A New Appreciation of Inflow Modelling for Autorotative Rotors

Yoh Murakami, M.AeroEng

Department of Aerospace Engineering
University of Glasgow
July 2008

Thesis submitted to the Faculty of Engineering, University of Glasgow,
in fulfilment of the requirements for the
degree of Doctor of Philosophy.

This thesis is based on research conducted between October 2004 and September 2007
at the Department of Aerospace Engineering, University of Glasgow.

Yoh Murakami
July 2008

Abstract

A dynamic inflow model is a powerful tool for predicting the induced velocity distribution over a rotor disc. On account of its closed form and simplicity, the model is highly practical especially for studying flight mechanics and designing control systems for helicopters. However, scant attention has been so far paid to applying this model to analyse autorotative rotors (i.e. rotors in the windmill-brake state), which differ from powered helicopter rotors (i.e. rotors in the normal working state) in that the geometric relation between the inflow and the rotor disc.

The principal aim of this research is to theoretically investigate the applicability of existing dynamic inflow models for autorotative rotors, and if necessary, to provide a new dynamic inflow model for autorotative rotors.

The contemporary dynamic inflow modelling is reviewed in detail from first principles in this thesis, and this identifies a modification to the mass-flow parameter for autorotative rotors. A qualitative assessment of this change indicates that it is likely to have a negligible impact on the trim state of rotorcraft in autorotation, but a significant effect on the dynamic inflow modes in certain flight conditions.

In addition, this thesis includes a discussion about the small wake skew angle assumption, which is invariably used in the derivation of Peters and He model. The mathematical validity of the assumption is cast doubt, despite the resultant model has experimentally been fully validated. This author discusses on a theoretical ground the possible reason why the Peters and He model works well in spite of its inconsistent derivation.

Declaration

The author hereby declares that this dissertation is a record of work carried out in the Department of Aerospace Engineering at the University of Glasgow during the period of October 2004 to September 2007.

The ideas and results in this dissertation are original in content except where otherwise stated.

Yoh Murakami
July 2008

Permission to Copy

Yoh Murakami

A New Appreciation of Inflow Modelling for Autorotative Rotors

Department of Aerospace, University of Glasgow

I, the undersigned, request that this thesis should be restricted either to inter-library lending, to use in another library or to photocopy in part or in full, for three months after this thesis is finally accepted by the Department of Aerospace Engineering, University of Glasgow.

After the restriction period, I, the undersigned, am willing that this thesis should be made available for consultation in the Library of Glasgow University for inter-library lending, for use in another library or for photocopy in part or in full - at the discretion of the Librarian - on the understanding that users are made aware of their obligations under copyright.

Yoh Murakami
July 2008

Acknowledgements

I would like to express my sincere appreciation to my supervisor, Dr. Stewart Houston, for his many hours of advice, constant assistance, supervision and encouragement.

I need to thank all the people in the department for creating a superb academic environment. Special thanks must go to Pauline Yearwood, David Suttie, Adriano Gagliardi, Lucy Schiavetta, Joseph Trchalik, Przemyslaw Marek, Nita Nathan and Giangicomo Gobbi for their friendship and encouragement.

I would also like to thank all of my friends in Glasgow, especially members of the Kelvin Ensemble, Glasgow Orchestra Society, St. Vincent Baroque Players, Harts String Quartet and Stone String Quartet for their having provided me with a wonderful musical life (music has always been the best pastime), and Rinako Nakagawa and Taro Fujita for their friendship and invaluable help.

I would also like to express my heartfelt gratitude to Dr. Darren Wall and Dr. Douglas Thomson, who patiently proof-read the final draft.

I also have to express my profound gratitude in this edition to Dr. Roy Bradley, who was the external examiner, and Dr. Eric Gillies, the internal, for their tough and strict but professional and instructive examination, suggestions and advice. When looking back to this experience in some decades, my gratitude shall be more profound; at least I must make my own future so that I can feel so both for them and myself.

Last but not least, I would like to express my deepest gratitude to my mother, Luna, who encouraged me and supported my study at all times in every aspect.

This work shall simply be dedicated to her.

Yoh Murakami
July 2008

Contents

Appendices

Nomenclature

Acronyms and Abbreviations

ARAIC	Aircraft and Railway Accidents Investigation Commission (of Japan)
ARMCOP	ARMy heliCOPter
CAA	Civil Aviation Authority
CFD	Computational Fluid Dynamics
DIY	Do It Yourself
DOF	Degree Of Freedom
KIAS	Knots, Indicated Air Speed
NACA	National Advisory Committee for Aeronautics
NASA	National Aeronautics and Space Administration
ONERA	Office National d'Études et de Recherches Aérospatiales
RASCAL	Rotorcraft Aeromechanics Simulation for Control AnaLysis
STOL	Short Take-Off and Landing
VTOL	Vertical Take-Off and Landing

General

$\mathbf{0}$	zero vector
$n!!$	double factorial, $n!! = n(n-2)(n-4)\cdots$
x	variable
$\mathbf{x}$	vector variable with implicit representation of elements (column vectors unless otherwise defined)
${}^t\mathbf{x}$	transposed vector of $\mathbf{x}$
(x_i)	column vector variable with explicit representation of elements
dx	infinitesimal variable
$[X]$	matrix variable with implicit representation of elements
$[X]^{-1}$	inverse matrix of $[X]$
$X[x_{ij}]$	matrix variable with explicit representation of elements
X_n^m	polynomials defined by two indices, m and n

Superscripts

$\bar{x}$	non-dimensionalised quantity
$\dot{x}$	derivative of x with respect to non-dimensional time, $\partial x/\partial \bar{t}$
x^c	indication of cosine
$x^{(c)}$	indication of the convective part of the Euler equation
x^m, x^r	terms associated with m-th or r-th harmonics
$x^{(M)}, x^{(L)}$	indication of apparent mass and gain matrices
x^s	indication of sine
$x^{(t)}$	indication of the time-derivative part of the Euler equation

Subscripts

x_0	indication of steady state; or indication of a value on rotor disc
x_n, x_j	terms associated with n-th or j-th polynomials
x_x, x_y, x_z	indication of coordinates

Latin Symbols

a	= acceleration, m/s^2
a_j^r, b_j^r	= Fourier coefficients for the representation of induced velocity
a_n, b_n	= arbitrary Fourier coefficients
a_x^{hinge}, a_z^{hinge}	= hinge acceleration components, m/s^2
A	= rotor area, m^2
$[A]$	= transformation matrix, $A_{jn}^{rm} = \int_0^1 \bar{P}_j^r \Psi_n^m \nu d\nu$
$[A]$	= linearised model system matrix
b	= number of blades
$[B]$	= transformation matrix, $B_{jn}^{rm} = \int_0^1 (1/\nu) \bar{P}_j^r \bar{P}_n^m \nu d\nu$
$[B]$	= linearised model control matrix
c	= blade chord, m
c_r	= blade root-cut, m
$\mathcal{C}$	= linear operator representation of $\partial/\partial z$
$C(k)$	= Theodorsen's lift deficiency function
C_L, C_M	= aerodynamic perturbations in roll and pitch moment,

non-dimensionalised on $\rho\Omega_0^2 R^5$

C_{2L}, C_{2M} = second harmonic aerodynamic perturbations in roll and pitch moment, non-dimensionalised on $\rho\Omega_0^2 R^5$

C_n^m, D_n^m = Fourier coefficients for Prandtl's potential function

C_T = aerodynamic perturbation in thrust, non-dimensionalised on $\rho\Omega_0^2 R^5$

D = drag, non-dimensionalised on $\rho\Omega_0^2 R^4$

$\mathcal{D}$ = linear operator representation of $(1/V)\int_\infty^0 \frac{\partial}{\partial z}....d\xi$

$\mathbf{e}_\nu, \mathbf{e}_\psi, \mathbf{e}_\eta$ = unit base vectors in ellipsoidal coordinates

f = function defined as $f(\nu) = \int_{-\infty}^0 \left(\frac{\partial}{\partial \bar{r}} + \frac{\mp m}{\bar{r}}\right) \bar{P}_n^m(\nu)\bar{Q}_n^m(\nu)dz$

F = force, N

$\mathbf{F}$ = force vector, N

h_1, h_2, h_3 = metric factors

H_n^m = coefficient defined as $H_n^m = (n+m-1)!!(n-m-1)!!/[(n+m)!!(n-m)!!]$

i = imaginary number, $i = \sqrt{-1}$

$I_{flap}, I_{pitch}, I_{lag}$ = blade inertia, Nm^2

$I_{xx}, I_{yy}, I_{zz}, I_{xz}$ = rotor inertia, Nm^2

J = function defined as $J = \sqrt{[(1+\eta^2)(1-\nu^2) - y_0^2](1 - y_0^2 - \nu_0^2)}$

K = function defined as $K = \eta^2(\eta^2+1) + \nu_0^2(\eta^2+1)\cos^2\chi - \eta^2 y_0^2 \sin^2\chi$

$[K]$ = matrix representation of $\mathcal{C}^{-1}$

K_c = longitudinal gradient of the induced flow distribution in Glauert's model

K_c, K_s = lateral and longitudinal wake curvatures

K_R = wake curvature

K_n^m = coefficient, $K_n^m = (2/\pi)H_n^m$

L = lift, non-dimensionalised on $\rho\Omega_0^2 R^4$

$[L]$ = gain matrix

$[\hat{L}]$ = gain matrix excluding the mass-flow parameter in the definition

$\mathbf{L}$ = aerodynamic moment vector, Nm

m = mass, kg

m = rotor mass, kg

M = mass of aircraft, kg

$[M]$ = apparent mass matrix

$M_{flap}, M_{pitch}, M_{lag}$ = moment acting on a blade, Nm

P = pressure, kg/ms^2

P_n = the Legendre function of the first kind

P_n^m = the associated Legendre function of the first kind

p, q, r = perturbed angular velocity components along airframe axes, rad/s

p_n, q_n = polynomials, defined as

$$p_n(x) = 1 - \frac{n(n+1)}{2!}x^2 + \frac{(n-2)n(n+1)(n+3)}{4!}x^4 - \cdots,$$
$$q_n(x) = x - \frac{(n-1)(n+2)}{3!}x^3 + \frac{(n-3)(n-1)(n+2)(n+4)}{5!}x^5 - \cdots.$$

$\mathbf{q}$ = perturbed velocity vector, $\mathbf{q} = (u, v, w)$, non-dimensionalised on $\Omega_0 R$

Q_n = the Legendre function of the second kind

Q_n^m = the associated Legendre function of the second kind

r = radial position on rotor disc, m

r_{cg} = position of centre of mass, m

r_{hinge} = position of flap, lag and feather hinge, m

r_{hub} = position of rotor hub, m

$\bar{r}, \psi, z$ = cylindrical coordinates

R = rotor radius, m

$\mathbb{R}$ = set of real numbers

t = time, s

t = $\tan\chi$

$[T_1], [T_2], [T_3]$ = transformation matrices

$\mathbf{u}$ = velocity vector, m/s

$\mathbf{u}$ = control vector

$\mathbf{U}$ = total velocity vector, non-dimensionalised on $\Omega_0 R$

u, v, w = perturbed velocity components along airframe axes, non-dimensionalised on $\Omega_0 R$

v = dimensional induced velocity, m/s

v_0 = dimensional uniform induced velocity, m/s

v_i = dimensional induced velocity, m/s

v_{1s} = dimensional induced velocity component, longitudinal, m/s

v_{1c} = dimensional induced velocity component, lateral, m/s

v_m = dimensional mass-flow parameter, m/s

v_{m+} = dimensional mass-flow parameter for normal working state, m/s

v_{m-} = dimensional mass-flow parameter for windmill-brake state, m/s

V = modulus of $\mathbf{V}$, $V = |\mathbf{V}|$

$\mathbf{V}$ = steady velocity vector, non-dimensionalised on $\Omega_0 R$, $\mathbf{V} = (V_x, V_y, V_z)$

$\mathbf{V}$ = arbitrary vector function, $\mathbf{V} = (V_1, V_2, V_3)$

V_m = mass-flow parameter, dimensionless on $\Omega_0 R$

V_{m+} = mass-flow parameter for normal working state, dimensionless on $\Omega_0 R$

V_{m-} = mass-flow parameter for windmill-brake state, dimensionless on $\Omega_0 R$

$V_{m\pm}$ = unified form of V_{m+} and V_{m-}, dimensionless on $\Omega_0 R$

V_T = non-dimensional total flow at rotor disc, dimensionless on $\Omega_0 R$

V_∞ = free stream speed, non-dimensionalised on $\Omega_0 R$

x = variable for functions in general

$\mathbf{x}$ = state vector

x, y, z = rotor disc coordinates, non-dimensionalised on R

X = wake skew angle parameter, $\tan(\chi/2)$

$\mathbf{X}$ = rotor force vector, $\mathbf{X} = (X, Y, Z)$, N

$\mathbf{X}_{elem}, \mathbf{X}^{aero}_{elem}, \mathbf{X}^{inert}_{elem}$
= blade element contributions to rotor force: total, aerodynamic, inertial, N

y = arbitrary function of x, $y = y(x)$

y_{cg} = position of the centre of gravity

$[Y]$ = matrix representation of $\mathcal{D}$

Y = extended wake skew angle parameter
in the no-assumption model

Greek Symbols

α = angle between free stream and rotor disc, rad

α_e = effective rotor angle of attack, $\alpha_e = (\pi/2) - \chi$, rad

α^m_n = Fourier coefficients for induced velocity, cosine part

β = flapping angle, rad

β^m_n = Fourier coefficients for induced velocity, sine part

Γ = Gamma function

Γ^{rm}_{jn} = coefficient defined as $\Gamma^{rm}_{jn} = \sum_{l=r+1}^{\infty} A^r_{jl} \Lambda^{rm}_{ln}$

δ = drag coefficient

δ_{ij} = Kronecker's delta

δ_r = rudder angle, deg

ζ = lag angle, rad

ζ^m_n = Fourier coefficients for the induced velocity, cosine part

η_c = lateral stick position, % (0% fully left)

η_s = longitudinal stick position, % (0% fully forward)

θ = collective pitch angle, deg

θ = perturbed pitch attitude, deg

θ_{1s} = longitudinal cyclic pitch , rad

θ_{1c} = lateral cyclic pitch, rad

θ_s = longitudinal tilt of the rotor shaft with respect to the airframe, rad

λ = non-dimensional total inflow

λ_0 = non-dimensional induced flow component, mean

λ_{1s} = non-dimensional induced flow component, longitudinal

λ_{1c} = non-dimensional induced flow component, lateral

λ_f = free stream inflow, $V\sin\alpha$

λ_m = non-dimensional inflow die to the rotor thrust

Λ_{jn}^{rm} = integral defined as $\Lambda_{jn}^{rm} = \int_0^1 \bar{P}_j^r(\nu) \int_{-\infty}^0 \Big(-\frac{\partial}{\partial \bar{r}} + \frac{\pm m}{\bar{r}} \Big) \bar{P}_n^m(\nu) \bar{Q}_n^m(\nu) dz d\nu$

μ = advance ratio in rotor coordinates, $V\cos\alpha$

μ_3 = axial component of inflow, $-V\sin\alpha$

ν = kinetic viscosity

ν, ψ, η = ellipsoidal coordinates

ξ = coordinate along free stream, positive upstream

ρ = density of air, kg/m^3

ρ_n^m = non-dimensionalising factor for P_n^m, $\rho_n^m = \sqrt{\frac{1}{2n+1} \cdot \frac{(n+m)!}{(n-m)!}}$

$[\tau]$ = time-constant matrix, $[L][M]$

τ_n^m = pressure coefficient

ϕ = perturbed roll attitude, deg

ϕ_s = lateral tilt of the rotor shaft with respect to the airframe, rad

Φ = pressure potential, non-dimensionalised on $\rho R^4 \Omega_0^2$

$\Phi^{(t)}$ = pressure potential corresponding to time-derivative terms in the Euler equation, non-dimensionalised on $\rho R^4 \Omega_0^2$

$\Phi^{(c)}$ = pressure potential corresponding to convection terms in the Euler equation, non-dimensionalised on $\rho R^4 \Omega_0^2$

$\tilde{\Phi}$ = pressure potential for the Pitt and Peters model, non-dimensionalised on $\rho R^4 \Omega_0^2$

χ = wake skew angle, rad

ψ = rotor azimuth, rad

ψ = perturbed roll attitude, deg

Ψ_n^m = general expansion function

ω = non-dimensionalised induced velocity

$\omega_x, \omega_y, \omega_z$ = blade angular velocities, m/s

ϖ_n^m = Fourier coefficients for the induced velocity, sine part

Ω = rotor speed, rad/s

Ω_p = propeller speed, rad/s

List of Figures

List of Tables

Chapter 1

Introduction

1.1 Overview

The primary aim of this thesis is to theoretically investigate the applicability of existing dynamic inflow models for autorotative rotors. Contemporary dynamic inflow models such as the Pitt and Peters model[(1)] have been developed for helicopter rotors in the normal working state. The literature suggests that this would be the first time that the possibility of applying the dynamic inflow model to autorotative rotors has been examined from a theoretical viewpoint.

Ever since the first gyroplane, Model C.4 designed by Juan de la Cierva, flew in 1923[(2,3,4)], it has always been a major problem how to describe the distribution of the airflow around the rotor. Although simple momentum theory can provide a key insight into the rotor performance in steady axial flight[(5,6)], a more sophisticated description about the inflow distribution is required to study the rotor performance, rotor stability and controllability in unsteady state or in forward flight, and to evaluate rotor loads, which are closely connected with the controls. The rotor loads are important also in relation to rotor vibration and structural fatigue. Historically, a variety of methods have been proposed to describe the detailed inflow distribution over rotors in the normal working state, either in steady or unsteady state for either axial or forward flight. Examples thereof include various dynamic inflow models.

In the following Sections in this Chapter, the characteristic features and historical development of the dynamic inflow model will be outlined. The discussion of this thesis shall mainly be focused on theoretical and mathematical aspects, but some numerical verification of the salient points are to be presented.

1.2 Organisation of this Thesis

An extensive literature review is given in Chapter 1 in relation to dynamic inflow models such as the Pitt & Peters and Peters & He models. In an attempt to outline the characteristic features of dynamic inflow modelling, the practical applications and

historical development are shown in comparison with other methods, such as lift deficiency functions and CFD methods. Furthermore, a brief history of gyroplanes and a description of the current problems in the field of gyroplane research are introduced so as to make clear the significance of this research.

In Chapter 2, the mathematical derivation of Peters and He model is carefully examined aiming to theoretically identify the necessary modifications to the model for its application to autorotative rotors. In this examination, the author seeks to improve the lucidity of the derivation of these models by examining the assumptions they are based on, presenting proofs to related theorems, as well as offering new approaches to interpreting these methods. A few potentially misleading typographical error in the original literature are also detailed. Although the author enunciates his own point of view in places, it must be herein emphasised that the results and derivations presented in this Chapter fundamentally rely on the work contained in Dr. C.-J. He's doctoral thesis[(7)].

In Chapter 3, the applicability of the existing dynamic inflow model for autorotative rotors is considered, and the necessary modification to the model for such applications are presented in terms of the geometric difference between rotors in the normal working and windmill-brake states with regard to the relation between the rotor angle of attack and the incoming flow. This difference always exists between rotors in those two states. Some computational simulations are also conducted to study the affect of the modification made in the mass-flow parameter.

In Chapter 4, *the small wake skew angle assumption*, which is a vital requirement in the derivation of Peters and He model, is examined. The analysis of Chapter 4 is based on that of Chapter 2, but the results are not limited to autorotative rotors. An alternative model, in which the small wake skew angle assumption is not used, is also presented. The reason why the Peters and He model practically works so well in spite of the questionable assumption is discussed on a theoretical ground.

In Chapter 5, an overview and discussion of the results presented in this thesis are provided together with recommendations for future research directions.

1.3 Focus of this Thesis

The primary focus of this research is the improvement of the performance of existing gyroplanes and the clarification of the dynamic behaviour of these aircraft. Following the advent of the helicopter[1], the gyroplane gradually gave way to the helicopter, and only a small number of studies were undertaken either on an academic, military or governmental basis after the Second World War[2]. In the mean time, the gyroplane has been developed generally by amateur home-builders and some small companies for sports or leisure flying, and consequently, a good number of pilots were killed in accidents without amply clarifying the possible causes of such accidents. Some fatal accidents could have been attributed to human error or technical malfunctions owing to inexpert weekend DIY manufacturing, but other accidents might have been caused by more fundamental design faults, or the control system. As the dead cannot speak in their own defence, it may be attributed to the authorities that closer investigations into the possible causes have not been pursued.

In the United Kingdom, CAA decided to ground all gyroplanes produced by Air Command International Inc. in 1991 after a series of six fatal accidents resulting in seven fatalities from 1989 to 1991, and this became the trigger for a series of research studies on gyroplanes at the University of Glasgow[(8,9,10)]. (Some accident reports in the U.K. are available from Ref. (11).) Compared to the U.K. and the U.S.A., where the gyroplane is relatively popular, the public recognition of the danger of gyroplanes is much smaller in other countries, and legislative systems such as airworthiness certificates and relevant air traffic laws can also be less developed.

For example, in Japan, where no official licensing system is set up for the gyroplane, there were 23 accidents between 1974 and 2006, including 8 accidents involving Air Command Gyroplanes, with 18 pilots killed. Given that there are only 120 or so officially registered gyroplanes in Japan, this accident rate is clearly significant. The Secretariat of ARAIC concluded that 19 accidents thereof could simply be attributed to human error and 1 to improper maintenance[(12)]. Considering the fact that all Air

[1] It is controversial to whom the title of the first inventor of the helicopter should be credited. Two Frenchmen, Louis Breguet (1880-1955) and Paul Cornu (1881-1944), independently insisted that they flew in 1907, but it is rather doubtful that their machines had enough power to take off. A Dane, Jens Ellehammer (1871-1946), flew in 1913, with the Crown Prince of Denmark witnessing the flight. It is more popularly accepted that the first flight is credited either to Focke Fw.61 in 1936[(13,14)] or to Breguet-Dorand's *Gyroplane Laboratoire* in 1935. In any case, the helicopter was not practical maturity until Sikorsky's Type R-4 was put into production in 1942[(15)].

[2] Quite a few research studies were made before the Second World War including Refs. (2-4,16-22). However, the number of such works published after the war is considerably few. References (23) and (24) are two such rare examples of studies undertaken after the Second World War before 1991.

Command Gyroplanes have been grounded in the U.K. due to the possible inherent instability, one may consider that there is a possibility that some of the accidents in Japan could be attributed to the inherent flight characteristics of the vehicles rather than human error.

There is thus a requirement to improve the basic understanding of the gyroplane aeromechanics, with both theoretical and experimental approaches necessary for this aim. In order to study flight mechanics of the gyroplane, a mathematical model of the induced velocity for autorotative rotors is an absolute necessity, and the dynamic inflow model should be better suited to this modelling task than other approaches to describing the inflow distribution, including various CFD methods. This forms the principal motivation for the present research.

As well as addressing safety issues as described above, there is also a belief that gyroplanes can still compete with other classes of V/STOL aircraft, including helicopters and tilt rotors, as a short-range transport of the future, and several projects to explore this possibility are presently under way. Thus, it is believed that a wide range of basic research, either theoretical or experimental, is necessary at this stage to realise those projects in time to come. Based on the view above, the possible contribution to the further development in gyroplanes also partly motivated this research.

Furthermore, autorotation is also of great importance for helicopters as the way of emergency landing, though it is an abnormal condition. Nevertheless, scant attention is paid to either the theoretical or experimental investigation, and this situation needs a suitable mathematical model which can be used in control analysis. Hence, further research on the flight state of autorotation should be meaningful not only for gyroplanes but also for helicopters in autorotation.

This background forms the motivation for this work, and it is hoped that this research will contribute to the study of control system and flight dynamics for the gyroplane and the autorotative state of the helicopter.

1.4 General Introduction to the Dynamic Inflow Model

In the following Subsections, the base principles of the dynamic inflow model and an outline of the schematic application thereof are briefly reviewed prior to Chapter 2, in

which the model will be derived and examined in depth from a rigorous mathematical perspective. The understanding of base principles beforehand is believed to make it easier to understand later Chapters. Also, it is aimed that the characteristic features of the dynamic inflow model are generally elucidated in comparison with other methods for describing the induced flow distribution over a rotor disc.

1.4.1 Base Principles

The dynamic inflow model is essentially an application of Newton's laws of motion. During the flight, the rotor is supported by the air, with this force called lift. By Newton's third law of motion, the rotor in turn exerts a force of the same magnitude as this lift in the right opposite direction (see Fig. 1-1). This force accelerates the air below the rotor according to Newton's second law of motion; the force equals the mass of the accelerated air multiplied by the acceleration,

$$ma = F. \tag{1.1}$$

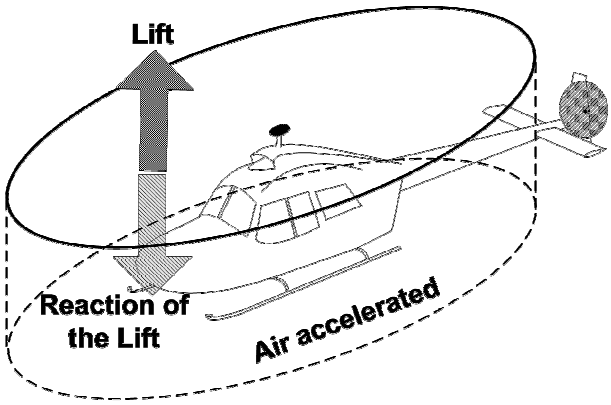

Fig. 1-1 [The first principle of the dynamic inflow model.]

There are two points which need attention here. Firstly, the equation of motion of inviscid incompressible flow is called Euler's Equations (or Eulerian Equations of motion), and it takes a slightly different form than Eq. (1.1), though essentially the same. The derivation of Eq. (1.2) from Eq. (1.1) should be found in most of textbooks on fluid mechanics such as Refs. (25) or (26).

$$\rho\frac{\partial \mathbf{u}}{\partial t} + \rho(\mathbf{u}\cdot\nabla)\mathbf{u} = -\nabla P, \tag{1.2}$$

where $\mathbf{u}$, t, ρ and P denote fluid velocity, time, fluid density and pressure, respectively.

Secondly, the total mass of the air flow accelerated is not as straightforward as in the motion of point masses, and thus the determination of the apparent mass of the flow forms a problem that must also be considered. Still, the reader should be encouraged to remember that the dynamic inflow model is in essence simply an application of Newton's laws of motion. Note that when applying Eq. (1.1) or (1.2), the rotor may be regarded as a thin flat continuous surface, which accelerates the air underneath the rotor to generate discontinuities in the pressure and velocity between upper and lower sides thereof. This assumption is called *actuator disc theory*.

The dynamic inflow model is typically represented in the form of a matrix equation.

$$[M]\ \dot{\mathbf{u}} + [L]^{-1}\mathbf{u} = \mathbf{F}, \tag{1.3}$$

where $\mathbf{u}$ and $\mathbf{F}$ are state vectors of the induced flow and the lift (rotor thrust and moments)[3], a dot (.) denotes differentiation with respect to time, $\partial/\partial\bar{t}$. At this stage, it may be noted that Eq. (1.3) is, very roughly speaking, in the same form as of Eq. (1.2), which is itself a rewriting of Eq. (1.1) for an ideal fluid. (Note that since the differential operators of $\partial/\partial\bar{t}$ is linear, it can be expressed as a matrix in Hilbert space. However, the differential operator of $(u \cdot \nabla)$ in Eq. (1.2) is not linear, and hence it should be invariably linearised to result in a linear form.) Given Newton's laws of motion, the derivation of the dynamic inflow model in the form of Eq. (1.3) from Eq. (1.2) is thus straightforward. Note that the $[M]$ and $[L]$ matrices in Eq. (1.3) are conventionally called *apparent mass matrix* and *gain matrix*, and their product, $[\tau] = [L][M]$, is called *time constant matrix*. These epithets will be occasionally used also in this thesis.

1.4.2 The Characteristics of the Dynamic Inflow Model

In this Section, a general appraisal of the dynamic inflow model is described, aiming to sketch out its features (i.e., strength, weakness, usefulness, limitation, etc.) in a practical context compared to other models. The characteristic features of the dynamic inflow model can be outlined as follows:

i. the dynamic inflow model is a mathematical model describing the unsteady dynamic

[3] It is difficult to identify who first introduced the matrix form because the dynamic inflow model was developed by many researchers in a parallel manner in the early stages. Reference (27) is one of the earliest works in which the matrix form is used, and Ref. (1) is believed to be most instrumental in establishing the matrix form.

distribution of the induced velocity at/near a rotor in terms of aerodynamic loads acting on the rotor;

ii. it may be associated with practical modifications or empirical corrections, and can be extended so as to incorporate additional effects such as aeroelasticity, compressibility, ground effect, blade root-cut, tip-loss, wake distortion and so on;

iii. it can be represented by relatively simple equations, especially when described by finite state variables, and is thus computationally light;

iv. it can be represented in a closed form, and thus can be applied for eigenvalue analysis and Floquet analysis. Especially when described by finite state variables, it is of particular use in analysing rotor control, stability, handling qualities and so on.

The versatility and flexibility described by point (ii) above are considered to be among the major advantages of a dynamic inflow model. Also, no restriction or assumption is required for the representation of lift in order to associate the lift with the induced flow in the frame of dynamic inflow models. The model can be thus flexibly coupled with any lift theory.

Regarding point (iii) above, although expressions of apparent mass and gain matrices in Eq. (1.3) by finite dimensional matrices are mathematically an approximation, the dynamic inflow model often needs to be formulated by a small number of state variables, and this mathematical simplicity makes it possible to compute the induced flow distribution within a limited time. Note that the number of state variables (i.e. Fourier coefficients) can be increased as much as required though, it only means improving the accuracy of the representation of lift or induced flow based on actuator disc theory. Since actuator disc theory itself is an extreme simplification of the rotor, this is arguably a limitation of the dynamic inflow model. More comprehensive CFD methods based on vortex methods are thus usually more suitable for studying detailed blade geometry and the relevant aerodynamic effects. Still, it is known that the dynamic inflow model imparts reasonable, at least practically sufficient, distributions of the induced velocities for most flight conditions of helicopters. For example, in a major seminal review, Chen shows comparisons between various dynamic inflow models expressed by 3×3 matrices, experimental data and computational methods, and concludes that "*all the first-harmonic inflow models predict the induced velocity as well (as poorly) as the free-wake methods...*"[28]. Considering the acceptable accuracy in the representation of the induced flow field, the extremely simple form of the dynamic inflow model can be considered as a superior strength, especially when iteratively

conducting real-time simulations[4].

The following schematic diagram illustrates how to couple the dynamic inflow model with other theories. Similar diagrams are frequently sketched by Peters and his coworkers[1,29].

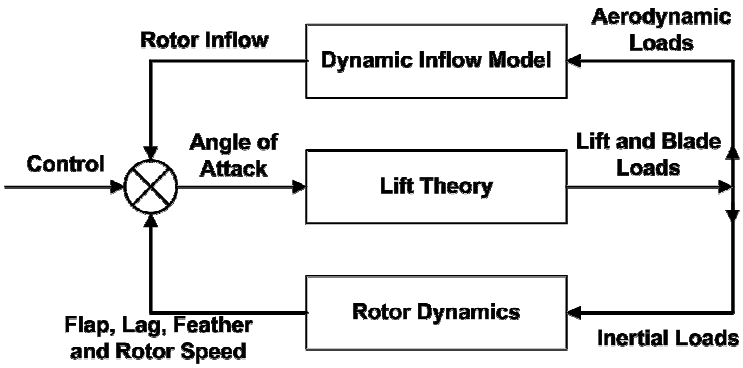

Fig. 1-2 [Schematic diagram for the typical use of the dynamic inflow model.]

Since the dynamic inflow model describes the induced velocity as a function of the lift, the diagram shows the typical combination of the dynamic inflow model with the lift theory, which describes the rotor lift, and the blade dynamics, which explains local angle of attack of the rotor. Still, this loop can be easily changed or extended by adding extra components such as body dynamics[5].

The closed loop described in Fig. 1-2 is the key to eigenvalue analysis that arises in considering stability[30-33] with respect to point (iv) above. Note that open loop models including free-wake and prescribed-wake methods, which are effective at time-marching problems, are usually not well-matched with such stability analyses.

In general, the lift theory and the rotor dynamics are much more advanced than the inflow model, and they can be tailor-made for individual blades incorporating root-cut, tip-loss, detailed blade shape and even aeroelastic deformation. Since a blade is quite flexible and hence experiences various airspeeds per revolution, such an advanced theory should be highly useful for structural analysis. However, from the control point

[4] The amazingly rapid development in computational methods made thereafter must, of course, also be taken into account today.

[5] A dynamic inflow model in the form of Eq. (1.3) is often synonymously called finite-state model, though this can not be a precise usage in the sense that any feasible method in reality should be expressed in terms of a finite number of variables. The connotation may imply that in comparison with dynamic inflow models, CFD methods need millions of states, which correspond to the number of their mesh, nodes, or grid points, and that it is thus impractical to use these methods for eigenvalue analysis.

of view, it is more important that there should be a balance between each theory shown in Fig. 1-2, because it is often the case that the combination of crude models yields better stability analysis results than those found for a crude model coupled with a detailed model[6(34-36)]. It is regrettable that these advanced blade dynamic models should be still often used in combination with simple momentum theory or quasi-steady inflow model. Examples of more advanced inflow models popularly used today include the Pitt and Peters model[(1)] and the Peters and He model[(37)], but their applicability to autorotative rotors has never been rigorously examined.

Based on the discussion above, this author believes that further sophistication and validation of the unsteady inflow model on a theoretical basis is of prime importance for the development of the analysis of autorotative rotors.

1.5 Concise History of the Attempts to Describe the Induced Flow Distribution

In this Section, the historical development of the dynamic inflow model is outlined in parallel with the history of other theories such as lift deficiency function, equivalent Lock number and CFD methods. It is generally difficult to clearly put theories into different categories, because all theories have been developed with mutually affecting each other. Sometimes it is the case that one theory comes to be hierarchically implied by another even though their start points were quite different. In this discussion, it is intended to focus on the role that the dynamic inflow model played in the development of models in this area.

1.5.1 From Classical Theory to the Pitt and Peters Model

In the simplest and oldest inflow model, it was assumed that the induced flow is steady and uniform over the rotor (see Fig. 1-3, top). The magnitude of the uniform induced velocity can be easily calculated from momentum theory, yet this simple model can yield a surprising level of information concerning the power required and the basic

[6] The dynamic inflow model with higher harmonics, which means larger $[M]$ and $[L]$ matrices, does not always give better results than of the first harmonic inflow model with 3×3 order matrices[(38)]. This might be also partly because of the unbalance of the accuracy between the description of the inflow distribution and the model itself, since the dynamic inflow model is based on linearised Euler's Equations, which are already hugely simplified from the Navier-Stokes Equations. In order to clarify the dynamic and aerodynamic couplings of the rotor in the higher frequency region, it is awaited to improve the dynamic inflow model with higher harmonics, which may require some empirical corrections. Reference (39) discusses why the second harmonic inflow model with 5×5 order matrices performs worse than the first harmonic model in Ref. (40), suggesting that the time-constant was underestimated. In any case, a dynamic inflow model with higher harmonics has not yet been successfully proposed.

flight performance in hover[5]. In the forward flight, however, the blades have different relative airspeeds at different positions on the rotor, and the uniform distribution cannot be realistically applied. Glauert proposed a linear distribution in which a longitudinal gradient is considered[5,41].

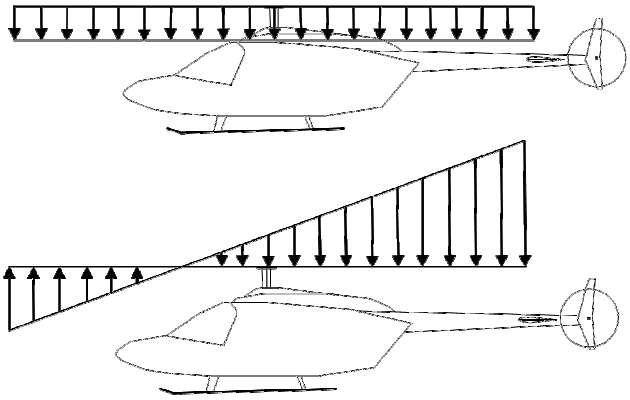

Fig. 1-3 [Comparison between the uniform distribution and Glauert's model.]

Glauert's model is effectively a first order linear approximation, and is too simple to provide an accurate representation for the complicated induced flow distribution found in practice, but yields reasonable results when applied with an appropriate gradient. The induced flow field in Glauert's model is described as follows,

$$v = v_0(1 + K_c\frac{r}{R}\cos\psi), \tag{1.4}$$

where K_c represents the longitudinal gradient of the distribution, and v, v_0, r, R and ψ denote the (axial) induced velocity, the uniform induced velocity, radial position on the rotor disc, the rotor radius and the rotor azimuth, respectively. (See Fig. 1-3, bottom.) Many values were theoretically or experimentally proposed for K_c, and the examples are found in Refs. (16) and (42). Coleman and Feingold[43] suggested $K_c = \tan(\chi/2)$, and this was the first time that K_c had been represented as a function of wake skew angle, χ. This was a marked improvement, because the distribution of the induced velocity heavily depends on the wake skew angle. Stepniewski introduces in Ref. (44) a broader variety of presupposed static distributions of the induced velocity.

Note that in momentum theory, the magnitude of induced velocity is evaluated regardless of the number of blades, airfoil section, chord length, blade twist, planform, rotor speed and so on. In order to include these detailed aspects of rotor, there was a school of attempts starting from blade element theory to describe the induced velocity,

examples of which can be found in Refs. (44) and (45).

Harris and McVeigh assumed that the local angle of attack of a blade should be zero at the root and tip so that the lift should be zero, which means that induced velocity forms a zero relative angle of attack at these points even in forward flight[(45)]. These works based on blade element theory helped to promote the improvement in the theory of non-uniform induced flow distribution. Harris further studied full-articulated rotors at low advance ratios, which exhibit an excessive amount of lateral flapping, correlating wind tunnel test data with several classical inflow theories and numerical simulations based on the prescribed wake method[(46)]. Harris concluded that none of those theories were satisfactory in predicting the lateral flapping at low advance ratios. This result indicated that an essential improvement in the theoretical models was still necessary.

The first attempt to rigorously describe the distribution in a theoretical manner in the frame of actuator disc theory can be traced back to Kinner[(47)], who introduced the ellipsoidal coordinate system to describe the induced flow, and represented the distribution of lift in the form of a functional series of the associated Legendre functions. Note that these works introduced above are related not to the unsteady inflow distribution, but to the steady distribution of the induced flow.

After the Second World War, the heyday of gyroplanes had passed, and the helicopter came to be a practical class of aerocraft. Some important works concerning the unsteady induced velocity were done in the 1950's in the context of helicopter flight mechanics. NACA engineers found through rotor whirl-tower tests in the 1950's that when increasing the collective pitch rapidly, there arises an overshoot of thrust[(15)]. The reason for this is that the delay of the induced flow in reaction to the change in the collective pitch leaves the local angle of attack high until the angle is decreased by the newly developed induced velocity[7]. This finding attracted the attention of rotorcraft aerodynamicists at the time to unsteady phenomena of the induced flow.

Mangler and Squire conducted one of the most important studies considering the

[7] One important aspect with this phenomenon is that the airfoil may generate lift at a higher angle of attack than its stall angle, because there is also a delay in the occurrence of stall. As a result, the overshoot of thrust sometimes can be as large as double the maximum lift in the steady state. This phenomenon is called *dynamic stall*. Examples of such radical overshoot of thrust include a rapid yaw control of helicopters, and this led to the possibility of serious damage in the tail rotor because the overshoot of tail rotor thrust surpasses the maximum steady state value, upon which the structure was designed. The induced velocity delayed in the response is now called *dynamic inflow* and this is the root of the name of the dynamic inflow model[(15)].

modelling of an unsteady distribution of the induced flow undertaken in this period[48]. They first associated Kinner's distribution of lift, which satisfies Laplace's equation and can describe the pressure discontinuity across the rotor, with the induced velocity field in the form of Euler's Equations. In their model, the rotor is treated as a solid circular disc as in actuator disc theory, and a lift distribution is assumed so as to satisfy the desired hub load. Mangler and Squire's model can be regarded as the theoretical archetype of the dynamic inflow model in the sense that the acceleration of the induced flow was therein implied. However, the method of coupling the rotor load with induced velocity was not as sophisticated as that of modern dynamic inflow models[8]. Joglker and Loewy extended Mangler and Squire's theory to incorporate the wake geometry[49][9].

Carpenter and Friedvich[50] presented another important work that also took the dynamic inflow effect into consideration, motivated by the "*jump take-off*" of overloaded helicopters. Some gyroplanes in the 1930's already practised jump take-off, which is a vertical take-off achieved by suddenly increasing the collective pitch of the rotor, which is sufficiently prerotated at the minimum collective pitch. Jump take-off is often explained as a sudden conversion of the excess kinetic energy stored in the rotor into the rotor work, but the overshoot of thrust due to the dynamic inflow effect is also important. Unfortunately, the dynamic inflow effect was not well understood by gyroplane engineers at that time. Carpenter and Friedvich's approach was quite different from Mangler's; they simply extended momentum theory by adding an extra term, *apparent mass term*, which accounts for the delay in the induced flow to respond to changes in collective pitch. Their model is now called *unsteady momentum theory*. The remaining problem therewith is how to evaluate the apparent mass, and they adopted the value of $8/3\pi \simeq 63.7$ % of the air mass in a sphere with the same diameter as the rotor, following Ref. (51). Their unsteady momentum theory can be simultaneously coupled with other equations about blade dynamics, and the computed results agreed well with experimental data for hovering flight.

Whereas the phenomenon caused by the dynamic inflow have been increasingly attracting the interest of helicopter aerodynamicists since the 1950's, most of the efforts in modelling the induced velocity distribution was still focused on the static distribution, in part because more basic information about the inflow distribution was first required

[8] Reference (57) shows that Mangler and Squire's model does not agree well with experimental data. See also Ref. (28) about the accuracy of the model.

[9] Although the whole picture of their model is highly complicated, one particularly instructive feature of Ref. (49) is that it presents a lucid and detailed rearrangement of the equations for aerodynamic coefficients expressed in ellipsoidal coordinates, which are seldom provided in other literature.

at that time[52-54].

In the meantime, Sissingh developed a new model in which the roll and pitch coupling of a rotor and their damping effect were linked with the variation of the dynamic inflow[55]. This cross-coupled damping effect was first reported in Ref. (56), but was not well explained by the existing theories in which a uniform distribution of the induced velocity was assumed. Sissingh assumed non-uniform distribution of the induced velocity, and associated the variation with the first harmonic variation of the lift coefficient. The idea of explaining the cross-coupled damping effect by non-uniform inflow variation was novel, and led to the contemporary dynamic inflow model, Eq. (1.3). Sissingh's results agreed with the experimental data of Amer so well that his approach was adopted in Lockheed REXOR Program and McDonnell-Douglas' (formerly Hughes) simulation program FLYRT[29]. However, Sissingh assumed that the reaction of the inflow should occur instantaneously, and did not take the dynamic delay into account. His model is therefore called *quasi-steady model*. Moreover, Sissingh formulated the inflow distribution as a Fourier series dependent only on the azimuth, but did not consider the radial variation.

Wheatley mentioned the close relation between the induced flow and the rotor load, and the possible problems with noise and vibration[16] as early as in the 1930's, but it was not until the 1960's that this relationship attracted more general attention, partly because of the advent of hingeless rotor, which was first adopted in the Messerschmidt-Bölkow BO105 in the late 1960's by virtue of the development in composite materials. The hingeless rotor is more sensitive to the variation of rotor load than full-articulated rotors, and hence the inclusion of inflow distribution into the model of the control system came to be considered as a vital necessity.

Curtiss and Shupe associated non-uniform rotor load with perturbations in pitching and rolling moments for hingeless rotors in axial flight in the frame of a quasi-steady model in 1971[58]. Instead of fully incorporating dynamic inflow effects, they modified the Lock number to account for the dynamic change in lift. Note that the reduced Lock number[10], which is usually called the *equivalent Lock number*, can be identified with Loewy's or Miller's lift deficient function. Bannerjee *et al*. compared both the equivalent Lock number method and the dynamic inflow model with experimental data,

[10] The Lock number is defined as $\gamma = \rho a c R^4 / I$. Reducing the Lock number is thus intuitively equivalent to assuming a heavier blade.

and concluded that the dynamic inflow model works better at low advance ratios up to 0.4[(59)].

The techniques of taking experimental measurements of the induced velocity distributions have been developed since the 1960's onwards, and examples include Refs. (60) and (61). Gaonkar and Peters later described the situation, "... *the theory of dynamic inflow has been driven constantly by the impetus of experimental data*." in Ref. (62). In point of fact, those experiments showed that unsteady momentum theory does not agree sufficiently well with experimental data, and this became the trigger to further develop the dynamic inflow model to cover forward flight conditions. Wood and Hermes tried to combine momentum theory and blade element theory to describe the induced flow in forward flight[(63)], and Azuma and Kawachi proposed *the local momentum theory*, in which instantaneous momentum balance at a local blade element is considered, and the blades are approximated as multiple wings, each of which has an elliptical circulation distribution[(64)]. The local momentum theory was so designed that the time-wise decay of the induced flow can be described by an attenuation coefficient even in unsteady forward flight.

In 1972, Ormiston developed the idea that the Fourier coefficients of the distributions of induced velocity and lift should be associated in the form of a matrix equation. Since he described the lift by circulation based on the Kutta-Joukowski theorem and blade flapping dynamics was also incorporated, the model resulted in an elaborate formulation[(27)]. The representation of induced velocity was not therein completed because only the time-averaged velocity distribution was considered in the model, and thus, as Ormiston himself stated in the paper, the major significance of the work should be in the mathematical rigour in the derivation.

Ormiston also developed a quasi-steady model with Peters to show that inclusion of the non-uniform distribution of the induced velocity of a hingeless rotor improved the agreement between the theory and experimental data[(65)]. Although their model was still partly based on complicated circulation theory, it was more accessible than the previous model in Ref. (27), and the correlation with experimental data was significantly improved. However, some elements of the gain matrices for this model were constant regardless of the wake skew angle or any other flight variables, and some non-diagonal terms are assumed to be zero, that is to say, cross-coupling effects are not sufficiently taken into consideration.

Peters further developed the model to the form of Eq. (1.3) including the apparent mass matrix[66], and demonstrated that the unsteady non-uniform induced velocity and the blade aeroelasticity have a significant effect on the response characteristics of the rotor system. However, the model is only appropriate for hovering flight, and thus the non-diagonal elements of the gain matrix were not therein considered. Moreover, the elements of matrices were not mathematically rigorously determined.

In 1976, Ormiston proposed an advanced mathematical model in which flapping angle, inflow components and pitch angle are expanded as a Fourier series, and the flapping angle and inflow components are unified in the form of a matrix equation, which is suitable for eigenvalue analysis[67]. Although only the first harmonics (i.e. longitudinal and lateral components) are therein considered, off-diagonal elements of matrices are also provided, and thus some cross-coupling behaviour of the rotor is also taken into account. The formulation is an important milestone towards the contemporary dynamic inflow models.

Various attempts at establishing the dynamic inflow model were made by many researchers at this time in rather a parallel manner, and the examples include Refs. (68), (69) and (70). White and Black's model[69] is quasi-steady, and Johnson's model[70] is similar to Carpenter and Friedvich's unsteady momentum theory. Although all of these references concluded that their models showed a considerable progress in correlation with experimental data such as Ref. (62), none of them could satisfactorily fully explain dynamic inflow effects. Crew, Hohenemser and Ormiston tried to formulate the reduction in control hub moment due to dynamic inflow effect in hover by either using the equivalent Lock number method or replacing the inflow term in the blade equations with an equivalent inflow term. Reference (71) has a brief summary of some of those various dynamic inflow models presented in this period. (Note that it is pointed out in Ref. (29) that the summary of Ref. (71) contains a misconception that the lateral and longitudinal components of the induced flow, λ_{1s} and λ_{1c}, are missed in the time-derivative part, i.e. the vector multiplied by the apparent mass matrix, resulting in an erroneous expression for the uniform component of induced velocity.)

Another important study of this period was conducted by Peters and Gaonkar[72]. These authors extended the equivalent Lock number approach[59], which was used in the frame of quasi-steady model for studying flapping stability, to the advanced dynamic inflow model for studying flap-lag stability. They conducted extensive calculations for

the following model types: no induced flow perturbations, quasi-steady momentum theory, unsteady momentum theory, an empirical model and the equivalent Lock number model. They concluded that the dynamic inflow effect significantly increases the flap-damping, and reduces the lag-damping. Some experimental attempts were also made to identify the elements of the gain matrix[73]. Gaonkar *et al*. studied the dynamic inflow effects on the flap-lag stability with a quasi-steady model using the equivalent Lock number[74].

The study of Van Holten, Ref. (75), is an important example of three-dimensional unsteady rotor modelling based on acceleration potential theory. This study cast a doubt on whether the classical lifting line model is valid for unsteady rotor dynamics, and represented the (incompressible) induced flow field in the form of asymptotic expansions. The theoretical basis and the limitation of Van Holten's model are examined in Ref. (76). Although Van Holten's model is mathematically rigorously derived, the model is represented in the form of integral equations, and is not well suited for flight dynamics applications.

The most important achievement in the history of dynamic inflow model was arguably made by Pitt and Peters[1], who extended the model of Ref. (65) for hovering to fully include forward flight. The characteristic features of this model are its versatility, possibly wide applications, the convenience it offers in being able to be used for stability and control analysis, and the quite mathematical presentation of its derivation. The equivalent Lock number approach is therein completely abandoned, and the gain matrix is described as a function of the wake skew angle. In Ref. (28), Chen presents intensive comparisons between the Pitt and Peters model and other dynamic inflow models including those models proposed in Refs. (43), (69) and (77). Chen concluded that the Pitt and Peters model shows an overall better agreement with experimental data than other models. Reference (78) introduces the derivation of the Pitt and Peters model in detail, together with an extensive literature review and comparison with other numerical models.

1.5.2 Lift Deficiency Function

Whether steady or unsteady, the idea of associating the induced velocity with rotor loads can be considered essentially based on simple Newtonian mechanics. On the other hand, there is a different approach, in which the distribution of induced flow is calculated from the distribution of vortices through the Biot-Savart law. The lift

distribution is also associated with the vortex distribution by means of the Kutta-Joukowski theorem. This approach generally becomes much more computationally intensive than the dynamic inflow model, but is more suitable for studying the detailed shape and behaviour of the rotor wake and for incorporating detailed blade geometry[11]. Moreover, the vortex method is suitable for studying unsteady aerodynamics by considering the interaction between unsteady vortices.

The study of unsteady rotor aerodynamics using the vortex method may be traced back to Glauert[(79)]. Theodorsen developed the study and introduced *Theodorsen's lift deficiency function*, $C(k)$, to account for the loss in circular lift due to the dynamic development of the wake of an oscillating blade[(80)]. Reference (5) presents the detailed mathematical derivation of the lift deficient function. Theodorsen's work was really a milestone in theoretical unsteady aerodynamics, yet the distribution of the induced flow is in reality much more complicated than what Theodorsen presumed, and thus the approach needed further sophistication. References about the development of lift deficiency functions include Refs. (81), (82) and (83). Greenberg coupled Theodorsen' lift deficiency function with the quasi-steady model. Willmer regarded the trailing wake from the outer part of a blade straight by neglecting its curvature, and succeeded in representing the azimuthal variation of lift, which showed a reasonable agreement with experimental data.

Miller introduced the concepts of the *near wake* and *far wake*, and concluded that the higher harmonic rotor loads are evident during forward flight and are subject to the far wake, and also that the higher harmonic loads are sensitive to the vertical spacing of the wake sheet layers[(85)]. Loewy improved Theodorsen's lift deficiency function by incorporating the spacing function to account for the influence of the shed vorticity, and this modification made the lift deficiency function much more useful in rotorcraft analysis. Loewy's work reconfirmed not only the importance of three-dimensional modelling of the rotor wake for rotorcraft analysis, but also the necessity of taking the dynamic inflow effect into consideration when studying critical flutter speed and so on[(86)]. Loewy's function is a great improvement from Theodorsen's though, only

[11] As is discussed in Section 1.3, the dynamic inflow model is based on simple actuator disc theory. Although the dynamic inflow model is highly flexible to combine with any other advanced blade dynamics theories[(7,36)], the start point (i.e. actuator disc theory) can be an inherent limitation of the approach. On the contrary, the vortex method is able to incorporate elaborate blade geometry and dynamics from the beginning, and can impart more intricate distribution. However, its minuteness sometimes leads to a lack of versatility, and the computational intensity may also be a problem. It should be noted here that these two theories are not incompatible, and can indeed be used in conjunction to overcome either of the single method's shortcomings. One example of such an attempt is found in Ref. (84).

two-dimensional vortex sheets are therein assumed, and hence the limitation of this assumption leads to the following shortcomings, which are pointed out by Peters and He[7]: (i) skewed helical vortex geometry, which is expected in forward flight, cannot be incorporated; (ii) the model has a singularity for the collective mode at the zero frequency, and the model is thus not suitable for low frequency problems; (iii) the theory is based on the frequency domain, and the applications coupled with other theories such as eigenvalue analysis flight dynamics are limited; and (iv) the model is not suitable to utilize for control systems.

Some attempts to improve Loewy's lift deficiency function include Refs. (87), (88) and (89). Jones and Rao[87] developed Loewy's lift deficiency function so as to incorporate the compressibility of air using the acceleration potential. Taking the compressibility of air into account was quite novel since most of precedent models presupposed only incompressible flow at that time. However, Jones and Rao did not consider time delay in the response of the air, and thus their model was also a quasi-steady model. This approach has the problem that compressible air needs some time to transmit a signal, and thus such a quasi-steady modelling should be valid only for incompressible flow.

Hammond and Pierce[88] improved Jones and Rao's model by incorporating the time-delay in the response of induced velocity. Friedmann and Venkatesen[89] modified Loewy's lift deficiency function in conjugation of quasi-steady inflow model of Greenberg[82], perturbation inflow model[71] or dynamic inflow models of Johnson[70], and studied the stability of the fuselage/rotor coupling dynamics in ground resonance. It is interesting that the final forms of these models, which are based on lift deficiency function, came quite close to the dynamic inflow model, which was introduced in the previous section, despite these models were developed from quite different start points.

The concept of lift deficiency function was originally simply a correction function based on two-dimensional wake theory and was defined in frequency domain, but Friedmann and Venkatesen converted the representation into time domain using classical control theory, in which Loewy's lift deficiency function is recognized as a transfer function relating the 3/4-chord induced velocity to the lift of the reference blade. This mathematical sophistication associates Loewy's lift deficiency function with the two-dimensional dynamic inflow model in the finite state form, and the contribution thereof to two-dimensional unsteady aerodynamics is both theoretically and practically

of great importance[90,91]. Friedmann and Venkatesen finally proposed a dynamic inflow model of the same form as Eq. (1.3)[90], which was developed from Loewy's lift deficiency function. Reference (92) gives a lucid explanation how classical lift deficiency functions can be hierarchically implied by more advanced dynamic inflow models.

1.5.3 Computational Method

Since there are a number of technical references published regarding various computational methods, which are most rapidly developing tools in this field, it should be out of scope of this thesis to introduce all their details. Instead, only characteristic features of computational methods shall be herein introduced in comparison with dynamic inflow models.

In Theodorsen's lift deficiency function theory, considerable simplifications and assumptions such as a two-dimensional wake sheet and constant vertical spacing between wake sheets are introduced. This was inevitable at that time in part because computers of the time were not able to track the complicated behaviour of vortices, which affect each other by their own induced velocity fields. Nowadays, owing to the rapid development in the computational technology, much more computationally intensive calculations can be conducted with smaller number of assumptions or simplifications at a much lower cost. These computational methods based on the vortex theory and the Biot-Savart law can be classified roughly into three types: (i) rigid wake model, (ii) prescribed wake model and (iii) free wake model. A rigid wake is assumed in the rigid wake model, and this is the strongest assumption, which in turn corresponds to the lightest computational load. In a prescribed wake model, the distribution of vortices is either empirically or semi-empirically prescribed at the initial state, and then the development of the wake distribution is computed through the Biot-Savart law. The free wake model is the most computationally intensive, and allows the wake distribution develop freely. Owing to the rapid development in computational resources, the free wake method is increasingly used and became the mainstream of contemporary CFD methods. The basic ideas of these methods are lucidly explained in Ref. (5), and the reader may refer to Refs. (77), (85), (93), (94) and (95) for further details concerning the historical development of these computational methods.

One characteristic feature of these computational methods, especially with free wake method, is that simulations of the development of the rotor wake can be conducted

based only on the first principles such as the Navier-Stokes equations, Biot-Savart law and vorticity transport equation(5) [12]. Recent rapid development in computational resources has made it possible to mesh the pertinent flow field and solid boundary (blades, hub, etc.) into millions of cells, and to simulate the resultant distortion in the three-dimensional wake distribution and the induced flow field in the time domain. The advantages of free wake analysis include the detailed description of the complicated flow field, the local treatment of airfoil dynamics, a thorough inclusion of complex interaction of vortices and specific boundary conditions, and the relatively low cost of conducting computations compared to full-scale experiments. Since the inflow is only globally treated in the dynamic inflow model, the detailed description from vortex methods is clearly better suited to examining locally complicated aerodynamic phenomena. Regarding the degree of reality of the wake description, it can be said that momentum theory is too simple, CFD methods are most convoluted, and the dynamic inflow method lies between these other two. Thus, momentum theory is most suitable for evaluating basic performance of rotor, CFD methods are for complicated local aerodynamic phenomena, while the dynamic inflow model is for analysing general stability (frequency, damping, modal information, etc.), control characteristics, vibration, handling qualities and transitional rotor dynamics[13].

A disadvantage of the CFD approach is that those vortex methods are not suitable for eigenvalue stability analysis because of the large number of states required to describe the unsteady wake. Another shortcoming in CFD simulations is that only the most stable state is presented in the simulation even when there are a plural of bifurcated non-linear solutions to the governing non-linear equations. Since the Navier-Stokes equations and the Euler equations are non-linear, they may give either non-linear solutions, which bifurcate from linear or other non-linear solutions, or isolated non-linear solutions, which do not bifurcate from any other solutions. These hidden secondary or tertiary solutions are usually neglected in numerical simulations because the most feasible solution is trailed step by step from the primary linear solution in a time-marching simulation, but, in fact, *non-linear jump* can happen in reality, i.e., it is possible that the physical state can change to an isolated state(97). Furthermore, eigenvalue stability

[12] Roughly speaking, a vortex is generated around a solid boundary, transported according to the induced flow, which other vortices induced, and vanish due to the viscosity of the fluid.

[13] Padfield suggested three levels of methods of rotorcraft simulation models in Ref. (96): in Level 1, the induced flow is described as a superposition of a finite number of simple flow states on the disc as a first-order model; in Level 2, the disc is replaced by individual blades; in Level 3, the entire rotor wake geometry is taken into consideration. According these three levels, it can be said that the momentum theory and advanced CFD methods correspond to the level 1 and 3, respectively, and the dynamic inflow model is supposed to cover more or less the level 2.

analysis is necessary in order to find bifurcated non-linear solutions. The free wake method is thus not suitable for stability analysis of non-linear solutions. Whereas dynamic inflow models are linear in general, they offer a greater flexibility to be combined with non-linear theories, and the examples include the study of Bassett[(98)], in which the Peters and He model[(37)] is used[14]. Houston and Brown showed a unique attempt to compare the dynamic inflow model with a vortex transport wake model focused on flight mechanics in autorotation[(99)], and concluded that the dynamic inflow model works satisfactorily for much of the autorotation regime except for steep descents, in which a comprehensive description of the inflow is essential.

1.5.4 From the Pitt and Peters Model to the State of the Art

The Pitt and Peters model is a significant milestone in the history of rotorcraft aerodynamics. It was the first truly practical dynamic inflow model which could be used for control system analysis, and well agreed with experimental data both for hovering and forward flight[(28,100)]. Dynamic inflow effects are so important in control and stability analysis that a convenient and versatile dynamic inflow model such as the Pitt and Peters model had been long-awaited. Nagabhushanam and Gaonkar[(101)] studied air resonance stability in forward flight by both the three-state and five-state models of Pitt and Peters. The torsional flexibility of the blades is also therein considered, and the stabilities of various modes are extensively examined. They concluded: the three-state model is more consistent than the five-state model in general; dynamic inflow tends to increase stability margins in general, that the air resonance characteristics are independent of the number of blades; and appropriate combination of aeroelastic coupling parameters can significantly improve air resonance stability. Reference (62) (or Ref. (102), which is almost identical to Ref. (62)) shows how dynamic inflow models were developed due to the desire to correlate with experimental data[15], and

[14] The dynamic inflow model is more suitable for stability analysis of non-linear solutions[(98,103)], though non-linear analysis in this field still awaits further development. Poiseille flow in a circular pipe is maybe an example of non-linear jump. No non-linear solutions bifurcated from the linear solution are hitherto found analytically, and the linear solution is analytically proven to be absolutely stable. However, as the Reynolds number increases, the flow changes from laminar to turbulent flow. This is considered to be a non-linear jump from the linear solution to an isolated non-linear solution, though any isolated solutions have yet been analytically found. Generally speaking, a turbulent flow may in practice be described by an orbit in phase space between two or more unstable equilibrium solutions to the governing equations, where these unstable equilibrium solutions cannot be found by simulation approaches.

[15] These authors concluded that the Pitt and Peters model agrees with experimental data quite well in hover. However, their correlations in forward flight or transient flight cases are poor, conceivably because of the lack of experimental data for these flight cases. The accuracy of Pitt and Peters model, which is at least as accurate as momentum theory, is predictable in hover because the model hierarchically implies momentum theory. The novel aspect with the Pitt and Peters model is the continuous representation of the gain matrix from axial to edgewise flight cases, and some further comparisons with experimental results to the model's performance for these cases is desirable. This author shall examine the Pitt and Peters model in Section 2.3.

presents a comparison between the results obtained from the Pitt and Peter model with experimental data including Ref. (61).

Dynamic inflow effects are of great importance in rotor stability analysis because dynamic inflow modes have nearly the same order of magnitude as those of flapping or lead-lag modes, and significantly affects the stability of various blade motions or aeromechanical phenomena such as ground resonance, air resonance, blade flapping, rotor-body coupling, pitch-roll coupling, flap-lag coupling and so on. Chen and Hindson extensively studied dynamic inflow effects on the stability in the vertical acceleration response of the helicopter in both the Carpenter and Friedvich model and the Pitt and Peters model with various thrust coefficients and blade Lock numbers. This study was conducted with the purpose of developing a super-augmented high-gain flight control system for military helicopters[(104)]. These authors reconfirmed the importance of dynamic inflow effects in control and stability analysis, reporting that both models performed well in comparison with NASA flight test results from CH-47B.

Although the Pitt and Peters model is widely used even now, it has the following weaknesses:

i. hub loads are therein used as the aerodynamic load on the rotor to associate with the induced velocity, that is to say, the model does not distinguish between different lift distributions that yield the same hub loads. However, a model that can distinguish specific lift distribution is required for blade structural analysis and aeroelastic analysis;
ii. the Pitt and Peters model is based on simple actuator disc theory, even though it is flexible enough to be coupled with more complicated blade element theory. This may reflect an inherent limitation of the model to account for the more complicated phenomena which are related to detailed blade geometry;
iii. the Pitt and Peters model is expressed in the perturbation form, but it is preferable for practical purposes that variable are described in terms of the overall variables;
iv. variables in the Pitt and Peters model are defined in the rotor coordinates, but for flight dynamics it would be more convenient to define the model in wind-axis coordinates.

Pitt and Peters themselves re-examined their model critically inspecting the assumptions such as actuator disc theory and the linearity of the distribution in

comparison with other inflow models[105,106]. In Ref. (40), Gaonkar and Peters defined the dynamic inflow effects as low frequency properties of the unsteady wake in contrast to conventional high frequency airfoil dynamics such as flutter, and showed a hierarchical relation between thirteen inflow models including quasi-steady, momentum theory, the equivalent Lock number approach and full unsteady models of 3DOF and 5DOF. This thorough comparison is highly instructive, and the authors remarked that there was no satisfactory replacement for momentum theory before the Pitt and Peters model appeared. They concluded that quasi-steady modelling is sufficient at high advance ratios, but that the dynamic inflow model of 5DOF is inadequate for a rotor having fewer than 5 blades, and that 3DOF model is overall more accurate than the 5DOF model. Results of this work indicate to what extent the dynamic inflow model needs to be sophisticated depending on the nature of individual problems. Regarding points (iii) and (iv) above, Peters and HaQuang proposed a non-linear version of Pitt and Peters model, in which all variables are treated not as perturbations but as in total amount[107], expressed in the wind-axis coordinate system.

The non-linear version was adopted in NASA Ames helicopter mathematical model, designated ARMCOP, and reportedly performed well[108]. Gaonkar and Peters summarised the historical development of the dynamic inflow model in Ref. (29), and showed an intensive comparison between various models. This review is also extremely instructive that it points out some misconceptions found in the past literature including Refs. (65), (71), (89), (105) and (106), and also limitations to the applicability of either the linear or non-linear dynamic inflow model.

The most important work which appeared after the Pitt and Peters model is arguably the Peters and He model[7], which forms the theoretical basis of this thesis. The derivation of this model is the most mathematically rigorous, and is consistent from the first principles compared to its preceding models. A concise version of the derivation is found in Ref. (37), and the model's validation and correlation with experimental data are shown in many research works, for example, in Refs. (30), (92), (109), (110), (111), (112) and (113). In the Peters and He model, the representations of both inflow and pressure distributions are generalised so that an arbitrary number of harmonics and radial shape functions can be used for each state.

Reference (92) presents a comparison between the Peters and He model and the experimental data from Refs. (114) - (116) using both rectangular and tapered blades,

and concluded that the model performs as well as or better than some computational codes of free-wake and prescribed-wake methods at a smaller computational cost. Reference (112) also compares the Peters and He model with classical theories and computational methods with contrasting their shortcomings, and demonstrates that the Peters and He model implicitly includes classical theories including Theodorsen's and Loewy's lift deficiency functions and Prandtl-Goldstein's tip-loss formula[16]. Reference (39) is a notably instructive study, since it compares the Peters and He model with various classical theories including Theodorsen's, Loewy's or Miller's lift deficiency functions and other finite-state methods. Reference (39) concluded that the Peters and He model is overall superior to classical unsteady models, but it cannot provide an accurate description of inflow in the close vicinity of the blade surface, nor can it account for wake roll-up. The Peters and He model has been further improved in some variations, with examples including Refs. (117) and (118), in which the ground effect is incorporated. The ground effect in this modelling is described as an extra term in the pressure potential in order to satisfy the boundary condition.

In applying the dynamic inflow model to a flight simulation code, there has been a mystery that the simulated results sometimes predict a completely opposite off-axis response in hover and low speed forward flight in comparison with the corresponding flight test data(119-123). A large number of publications related thereto suggested many possible causes for this phenomenon including gyroscopic force of the wake(124), aerodynamic interaction between the rotor and fuselage(125), dynamic twisting of the blade(126), wake distortion(127,128) and so on. It is highly likely that several of these mechanics are therein coupled in a complex manner. This problem is an active area of current research. Regarding the wake distortion, Ref. (129) proposes that the gain matrix in the Peters and He model should be modified as an *augmented L-matrix* so as to account for the effects due to wake curvature in non-hover flight conditions. Those models which have augmented gain matrix are called the *augmented Peters and He model* or *augmented Pitt and Peters model*, depending on the base model, and the literature about these augmented models includes Refs. (130) - (134). Note that the complicated wake distortion effects are incorporated in these models by wake curvature parameter, K_R, which is empirically determined. Reference (134) introduced the augmented Pitt and Peters model in which wake skew, wake curvature and wake spacing are incorporated as additional states in transitional flight.

[16] It may be rather odd that Pitt and Peters model is not compared with the Peters and He model at all either in Ref. (92) or (112) in spite of comparisons with many of more classical theories. This author will present his own view about the Pitt & Peters and Peters & He models in Section 2.3.

Zhao[135] presented a table of various values of K_R for comparison, and proposed augmented models for both the Pitt & Peters and Peters & He models including detailed mathematical derivations. In Ref. (135), a more refined description of the wake curvature which is expressed by lateral and longitudinal wake curvatures, K_c and K_s, is also proposed. The inclusion of the wake effects into dynamic inflow modelling is still an up-to-date issue in the field, and further improvement, validation and correlation with experimental and CFD simulation data are required, partly because the correction parameters must be essentially empirically determined.

References (136) and (137) propose a state-of-the-art methodology whose mathematical derivation is quite different from that of the Peters and He model. The model is based on the conservation equations of mass and momentum, and they are transformed into state-space forms by the Galerkin method so that the Peters and He model is therein hierarchically implied. A velocity potential is also therein considered on top of an acceleration potential, and both off- and on-disc flow are described by the set of three components. Although it seems that the Peters and Morillo model has not yet been widely utilized at present, it will likely be the leading next generation dynamic inflow model.

1.6 Literature on Autorotation

In this Section, the historical and current state of works on gyroplanes and helicopters in the windmill-brake state is briefly introduced in order to outline the importance of this research in the relevant context. Cierva himself made a huge contribution to the development in the theory of early gyroplanes from both theoretical and practical points of view[2,3,4,138]. (The left picture of Fig. 1-4 is Cierva's Type C.4, which made the first controlled gyroplane flight in 1923.) British aerodynamicists such as Lock and Glauert, whom Cierva vehemently criticised, made more rigorous theoretical work[20-22,41,79,139-143]. Concurrently, a number of experimental and theoretical studies were intensively conducted in the U.S.A. by NACA engineers such as Wheatley and others[16-19]. Indeed, there was a sound basis for further studying the characteristics and aerodynamics of the gyroplane at that time. The initial development in the Autogiro by Cierva is introduced in Ref. (144) in rather a story-telling manner, while Ref. (145) gives detailed background about the gyroplane both in historical and technical aspects. Despite the great success of gyroplanes in commercial and military fields in the 1930's, the mainstream of rotorcraft research shifted to the helicopter after the 1940's. Most of

the technical and theoretical achievements made by that time for the gyroplane such as flapping hinge, lead-and-lag hinge, cyclic blade feathering, gimballed or spider mechanism control system, blade element theory, momentum theory and so on were applied to the helicopter[17]. However, further developments thereafter were conducted only for the helicopter, and theoretical study on the gyroplane was almost forgotten.

In the meantime, gyroplanes were chiefly developed by small companies such as Bensen Aircraft Corporation, Rotary Air Force Inc., Air Command International and so on(146), or individual devotees such as Kenneth Wallis(147), mainly for sports flying. The most popular configuration for gyroplanes today, namely, one- or two-seater short fuselage with pusher propeller and cantilevered fin, was established by these developers. (The right picture of Fig. 1-4 is G7-R477 designed by a Japanese amateur gyroplane devotee, Masanori Kokubun, showing the typical configuration of contemporary light-weight sports gyroplanes.) However, little theoretical development was undertaken about the aerodynamic features of the vehicle in spite of a series of fatal accidents, and the developments were mainly structural for reducing the price or for making it easier to home-build without any backup either from the industrial sector or from academics. As a result, some models were poorly designed from the safety point of view, and hence a more comprehensive theory was required either to design a gyroplane or to investigate accidents[18].

Fig. 1-4 [Gyroplanes: C.4 and G7-R447.][19]

[17] It should be mentioned here that while most of today's helicopters have swash plates to control the cyclic pitch, most of modern gyroplanes have the direct control system, in which the direction of the rotor head is directly controlled by rods connected with the control stick.

[18] There were more mathematics-oriented researches about "autorotation" such as Refs. (160) and (161), yet their interests were focused on more general aerodynamic phenomena such as the gyration of sycamore seeds, fluttering of chuff, rotation of anemometre and so on, and their results are far from applying for home-built gyroplanes. There is probably a gap in the usage of the word "autorotation" between aeronautical aerodynamicists and mathematical hydrodynamicists.

[19] The picture of C.4 was kindly provided by Dr. Bruce Charnov of Hofstra University, and the picture of G7-R447 was kindly provided by Mr. Masanori Kokubun, with the copyrights approved.

As mentioned in Section 1.2, it was the first time after the Second World War that gyroplanes have been extensively investigated[20] at the University of Glasgow as part of CAA funded research programme following several grievous accidents in the United Kingdom[(148)]. The research topics include aerodynamic characteristics of various configurations[(8)], qualitative or quantitative control and stability analysis[(149,150)], rotorcraft flight dynamics in autorotation[(9,10)] and numerical simulation of autorotative flight[(151-153)]. Spathopoulos studied a mathematical model to simulate rotorcraft in autorotation[(154)], and Bagiev assessed gyroplane handling qualities using both flight tests and simulations[(155)]. Some new projects to revive the gyroplane are presently under way including a hybrid-gyroplane by Cartercopter[(156)], a turbine-powered gyroplane by Groen Bros. Inc.[(157)] and some more conceptual designs such as massive VTOL transport[(157)] and *airbike*[(158)]. The possibility of using a gyroplane as unmanned reconnaissance vehicle is also examined[(159)] in stability and dynamic characteristics[21]. Academic studies of gyroplanes have thus recently restarted, and the future outcome and scope of these projects are not yet clear.

The very first motivation of Cierva to invent the Autogiro was that he wanted to build a safe vehicle which is free from stall. In fact, Ref. (144) reads about Autogiro, "... *although not designed with the sporting purpose of increasing speed not with the commercial object of enlarging the radius of action, but with the humanitarian purpose of reducing to a minimum the number of accidents and the number of human lives sacrificed in the flight for the conquest of the air.*" It is thus quite ironical that the contemporary gyroplanes are designed chiefly for the sporting purpose, albeit not for the speed, and hence are associated with unacceptable casualty rates. The flight principle of the gyroplane itself is not in the wrong, and there still is a possibility that the gyroplane can regain a prominent position in aviation if updated with state-of-the-art advanced technology. What are urgently required now are further theoretical, practical or experimental works such as mathematical models, technical knowledge, experimental data and so on, to provide a sound technical basis either for improving contemporary gyroplanes or for developing new gyroplanes.

[20] In some projects of designing convertiplane, which is a mule of fixed-wing aircraft and rotarycraft, the flight principle of the gyroplane occasionally attracted some attention. These projects includes Fairy's Rotordyne[(162)], whose concept is now tried to revive by Groen Brothers Inc.[(157)] There were also some attempts to develop a gyroplane for commercial purpose, but they all resulted in failure.

[21] Interestingly, the authors concluded that the elevator control should be used together with longitudinal cyclic control, unlike the most of contemporary small gyroplanes, which usually have only small (or sometimes no) fixed horizontal stabilizer.

Chapter 2

Review of the Dynamic Inflow Model of Peters and He

2.1 Introduction

2.1.1 Overview

In this Chapter, the theoretical derivation of Peters and He model will be reviewed in depth and examined in detail. The general theory of dynamic inflow models has been extensively developed by Peters and his coworkers in the last two decades, and the Peters and He model is theoretically one of the most refined dynamic inflow models in existence today.

The later Chapters of this thesis are based on the Peters and He model, and thus it is necessary to first review the foundations of this model. As well as permitting the foundations of the work of the present thesis to be presented, a review of this model is also convenient since the relevant literature, including Refs. (1) and (7) offers a somewhat disjointed view of the model's derivation, which is not readily accessible. In particular, some assumptions and theorems therein used are not explicitly declared or proven in the original literature, and thus the present author tries to improve the lucidity of the explanation of the mathematical derivation of this model by complementing the details of some difficult rearrangements of equations and correcting some typographical error contained in the original references. Although the author also presents new explanations of some aspects of this derivation, it must be stressed here again that the general idea of this Chapter is based on the works of previous authors, including Peters, He and their coworkers. In particular, this Chapter is largely based on Ref. (7), which should be the most thorough source of the pertinent theory. Some complementary theorems and peripheral topics are discussed either in footnotes or appendices.

2.1.2 Notations

Symbols and notations are used so as to be as consistent with Refs. (1), (7) and (92) as possible, although it should be noted that there is a variation of notations even between these references. The author thus chose the most reasonable designations for the case. Readers are encouraged to confirm the definitions when reading a plurality of

literatures.

In this thesis, those variables that are related to the *time-derivative* and *convection* terms of the Euler equation are denoted by (t) and (c) as superscripts, respectively. This notation is original in this thesis, and it is hoped that it will facilitate a better understanding. The variables that are related to Fourier coefficients for cosine and sine functions are also given c and s as superscripts, respectively. For the Legendre functions, r, j, i, k, m and n are used as dummy indices. No matter how confusing they may look, the way of using letters in this Chapter is thus consistent. For example, $\hat{L}_{jn}^{rmc}$ denotes a Fourier coefficient having four indices of r, m, j and n, corresponding to a cosine function.

2.2 Review of the Dynamic Inflow Model of Peters and He

2.2.1 Fundamental Assumptions for the Mathematical Derivation of the Peters and He Model.

The Peters and He model is based on the following assumptions, (A1) - (A5):

(A1) the flow is inviscid. Thus, the induced flow is generated by the pressure potential (or acceleration potential), and governed by the Euler equations,

$$\frac{\partial \mathbf{U}}{\partial \bar{t}} + (\mathbf{U} \cdot \nabla)\mathbf{U} = -\nabla\Phi, \qquad (2.1)$$

where $\mathbf{U}, \bar{t}$ and Φ represent non-dimensionalised velocity, time and a pressure potential function, respectively[22];

(A2) the pressure distribution over the rotor disc is continuous, but it has a discontinuity across the rotor disc;

(A3) air flow is assumed to be incompressible and satisfies the equation of continuity,

$$\nabla \cdot \mathbf{U} = 0; \qquad (2.2)$$

(A4) the rotor disc can be regarded as a flat orientable disc.

The assumption (A1) explains why the flow is not governed by the Navier-Stokes equations, but by the Euler equations. Since the air flow around the rotor is sufficiently fast (for example, a typical Reynolds number about a helicopter blade is 10^5 - 10^6), the

[22] The Euler equations can be derived as a consequence of the conservation of momentum (Newton's law of motion), if assumptions (A3) and (A1) are valid. Thus, assumptions (A2) and (A4) can mathematically be implied in assumption (A1) if Newtonian mechanics is approved. Although it may sound needless to state, assumption (A1) may be interpreted that Newtonian mechanics is considered to be valid.

assumption (A1) can be reasonably used for most flight cases.

The assumptions (A2) and (A4) indicate that the model is based on actuator disc theory, and the assumption (A4) gives the theoretical grounds for regarding the lift working on the rotor disc as the pressure potential[23]. The assumption (A3) means that air compressibility and shock wave effect are negligible. While this is not always the case with high-speed helicopter flights, this assumption can still be reasonably valid for a wide range of helicopter flights and for most gyroplane flights.

2.2.2. The Representation of the Pressure Field

The mathematical derivation of the dynamic inflow model essentially relies on the principle of superposition of linear equations. Since Eq. (2.1) contains a non-linear term (i.e. the convection term), which must be linearised in advance for dynamic inflow modelling as follows (see also Appendix 2.1),

$$\frac{\partial \mathbf{q}}{\partial \bar{t}} - (\mathbf{V} \cdot \nabla)\mathbf{q} = -\nabla\Phi, \tag{2.3.1}$$

where $\mathbf{V}$ is the non-dimensionalised steady base flow, Φ is the pressure potential which drives the induced flow and $\mathbf{q}$ is the induced flow, which is regarded as a perturbation in this linearised equation. Note that the second term in the left-hand side of Eq. (2.3.1) has a minus sign unlike Eq. (2.1), because positive $\mathbf{q}$ and $\mathbf{V}$ are defined in opposite directions, as shall be seen in Fig. 2-2. In Cartesian coordinates, Eq. (2.3.1) can be separated into the following three equations,

$$\frac{\partial q_x}{\partial \bar{t}} - V_x\frac{\partial q_x}{\partial x} - V_y\frac{\partial q_x}{\partial y} - V_z\frac{\partial q_x}{\partial z} = -\nabla_x\Phi, \tag{2.3.2}$$

$$\frac{\partial q_y}{\partial \bar{t}} - V_x\frac{\partial q_y}{\partial x} - V_y\frac{\partial q_y}{\partial y} - V_z\frac{\partial q_y}{\partial z} = -\nabla_y\Phi, \tag{2.3.3}$$

$$\frac{\partial q_z}{\partial \bar{t}} - V_x\frac{\partial q_z}{\partial x} - V_y\frac{\partial q_z}{\partial y} - V_z\frac{\partial q_z}{\partial z} = -\nabla_z\Phi. \tag{2.3.4}$$

[23] Note that the dynamic inflow model based on actuator disc theory can be subsequently coupled with any lift distribution, in which each blade shape may be considered in detail. Still, this should be considered as a combination of different theories, and it should be explicitly emphasised that the derivation of Peters and He model is based on simple actuator disc theory.

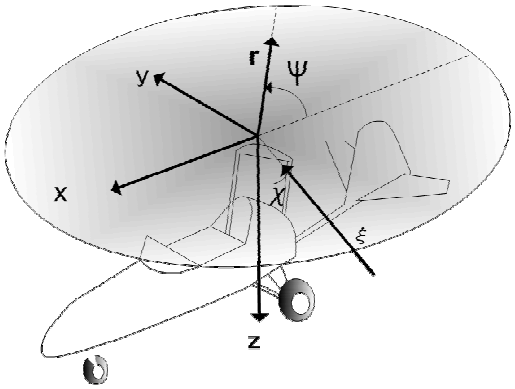

Fig. 2-1 [Vehicle coordinate systems; both for Helicopter and Gyroplane.]

Note that Eq. (2.3.1) is expressed in the vector form, with each of $\mathbf{q}, \mathbf{V}$ and $\nabla\Phi$ having three components, irrespective of the particular coordinate system that is adopted. For the purpose of the following discussion, the rotor coordinates, (x, y, z), and streamline coordinate, ξ, are introduced here. Note that $\mathbf{V}$ becomes one-dimensional along ξ. The cylindrical coordinate system on the rotor disc, $(\bar{r}, \psi, z)$, is also used (Fig. 2-1), where $\bar{r}$ is non-dimensionalised by the rotor radius as $\bar{r} = r/R$ (thus $0 \le \bar{r} \le 1$).

The transformations between the xyz- and $\bar{r}\psi z$-systems are detailed in Appendix 2.2. It is often the convention that only the z-component of $\mathbf{q}$ is called the induced velocity, in part because the z-component is far larger than the x- or y- component and maybe also because only the z-component of $\mathbf{q}$ is directly related to the lift and rotor thrust. The z-component of $\mathbf{q}$ is induced by the z-component of $\nabla\Phi$ in Eq. (2.3.1), which describes the aerodynamic pressure working on the rotor disc in the z-direction, namely, the lift.

The ξ-axis is skewed by the angle of χ with respect to the z-axis, Fig.2-2, and its positive direction is defined as the upstream direction, which is why the second term of Eq. (2.3.1) has a negative sign. Note that when comparing helicopter and gyroplane rotors, the ξ- and z-axes come to opposite sides, and thus the positive direction of rotor angle of attack, α, is defined in a different way, Fig. 2-3.

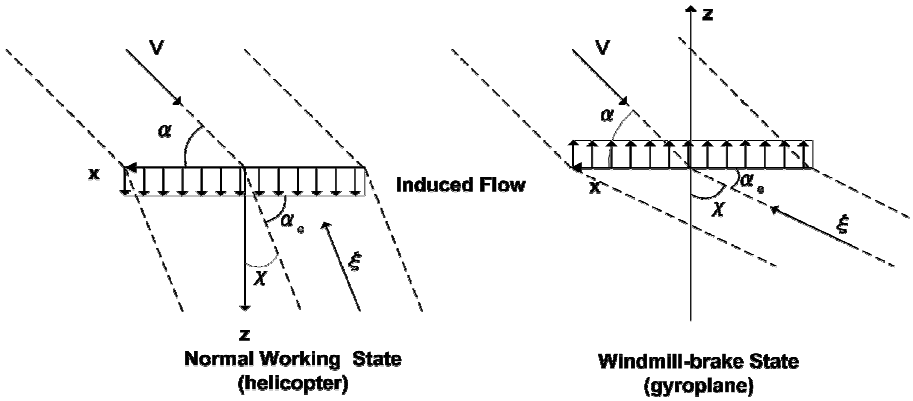

Fig. 2-2 [Difference in the aerodynamic configuration of the rotors of normal working and windmill-state states.]

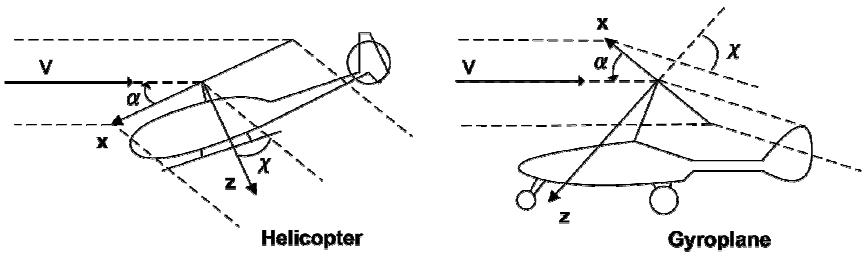

Fig. 2-3 [Difference in the rotor angle of attack of helicopter and gyroplane rotors.]

On account of the principle of superposition of linear equations, Eq. (2.3.1) can be decomposed into two equations,

$$\frac{\partial \mathbf{q}}{\partial \bar{t}} = -\nabla\Phi^{(t)}, \tag{2.4.1}$$

$$(\mathbf{V}\cdot\nabla)\mathbf{q} = \nabla\Phi^{(c)}, \tag{2.4.2}$$

where

$$\Phi^{(t)} + \Phi^{(c)} = \Phi\,. \tag{2.4.3}$$

Multiplying Eqs. (2.4.1) and (2.4.2) by ∇ and applying Eq. (2.2), the following Laplace's equations are obtained,

$$\triangle\Phi^{(t)} = 0, \tag{2.5.1}$$

$$\triangle\Phi^{(c)} = 0, \tag{2.5.2}$$

$$\triangle\Phi = \triangle\Phi^{(t)} + \triangle\Phi^{(c)} = 0\,. \tag{2.5.3}$$

The pressure function, Φ, can be given by solving these Laplace's equations under appropriate boundary conditions. The Peters and He model is based on the following boundary conditions:

(B1) Φ becomes zero at infinity;
(B2) Φ becomes zero at the edge of the rotor.

The pressure distribution on the rotor disc is considered to be linearly proportional to the distribution of induced velocity due to the linearity of Eq. (2.3)[24]. (Note that this property does not hold if Euler's equations are not linearised.) The problem of describing the distribution of induced velocity can then simply result in a Dirichlet problem for Laplace's equation under the boundary conditions of (B1) and (B2).

Note that if air is assumed to be perfectly incompressible, any perturbation of air (e.g. pressure, temperature, density, velocity, entropy, etc.) should theoretically propagate at once even to infinity. Thus, although the boundary condition (B1) can be considered to be intuitively reasonable as a physical assumption, it is mathematically not self-evidently acceptable. However, (B1) will be approved without further discussion in this Chapter following Peters and He.

Laplace's equation is separable either in Cartesian, circular cylindrical, conical, ellipsoidal, elliptic cylindrical, oblate spheroidal, parabolic, parabolic cylindrical, paraboloidal, prolate spheroidal or spherical coordinate system[(163,164)]. The choice of coordinate system should be decided according to the boundary conditions and the ellipsoidal coordinate system is generally believed to be the most suitable for rotorcraft problems, because the ellipsoidal coordinate system provides solutions to Laplace's equation expressed by the associated Legendre functions, which satisfy the boundary condition (B2) well and are suitable for representing the pressure gap between the upper and lower surfaces of the disc, namely the lift (see also Appendix 2.3).

In this coordinate system, the solution to Laplace's equation subject to boundary conditions of (B1) and (B2) is expressed as

[24] The application of linearised Euler equations for describing the distribution of induced flow of a rotor can be traced back to Mangler and Squire[(48)].

$$\Phi(\nu,\eta,\psi,\bar{t}) = \sum_{m=0}^{\infty}\sum_{n=1}^{\infty} P_n^m(\nu)Q_n^m(i\eta)\Big[C_n^m(\bar{t})\cos(m\psi) + D_n^m(\bar{t})\sin(m\psi)\Big], \quad (2.6.1)$$

$$m+n \equiv 1 \mod 2, \quad (2.6.2)$$

where $P_n^m(\nu)$ and $Q_n^m(i\eta)$ are the associated Legendre functions of the first and second kinds, respectively (see Appendix 2.4). Also, it is assumed here that the pressure potential, Φ, is a smooth continuous function which is differentiable as many times as required with respect to $\bar{r}$ and ψ, and that Φ is periodic with respect to ψ with a period of 2π. This solution is sometimes called *Prandtl's potential function*, for which Ref. (47) may be consulted for further details. Note that although the associated Legendre equations of the first and second kinds yield the four solutions of $P_n^m(\nu)$, $Q_n^m(i\eta)$, $P_n^m(i\nu)$ and $Q_n^m(\eta)$, only $P_n^m(\nu)$ and $Q_n^m(i\eta)$ can satisfy the boundary conditions (B1) and (B2), and so the other two solutions should be discarded. Moreover, when $m+n \equiv 0 \mod 2$, the boundary conditions are not satisfied (see Appendix 2.5), and hence only those m and n which satisfy $m+n \equiv 1 \mod 2$ should be chosen. Furthermore, with regard to the indices of the Legendre function of the first kind, $n \geq m$ is required from the definition (see Appendix 2.5). In summary, n should satisfy $n = m+1, m+3, m+5, \ldots.$

2.2.3. Normalisation of the Pressure Function

In the elliptic coordinate system, the region $z<0$ is described as $\nu>0$, idem quod $z>0$ as $\nu<0$. Thus, when Φ is described by only those m and n which satisfy $m+n \equiv 1 \mod 2$, the distribution of Φ becomes discontinuous at the surface $\nu=0$, namely, at the rotor disc. The rotor disc itself is described as $\eta=0,\ \nu=\sqrt{1-\bar{r}^2}$ in the elliptic coordinate system. The discontinuity of the pressure distribution across the rotor disc can be considered equal to the lift.

$$\begin{aligned} L(\bar{r},\psi,\bar{t}) &\equiv \Phi(\bar{r},\psi,\bar{t})\,\big|_{\nu<0,\eta=0} - \Phi(\bar{r},\psi,\bar{t})\,\big|_{\nu>0,\eta=0} \\ &= -2\sum_{m=0}^{\infty}\sum_{n=m+1,m+3,\ldots}^{\infty} P_n^m(\nu)Q_n^m(i0)\Big[C_n^m(\bar{t})\cos(m\psi) + D_n^m(\bar{t})\sin(m\psi)\Big] \quad (\nu>0) \\ &\equiv \sum_{m=0}^{\infty}\sum_{n=m+1,m+3,\ldots}^{\infty} \bar{P}_n^m(\nu)\Big[\tau_n^{mc}(\bar{t})\cos(m\psi) + \tau_n^{ms}(\bar{t})\sin(m\psi)\Big]. \end{aligned} \quad (2.7)$$

Note that $P_n^m(-\nu) = (-1)^{m+n}P_n^m(\nu)$, $\bar{P}_n^m(\nu)$, $\tau_n^{mc}(\bar{t})$ and $\tau_n^{ms}(\bar{t})$ are defined as follows[165],

$$\bar{P}_n^m(\nu) = (-1)^m \left(\frac{P_n^m(\nu)}{\rho_n^m} \right), \tag{2.8.1}$$

$$\rho_n^m = \sqrt{\frac{1}{2n+1} \cdot \frac{(n+m)!}{(n-m)!}}, \tag{2.8.2}$$

$$\tau_n^{mc} = (-1)^{m+1} 2 Q_n^m(i0) \rho_n^m C_n^m, \tag{2.8.3}$$

$$\tau_n^{ms} = (-1)^{m+1} 2 Q_n^m(i0) \rho_n^m D_n^m. \tag{2.8.4}$$

The function $\bar{P}_n^m(\nu)$ is the normalised associated Legendre function of the first kind, and its orthogonality is defined in the interval of $0 \le \nu \le 1$ as

$$\int_0^1 \bar{P}_n^m(\nu) \bar{P}_j^m(\nu) d\nu = \delta_{nj}, \tag{2.9.1}$$

$$\bar{P}_{m+1}^n(\nu) > 0, \tag{2.9.2}$$

where δ_{nj} is Kronecker's delta.

$$\delta_{nj} = \begin{cases} 1, & (n = j) \\ 0. & (n \neq j) \end{cases} \tag{2.9.3}$$

Equations (2.7), (2.9.1) and (2.9.2) indicate that the radial distribution of lift is expanded in the functional space spanned by the normalised associated Legendre functions of the first kind, where each of $\bar{P}_n^m(\nu)$ is a unit basis, and that the angular distribution of lift is also expanded in the functional space spanned by trigonometric functions, whose orthogonalities are given by

$$\frac{1}{\pi} \int_0^{2\pi} \sin mx \sin nx dx = \frac{1}{\pi} \int_0^{2\pi} \cos mx \cos nx dx = \delta_{mn}, \tag{2.10.1}$$

$$\int_0^{2\pi} \sin mx \cos nx dx = \int_0^{2\pi} \cos mx \sin nx dx = 0. \tag{2.10.2}$$

Equation (2.6.1) can also be normalised as

$$\Phi(\nu, \eta, \psi, \bar{t}) = -\frac{1}{2} \sum_{m=0}^{\infty} \sum_{n=m+1, m+3, \ldots}^{\infty} \bar{P}_n^m(\nu) \bar{Q}_n^m(i\eta) \left[\tau_n^{mc}(\bar{t}) \cos(m\psi) + \tau_n^{ms}(\bar{t}) \sin(m\psi) \right], \tag{2.11}$$

where $\bar{Q}_n^m(i\eta) = Q_n^m(i\eta)/Q_n^m(i0)$. Note that $\Phi^{(t)}$ and $\Phi^{(c)}$ also satisfy Laplace's equation under the same boundary conditions, Eqs. (2.5.1) - (2.5.3), i.e. they should be expressed in the same form as that of Φ,

$$\Phi^{(t)}(\nu,\eta,\psi,\bar{t}) = -\frac{1}{2}\sum_{m=0}^{\infty}\sum_{n=m+1,m+3,\ldots}^{\infty} \bar{P}_n^m(\nu)\bar{Q}_n^m(i\eta)\Big[\tau_n^{mc(t)}(\bar{t})\cos(m\psi) + \tau_n^{ms(t)}(\bar{t})\sin(m\psi)\Big], \tag{2.12.1}$$

$$\Phi^{(c)}(\nu,\eta,\psi,\bar{t}) = -\frac{1}{2}\sum_{m=0}^{\infty}\sum_{n=m+1,m+3,\ldots}^{\infty} \bar{P}_n^m(\nu)\bar{Q}_n^m(i\eta)\Big[\tau_n^{mc(c)}(\bar{t})\cos(m\psi) + \tau_n^{ms(c)}(\bar{t})\sin(m\psi)\Big]. \tag{2.12.2}$$

Based on the principle of superposition of linear equations, the lift described by Eq. (2.7) can also be decomposed into two parts corresponding to the time-derivative and the convection terms in the Euler equations, respectively,

$$L(\nu,\eta,\psi,\bar{t}) = L^{(t)}(\nu,\eta,\psi,\bar{t}) + L^{(c)}(\nu,\eta,\psi,\bar{t}), \tag{2.13.1}$$

$$L^{(t)}(\nu,\eta,\psi,t) \equiv \sum_{m=0}^{\infty}\sum_{n=m+1,m+3,\ldots}^{\infty} \bar{P}_n^m(\nu)\Big[\tau_n^{mc(t)}(\bar{t})\cos(m\psi) + \tau_n^{ms(t)}(\bar{t})\sin(m\psi)\Big], \tag{2.13.2}$$

$$L^{(c)}(\nu,\eta,\psi,\bar{t}) \equiv \sum_{m=0}^{\infty}\sum_{n=m+1,m+3,\ldots}^{\infty} \bar{P}_n^m(\nu)\Big[\tau_n^{mc(c)}(\bar{t})\cos(m\psi) + \tau_n^{ms(c)}(\bar{t})\sin(m\psi)\Big]. \tag{2.13.3}$$

In order to identify the Fourier coefficient functions, $\tau_n^{mc(t)}, \tau_n^{ms(t)}, \tau_n^{mc(c)}$ and $\tau_n^{ms(c)}$, an appropriate lift theory is required. Examples thereof include blade element theory[7], ONERA dynamic stall theory[30] and others. Reference (37) compares several lift models based on Ref. (166). Note that the representations of the lift as Eqs. (2.13.1) - (2.13.3) are expressed in general forms, and hence these equations are independent of any specific representation of lift. This makes it possible to flexibly combine the dynamic inflow model with any possible lift theory, which may vary depending on the class of the aircraft (i.e. helicopter, gyroplane, etc.), aerodynamic status of the rotor (i.e. normal working state, windmill-brake state, etc.) and so on.

2.2.4. The Relation between the Pressure Function and the Induced Velocity

The induced velocity is described by the pressure function by way of Eqs. (2.4.1) and (2.4.2), and the pressure function, Eq. (2.11), is represented by the normalised

associated Legendre function of the first kind and trigonometric functions. Thus the next step is the expression of the distribution of the induced velocity in the form of a Fourier series by appropriate orthogonal functions, and make clear the relation between its Fourier coefficients and their counterparts in the lift distribution, i.e. $\tau_n^{mc(t)}, \tau_n^{ms(t)}, \tau_n^{mc(c)}$ and $\tau_n^{ms(c)}$. Integrating Eq. (2.4.2) along the streamline yields

$$\mathbf{q} = -\frac{1}{V}\int_0^\infty \nabla\Phi^{(c)} d\xi. \tag{2.14}$$

Note that although $\mathbf{V}$ in Eq. (2.4.2) is a vector, it can be reduced to a scalar along the ξ-axis, and thus the integration along the ξ-axis allows $\mathbf{V}$ to be replaced with $V = |\mathbf{V}|$. Suppose $\mathbf{q} = (u, v, w)$, where w can be expressed by the z-component of Eq. (2.14) as

$$w = \frac{1}{V}\int_\infty^0 \frac{\partial\Phi^{(c)}}{\partial z} d\xi. \tag{2.15}$$

The value of $\Phi^{(c)}$ at infinity is to be determined from the boundary condition (B1). From the z-component of Eq. (2.4.1), the time-derivative of w is given in the same manner as

$$\frac{\partial w}{\partial \bar{t}} \equiv -\frac{\partial\Phi^{(t)}}{\partial z}\Big|_{\eta=0}. \tag{2.16}$$

Note that specific mappings between the ξ-axis and xyz-axes are not required at this stage. Since $\Phi^{(t)}$ and $\Phi^{(c)}$ described by Eqs. (2.12.1) and (2.12.2) are linear functions with respect to $\tau_n^{mc(t)}, \tau_n^{ms(t)}, \tau_n^{mc(c)}$ and $\tau_n^{ms(c)}$, the actions of the differentiation and integration in Eqs. (2.15) and (2.16) can be represented in the form of linear operators in Hilbert space,

$$\frac{\partial w}{\partial \bar{t}} \equiv -\frac{\partial\Phi^{(t)}}{\partial z}\Big|_{\eta=0} \equiv \mathcal{C}[\Phi^{(t)}], \tag{2.17}$$

$$w = \frac{1}{V}\int_\infty^0 \frac{\partial\Phi^{(c)}}{\partial z} d\xi \equiv \mathcal{D}[\Phi^{(c)}], \tag{2.18}$$

where $\mathcal{C}$ and $\mathcal{D}$ are appropriate mappings from the Hilbert space, where $\Phi^{(t)}$ and $\Phi^{(c)}$ are defined, into another functional space where w and $\partial w/\partial \bar{t}$ are defined. Since the induced velocity is always uniquely induced in reaction to the pressure gradient from

the physical point of view, the mappings need to be injections, thus $\mathcal{C}$ and $\mathcal{D}$ may be assumed to be isomorphic linear operators to have inverse mappings[25]. The following rearrangements are thus always assured[26],

$$\mathcal{D}^{-1}[w] = \Phi^{(c)}, \tag{2.19}$$

$$\mathcal{C}^{-1}[\dot{w}] = \Phi^{(t)}, \tag{2.20}$$

$$\mathcal{C}^{-1}[\dot{w}] + \mathcal{D}^{-1}[w] = \Phi^{(t)} + \Phi^{(c)} = \Phi\,. \tag{2.21}$$

2.2.5 Matrix Representations

Suppose that w in Eq. (2.17) can be expressed in the form of a Fourier series as

$$w(\bar{r},\psi,\bar{t}) = \sum_{m=0}^{\infty} \sum_{n=m+1,m+3,\ldots}^{\infty} \Psi_n^{m(M)}(\nu)[\alpha_n^m(\bar{t})\cos(m\psi) + \beta_n^m(\bar{t})\sin(m\psi)], \tag{2.22}$$

where $\Psi_n^{m(M)}$ is an appropriate function that can form a complete orthogonal system of functions for each of m in the interval of $0 \le \nu \le 1$. Inserting Eqs. (2.22) and (2.12.1) into Eq. (2.20) yields

$$\tau_n^{mc(t)} = K[\alpha_j^r], \tag{2.23.1}$$

$$\tau_n^{ms(t)} = K[\beta_j^r], \tag{2.23.2}$$

where K is the matrix representation of the linear operator C^{-1}, and Fourier coefficients α_j^r, β_j^r, $\tau_j^{rc(t)}$ and $\tau_j^{rs(t)}$ are defined in the vector space spanned by $\cos r\psi$ and $\sin r\psi$ $(r = 1, 2, \ldots)$ according to an integer of j, which satisfies $j = r+1, r+3, \ldots$.[27] Note that a linear operator in Hilbert space can be represented as a matrix in $\mathbb{R}^{\infty}$. Here, α_j^r, β_j^r, $\tau_j^{rc(t)}$ and $\tau_j^{rs(t)}$ are represented as column vectors, each of whose

[25] Physically, it is obvious that a unique induced flow distribution is caused in response to a pressure distribution over a rotor. However, the discussion about the invertibility of $\mathcal{C}$ and $\mathcal{D}$ lacks rigour because these mappings of $\mathcal{C}$ and $\mathcal{D}$ have not been mathematically proven to be bijections. Peters and He did not discuss this point in depth, and the present Chapter will also assume $\mathcal{C}$ and $\mathcal{D}$ are invertible without further discussion.

[26] Note that when the model is based on the non-linear Euler equations, it is not self-evident whether $\mathcal{C}$ and $\mathcal{D}$ have inverse mappings because the pressure function would possibly be a multi-valued function giving a plural of bifurcated solutions. In general, the theory of non-linear operators in Hilbert space is not yet sufficiently developed in mathematics.

[27] Note that in the following discussion, dummy indices r and j will be used in addition to m and n, when necessary, following the notation of Peters[7,37]. Readers should not confuse r with $\bar{r}$, which denotes the non-dimensional radial position.

elements is itself a vector again, following the convention in flight dynamics (i.e. $1 \times rj$ matrix).

$$\alpha_j^r = {}^t(\alpha_2^1, \alpha_4^1, ...; \alpha_3^2, \alpha_5^2, ...; \alpha_{r+1}^r, \alpha_{r+3}^r, ...), \tag{2.24.1}$$

$$\beta_j^r = {}^t(\beta_2^1, \beta_4^1, ...; \beta_3^2, \beta_5^2, ...; \beta_{r+1}^r, \beta_{r+3}^r, ...), \tag{2.24.2}$$

$$\tau_n^{mc(t)} = {}^t(\tau_2^{1c(t)}, \tau_4^{1c(t)}, ...; \tau_3^{2c(t)}, \tau_5^{2c(t)}, ...; \tau_{m+1}^{mc(t)}, \tau_{m+3}^{mc(t)}, ...), \tag{2.24.3}$$

$$\tau_n^{ms(t)} = {}^t(\tau_2^{1s(t)}, \tau_4^{1s(t)}, ...; \tau_3^{2s(t)}, \tau_5^{2s(t)}, ...; \tau_{m+1}^{ms(t)}, \tau_{m+3}^{ms(t)}, ...). \tag{2.24.4}$$

The matrix K is the representation of the linear operator that transforms both α_j^r to $\tau_j^{rc(t)}$ or β_j^r to $\tau_j^{rs(t)}$, and it is assured that K is non-singular with its inverse matrix, K^{-1}, for the same reasons that C and D have their inverse matrices. K can be represented as a partitioned matrix, and its elements can be expressed as K_{nj}^{mr}, where m and r indicate the row- and column-positions of the partition, respectively, and n and j indicate the row- and column-positions in the mr partition. (See Fig. 2-4.)

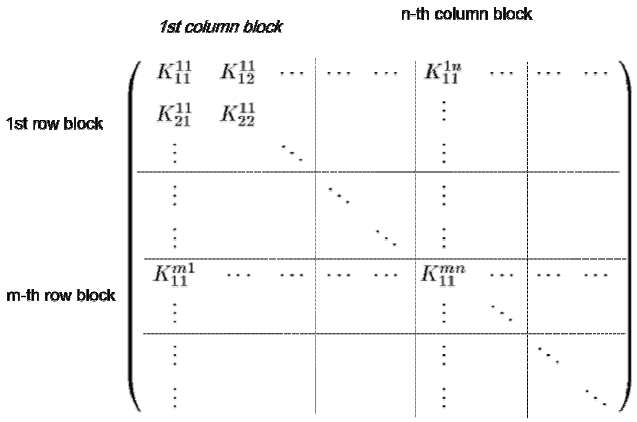

Fig. 2-4 [Matrix representation of C^{-1}.]

For its inverse matrix to exist, the matrix K needs to be regular[28]. Suppose also that w in Eq. (2.18) can be expressed in the same form as ω in Eq. (2.22),

$$w(\bar{r},\psi,\bar{t}) = \sum_{m=0}^{\infty} \sum_{n=m+1,m+3,\ldots}^{\infty} \Psi_n^{m(L)}(\nu)[\zeta_n^m(\bar{t})\cos(m\psi) + \varpi_n^m(\bar{t})\sin(m\psi)], \tag{2.25}$$

where $\Psi_n^{m(L)}$ is also an appropriate function which can form a complete orthogonal system of functions for each m in the interval of $0 \le \nu \le 1$. Note that $\Psi_n^{m(L)}$ in Eq. (2.25) may be different from $\Psi_n^{m(M)}$ in Eq. (2.22), because Eqs. (2.19) and (2.20) are independent. Inserting Eqs. (2.25) and (2.12.2) into Eq. (2.19) yields the following equations,

$$\tau_n^{mc(c)} = Y^{-1}[\zeta_j^r], \tag{2.26}$$

$$\tau_n^{ms(c)} = Y^{-1}[\varpi_j^r], \tag{2.27}$$

where Y is the matrix representation of the linear operator D. Here again, ζ_j^r, ϖ_j^r, $\tau_j^{rc(c)}$ and $\tau_j^{rs(c)}$ are defined in the functional space spanned by $\cos r\psi$ and $\sin r\psi$ ($r = 1, 2, \ldots$) according to an integer j, which satisfies $j = r+1, r+3, \ldots$.

$$\zeta_j^r = {}^t(\zeta_2^1, \zeta_4^1, \ldots; \zeta_3^2, \zeta_5^2, \ldots; \zeta_{r+1}^r, \zeta_{r+3}^r, \ldots), \tag{2.28.1}$$

$$\varpi_j^r = {}^t(\varpi_2^1, \varpi_4^1, \ldots; \varpi_3^2, \varpi_5^2, \ldots; \varpi_{r+1}^r, \varpi_{r+3}^r, \ldots), \tag{2.28.2}$$

$$\tau_n^{mc(c)} = {}^t(\tau_2^{1c(c)}, \tau_4^{1c(c)}, \ldots; \tau_3^{2c(c)}, \tau_5^{2c(c)}, \ldots; \tau_{m+1}^{mc(c)}, \tau_{m+3}^{mc(c)}, \ldots), \tag{2.28.3}$$

$$\tau_n^{ms(c)} = {}^t(\tau_2^{1s(c)}, \tau_4^{1s(c)}, \ldots; \tau_3^{2s(c)}, \tau_5^{2s(c)}, \ldots; \tau_{m+1}^{ms(c)}, \tau_{m+3}^{ms(c)}, \ldots). \tag{2.28.4}$$

The matrix Y has its inverse matrix Y^{-1} for the same reason why the inverse of K exists. The matrix Y may be considered as a partitioned matrix, transforming both ζ_j^r to $\tau_n^{mc(c)}$ and ϖ_j^r to $\tau_n^{ms(c)}$. The elements of the matrix Y can be expressed as Y_{nj}^{rm}, where m and r indicate the row- and column-block positions in a partitioned matrix,

[28] The matrix K may be intuitively considered as a square matrix, although both m and r are ideally in the range 0 to ∞.

respectively, and n and j indicate the row- and column-positions in the mr partition, respectively, as illustrated in Fig. 2-4. Equations (2.4.3), (2.23.1), (2.23.2), (2.26) and (2.27) yield the following matrix equations,

$$\left[\quad K_{nj}^{mr}\quad\right]\left(\dot{\alpha}_j^r\right)+\left[\quad Y_{nj}^{mrc}\quad\right]^{-1}\left(\zeta_j^r\right)=\left(\tau_n^{mc(t)}\right)+\left(\tau_n^{mc(c)}\right)=\left(\tau_n^{mc}\right), \tag{2.29.1}$$

$$\left[\quad K_{nj}^{mr}\quad\right]\left(\dot{\beta}_j^r\right)+\left[\quad Y_{nj}^{mrs}\quad\right]^{-1}\left(\varpi_j^r\right)=\left(\tau_n^{ms(t)}\right)+\left(\tau_n^{ms(c)}\right)=\left(\tau_n^{ms}\right). \tag{2.29.2}$$

Note that while $m\geq 0$ in Eq. (2.29.1), $m\geq 1$ in Eq. (2.29.2). Note also that n should satisfy $n>m,\ n+m\equiv 1 \mod 2$ (i.e. $n=m+1,m+3,m+5,\ldots$) in both equations. When these equations are numerically computed, the integers m,r,n and j need to be truncated at an appropriate finite number so that K_{nj}^{rm} and Y_{nj}^{rm} should be finite-dimensional square matrices, for which $\max\{r\}=\max\{m\}$ is necessary.

2.2.6 The Unified Representation of the Induced Flow Fields

Equations (2.29.1) and (2.29.2) are expressed in terms of Fourier coefficients $\alpha_j^r,\beta_j^r,\zeta_j^r$ and ϖ_j^r to represent the same induced velocity distribution, but, in fact, only two of these sets of coefficients are sufficient to represent any flow field. Thus, appropriate transformations represented by matrices A_{ij}^{kr} and B_{ij}^{kr} are introduced to unify the representations such that

$$\left[\quad K_{ni}^{mk}\quad\right]\left[\quad A_{ij}^{kr}\quad\right]\left(\dot{a}_j^r\right)+\left[\quad Y_{ni}^{mkc}\quad\right]^{-1}\left[\quad B_{ij}^{kr}\quad\right]\left(a_j^r\right)=\left(\tau_n^{mc(t)}\right)+\left(\tau_n^{mc(c)}\right)=\left(\tau_n^{mc}\right), \tag{2.30.1}$$

$$\left[\quad K_{ni}^{mk}\quad\right]\left[\quad A_{ij}^{kr}\quad\right]\left(\dot{b}_j^r\right)+\left[\quad Y_{ni}^{mks}\quad\right]^{-1}\left[\quad B_{ij}^{kr}\quad\right]\left(b_j^r\right)=\left(\tau_n^{ms(t)}\right)+\left(\tau_n^{ms(c)}\right)=\left(\tau_n^{ms}\right), \tag{2.30.2}$$

where

$$\left[\quad A_{ij}^{kr}\quad\right]\left(\dot{a}_j^r\right)=\left(\dot{\alpha}_i^k\right), \tag{2.31.1}$$

$$\left[\quad A_{ij}^{kr}\quad\right]\left(\dot{b}_j^r\right)=\left(\dot{\beta}_i^k\right), \tag{2.31.2}$$

$$\left[\quad B_{ij}^{kr}\quad\right]\left(a_j^r\right)=\left(\zeta_i^k\right), \tag{2.31.3}$$

$$\left[\quad B_{ij}^{kr}\quad\right]\left(b_j^r\right)=\left(\varpi_i^k\right), \tag{2.31.4}$$

$$w(r,\psi,t)=\sum_{r=0}^{\infty}\sum_{j=r+1,r+3,\ldots}^{\infty}\Psi_j^r(\nu)[a_j^r(t)\cos(r\psi)+b_j^r(t)\sin(r\psi)]. \tag{2.32}$$

Equations (2.30.1) and (2.30.2) can be rewritten as

$$\left[\quad M_{nj}^{mr}\quad\right]\left(\dot{a}_j^r\right)+\left[\quad L_{nj}^{mrc}\quad\right]^{-1}\left(a_j^r\right)=\left(\tau_n^{mc(t)}\right)+\left(\tau_n^{mc(c)}\right)=\left(\tau_n^{mc}\right), \tag{2.33.1}$$

$$\left[\quad M_{nj}^{mr}\quad\right]\left(\dot{b}_j^r\right)+\left[\quad L_{nj}^{mrc}\quad\right]^{-1}\left(b_j^r\right)=\left(\tau_n^{ms(t)}\right)+\left(\tau_n^{ms(c)}\right)=\left(\tau_n^{ms}\right), \tag{2.33.2}$$

where

$$\left[\quad M_{nj}^{mr}\quad\right]=\left[\quad K_{ni}^{mk}\quad\right]\left[\quad A_{ij}^{kr}\quad\right], \tag{2.34.1}$$

$$\left[\quad L_{nj}^{mrc}\quad\right]^{-1}=\left[\quad Y_{ni}^{mkc}\quad\right]^{-1}\left[\quad B_{ij}^{kr}\quad\right], \tag{2.34.2}$$

$$\left[\quad L_{nj}^{mrs}\quad\right]^{-1}=\left[\quad Y_{ni}^{mks}\quad\right]^{-1}\left[\quad B_{ij}^{kr}\quad\right]. \tag{2.34.3}$$

Equations (2.33.1) and (2.33.2) can be decomposed again into a time-derivative and convection parts as, respectively,

$$\left[\quad M_{nj}^{mr}\quad\right]\left(\dot{a}_j^r\right)=\left(\tau_n^{mc(t)}\right), \tag{2.35.1}$$

$$\left[\quad M_{nj}^{mr}\quad\right]\left(\dot{b}_j^r\right)=\left(\tau_n^{ms(t)}\right), \tag{2.35.2}$$

$$\left[\quad L_{nj}^{mrc}\quad\right]^{-1}\left(a_j^r\right)=\left(\tau_n^{mc(c)}\right), \tag{2.35.3}$$

$$\left[\quad L_{nj}^{mrs}\quad\right]^{-1}\left(b_j^r\right)=\left(\tau_n^{ms(c)}\right). \tag{2.35.4}$$

These matrix equations of Eqs. (2.33.1) and (2.33.2) are well-known as the typical forms of the dynamic inflow model, though the basic structures of these equations are essentially those of the Euler equations, Eq. (2.3). Whereas Ψ_j^r may be any appropriate function in so far as it can form a complete orthogonal system of functions for each m in the interval of $[0,1]$, Peters recommended purely from a practical point of view in Refs. (37) and (92) that $(1/\nu)\bar{P}_j^r(\nu)$ may be the best choice on account of the rapid convergence of these functions around $\bar{r}=1$ (i.e. around the blade tip), and also of the practical feasibility that arises from the fact that computations with these functions may be carried out analytically in a closed form[37][92],

$$\Psi_j^r = \frac{1}{\nu}\bar{P}_j^r(\nu). \tag{2.36}$$

The remaining problem is how to define $\Psi_n^{m(L)}$ and $\Psi_n^{m(M)}$, and Peters also recommended the following representations again from a practical point of view.

$$\Psi_j^{r(M)} = \frac{1}{\nu}\bar{P}_j^r(\nu), \tag{2.37.1}$$

$$\Psi_j^{r(L)} = \bar{P}_j^r(\nu). \tag{2.37.2}$$

As well as the fact that $(1/\nu)\bar{P}_j^r(\nu)$ forms a complete orthogonal system of functions, it can also be expressed in terms of only the radial position of the rotor disc, $\bar{r}=\sqrt{1-\nu^2}$, and this property hugely simplifies the practical treatment of the equations in relation to the blade element theory (see also Appendix 2.7),

$$\frac{1}{\nu}\bar{P}_n^m(\nu) = \sqrt{(2n+1)H_n^m}\sum_{q=m,m+2,m+4,\ldots}^{n-1}\frac{(-1)^{\frac{q-m}{2}}(n+q)!!}{(q-m)!!(q+m)!!(n-q-1)!!}\bar{r}^q, \tag{2.38}$$

where

$$H_n^m = \frac{(n+m-1)!!(n-m-1)!!}{(n+m)!!(n-m)!!}. \tag{2.39}$$

For the case when $n=m+1$, Eq. (2.38) can be further simplified as follows[92],

$$\frac{1}{\nu}\bar{P}_{m+1}^m(\nu) = \sqrt{\frac{(2m+3)!!}{(2m)!!}}\bar{r}^m. \tag{2.40}$$

In the later discussion, Ψ_j^r is to be integrated over the rotor disc, and the fact that $(1/\nu)\bar{P}_n^m(\nu)$ is a function of $\bar{r}$ alone makes the integration much simpler. Equation (2.40) is of particular use for that case[29]. Equations (2.33.1), (2.34.1) and (2.35.1) allow of the assumption that, without the loss of generality,

$$A_{ij}^{kr} = \delta_{ij}, \tag{2.41}$$

$$\alpha_j^r = a_j^r. \tag{2.42}$$

Thus, the matrix A_{ij}^{kr} becomes the unit matrix. In this case, the matrix B_{ij}^{kr} should be determined through substituting Eqs. (2.26), (2.31.3), (2.31.4), (2.34.2), (2.34.3), (2.35.3), (2.35.4), (2.36) and (2.27) into Eq. (2.18) and equating coefficients. Regarding the cosine terms, substituting Eqs (2.23.2), (2.25), (2.36) and (2.37.2) into Eq. (2.34.2) yields

$$\sum_{r=0}^{\infty}\sum_{j=r+1,r+3,\ldots}^{\infty}\frac{1}{\nu}\bar{P}_j^r(\nu)[a_j^r(\bar{t})\cos(r\psi)+b_j^r(\bar{t})\sin(r\psi)]$$
$$=\sum_{k=0}^{\infty}\sum_{i=k+1,k+3,\ldots}^{\infty}\bar{P}_i^k(\nu)[\zeta_i^k(\bar{t})\cos(k\psi)+\varpi_i^k(\bar{t})\sin(k\psi)]. \tag{2.43}$$

On account of the orthogonality of normalised associated Legendre functions of the first kind over $[0,1]$, Eq.(2.9.1), and of the trigonometric functions over $[0,2\pi]$ (Eq. (2.10.1) and (2.10.2)), ζ_i^k and ϖ_i^k can be determined as

$$\zeta_i^k = \frac{1}{\pi}\int_0^{2\pi}\int_0^1\left(\sum_{r=0}^{\infty}\sum_{j=r+1,r+3,\ldots}^{\infty}\frac{1}{\nu}\bar{P}_j^r(\nu)[a_j^r(t)\cos(r\psi)+b_j^r(t)\sin(r\psi)]\right)\bar{P}_i^k(\nu)\cos(k\psi)d\nu d\psi$$
$$=\left(\int_0^1\frac{1}{\nu}\bar{P}_j^r(\nu)\bar{P}_i^k(\nu)d\nu\right)a_j^r, \tag{2.44}$$

[29] Also, as is often the case with application to flight control systems, only a crude approximation is required where n is simply considered to be $m+1$.

$$\varpi_i^k = \frac{1}{\pi}\int_0^{2\pi}\int_0^1 \left(\sum_{r=0}^{\infty}\sum_{j=r+1,r+3,\ldots}^{\infty}\frac{1}{\nu}\bar{P}_j^r(\nu)[a_j^r(t)\cos(r\psi)+b_j^r(t)\sin(r\psi)]\right)\bar{P}_i^k(\nu)\sin(k\psi)d\nu d\psi$$

$$= \left(\int_0^1 \frac{1}{\nu}\bar{P}_j^r(\nu)\bar{P}_i^k(\nu)d\nu\right)b_j^r. \qquad (2.45)$$

Thus, from Eqs. (2.31.1) and (2.31.4),

$$B_{ij}^{kr} = \int_0^1 \frac{1}{\nu}\bar{P}_j^r(\nu)\bar{P}_i^k(\nu)d\nu. \qquad (2.46.1)$$

Note that matrix $[B_{ij}^{kr}]$ does not have to have non-zero values for its entries; in fact, a diagonal partition matrix suffices for the transformation required in Eqs. (2.31.3) and (2.31.4).

$$B_{ij}^{k} = \int_0^1 \frac{1}{\nu}\bar{P}_j^k(\nu)\bar{P}_i^k(\nu)d\nu. \qquad (2.46.2)$$

This integration can be analytically expressible and the formula is found in Ref. (167).

$$\int_0^1 \frac{1}{\nu}\bar{P}_j^k(\nu)\bar{P}_i^k(\nu)d\nu = (-1)^{i+j-2r-2}\sqrt{(2i+1)(2j+1)\frac{H_j^k}{H_i^k}}\sum_{q=r,r+2,\ldots}^{j-1}\frac{(2q+1)}{(i-q)(i+q+1)}H_q^k. \qquad (2.47)$$

The inverse matrix of B_{ij}^k was found by He (Ref. (7), page 30),

$$\left[B_{ij}^k\right]^{-1} = \frac{(-1)^{\frac{i+j-2r}{2}}}{\sqrt{H_j^k H_i^k}}\cdot\frac{2\sqrt{(2i+1)(2j+1)}}{(i+j)(i+j+2)[(i-j)^2-1]}, \qquad (2.48)$$

where this expression will be highly convenient for the later discussion of L_{nj}^{mrc} and L_{nj}^{mrs}.

2.2.7 The Apparent Mass Matrix, M

In order to combine Eq. (2.36) with Eq. (2.17), the z-derivative in Eq. (2.17) should be transformed into ellipsoidal coordinates[30] (see Appendix 2.3). In general,

$$\frac{\partial}{\partial z} = -\frac{1}{\nu^2+\eta^2}\left[\eta(1-\nu^2)\frac{\partial}{\partial \nu} + \nu(1+\eta^2)\frac{\partial}{\partial \eta}\right]. \tag{2.49}$$

In particular, on the rotor disc $\eta = 0$, and hence Equation (2.49) can be simplified to

$$\frac{\partial}{\partial z}\Big|_{rotor\ \ disc} = -\frac{1}{\nu}\cdot\frac{\partial}{\partial \eta}. \tag{2.50}$$

Equations (2.17) and (2.50) yield

$$\dot{v}_i = \dot{w} \equiv -\frac{\partial \Phi^{(t)}}{\partial z}\Big|_{\eta=0} = \frac{1}{\nu}\cdot\frac{\partial \Phi^{(t)}}{\partial \eta}\Big|_{\eta=0}. \tag{2.51}$$

On the other hand, Eqs. (2.12.1) and (2.22) give

$$\frac{1}{\nu}\cdot\frac{\partial \Phi^{(t)}}{\partial \eta}\Big|_{\eta=0} = -\frac{1}{2}\sum_{m=0}^{\infty}\sum_{n=m+1,m+3,\ldots}^{\infty}\frac{1}{\nu}\bar{P}_n^m(\nu)\frac{\partial \bar{Q}_n^m(i\eta)}{\partial \eta}\left[\tau_n^{mc(t)}(\bar{t})\cos(m\psi) + \tau_n^{ms(t)}(\bar{t})\sin(m\psi)\right]\Big|_{\eta=0}, \tag{2.52}$$

$$\dot{w} = \sum_{r=0}^{\infty}\sum_{j=r+1,r+3,\ldots}^{\infty}\frac{1}{\nu}\bar{P}_j^r(\nu)[\dot{a}_j^r(\bar{t})\cos(r\psi) + \dot{b}_j^r(\bar{t})\sin(r\psi)]. \tag{2.53}$$

Substituting Eqs. (2.50), (2.52) and (2.53) into Eq. (2.17) yields

$$\begin{aligned}\sum_{r=0}^{\infty}\sum_{j=r+1,r+3,\ldots}^{\infty}&\bar{P}_j^r(\nu)[\dot{a}_j^r(\bar{t})\cos(r\psi) + \dot{b}_j^r(\bar{t})\sin(r\psi)] \\ &= -\frac{1}{2}\sum_{m=0}^{\infty}\sum_{n=m+1,m+3,\ldots}^{\infty}\bar{P}_n^m(\nu)\frac{\partial \bar{Q}_n^m(i\eta)}{\partial \eta}\left[\tau_n^{mc(t)}(\bar{t})\cos(m\psi) + \tau_n^{ms(t)}(\bar{t})\sin(m\psi)\right]\Big|_{\eta=0}.\end{aligned} \tag{2.54}$$

Multiplying Eq. (2.54) by $\bar{P}_j^r(\nu)$ and $\cos(r\psi)$, and integrating by ν over $[0,1]$ and by ψ over $[0,2\pi]$, the orthogonality of the normalised associated Legendre function of

[30] References (1) and (35) contain the same typographical error in the representation of Eq. (2.49).

the first kind and the trigonometric functions, Eqs. (2.9.1) and (2.10.1), yield the following relations,

$$(left-hand\ \ term)=\pi\sum_{r=0}^{\infty}\sum_{j=r+1,r+3,\ldots}^{\infty}\dot{a}_j^r(\bar{t}), \tag{2.55.1}$$

$$(right-hand\ \ term)=-\frac{\pi}{2}\sum_{r=0}^{\infty}\sum_{n=r+1,r+3,\ldots}^{\infty}\delta_{jn}\frac{\partial\bar{Q}_n^r(i\eta)}{\partial\eta}\bigg|_{\eta=0}\tau_n^{rc(t)}(\bar{t}). \tag{2.55.2}$$

Therefore,

$$\dot{a}_j^r=-\frac{1}{2}\cdot\frac{\partial\bar{Q}_j^r(i\eta)}{\partial\eta}\bigg|_{\eta=0}\tau_j^{rc(t)}(\bar{t}). \tag{2.56}$$

Similarly, multiplying Eq. (2.54) by $\bar{P}_j^r(\nu)$ and $\sin(r\psi)$, and integrating by ν over $[0,1]$ and by ψ over $[0,2\pi]$ yields

$$\dot{b}_j^r=-\frac{1}{2}\cdot\frac{d\bar{Q}_j^r(i\eta)}{d\eta}\bigg|_{\eta=0}\tau_j^{rs(t)}. \tag{2.57}$$

Equations (2.56) and (2.57) can be further simplified by the following formula,

$$-\frac{d\bar{Q}_j^r(i\eta)}{d\eta}\bigg|_{\eta=0}=\frac{\pi(j+r)!!(j-r)!!}{2(j+r-1)!!(j-r-1)!!}\equiv\frac{\pi}{2}\big(H_j^r\big)^{-1}. \tag{2.58}$$

Comparing Eqs. (2.56) and (2.57) with Eqs. (2.35.1) and (2.35.2), $r=m$ and $j=n$ are required, that is to say, M is a diagonal matrix. From Eq. (2.58), the elements of matrix M can be obtained as

$$\begin{aligned}M_{nj}^{mr}&=\bigg[-\frac{1}{2}\delta_{mr}\delta_{nj}\frac{d\bar{Q}_n^m(i\eta)}{d\eta}\bigg|_{\eta=0}\bigg]^{-1}\\&=\frac{4}{\pi}H_n^m\delta_{mr}\delta_{nj}\\&=\frac{4(n+m-1)!!(n-m-1)!!}{\pi(n+m)!!(n-m)!!}\delta_{mr}\delta_{nj}.\end{aligned} \tag{2.59}$$

Note that only such combinations of m and n that $m+n \equiv 1 \mod 2$ are chosen. Table 2-1 shows some examples of the value of M_n^m.

	$n=0$	$n=1$	$n=2$	$n=3$	$n=4$	$n=5$	$n=6$	$n=7$
$m=0$		$\frac{4}{\pi}$		$\frac{16}{9\pi}$		$\frac{256}{225\pi}$		$\frac{1024}{1225\pi}$
$m=1$	-		$\frac{8}{3\pi}$		$\frac{64}{45\pi}$		$\frac{512}{525\pi}$	
$m=2$	-	-		$\frac{32}{15\pi}$		$\frac{128}{105\pi}$		$\frac{4096}{4725\pi}$
$m=3$	-	-	-		$\frac{64}{35\pi}$		$\frac{1024}{945\pi}$	
$m=4$	-	-	-	-		$\frac{512}{315\pi}$		$\frac{2048}{2079\pi}$
$m=5$	-	-	-	-	-		$\frac{1024}{693\pi}$	
$m=6$	-	-	-	-	-	-		$\frac{4096}{3003\pi}$

Table 2-1. [Examples of M_n^m.]

2.2.8. The Gain Matrix, L - part 1 - *The General Representation*

While the representation of matrix M_{nj}^{mr} is common to both Eqs. (2.35.1) and (2.35.2), Eqs. (2.35.3) and (2.35.4) have different matrices for L_{nj}^{mrc} and L_{nj}^{mrs}. Substituting Eqs. (2.12.2), (2.32), (2.36) and (2.37.2) into Eq. (2.18) yields

$$\sum_{r=0}^{\infty}\sum_{j=r+1,r+3,\ldots}^{\infty}\bar{P}_j^r(\nu)[\zeta_j^r(\bar{t})\cos(r\psi)+\varpi_j^r(\bar{t})\sin(r\psi)]$$
$$=\frac{1}{2V}\int_0^{\infty}\frac{1}{\nu}\frac{\partial}{\partial\eta}\left(\sum_{m=0}^{\infty}\sum_{n=m+1,m+3,\ldots}^{\infty}\bar{P}_n^m(\nu)\bar{Q}_n^m(i\eta)\left[\tau_n^{mc(c)}(\bar{t})\cos(m\psi)+\tau_n^{ms(c)}(\bar{t})\sin(m\psi)\right]\right)d\xi. \tag{2.60}$$

Multiplying Eq. (2.60) by either $\bar{P}_n^m(\nu_0)\cos(r\psi_0)$ or $\bar{P}_n^m(\nu_0)\sin(r\psi_0)$, where ν_0 and ψ_0 indicate a fixed point on the rotor disc, from which the reference streamline, along

which a ξ-axis is defined, is generated in the downstream direction. Note that (x_0, y_0) is the Cartesian representation of the point on the rotor disc $(\sqrt{1-\nu_0}, \psi_0)$ expressed in polar coordinates, as shown in Fig. 2-5.

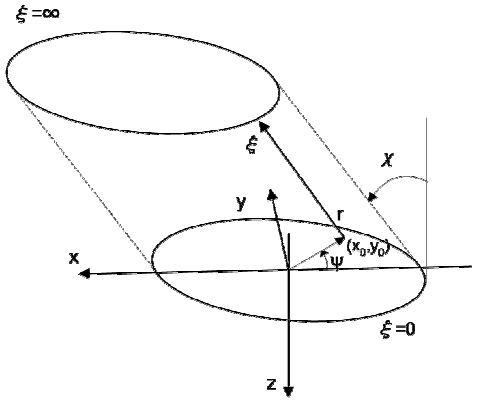

Fig. 2-5 [Skewed cylindrical description for the rotor wake.]

The ξ-coordinate in Fig. 2-5 is pointing in the opposite direction to the z-axis, and this is typical of the normal working state of a helicopter rotor[31].

Incidentally, readers are encouraged to bear in mind that the representation of wake tube as an infinitely long skewed cylinder is a hugely simplified approximation; the flow in the rotor wake in reality becomes strongly turbulent within a distance of several rotor radii from the rotor. Figure 2-6 shows an example of more realistic description of the wake tube simulated by the vortex transportation method[32]. In this thesis, the skewed cylindrical representation is used following He and Peters, whereas there possibly is much room in the description of wake tube for further improvements and sophistications for the analytical representation.

Fig. 2-6 [Wake tube description by the vortex transportation method.]

[31] The case of an autorotative rotor (i.e. the windmill-brake state) will be discussed in Chapter 3.
[32] Figure 2-5 is kindly provided by Prof. Richard Brown of Glasgow University, with the copyright approved.

Integrating Eq. (2.60) by ν_0 over $[0,1]$ and by ψ over $[0,2\pi]$, the orthogonality of the normalised associated Legendre functions of the first kind and trigonometric functions give the following relations,

$$\pi\sum_{r=0}^{\infty}\sum_{j=r+1,r+3,\ldots}^{\infty}\zeta_j^r(\bar{t}) = \left[\int_0^{2\pi}\int_0^1\frac{1}{2V\nu}\int_0^{\infty}\frac{\partial}{\partial\eta}\left(\sum_{m=0}^{\infty}\sum_{n=m+1,m+3,\ldots}^{\infty}\bar{P}_n^m(\nu)\bar{Q}_n^m(i\eta)\cos(m\psi)\right)d\xi\cdot\bar{P}_j^r(\nu_0)\cos(r\psi)d\nu_0 d\Psi\right]\tau_n^{mc(c)}(\bar{t}), \tag{2.61}$$

$$\pi\sum_{r=0}^{\infty}\sum_{j=r+1,r+3,\ldots}^{\infty}\varpi_j^r(\bar{t}) = \left[\int_0^{2\pi}\int_0^1\frac{1}{2V\nu}\int_0^{\infty}\frac{\partial}{\partial\eta}\left(\sum_{m=0}^{\infty}\sum_{n=m+1,m+3,\ldots}^{\infty}\bar{P}_n^m(\nu)\bar{Q}_n^m(i\eta)\sin(m\psi)\right)d\xi\cdot\bar{P}_n^m(\nu_0)\sin(r\psi)d\nu_0 d\Psi\right]\tau_n^{ms(c)}(\bar{t}). \tag{2.62}$$

From Eqs. (2.35.3), (2.35.4), (2.61) and (2.62), the elements of matrices $\hat{L}_{jn}^{rmc}$ and $\hat{L}_{jn}^{rms}$ can be expressed as follows,

$$L_{nj}^{mrc} = \frac{1}{2\pi V}\int_0^{2\pi}\int_0^1\int_0^{\infty}\frac{\partial}{\nu\partial\eta}\left(\bar{P}_n^m(\nu)\bar{Q}_n^m(i\eta)\cos(m\psi)\right)d\xi\cdot\bar{P}_j^r(\nu_0)\cos(r\psi)d\nu_0 d\psi, \tag{2.63}$$

$$L_{nj}^{mrs} = \frac{1}{2\pi V}\int_0^{2\pi}\int_0^1\int_0^{\infty}\frac{\partial}{\nu\partial\eta}\left(\bar{P}_n^m(\nu)\bar{Q}_n^m(i\eta)\sin(m\psi)\right)d\xi\cdot\bar{P}_j^r(\nu_0)\sin(r\psi)d\nu_0 d\psi. \tag{2.64}$$

Regarding the definition of the gain matrix, Peters presented a different form[37], in which the mass-flow parameter, V, is excluded. This form is distinguished from Eqs. (2.63) and (2.64) by hat symbol, (^), following Peters' notation.

$$\hat{L}_{jn}^{rmc} = \frac{1}{2\pi}\int_0^{2\pi}\int_0^1\int_0^{\infty}\frac{\partial}{\nu\partial\eta}\left(\bar{P}_n^m(\nu)\bar{Q}_n^m(i\eta)\cos(m\psi)\right)d\xi\cdot\bar{P}_j^r(\nu_0)\cos(r\psi)d\nu_0 d\psi, \tag{2.65.1}$$

$$\hat{L}_{jn}^{rms} = \frac{1}{2\pi}\int_0^{2\pi}\int_0^1\int_0^{\infty}\frac{\partial}{\nu\partial\eta}\left(\bar{P}_n^m(\nu)\bar{Q}_n^m(i\eta)\sin(m\psi)\right)d\xi\cdot\bar{P}_j^r(\nu_0)\sin(r\psi)d\nu_0 d\psi, \tag{2.65.2}$$

$$\hat{L}_{jn}^{0mc} = \frac{1}{4\pi}\int_0^{2\pi}\int_0^1\int_0^{\infty}\frac{\partial}{\nu\partial\eta}\left(\bar{P}_n^m(\nu)\bar{Q}_n^m(i\eta)\cos(m\psi)\right)d\xi\cdot\bar{P}_j^0(\nu_0)d\nu_0 d\psi. \tag{2.65.3}$$

Note that $\hat{L}_{jn}^{0mc}$ has the coefficient of $1/4$ while $\hat{L}_{jn}^{rmc}$ and $\hat{L}_{jn}^{rms}$ have $1/2$. (See Appendix 2.8 thereabout.) Note also that when $r=0$, the associated Legendre function of the first kind reduces to the Legendre function of the first kind (see Appendix 2.5). The integrations of Eqs. (2.65.1) - (2.65.3) will be discussed in the next Subsection[33].

2.2.9 The Gain Matrix, L - part 2 - *Skewed Cylindrical Representation for the Wake Tube*

Using Eqs. (2.12.2) and (2.50), Eqs (2.65.1) - (2.65.3) can be rearranged as

$$\hat{L}_{jn}^{rmc} = \frac{1}{2\pi}\int_0^{2\pi}\int_0^1\int_0^\infty \frac{\partial \Phi_n^{mc(c)}}{\partial z} d\xi \cdot \bar{P}_j^r(\nu_0)\cos(r\psi) d\nu_0 d\psi, \tag{2.66.1}$$

$$\hat{L}_{jn}^{rms} = \frac{1}{2\pi}\int_0^{2\pi}\int_0^1\int_0^\infty \frac{\partial \Phi_n^{ms(c)}}{\partial z} d\xi \cdot \bar{P}_j^r(\nu_0)\sin(r\psi) d\nu_0 d\psi, \tag{2.66.2}$$

$$\hat{L}_{jn}^{0mc} = \frac{1}{4\pi}\int_0^{2\pi}\int_0^1\int_0^\infty \frac{\partial \Phi_n^{mc(c)}}{\partial z} d\xi \cdot \bar{P}_j^0(\nu_0) d\nu_0 d\psi. \tag{2.66.3}$$

In spite of the apparent complicated forms of these expressions, it is shown by He that these integrations are analytically expressible in closed forms in Ref. (7), and his method will be revisited in this Subsection. First of all, it should be confirmed that He's method is based on the following assumptions[34]:

(C1) the wake tube should be described as a skewed cylinder with the wake skew angle of χ to the rotor disc, as is shown in Fig. 2-5[35];
(C2) the wake skew angle, χ, should be small[36].

Suppose the rotor wake is expressed in the shape of skewed cylinder following He,

[33] With regard to the coefficient of $\hat{L}_{nj}^{mr}$, there are variations in the literature: for example, Refs. (92) and (37) introduce different $\hat{L}_{nj}^{mr}$ where the former is double as of the latter. See Appendix 2.9 about the variation in the definition.

[34] These assumptions are not mentioned at all in Refs. (1), (37), (92) and (112), and are mentioned only in an appendix of Ref. (7). Most readers who have not read Ref. (7) may thus perhaps struggle to execute the integrations of Eq. (2.65) and how to determine the elements of the gain matrix.

[35] As mentioned in the previous Subsection, assumption (C1) is controversial. However, it is highly likely impossible to analytically perform the complicated integrations in Eqs. (2.66.1) - (2.66.3) without the simplification. Even in more advanced augmented dynamic inflow models (e.g. Ref. (129)), in which more convoluted wake distortion is considered, only ad hoc coefficients modifying the Peter and He model are used to represent the wake distortion. It is likely that this is due to the hopeless complexity of those integrations when incorporating the wake distortion into the analytical calculation at this stage.

[36] In high speed forward flight, the wake skew angle cannot be considered small. Thus for this flight situation, the justification for assumption (C2) also weakens. However, the validity of this assumption is not discussed in any of the previous studies, although the Peters and He model is widely used for flight dynamics applications even in full forward flight condition. The assumption shall be further discussed in Chapter 4.

these integrations can be considered as volume integrations throughout the skewed cylindrical domain shown in Fig. 2-5. The one-dimensional ξ-coordinate is defined inside the skewed cylinder along a streamline. A point inside the skewed cylinder, (x, y, z), can be described by ξ and (x_0, y_0), which is a specific point on the rotor disc from which the reference streamline develops in the downstream direction (see also Appendix 2.2).

$$x = \xi \sin\chi + x_0, \tag{2.67.1}$$

$$y = y_0, \tag{2.67.2}$$

$$z = -\xi \cos\chi, \tag{2.67.3}$$

where

$$x_0 = -\bar{r}\cos\psi, \tag{2.68.1}$$

$$y_0 = \bar{r}\sin\psi. \tag{2.68.2}$$

Equations (2.67.1), (2.67.2) and (2.67.3) in turn give the following relations,

$$d\xi = -\frac{1}{\cos\chi} dz, \tag{2.69.1}$$

$$\frac{\partial}{\partial\xi} = \frac{\partial x}{\partial\xi}\cdot\frac{\partial}{\partial x} + \frac{\partial y}{\partial\xi}\cdot\frac{\partial}{\partial y} + \frac{\partial z}{\partial\xi}\cdot\frac{\partial}{\partial z} = \sin\chi\frac{\partial}{\partial x} - \cos\chi\frac{\partial}{\partial z}. \tag{2.69.2}$$

Note that $\cos\chi \neq 0$ is necessary when deriving Eq. (2.69.1) from Eq. (2.67.3), thus edgewise flight ($\chi = \pi/2$) should be excluded from the model hereinafter[37].

From Eq. (2.69.2),

$$\frac{\partial}{\partial z} = -\frac{1}{\cos\chi}\cdot\frac{\partial}{\partial\xi} + \tan\chi\frac{\partial}{\partial x}. \tag{2.70}$$

Using Eq. (2.70), Eq. (2.66.1) can be rearranged as

$$\begin{aligned}\hat{L}_{jn}^{rmc} &= \frac{1}{2\pi}\int_0^{2\pi}\int_0^1\int_0^\infty \frac{\partial\Phi_n^{mc(c)}}{\partial z} d\xi\cdot\bar{P}_j^r(\nu_0)\cos(r\psi)d\nu_0 d\psi \\ &= -\frac{1}{2\pi\cos\chi}\int_0^{2\pi}\int_0^1\int_0^\infty \frac{\partial\Phi_n^{mc(c)}}{\partial\xi} d\xi\cdot\bar{P}_j^r(\nu_0)\cos(r\psi)d\nu_0 d\psi \\ &\quad + \frac{\tan\chi}{2\pi}\int_0^{2\pi}\int_0^1\int_0^\infty \frac{\partial\Phi_n^{mc(c)}}{\partial x} d\xi\cdot\bar{P}_j^r(\nu_0)\cos(r\psi)d\nu_0 d\psi.\end{aligned} \tag{2.71}$$

[37] However, the resultant model based on these equations will later be extended up to $\chi = \pi/2$ owing to *the small wake skew angle assumption*. The extension of the model apparently contradicts the necessary condition for rearranging Eq. (2.67.3) to Eq. (2.69.1). This author will discuss this point in depth in Chapter 4.

The first term on the right-hand side of Eq. (2.71) can be straightforwardly integrated as

$$
\begin{aligned}
(first\ \ term) &= -\frac{1}{2\pi\cos\chi}\int_0^{2\pi}\int_0^1 \left[\Phi_n^{mc(c)}\right]_0^{\infty}\cdot \bar{P}_j^r(\nu_0)\cos(r\psi)d\nu_0 d\psi \\
&= \frac{1}{2\pi\cos\chi}\int_0^{2\pi}\int_0^1 \Phi_n^{mc(c)}\Big|_{\xi=0}\cdot \bar{P}_j^r(\nu_0)\cos(r\psi)d\nu_0 d\psi \\
&= \frac{1}{2\pi\cos\chi}\int_0^{2\pi}\int_0^1 \left(\bar{P}_n^m(\nu_0)\cos(m\psi)\right)\bar{P}_j^r(\nu_0)\cos(r\psi)d\nu_0 d\psi \\
&= \frac{1}{2\cos\chi}\delta_{mr}\delta_{nj}. \qquad (2.72)
\end{aligned}
$$

Note that $\Phi_n^{mc(c)}\Big|_{\xi=\infty} = 0$ by applying the boundary condition (B1). Using Eq. (2.69.1), the second term on the right-hand side of Eq. (2.71) can be rearranged as

$$
(second\ \ term) = -\frac{\tan\chi}{2\pi\cos\chi}\int_0^{2\pi}\int_0^1\int_0^{-\infty}\frac{\partial\Phi_n^{mc(c)}}{\partial x}dz\cdot\bar{P}_j^r(\nu_0)\cos(r\psi)d\nu_0 d\psi. \qquad (2.73)
$$

The same discussion can be applied to Eq. (2.66.2),

$$
\begin{aligned}
\hat{L}_{jn}^{rms} &= \frac{1}{2\pi}\int_0^{2\pi}\int_0^1\int_0^{\infty}\frac{\partial\Phi_n^{ms(c)}}{\partial z}d\xi\cdot\bar{P}_j^r(\nu_0)\sin(r\psi)d\nu_0 d\psi \\
&= -\frac{1}{2\pi\cos\chi}\int_0^{2\pi}\int_0^1\int_0^{\infty}\frac{\partial\Phi_n^{ms(c)}}{\partial\xi}d\xi\cdot\bar{P}_j^r(\nu_0)\sin(r\psi)d\nu_0 d\psi \\
&\quad + \frac{\tan\chi}{2\pi}\int_0^{2\pi}\int_0^1\int_0^{\infty}\frac{\partial\Phi_n^{ms(c)}}{\partial x}d\xi\cdot\bar{P}_j^r(\nu_0)\sin(r\psi)d\nu_0 d\psi, \qquad (2.74)
\end{aligned}
$$

where

$$
\begin{aligned}
(first\ \ term) &= -\frac{1}{2\pi\cos\chi}\int_0^{2\pi}\int_0^1\left[\Phi_n^{ms(c)}\right]_0^{\infty}\cdot\bar{P}_j^r(\nu_0)\sin(r\psi)d\nu_0 d\psi \\
&= \frac{1}{2\cos\chi}\delta_{mr}\delta_{nj}, \qquad (2.75)
\end{aligned}
$$

$$
(second\ \ term) = -\frac{\tan\chi}{2\pi\cos\chi}\int_0^{2\pi}\int_0^1\int_0^{-\infty}\frac{\partial\Phi_n^{ms(c)}}{\partial x}dz\cdot\bar{P}_j^r(\nu_0)\sin(r\psi)d\nu_0 d\psi. \qquad (2.76)
$$

Equation (2.66.3) is a special case of Eq. (2.66.1) in which $r = 0$. In summary, Eqs. (2.66.1) - (2.66.3) can be rearranged as follows,

$$\hat{L}_{jn}^{rmc} = \frac{1}{2\cos\chi}\delta_{mr}\delta_{nj} - \frac{\tan\chi}{2\pi\cos\chi}\int_0^{2\pi}\int_0^1\left(\int_0^{-\infty}\frac{\partial\Phi_n^{mc(c)}}{\partial x}dz\right)\bar{P}_j^r(\nu_0)\cos(r\psi)d\nu_0 d\psi, \quad (2.77.1)$$

$$\hat{L}_{jn}^{rms} = \frac{1}{2\cos\chi}\delta_{mr}\delta_{nj} - \frac{\tan\chi}{2\pi\cos\chi}\int_0^{2\pi}\int_0^1\left(\int_0^{-\infty}\frac{\partial\Phi_n^{ms(c)}}{\partial x}dz\right)\bar{P}_j^r(\nu_0)\sin(r\psi)d\nu_0 d\psi, \quad (2.77.2)$$

$$\hat{L}_{jn}^{0mc} = \frac{1}{4\cos\chi}\delta_{mr}\delta_{nj} - \frac{\tan\chi}{4\pi\cos\chi}\int_0^{2\pi}\int_0^1\left(\int_0^{-\infty}\frac{\partial\Phi_n^{mc(c)}}{\partial x}dz\right)\bar{P}_j^r(\nu_0)d\nu_0 d\psi. \quad (2.77.3)$$

2.2.10 The Gain Matrix, L - part 3 - *The Pressure Function*

From Eq. (2.12.2), $\Phi_n^{mc(c)}$ and $\Phi_n^{ms(c)}$ can be expressed as follows,

$$\Phi_n^{mc(c)} = \bar{P}_n^m(\nu)\bar{Q}_n^m(i\eta)\cos(m\psi) = \frac{e^{im\psi}+e^{-im\psi}}{2}\bar{P}_n^m(\nu)\bar{Q}_n^m(i\eta), \quad (2.78.1)$$

$$\Phi_n^{ms(c)} = \bar{P}_n^m(\nu)\bar{Q}_n^m(i\eta)\sin(m\psi) = \frac{e^{im\psi}-e^{-im\psi}}{2i}\bar{P}_n^m(\nu)\bar{Q}_n^m(i\eta). \quad (2.78.2)$$

Note that the partial derivative with respect to x can be expressed in polar coordinates as

$$\frac{\partial}{\partial x} = \frac{1}{2}\left\{e^{i\psi}\left(-\frac{\partial}{\partial\bar{r}} + \frac{1}{i\bar{r}}\cdot\frac{\partial}{\partial\psi}\right) - e^{-i\psi}\left(\frac{\partial}{\partial\bar{r}} + \frac{1}{i\bar{r}}\cdot\frac{\partial}{\partial\psi}\right)\right\}. \quad (2.79)$$

Equations (2.78.1) and (2.79) yield the expression of the successive differentiation of $\Phi_n^{mc(c)}$ with respect to x.

$$\frac{\partial^k\Phi_n^{mc(c)}}{\partial x^k} = \frac{1}{2^{k+1}}\left\{e^{i\psi}\left(-\frac{\partial}{\partial\bar{r}} + \frac{1}{i\bar{r}}\cdot\frac{\partial}{\partial\psi}\right) - e^{-i\psi}\left(\frac{\partial}{\partial\bar{r}} + \frac{1}{i\bar{r}}\cdot\frac{\partial}{\partial\psi}\right)\right\}^k (e^{im\psi}+e^{-im\psi})\bar{P}_n^m(\nu)\bar{Q}_n^m(i\eta), \quad (2.80.1)$$

$$\frac{\partial^k\Phi_n^{ms(c)}}{\partial x^k} = \frac{1}{2^{k+1}i}\left\{e^{i\psi}\left(-\frac{\partial}{\partial\bar{r}} + \frac{1}{i\bar{r}}\cdot\frac{\partial}{\partial\psi}\right) - e^{-i\psi}\left(\frac{\partial}{\partial\bar{r}} + \frac{1}{i\bar{r}}\cdot\frac{\partial}{\partial\psi}\right)\right\}^k (e^{im\psi}-e^{-im\psi})\bar{P}_n^m(\nu)\bar{Q}_n^m(i\eta). \quad (2.80.2)$$

For example, the first and second derivatives of $\Phi_n^{mc(c)}$ and $\Phi_n^{ms(c)}$ are expressed as follows[38],

$$\frac{\partial \Phi_n^{mc(c)}}{\partial x} = \frac{1}{2^2}\Bigg\{ (e^{i(m+1)\psi} + e^{-i(m+1)\psi})\Bigg(-\frac{\partial}{\partial r} + \frac{m}{r}\Bigg) + (e^{i(m-1)\psi} + e^{-i(m-1)\psi})\Bigg(-\frac{\partial}{\partial r} - \frac{m}{r}\Bigg)\Bigg\} \bar{P}_n^m(\nu)\bar{Q}_n^m(i\eta), \tag{2.81.1}$$

$$\frac{\partial^2 \Phi_n^{mc(c)}}{\partial x^2} = \frac{1}{2^2}\Bigg\{ (e^{i(m+2)\psi} + e^{-i(m+2)\psi})\Bigg(-\frac{\partial}{\partial r} + \frac{m+1}{r}\Bigg)\Bigg(-\frac{\partial}{\partial r} + \frac{m}{r}\Bigg) + (e^{i(m-2)\psi} + e^{-i(m-2)\psi})\Bigg(-\frac{\partial}{\partial r} - \frac{m-1}{r}\Bigg)\Bigg(-\frac{\partial}{\partial r} - \frac{m}{r}\Bigg) + 2(e^{im\psi} + e^{-im\psi})\Bigg(\frac{\partial^2}{\partial r^2} + \frac{1}{r}\frac{\partial}{\partial \bar{r}} - \frac{m^2}{r^2}\Bigg)\Bigg\} \bar{P}_n^m(\nu)\bar{Q}_n^m(i\eta), \tag{2.81.2}$$

$$\frac{\partial \Phi_n^{ms(c)}}{\partial x} = \frac{1}{2^2 i}\Bigg\{ (e^{i(m+1)\psi} - e^{-i(m+1)\psi})\Bigg(-\frac{\partial}{\partial r} + \frac{m}{r}\Bigg) + (e^{i(m-1)\psi} + e^{-i(m-1)\psi})\Bigg(-\frac{\partial}{\partial r} - \frac{m}{r}\Bigg)\Bigg\} \bar{P}_n^m(\nu)\bar{Q}_n^m(i\eta), \tag{2.82.1}$$

$$\frac{\partial^2 \Phi_n^{ms(c)}}{\partial x^2} = \frac{1}{2^3 i}\Bigg\{ (e^{i(m+2)\psi} - e^{-i(m+2)\psi})\Bigg(-\frac{\partial}{\partial r} + \frac{m+1}{r}\Bigg)\Bigg(-\frac{\partial}{\partial r} + \frac{m}{r}\Bigg) + (e^{i(m-2)\psi} + e^{-i(m-2)\psi})\Bigg(-\frac{\partial}{\partial r} - \frac{m-1}{r}\Bigg)\Bigg(-\frac{\partial}{\partial r} - \frac{m}{r}\Bigg) + 2e^{im\psi}\Bigg(\frac{\partial^2}{\partial r^2} + \frac{1}{r}\frac{\partial}{\partial \bar{r}} - \frac{m^2}{r^2}\Bigg)\Bigg\} \bar{P}_n^m(\nu)\bar{Q}_n^m(i\eta). \tag{2.82.2}$$

2.2.11 The Gain Matrix, L - part 4 - *The Small Wake Skew Angle Assumption*

When the flight condition is close to axial flight, the wake skew angle, χ, can be regarded sufficiently small, and the trigonometric functions can be approximated as follows,

$$\cos\chi = \frac{1-X^2}{1+X^2} = (1-X^2)(1+X^2)^{-1} \simeq (1-X^2)^2 \simeq 1, \tag{2.83.1}$$

[38] Reference (7) has a typographical error in Eq. (2.81.2)

$$\sin\chi = \frac{2X}{1+X^2} = 2X(1+X^2)^{-1} \simeq 2X(1-X^2) \simeq 2X, \tag{2.83.2}$$

$$\tan\chi = \frac{2X}{1-X^2} = 2X(1-X^2)^{-1} \simeq 2X(1+X^2) \simeq 2X, \tag{2.83.3}$$

where

$$X = \tan\frac{\chi}{2}. \tag{2.83.4}$$

Using Eqs. (2.67.3) and (2.83.3), the pressure function can be expanded in the form of a Taylor series around $(x_0, y_0, 0)$ to describe the pressure field in the neighbourhood of the rotor disc,

$$\begin{aligned}\Phi_n^{mc(c)}(x,y,z) &= \Phi_n^{mc(c)}(\xi\sin\chi + x_0, y_0, z)\\ &= \Phi_n^{mc(c)}(-z\tan\chi + x_0, y_0, z)\\ &\simeq \Phi_n^{mc(c)}(x_0 - 2Xz, y_0, z)\\ &= \sum_{k=0}^{\infty}\frac{(-1)^k}{k!}(2Xz)^k\frac{\partial^k\Phi_n^{mc(c)}}{\partial x^k}\bigg|_{x=x_0}.\end{aligned} \tag{2.84}$$

Equations (2.79), (2.83.1), (2.83.3) and (2.84) allow Eq. (2.77.1) to be rearranged as

$$\begin{aligned}\hat{L}_{jn}^{rmc} &= \frac{1}{2\cos\chi}\delta_{rm}\delta_{jn} + \frac{\tan\chi}{2\pi\cos\chi}\int_0^{2\pi}\int_0^1 \bar{P}_j^r(\nu)\cos(r\psi)\int_{-\infty}^0\frac{\partial\Phi_n^{mc(c)}}{\partial x}dz d\nu d\psi\\ &\simeq \frac{1}{2\cos\chi}\delta_{rm}\delta_{jn}\\ &\quad + \frac{\tan\chi}{2\pi\cos\chi}\sum_{q=0}^{\infty}\int_0^{2\pi}\int_0^1 \bar{P}_j^r(\nu)\cos(r\psi)\int_{-\infty}^0\sum_{k=0}^{\infty}\frac{(-1)^k}{k!}(2Xz)^k\frac{\partial^{k+1}\Phi_n^{mc(c)}}{\partial x^{k+1}}\bigg|_{x=x_0} dz d\nu d\psi\\ &\simeq \frac{1}{2}\delta_{rm}\delta_{jn} + \frac{X}{2\pi}\int_0^{2\pi}\int_0^1 \bar{P}_j^r(\nu)\cos(r\psi)\int_{-\infty}^0\sum_{k=0}^{\infty}\frac{(-1)^k}{k!}(Xz)^k\bigg\{e^{i\psi}\bigg(-\frac{\partial}{\partial\bar{r}} + \frac{1}{ir}\frac{\partial}{\partial\psi}\bigg)\\ &\quad - e^{-i\psi}\bigg(\frac{\partial}{\partial\bar{r}} + \frac{1}{i\bar{r}}\frac{\partial}{\partial\psi}\bigg)\bigg\}^{k+1}\Phi_n^{mc(c)}\bigg|_{x=x_0} dz d\nu d\psi\\ &\simeq \frac{1}{2}\delta_{rm}\delta_{jn} + \frac{1}{4\pi}\sum_{k=0}^{\infty}\int_0^{2\pi}\exp[i(|r|+|m|+|k+1|)\psi]d\psi\\ &\quad \int_0^1 \bar{P}_j^r(\nu)\int_{-\infty}^0\bigg\{\prod_{q=0}^{k}\bigg(-\frac{\partial}{\partial r} + \frac{|m|+q}{r}\bigg)\bigg\}\frac{X^{k+1}z^k}{k!}\bar{P}_n^m(\nu)\bar{Q}_n^m(\nu)dz d\nu.\end{aligned} \tag{2.85}$$

Regarding the integration of ψ in Eq. (2.85), only certain combinations of r, m and k can give non-zero values since

$$\frac{1}{2\pi}\int_0^{2\pi} \exp[i(|r| + |m| + |k+1|)\psi] = \delta_{0p}, \tag{2.86}$$

where $p = |r| + |m| + |k+1|$.[39] For non-zero elements of $\hat{L}^{rmc}_{jn}$, the possible combination is either of the following two cases: when $r > m$, $\pm r \mp m \mp (k+1) = 0$; when $r < m$, $\pm r \mp m \pm (k+1) = 0$. These two cases can be unified as a single expression of $k+1$ as $k+1 = \pm(r \mp m) = |r \pm m|$, and thus Eq. (2.85) can be further simplified as

$$\hat{L}^{rmc}_{jn} = \frac{1}{2}\delta_{rm}\delta_{jn} + \frac{1}{2}X^{|r\pm m|}\sum_{k=0}^{\infty}\int_0^1 \bar{P}^r_j(\nu)\int_{-\infty}^0 \left\{\prod_{q=0}^{k}\Big(-\frac{\partial}{\partial\bar{r}} + \frac{\pm m + q}{\bar{r}}\Big)\right\}\frac{z^k}{k!}\bar{P}^m_n(\nu)\bar{Q}^m_n(\nu)dzd\nu. \tag{2.87}$$

Regarding the right-hand terms of Eq. (2.87), it is convenient to define the following two functions,

$$\Lambda^{rm}_{jn} = \int_0^1 \bar{P}^r_j(\nu)\int_{-\infty}^0 \Big(-\frac{\partial}{\partial\bar{r}} + \frac{\pm m}{\bar{r}}\Big)\bar{P}^m_n(\nu)\bar{Q}^m_n(\nu)dzd\nu, \tag{2.88.1}$$

$$f(\bar{r}) = f(\nu) = \int_{-\infty}^0 \Big(\frac{\partial}{\partial\bar{r}} + \frac{\mp m}{\bar{r}}\Big)\bar{P}^m_n(\nu)\bar{Q}^m_n(\nu)dz. \tag{2.88.2}$$

Equations (2.88.1) and (2.88.2) are useful when working on the $k = 0$ case of Eq. (2.87). Equation (2.88.2) yields

$$\begin{aligned}\frac{df(r)}{dr} &= \int_{-\infty}^0 \Big(\frac{\partial^2}{\partial r^2} \mp \frac{m}{r}\frac{\partial}{\partial r} \pm \frac{m}{r^2}\Big)\bar{P}^m_n(\nu)\bar{Q}^m_n(\nu)dz \\ &= \int_{-\infty}^0 \Big(-\frac{\partial^2}{\partial z^2} + \frac{\mp m - 1}{r}\frac{\partial}{\partial r} + \frac{m^2 \pm m}{r^2}\Big)\bar{P}^m_n(\nu)\bar{Q}^m_n(\nu)dz \\ &= -\int_{-\infty}^0 \frac{\partial^2}{\partial z^2}\bar{P}^m_n(\nu)\bar{Q}^m_n(\nu)dz + \frac{\mp m - 1}{r}f(r),\end{aligned} \tag{2.89}$$

[39] Peters and He used the compound sign of $\pm$ instead of modulus for Eq. (2.85) in Refs. (7) and (37). However, for example, $\pm r \pm m$ is conventionally interpreted as either $+r+m$ or $-r-m$, excluding $+r-m$ or $-r+m$. Since the combination of + and - is herein completely arbitrary, this author believes that modulus signs are more appropriate for use in Eqs. (2.85) and (2.86).

where it is implied that the pressure function satisfies Laplace's equation,

$$\triangle\Phi_n^{mc(c)} = \left(\frac{\partial^2}{\partial z^2} + \frac{\partial^2}{\partial r^2} + \frac{1}{r}\frac{\partial}{\partial r} - \frac{m^2}{r^2}\right)\bar{P}_n^m(\nu)\bar{Q}_n^m(\nu) = 0. \tag{2.90}$$

Note that the first term on the right-hand side of Eq. (2.89) can be transformed as

$$\int_{-\infty}^{0}\frac{\partial^2}{\partial z^2}\bar{P}_n^m(\nu)\bar{Q}_n^m(\nu)dz = \frac{d}{dz}\Big[\bar{P}_n^m(\nu)\bar{Q}_n^m(\nu)\Big]_{z=-\infty}^{z=0} = \frac{1}{\nu K_n^m}\bar{P}_n^m(\nu). \tag{2.91}$$

Equations (2.89) and (2.91) result in a linear ordinary differential equation for $f(r)$.

$$\frac{df}{dr} + \frac{\pm m + 1}{r}f + \frac{1}{\nu K_n^m}\bar{P}_n^m(\nu) = \frac{1}{r^{\pm m+1}}\frac{d}{dr}(r^{\pm m+1}f) + \frac{1}{\nu K_n^m}\bar{P}_n^m(\nu) = 0, \tag{2.92.1}$$

where

$$K_n^m = \frac{2}{\pi}H_n^m = \frac{2}{\pi}\cdot\frac{(n+m-1)!!(n-m-1)!!}{(n+m)!!(n-m)!!}. \tag{2.92.2}$$

Equation (2.92.1) is easy to solve analytically, and $f(r)$ is obtained as

$$f = \frac{1}{\bar{r}^{\pm m+1}}\left\{\int_0^{\bar{r}}\frac{\bar{r}^{\pm m+1}}{\nu K_n^m}\bar{P}_n^m(\nu)d\bar{r} + C\right\}, \tag{2.93}$$

where C is an arbitrary constant. Since $\bar{r} = \sqrt{1-\nu^2}$, Eq. (2.93) can be rearranged as follows upon using $d\bar{r} = \frac{-\nu}{\sqrt{1-\nu^2}}d\nu = -\frac{\nu}{\bar{r}}d\nu$,

$$f = \frac{1}{\bar{r}^{\pm m+1}K_n^m}\left\{\int_0^{\nu}\bar{r}^{\pm m}\bar{P}_n^m(\nu)d\nu + C\right\}. \tag{2.94.1}$$

Especially when $k = 0, m = r+1$,

$$f = \frac{\bar{r}^{m-1}}{K_n^m}\left\{\int_0^{\nu}\bar{r}^{-m}\bar{P}_n^m(\nu)d\nu + C\right\}. \tag{2.94.2}$$

Note that the normalised Legendre function of the first kind satisfies

$$\bar{r}^{-m}\bar{P}_n^m(\nu)=\frac{\rho_n^{m-1}}{\rho_n^m}\cdot\frac{d}{d\nu}\Big[-\bar{r}^{-m+1}\bar{P}_n^{m-1}(\nu)\Big]. \tag{2.95}$$

By Eq. (2.95), Eq. (2.94.1) can be further rearranged as

$$\begin{aligned}
f&=\frac{\bar{r}^{m-1}}{K_n^m}\Big\{\int_0^\nu \bar{r}^{-m}\bar{P}_n^m(\nu)d\nu+C\Big\}\\
&=-\frac{\bar{r}^{m-1}}{K_n^m}\Big[\frac{\rho_n^{m-1}}{\rho_n^m}(1-\nu^2)^{\frac{1-m}{2}}\bar{P}_n^{m-1}(\nu)\Big]_0^\nu+\frac{\bar{r}^{m-1}}{K_n^m}C\\
&=-\frac{1}{K_n^m}\Big[\frac{\rho_n^{m-1}}{\rho_n^m}\bar{P}_n^{m-1}(\nu)-\bar{r}^{m-1}\frac{\rho_n^{m-1}}{\rho_n^m}\bar{P}_n^{m-1}(0)\Big]+\frac{\bar{r}^{m-1}}{K_n^m}C\\
&=\frac{1}{K_n^m}\cdot\frac{\rho_n^{m-1}}{\rho_n^m}\bar{P}_n^{m-1}(\nu),
\end{aligned} \tag{2.96}$$

where the integration constant of C is chosen as $C=\frac{\rho_n^{m-1}}{\rho_n^m}\bar{P}_n^m(0)$ so that $f(0)=0$. Equation (2.88.1) can be thus simply expressed as

$$\Lambda_{jn}^{rm}=-\frac{1}{K_n^m}\cdot\frac{\rho_j^r}{\rho_n^m}\int_0^1\bar{P}_j^r(\nu)\bar{P}_n^r(\nu)d\nu. \tag{2.97}$$

Recall that this is only for the case that $m=r+1$. Equation (2.97) gives the explicit representation of Λ_{jn}^{rm} in accordance with the relation between r,m,j and n:

(i) $n<r,\ \ r+m\equiv 1\ \mathrm{mod}.2;$

$$\begin{aligned}
&\bar{P}_n^r(\nu)\equiv 0, H_n^r\equiv 0,\\
&\therefore\quad \Lambda_{jn}^{rm}=0,
\end{aligned} \tag{2.98.1}$$

(ii) $m>r,\ \ n\geq r,\ \ r+m\equiv 1\ \mathrm{mod}.2;$

$$\Lambda_{jn}^{rm}=(-1)^{\frac{n+j-2r+1}{2}}\frac{\pi}{2}\cdot\frac{H_n^r}{\sqrt{H_n^mH_j^r}}\cdot\frac{\sqrt{(2j+1)(2n+1)}}{(j-n)(n+j+1)}, \tag{2.98.2}$$

(iii) $n \geq r,\ \ m > r,\ \ r+m \equiv 0 \mod 2;$

$$\Lambda_{jn}^{rm} = \delta_{jn}\sqrt{\frac{H_n^r}{H_n^m}}, \tag{2.98.3}$$

(iv) $n < r,\ \ m > r,\ \ r+m \equiv 0 \mod 2;$

$$\Lambda_{jn}^{rm} = (-1)^{\frac{n+j-2r}{2}}\frac{1}{\sqrt{H_n^m H_j^r}}\cdot\frac{(n+r-1)!!(r-n-2)!!}{(n+r)!!(r-n-1)!!}\cdot\frac{\sqrt{(2j+1)(2n+1)}}{(j-n)(n+j+1)}. \tag{2.98.4}$$

2.2.12 The Gain Matrix, L - part 5 -*The Elements in Closed Forms*

Using the results of the previous Subsection, the integrals of Eqs. (2.66.1) - (2.66.3) can be explicitly represented in the following forms[7],

$$[\hat{L}_{jn}^{0m}]^c = (X^m)[\Gamma_{jn}^{0m}], \tag{2.99.1}$$

$$[\hat{L}_{jn}^{rm}]^c = [X^{|r-m|} + (-1)^{min(r,m)}X^{|r+m|}][\Gamma_{jn}^{rm}], \tag{2.99.2}$$

$$[\hat{L}_{jn}^{rm}]^s = [X^{|r-m|} - (-1)^{min(r,m)}X^{|r+m|}][\Gamma_{jn}^{rm}], \tag{2.99.3}$$

where Γ is a function defined as follows,

$$\Gamma_{jn}^{rm} = \sum_{l=r+1}^{\infty} A_{jl}^r \Lambda_{ln}^{rm}. \tag{2.100}$$

Note that Γ takes different values depending on whether $r+m$ is odd or even

(i) $r+m \equiv 0 \mod 2;$

$$\Gamma_{jn}^{rm} = \sqrt{\frac{H_n^r}{H_n^m}}\sum_{l=r+1}^{\infty}\int_0^1 A_{jl}^r \bar{P}_l^r(\nu)\bar{P}_n^r(\nu)d\nu$$

$$= \sqrt{\frac{H_n^r}{H_n^m}}\int_0^1 \nu\bar{P}_j^r(\nu)\bar{P}_n^r(\nu)d\nu$$

$$= \sqrt{\frac{H_n^r}{H_n^m}} A_{jn}^r$$

$$= \frac{(-1)^{\frac{n+j-2r}{2}}}{\sqrt{H_n^m H_j^r}} \cdot \frac{2\sqrt{(2n+1)(2j+1)}}{(n+j)(n+j+2)[(n-j)^2-1]}, \qquad (2.101.1)$$

(ii) $r+m \equiv 0 \mod 1$, $j = n \pm 1$;

$$\Gamma_{jn}^{rm} = \operatorname{sgn}(r-m)\frac{\pi}{2} \cdot \sqrt{\frac{H_n^r}{H_n^m}} \sum_{l=r+1}^{\infty} \int_0^1 A_{jl}^r \bar{P}_l^r(\nu) \bar{P}_n^r(\nu) d\nu$$

$$= \operatorname{sgn}(r-m)\frac{\pi}{2} \cdot \sqrt{\frac{H_n^r}{H_n^m}} \int_0^1 \nu \bar{P}_j^r(\nu) \bar{P}_n^r(\nu) d\nu$$

$$= \operatorname{sgn}(r-m)\frac{\pi}{2} \cdot \sqrt{\frac{H_n^r}{H_n^m}} \left\{ \sqrt{\frac{(n+1+r)(n+1-r)}{(2n+3)(2n+1)}} \int_0^1 \nu \bar{P}_j^r(\nu) \bar{P}_{n+1}^r(\nu) \right.$$

$$\left. + \sqrt{\frac{(n-1)(n+r)}{(2n+1)(2n-1)}} \int_0^1 \nu \bar{P}_j^r(\nu) \bar{P}_{n-1}^r(\nu) d\nu \right\}$$

$$= \operatorname{sgn}(r-m)\frac{\pi}{2} \cdot \sqrt{\frac{H_n^r}{H_n^m}} \left\{ \sqrt{\frac{1}{H_{n+1}^r}} \frac{1}{\sqrt{(2n+1)(2n+3)}} \delta_{j,n+1} \right.$$

$$\left. + \sqrt{\frac{1}{H_{n-1}^r}} \frac{1}{\sqrt{(2n+1)(2n-1)}} \delta_{j,n-1} \right\}$$

$$= \frac{\pi}{2\sqrt{H_n^m H_j^r}} \cdot \frac{\operatorname{sgn}(r-m)}{\sqrt{(2n+1)(2j+1)}} \delta_{j,n\pm1}, \qquad (2.101.2)$$

(iii) $r+m \equiv 1 \mod 2$, $j \neq n \pm 1$;

$$\Gamma_{jn}^{rm} = 0. \qquad (2.101.3)$$

Note that Eqs. (2.101.1) - (2.101.3) indicate that every other element of the gain matrix, whether moving along a row or a column, is zero (i.e. the matrix looks like a chessboard). Note also that the only variable of the gain matrix is the wake skew angle, χ. Some specific examples of Eqs. (2.101.1) - (2.101.3) are shown below, using both χ

and α_e[40],

$$\hat{L}_{11}^{00c} = \frac{3}{2}, \tag{2.102.1}$$

$$\hat{L}_{12}^{01c} = -\frac{2\pi}{\sqrt{10}}\tan\frac{\chi}{2} = -\frac{2\pi}{\sqrt{10}}\sqrt{\frac{1-\sin\alpha_e}{1+\sin\alpha_e}}, \tag{2.102.2}$$

$$\hat{L}_{21}^{10c} = \frac{2\pi}{\sqrt{10}}\tan\frac{\chi}{2} = \frac{2\pi}{\sqrt{10}}\sqrt{\frac{1-\sin\alpha_e}{1+\sin\alpha_e}}\ , \tag{2.102.3}$$

$$\hat{L}_{22}^{11s} = \frac{5}{4}\Big(1+\tan^2\frac{\chi}{2}\Big) = \frac{5}{2(1+\sin\alpha_e)}, \tag{2.102.4}$$

$$\hat{L}_{22}^{11c} = \frac{5}{4}\Big(1-\tan^2\frac{\chi}{2}\Big) = \frac{5\sin\alpha_e}{2(1+\sin\alpha_e)}, \tag{2.102.5}$$

where the following trigonometric formulae are used.

$$\tan^2\frac{\chi}{2} = \frac{1-\cos\chi}{1+\cos\chi} = \frac{1-\sin\alpha_e}{1+\sin\alpha_e}, \tag{2.103.1}$$

$$1+\tan^2\frac{\chi}{2} = \frac{2}{1+\cos\chi} = \frac{2}{1+\sin\alpha_e}, \tag{2.103.2}$$

$$1-\tan^2\frac{\chi}{2} = \frac{2\cos\chi}{1+\cos\chi} = \frac{2\sin\alpha_e}{1+\sin\alpha_e}. \tag{2.103.3}$$

The simplest example of the gain matrix is a 3×3 matrix for the three-state model, which comprised only those elements in which $r=0$, m is either 0 or 1 depending on $r+m \mod 2$, and $j=r+1,\ n=m+1$.

$$\begin{pmatrix} M_{11}^{00} & 0 & 0 \\ 0 & M_{22}^{11} & 0 \\ 0 & 0 & M_{22}^{11} \end{pmatrix} \begin{pmatrix} \dot{a}_1^{0c} \\ \dot{b}_2^{1s} \\ \dot{a}_2^{1c} \end{pmatrix} + \begin{pmatrix} L_{11}^{00c} & 0 & L_{12}^{01c} \\ 0 & L_{22}^{11s} & 0 \\ L_{21}^{10c} & 0 & L_{22}^{11c} \end{pmatrix}^{-1} V \begin{pmatrix} a_1^{0c} \\ b_2^{1s} \\ a_2^{1c} \end{pmatrix} = \begin{pmatrix} \tau_1^{0c(t)} \\ \tau_2^{1s(t)} \\ \tau_2^{1c(t)} \end{pmatrix} + \begin{pmatrix} \tau_1^{0c(c)} \\ \tau_2^{1s(c)} \\ \tau_2^{1c(c)} \end{pmatrix} = \begin{pmatrix} \tau_1^{0c} \\ \tau_2^{1s} \\ \tau_2^{1c} \end{pmatrix}. \tag{2.104}$$

[40] In Ref. (28), the effective angle of attack, $\alpha_e = \frac{\pi}{2} - \chi = \tan^{-1}\left|\frac{\lambda}{\mu}\right|$, is used instead of χ in the representation of the gain matrix. Unless reference is made to Eqs. (2.103.1) - (2.103.3), it may appear that the gain matrix for Chen's model has quite different entries from those in which the wake skew angle is used. He also recommended in Ref. (7) that the effective angle of attack should be used instead of the wake skew angle in relation to Peters and HaQuang's non-linear model, but the reason is not therein stated. This author believes that the difference is not mathematically essential so far as Eqs. (2.103.1) - (2.103.3) are valid.

In Eq. (2.104), τ_1^{0c}, τ_2^{1s} and τ_2^{1c} should be associated with an appropriate lift theory. References (7), (37), (92) and (112) describe some examples of the possible lift theories.

2.3 The Pitt and Peters model

The Pitt and Peters model[(1)] is a predecessor to the Peters and He model, but is still arguably one of the most popular dynamic inflow models widely used today. Although these two models look similar at a glance, the mathematical derivation and the resultant matrices are quite different, and the relation between these two models has not been fully explained in the pertinent literature. Reference (101) should be a rare reference which shows that the Pitt and Peter model forms a special case of the Peters and He model for axial flight cases, but for other flight scenarios between these two models has not been fully theoretically elucidated, and the correlation was shown only experimentally[41].

In this Section, the relation between the Pitt and Peters model and the Peters and He model shall be theoretically examined aiming to make clear the connection between the two models.

2.3.1 The Apparent Mass Matrix, M

The main difference between the two models lies in the fact that while in the Peters and He model the induced flow is associated with lift coefficients, τ_n^m, in the Pitt and Peters model, the induced flow is associated with rotor loadings, C_T, C_M and C_L.

The thrust coefficient is defined as

$$C_T \equiv \iint \Phi d\bar{A} \Big|_{\eta=0, \nu=\sqrt{1-\bar{r}^2}}, \tag{2.105}$$

where

$$\Phi(\nu,\eta,\psi,\bar{t}) = \sum_{m=0}^{\infty} \sum_{n=m+1,m+3,\ldots}^{\infty} P_n^m(\nu) Q_n^m(i\eta) \Big[C_n^m(\bar{t}) \cos(m\psi) + D_n^m(\bar{t}) \sin(m\psi) \Big]. \tag{2.106}$$

Since those terms in which $m \neq 0$ will be zero when integrated over $[0, 2\pi]$ with respect to ψ, Eq. (2.105) simply results in

---

41 The Pitt and Peters model was seldom theoretically compared with the Peters and He model, in a published paper available, despite other wake models were compared with the Peters and He model to validate the model[(92)]. In fact, References (63) and (101) are only references, to the best knowledge of the present author, in which the relationship between these two models is discussed. However, the discussion is limited to an experimental result, and the mathematical relationship is not clarified at all.

$$C_T = \iint \Phi d\bar{A}$$

$$= \frac{1}{\pi}\int_0^{2\pi}\int_0^1 \left\{ \bar{r}\sqrt{1-\bar{r}^2}\,C_1^0 - \frac{1}{3}\bar{r}\sqrt{1-\bar{r}^2}\,(2-5\bar{r}^2)C_3^0 - \ldots \right) d\bar{r}d\psi$$

$$= \frac{4}{3}C_1^0. \qquad (2.107)$$

Note that as long as Eq. (2.107) is satisfied, any distribution of C_T will suffice because all terms which contain C_k^0 for $k \geq 3$ will vanish when integrated over $[0,1]$ with regard to $\bar{r}$. Thus, C_k^0 $(k \geq 3)$ should be determined by extra boundary conditions on the rotor pressure when necessary. Figure 2-7 shows two examples of the possible pressure distribution where Eq. (2.107) is satisfied[42]: the top diagram is of the simplest case where only C_1^0 term is considered and thus $\Phi = \sqrt{1-\bar{r}^2}$; and the bottom is the next simplest case where C_1^0 and C_3^0 terms are considered with an additional boundary condition that the pressure should be zero at the hub centre, $\Phi = 0\,\big|_{\bar{r}=0}$, i.e. $\Phi = \frac{5}{2}\bar{r}^2\sqrt{1-\bar{r}^2}$.

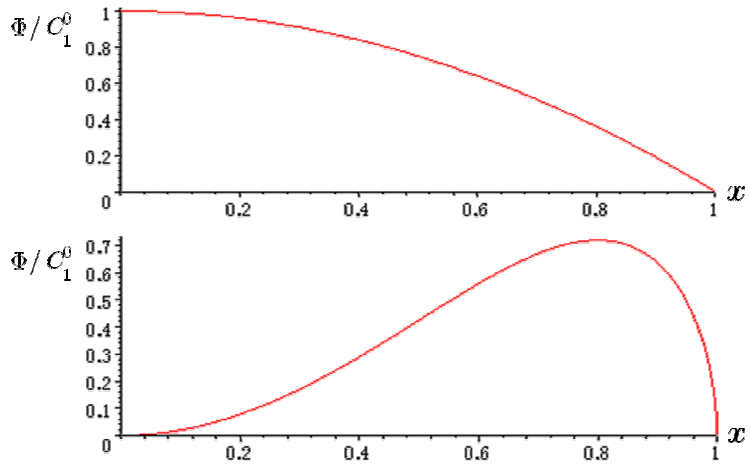

Fig .2-7 [Lift distributions on a blade described by the associated Legendre function; the first and second harmonics.]

[42] The Pitt and Peters model is fundamentally based on actuator disc theory and momentum theory. Both actuator disc theory and momentum theory are independent of detailed rotor information such as number of blades, planform of blades, airfoil and the 3-dimensional pressure distribution on the blades. What is required in the Pitt and Peters model is thus only the mean value of the pressure working on the rotor, and this gives a variety of possible pressure distributions, so far as they give the same hub loadings.

On the other hand, C_T is related to τ_n^m as follows,

$$\begin{aligned} C_T &\equiv \frac{1}{\pi}\int_A L d\bar{A} = \frac{1}{\pi}\int_0^{2\pi}\int_0^1 \bar{P}_1^0(\nu)\tau_1^{0c}(\bar{t})\bar{r}d\bar{r}d\psi \\ &= \frac{1}{\pi}\int_0^{2\pi}\int_0^1 \sqrt{3}\, r\sqrt{1-r^2}\, d\bar{r}d\psi \cdot \tau_1^{0c}(\bar{t}) \\ &= \frac{2}{\sqrt{3}}\tau_1^{0c}. \end{aligned} \tag{2.108}$$

Regarding the definition of lift coefficients of higher harmonics (i.e. roll and pitch moments), Mangler suggested the following form[5,48],

$$L(\bar{r},\psi) = \frac{1}{2}C_0 + C_L\sin\psi + C_M\cos\psi + C_{2L}\sin 2\psi + C_{2M}\cos 2\psi + \cdots. \tag{2.109}$$

However, Peters did not mention in the literature the factor of $1/2$ appearing in the first term. It is thus reasonable to assume that the lift coefficients of Pitt and Peters model are defined as follows,

$$L(\bar{r},\psi) = C_0 + 2(C_L\sin\psi + C_M\cos\psi + C_{2L}\sin 2\psi + C_{2M}\cos 2\psi + \cdots). \tag{2.110}$$

Note that the difference in the definition is of course minor, having no influence on results so long appropriate attention is paid to these factors[43]. Coefficients C_L and C_M can be associated with lift coefficients, τ_2^{1s} and τ_2^{1c}, respectively[44],

[43] Reference (37) does not have a clear definition of lift coefficients, while Reference (1) has a typographical error in the calculation of the lift coefficients. At least in those studies of Peters that appear in the bibliography of this thesis, the lift coefficients are not explicitly defined. There are some other variations in the definition[27][86], and this situation should confuse readers.

[44] Higher harmonics can be defined and determined in the same manner when required. Examples include $C_{2L} \equiv \frac{1}{\pi}\int_A L(-r^2\sin 2\Psi)d\bar{A} - \frac{8}{\sqrt{105}}\tau_3^{2s}(t)$ and $C_{2M} \equiv \frac{1}{\pi}\int_A L(-r^2\cos 2\Psi)d\bar{A} = -\frac{8}{\sqrt{105}}\tau_3^{2c}(t)$.

$$C_L \equiv \frac{4}{\pi}\int_A L(\bar{r},\psi)(-\,\bar{r}\sin\psi)d\bar{A}$$
$$= -\frac{4}{\pi}\int_0^{2\pi}\int_0^1 \bar{P}_2^1(\nu)\tau_2^{1s}(\bar{t})r^2\sin^2\psi d\bar{r}d\psi$$
$$= -\frac{8}{\sqrt{15}}\tau_2^{1s}(\bar{t}), \tag{2.111}$$

$$C_M \equiv \frac{4}{\pi}\int_A L(\bar{r},\psi)(-\,\bar{r}\cos\psi)d\bar{A}$$
$$= -\frac{4}{\pi}\int_0^{2\pi}\int_0^1 \bar{P}_2^1(\nu)\tau_2^{1c}(\bar{t})\bar{r}^2\cos^2\psi d\bar{r}d\psi$$
$$= -\frac{8}{\sqrt{15}}\tau_2^{1c}(\bar{t}). \tag{2.112}$$

In the Pitt and Peters model, the induced flow is also considered in the following form,

$$w = \lambda_0 + \lambda_{1s}r\sin\psi + \lambda_{1c}r\cos\psi + \lambda_{2s}r^2\sin 2\psi + \lambda_{2c}r^2\cos 2\psi + \cdots. \tag{2.113}$$

Equating Eqs. (2.113), (2.22) and Eq. (2.36) yields

$$\lambda_0 \equiv \frac{1}{\pi}\int_A w dA = \sqrt{3}\,\alpha_1^0(\bar{t}), \tag{2.114}$$
$$\lambda_{1s} \equiv \frac{4}{\pi}\int_A w(\bar{r}\sin\psi)dA = -\,2\sqrt{15}\,\beta_2^1(\bar{t}), \tag{2.115}$$
$$\lambda_{1c} \equiv \frac{4}{\pi}\int_A w(\bar{r}\sin\psi)dA = -\,2\sqrt{15}\,\alpha_2^1(\bar{t}). \tag{2.116}$$

Thus,

$$\begin{pmatrix} \frac{4}{\pi} & 0 & 0 \\ 0 & \frac{8}{3\pi} & 0 \\ 0 & 0 & \frac{8}{3\pi} \end{pmatrix} \begin{pmatrix} \dot{a}_1^{0c} \\ \dot{b}_2^{1s} \\ \dot{a}_s^{1c} \end{pmatrix} = \begin{pmatrix} \tau_1^{0c(t)} \\ \tau_2^{1s(t)} \\ \tau_s^{1c(t)} \end{pmatrix} \quad \Leftrightarrow \quad \begin{pmatrix} \frac{8}{3\pi} & 0 & 0 \\ 0 & \frac{16}{45\pi} & 0 \\ 0 & 0 & \frac{16}{45\pi} \end{pmatrix} \begin{pmatrix} \dot{\lambda}_0 \\ \dot{\lambda}_{s1} \\ \dot{\lambda}_{c1} \end{pmatrix} = \begin{pmatrix} C_T \\ C_L \\ C_M \end{pmatrix}. \tag{2.117}$$

The matrix appearing on the right-hand side of Eq. (2.117) is well-known as the apparent mass matrix in the Pitt and Peters model[(1)45.] It is thus confirmed that the apparent mass matrix in the Pitt and Peters model is consistently and hierarchically implied as a special case of the Peters and He model.

2.3.2 The Gain Matrix, L

For the gain matrix, Eq. (2.25) is assumed to represent the inflow distribution in the previous discussion. For a special flight case where $\frac{\partial}{\partial \bar{t}} = 0$ (steady) and $z = -\xi$ (axial flight), Eq. (2.15) results in a simple forms,

$$\Phi^{(t)} = 0, \tag{2.118}$$

$$\Phi = \Phi^{(c)}, \tag{2.119}$$

$$w \equiv \frac{1}{V}\int_{\infty}^{0} \frac{\partial \Phi^{(c)}}{\partial z} d\xi = -\frac{1}{V}\Phi \Big|_{\eta=0}. \tag{2.120}$$

From Eqs. (2.6.1) and (2.120),

$$\begin{aligned}
\lambda_0 &= \frac{1}{\pi}\int_0^{2\pi}\int_0^1 w\bar{r}d\bar{r}d\psi \\
&= \frac{1}{2\pi V}\int_0^{2\pi}\int_0^1 \sum_{m=0}^{\infty}\sum_{n=m+1,m+3,\ldots}^{\infty} \bar{P}_n^m(\nu)\bar{Q}_n^m(0)\left[\tau_n^{mcc}(\bar{t})\cos(m\psi) + \tau_n^{msc}(\bar{t})\sin(m\psi)\right]\bar{r}d\bar{r}d\psi \\
&= \frac{1}{V}\int_0^1 \sum_{n=1,3,5,\ldots}^{\infty} \bar{P}_n^0(\nu)\bar{r}d\bar{r}\cdot\zeta_n^{0c(c)}(\bar{t}).
\end{aligned} \tag{2.121}$$

Especially for $n = 1$,

$$\lambda_0 = \frac{1}{V}\int_0^1 \bar{P}_1(\nu)\bar{r}d\bar{r}\cdot\tau_1^{0c(c)}(\bar{t}) = \frac{1}{2V}\cdot\zeta_1^{0c(c)}. \tag{2.122}$$

Indeed, the proportionality coefficient obtained from Eq. (2.122), $1/2$, agrees with the L_{11} entry of the gain matrix in the Pitt and Peters model. This result also agrees with the relation between C_T, V_T (the non-dimensionalised total flow at the rotor plane) and λ_0 for a steady axial flight case, in which they can be simply obtained from momentum theory, Eq. (2.123), if replacing V and $\zeta_1^{0c(c)}$ in Eq. (2.122) with V_T and C_T, respectively,

[45] In some references such as Ref. (107), a matrix having $-16/45\pi$ for the $(2,2)$ and $(3,3)$ entries is introduced as the apparent mass matrix of the Pitt and Peters model. This difference in the sign is caused by a difference in the definitions of C_L and C_M.

$$C_T = 2V_T\lambda_0, \tag{2.123}$$

This is not an unexpected coincidence because steady axial flight is presupposed in the Pitt and Peters model to determine the L_{11} entry. However, the L_{11} entry of the gain matrix obtained from Eq. (2.122) should not be adopted as it is in the unified model, because the induced flow in Eq. (2.122) is represented by the Fourier coefficient of ζ, which is different from α and β in the previous Subsection.

In Ref. (1), the Pitt and Peters model was derived by determining each element of the apparent mass and gain matrices by presupposing a specialised flight case, such as steady axial or edgewise flight. Those entries are collected together into the matrices at the final stage(1), but the necessary transformation for unifying the model (recall Subsection 2.2.6) is arguably lacking in the derivation, resulting in a model in which vectors (α, β) and (ζ, ϖ) are mixedly used to represent the same induced flow distribution.

Whereas some flight cases which are dominated by either $\Phi^{(c)}$ or $\Phi^{(t)}$ alone (i.e. only one of (α, β) or (ζ, ϖ) is therein dominant and the other is negligible) may be practically described well by the Pitt and Peters model, this author therefore doubts for the reason above that there is a problem with the representation of the inflow components in the Pitt and Peters model.

2.4 The Mass-flow Parameter and Non-linear Versions

The flow parameter in the Peters and He model, V, can be the non-dimensionalised freestream speed, V_∞. However, it is better to account for energy *added* to the flow from the rotor in order to describe the induced flow in the wake, and Ref. (1) recommends to replace V with the mass-flow parameter, V_m, which is defined as

$$V_m = \frac{\mu^2 + \lambda(\lambda + \lambda_m)}{\sqrt{\mu^2 + \lambda^2}} = \frac{\mu^2 + \lambda(\lambda + \lambda_m)}{V_T}, \tag{2.124}$$

where μ, λ and λ_m are advance ratio, the total inflow, inflow due to the rotor thrust, respectively. Figure 2-8 shows the relation between these parameters.

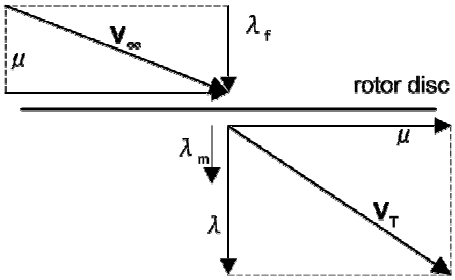

Fig. 2-8 [Inflow components in the wind axes.]

Note that these parameters are defined in the wind axes. In Fig. 2-8, λ_f is the normal component of V_∞ and satisfies

$$\lambda = \lambda_f + \lambda_m. \tag{2.125}$$

In a steady case, λ_m is simply given by momentum theory and is equal to the uniform component of the induced flow[1,92],

$$\lambda_m = \frac{C_T}{2V_T} = \lambda_0. \tag{2.126}$$

However, in an unsteady case, λ_m does not generally coincides with λ_0, and is defined by the first row of the gain matrix as[107]

$$\lambda_m = \frac{1}{2}(1,0,0)\begin{bmatrix} \\ L \\ \\ \end{bmatrix}^{-1}\begin{pmatrix} \lambda_0 \\ \lambda_{1s} \\ \lambda_{1c} \end{pmatrix}. \tag{2.127}$$

With regard to the flow parameter, Peters and HaQuang proposed an extended version for the Pitt and Peters model[107], which is obtained by the following process:

i. swapping the flow parameter, V, with the *mass-flow parameter matrix,*

$$V \mapsto \begin{pmatrix} V_T & 0 & 0 \\ 0 & V_m & 0 \\ 0 & 0 & V_m \end{pmatrix}; \tag{2.128}$$

ii. treating all variables as total flow rather than perturbation.

Due to the non-linearity between the mass-flow parameters and inflow components, this model is called the *non-linear version of the Pitt and Peters model* or *Peters and*

HaQuang's non-linear model.

This modification should give a better description of induced flow, because the thrust is more directly related to the total inflow and the induced velocity based on momentum theory than the roll and pitch moments are. The roll and pitch moments are more sensitive to the variation in the inflow, and this is indeed the case with this formulation[46]. The process (ii) above is done by integrating the perturbation version of Pitt and Peters model over the rotor disc.

The Peters and He model can also be extended to its non-linear version by replacing the flow parameter with the mass-flow parameter matrix, in which λ_m is defined as

$$\lambda_m = \frac{2}{\sqrt{3}}(1,0,0,...,0)\left[\ \hat{L}_{jn}^{rmc}\ \right]^{-1}\left(a_n^m\right). \tag{2.129}$$

This relation can be derived from Eq. (2.108), (2.126) and

$$\lambda_0 \simeq \sqrt{3}\,\bar{a}_1^0 \tag{2.130}$$

where $\bar{a}_1^0$ is the steady uniform induced flow[(1,7)]. This approximation is introduced in Ref. (7). The non-linear version of Pitt and Peters model is verified in Refs. (62) and (102). The non-linear version of the Peters and He model is verified in Refs. (7), (92) and (112) and is widely used today.

The present author has no objection to the validity of those non-linear models at all, but is of the personal opinion that the naming of "non-linear" might be misleading; in the context of fluid mechanics, the term of non-linearity is usually associated with the convection term in the Euler equations or the Navier-Stokes equations. The non-linear dynamic inflow models are not fully non-linear in this sense, because the derivation of the model essentially depends on the linearised Euler equations. (The process of non-linearisation is always a process of deleting infinitesimal variables of higher orders, and it is impossible to recover those deleted terms at a later stage.) The non-linearity in the non-linear dynamic inflow models indicates only the non-linear relationships

[46] Reference (71) discusses in its Section 10-6 why a different flow parameter for rotor moments than that for the rotor thrust is required for unsteady flight cases.

between flow parameters and rotor forces considering momentum theory, and thus this appellation may be confusing.

2.5 Discussion

In this Chapter, the Peters and He model was thoroughly reviewed in detail. In order to explore the possibility of applying the dynamic inflow model to autorotative rotors, a comprehensive examination of the theoretical derivation of the theory from the first principles is essential together with the consideration of the assumptions therein used.

In the course of examining the derivation of the model, the assumptions upon which the Peters and He model is based, (A1) - (C2), are clearly identified in this Chapter.

Among these assumptions, the small wake skew angle assumption, (C2), is arguably the most objectionable because the wake skew angle can be quite large in forward flight, and indeed, the Peters and He model was intended to be used for a wide range of wake skew angles from $0°$ to $90°$. Since the assumption forms a fundamental step of the derivation, this should be considered as a contradiction, and hence lucid explanation must be made concerning its validity. Unfortunately, the literature suggests no answer to this contradiction. The present author shall discuss this problem in Chapter 4 in depth.

With reference to past studies, it appears that the present thesis is the first study to consider the mathematical relation between the Pitt and Peters model and the Peters and He model. The present Chapter casts some doubt over whether the Peters and He model hierarchically includes the Pitt and Peters model. It may be premature to make a conclusive remark about this matter because this is a type of problem which needs to be concluded through a plural of more concrete proofs by authorities including the original authors. It is hoped that this thesis would provoke further discussion of this issue.

2.6 Chapter Summary

This Chapter was written with the objective of providing a sound theoretical basis for the subsequent Chapters of this thesis. Chapters 3 and 4 are essentially based on the theoretical considerations of this Chapter, and thus it is believed that the objective above is attained.

This Chapter can be summarised as follows:

1. The derivation of Peters and He model has been thoroughly re-examined;
2. All assumptions which are used in the derivation have been clearly identified;
3. The limitations of these assumptions and possible modifications have been considered;
4. The Pitt and Peters model has been reviewed in relation to the Peters and He model, with some doubt cast on the statement in Ref. (102) that the Peters and He model hierarchically includes the Pitt and Peters model;
5. The logical inconsistency of the small wake skew angle assumption has been described.

Chapter 3

Dynamic Inflow Modelling for Autorotative Rotors

N.b.) The content of this Chapter is shortened and published as Ref. (168).

3.1 Introduction

In the history of the development of dynamic inflow modelling, scant attention has been paid so far in analysing autorotative rotors. References. (9), (10) and (151) may be recherché examples in which the Pitt and Peters model is used for rotors in the windmill-brake state. Still, little theoretical attention as to the applicability of the model was paid.

Important theoretical attempts recently made to extend the dynamic inflow model include Refs. (169) and (170), in which the original model was enhanced to cover the vortex-ring and windmill-brake states. Although Refs. (169) and (170) are mainly focused on the vortex ring state and its smooth transition in the context of helicopter applications, such theoretical works should also be of great importance for gyroplane engineers.

The aim of this Chapter is to identify a necessary modification to the dynamic inflow model when applied to an autorotative rotor through reviewing the derivation of dynamic inflow model from the first principles. Whereas the Peters & He or Pitt and Peters model is kept in mind as a specific example in the following Sections, the essence of the discussion is not limited to any particular model, but can be applied for other variations of dynamic inflow models in general. Results of numerical simulations are also presented to compare the original and modified models.

3.2 The Applicability of the Dynamic Inflow Model to an Autorotative Rotor

3.2.1 Examination on Matrix Elements of Dynamic Inflow Models

There is a major geometric difference between a powered helicopter rotor and an autorotating rotor:

(D1) the free stream is coming toward an autorotating rotor from below, while it is coming from above to a rotor in normal working state (see Fig. 2-3).

Although the terms of *the normal working state* and *the windmill-brake state* are already used in Chapter 1 to describe the rotor states of the helicopter and the gyroplane, they need to be given more strict definitions here; the state in which a rotor is receiving the incoming flow from below is hereinafter referred to as the windmill-brake state, and the state in which a rotor is receiving the inflow from above is referred to as the normal working state following Ref. (5)[47]. Point (D1) above can be considered as a fundamental geometric dissimilitude between windmill-brake and normal working states, and how the difference in the underlying configuration is reflected on the equations of the dynamic inflow model is to be discussed in this Chapter. As was seen in Chapter 2, the entire derivation of Peters and He's dynamic inflow model is highly mathematical and complicated though, it is not necessary to trace each and every line of the derivation to examine the applicability of the model for autorotative rotors. What are required to discuss point (D1) above are only the base equations, viz., the linearised Euler equations,

$$\frac{\partial \mathbf{q}}{\partial t} - V\nabla \mathbf{q} = -\nabla \Phi, \tag{3.1}$$

in which the flow components, $\mathbf{q}$, are defined along a streamline coordinate, ξ, whose positive direction is defined to be upstream. The reason why the second term on the left-hand side has the sign of minus is that the direction of V is defined to be opposite

[47] The definition of these geometric attitudes of a rotor towards the inflow should be independent of whether or not the rotor speed is mechanically retained constant. However, the normal working state conventionally implies that the rotor is governed by an engine, and the wind-mill brake state implies that the rotor is not mechanically driven. Indeed, the fact that an autorotative rotor is not mechanically driven is another major difference from an powered helicopter rotor, but the DOF in the rotor speed can be implemented in a mathematical model with regard to blade dynamics (see Fig. 1-2), and thus any change in the rotor speed can be calculated in the loop in a quasi-steady manner. Thus, this thesis does not pay special attention to the extra DOF in the rotor speed of an autorotative rotor.

to the positive direction of ξ-axis. Since this is the case both for the normal working and windmill-brake states by definition (see figure 2-2 about this comparison between two states of a rotor easier), the left hand side of Eq. (3.1) holds the same for both rotor states in the vector form.

When focusing only on the z-components of Eq. (3.1), it can be noticed that (i) the direction of lift against the free stream is different as is shown in Fig. 2-2, and (ii) the direction of the z-axis and the induced flow in the windmill-brake state are opposite to those in the normal working state. (Figure 2-2 is obtained by re-drawing Fig. 2-3 so that the rotor plane should be put horizontally and that the free stream should come from the upper left side of the rotor in the diagram.) The derivation of dynamic inflow models are based on the z-component of the linearised Euler equation, thus the model for the windmill-brake state needs to change the signs of both $\mathbf{q}$ and Φ in Eq. (3.1). This leads to the identical form with that for the normal working state, and therefore it can be ascertained that each element of the matrices in a dynamic inflow model holds the same both for normal working and windmill-brake states.

Note that the discussion above is not limited only to the Peters and He model, but also to other models such as the Pitt and Peters model as long as their derivations are based on the linearised Euler equations.

3.2.2 Definitions of the Wake Skew Angle

In Fig. 2-2, the wake skew angle, χ, is defined as follows for both normal working and windmill-brake states[37],

$$\chi = \tan^{-1}\left|\frac{\mu}{\lambda}\right|. \tag{3.2}$$

Note that although the general matrix representation of a dynamic inflow model remains the same, the direction of such parameters as α and χ must be different because of the difference in the direction of inflow towards the z-axis of the airframe (see Fig. 2-2).

When applying a dynamic inflow model to the windmill-brake state, it may happen that one would misinterpret the inflow angle, α, should be in the range from 90° to 180° for the windmill-brake state unless the definition of α is changed. As a matter of

fact, Chen introduced a different definition of χ from Eq. (3.2) in that it does not have the modulus[28], and thus according to this definition, the rotor angle of attack, α, should be in the range from 90° to 180° for the windmill-brake.

Chen's definition may look versatile at a glance, because the model could be used both for normal working and windmill-brake states without any changes in the definition so that angles of $0^\circ \le \chi \le 90^\circ$ and angles of $90^\circ \le \chi \le 180^\circ$ therein indicate the normal working and windmill-brake states, respectively. However, Chen's definition would entail unfavourable divergences of some gain matrix elements which contain $\tan(\chi/2)$ to ∞ at $\chi = 180^\circ$. Still, that χ equals 180° means axial descent cases in the windmill-brake state, which is practically quite a possible operational state for gyroplanes, and thus the unfavourable divergence has been a problem with dynamic inflow modelling when applying Chen's formulation to autorotative rotors.

Intuitively, the windmill-brake state can be regarded upside-down to the normal working state (Fig. 2-2), and thus α and χ must be defined so as to come in the range of 0° and 90° for both states. The modulus sign in the definition should not be dropped off for this reason.

3.2.3 Examination on the Mass-flow Parameter

Now the mass-flow parameter should be examined. The flow parameter V is recommended to be replaced with V_m in order to account for energy added in the wake by the rotor[1,7,66,92]. The added energy can also be interpreted as the acceleration of inflow and the contraction of the wake tube in the normal working state. The mass-flow parameter defined for the normal working state is to be referred to as V_{m+} hereinafter,

$$\begin{aligned} V_{m+} &\equiv V_T + \lambda_m \frac{\partial V_T}{\partial \lambda_m} \\ &= \frac{\mu^2 + (\lambda_f + \lambda_m)(\lambda_f + 2\lambda_m)}{V_T} = \frac{\mu^2 + \lambda(\lambda + \lambda_m)}{\sqrt{\mu^2 + \lambda^2}}, \end{aligned} \tag{3.3}$$

where the definition of λ_m is given as Eq. (2.127).

However, the definition of V_m should be changed for the windmill-brake state, because a rotor in the wind-mill brake state is not adding but receiving energy from the

free stream (this can be interpreted as the deceleration of inflow or the expansion of the wake tube). This shall be reflected upon the sign of the second term of Eq. (3.3), and so the mass-flow parameter for the wind-mill brake state should be defined as

$$V_{m-} \equiv V_T - \lambda_m \frac{\partial V_T}{\partial \lambda_m}$$
$$= \frac{\mu^2 + (\lambda_f + \lambda_m)\lambda_f}{V_T} = \frac{\mu^2 + \lambda(\lambda - \lambda_m)}{\sqrt{\mu^2 + \lambda^2}}. \tag{3.4}$$

The V_m defined for the windmill-brake state in this manner is to be referred to as V_{m-} hereinafter.

In Eqs. (3.3) and (3.4), λ can consistently be defined as

$$\lambda = \lambda_f + \lambda_m, \tag{3.5}$$

where $\lambda_m < 0$ for the windmill-brake state and $\lambda_m > 0$ for the normal working state. The difference in the sign of λ_m is the reflection of the geometric difference between the two states. The following equations are intuitively evident from Fig. 2-2,

$$|\lambda| = |\lambda_f| + |\lambda_m|, \qquad \text{(for the normal working state)} \tag{3.6}$$

$$|\lambda| = ||\lambda_f| - |\lambda_m||. \qquad \text{(for the windmill-brake state)} \tag{3.7}$$

Note that the difference between V_{m+} and V_{m-} is not naturally accommodated in the definition of V_m because the difference is the reflection of the physical difference in those two rotor states in terms of the energy flow, and thus this is independent of the choice of coordinate system[48].

3.2.4 Unified form of V_{m+} and V_{m-}

The necessity of separating V_m into V_{m+} and V_{m-} can be more mathematically enunciated than the physical and rather intuitive discussion in the previous Subsection. Differentiating $V_T^2 = \mu^2 + \lambda^2 = \mu^2 + (\lambda_f + \lambda_m)^2$ with respect to λ_m yields

[48] If the sign of λ_m alone is changed, V_{m+} and V_{m-} will mutually invert to each other. This can intuitively interpreted as the reflection of the fact that a rotor in the windmill-brake state can be regarded upside-down to a rotor in the normal working state. An error in the definition of λ_m would lead to wrongly swapping V_{m+} and V_{m-}.

$$\frac{\partial V_T}{\partial \lambda_m} = \frac{\lambda}{V_T} = \cos\chi \tag{3.8}$$

for the normal working state. Especially when in high-speed forward flight,

$$\cos\chi \simeq \sin\alpha \simeq \tan\alpha. \tag{3.9}$$

Note that $\tan\alpha$ should be always positive due to the modulus sign in Eq. (3.2), and thus λ/V_T in Eq. (3.9) is also required to be positive. When in the normal working state, this is indeed the case because $V_T > 0$ and $\lambda > 0$. However, $\lambda < 0$ when in autorotation. Hence, this further requires that $\cos\chi$ should be defined as $|\lambda|/V_T$ in order to be consistent with Eq. (3.2), if it is supposed to cover both the normal working and windmill-brake states. Indeed, the minus sign on the right-hand side of Eq. (3.4) is equivalent to the modulus sign in effect.

In fact, V_{m+} and V_{m-} can be unified by using modulus sign as

$$V_{m\pm} \equiv V_T \pm \lambda_m \frac{\partial V_T}{\partial \lambda_m} = \frac{\mu^2 + \lambda^2 + \lambda_m|\lambda|}{V_T}. \tag{3.10}$$

Equation (3.10) can consistently be used both in the normal working and windmill-brake states and is consistent with Eq. (3.2). In Ref. (104), Peters defined $\tan\alpha$ (Eq. (19), p.66) and reads, "α is always positive, whether the flow is from above or below". As discussed above, the mass-flow parameter should be defined as Eq. (3.10) to be consistent with Peters' own definition of $\tan\alpha$, Eq. (3.2)[49]. Further discussion about this issue shall be held in Appendix 3.1.

3.3 Numerical Simulation

The difference between V_{m+} and V_{m-} came from rather an elementary and intuitive discussion, but this would appear to be the first time that the difference has been explicitly highlighted in relation to the dynamic inflow model. The comparison of V_{m+} and V_{m-} is conducted by numerical simulation using a generic rotorcraft simulation code RASCAL at the University of Glasgow, which was already used for some studies[9,10,151,154,155], and whose validation was evident in Ref. (152). The non-linear version of Pitt and Peters model is used in the simulation model to describe the induced

[49] The mass-flow parameter, V_m, first appeared in Ref. (66) and has been used in dynamic inflow models of Peters. However, its mathematical derivation is not elucidated in published papers.

velocity field, and local aerodynamic loads on a blade can be thereby given through blade element approach. It should be acknowledged that the algorithms are implemented in RASCAL by Dr. Stewart Houston at the University of Glasgow.

On the other hand, inertial loads are therein described by the Euler equations of rigid body as below.

$$I_{flap}(\dot{\omega}_x - \omega_y\omega_z) - my_{cg}a_z^{hinge} = M_{flap}, \tag{3.11}$$

$$I_{pitch}(\dot{\omega}_y - \omega_x\omega_z) = M_{pitch}, \tag{3.12}$$

$$I_{lag}(\dot{\omega}_z - \omega_x\omega_y) - my_{cg}a_x^{hinge} = M_{lag}, \tag{3.13}$$

where blades are considered rigid. Reference (152) is to be referred about the detailed derivation of $\omega_x, \omega_y, \omega_z$, a_x^{hinge} and a_z^{hinge}.

The rotor forces and moments in the airframe coordinate system are represented by the integration of those moments and lift on each blade element. Using transform matrices, $[T_1], [T_2]$ and $[T_3]$, from blade element coordinate system to the airframe one, rotor loads and moments can be written as

$$\mathbf{X} = [T_1]^{-1} \sum_{j=1}^{b} \Big[[T_2]^{-1}[T_3]^{-1} \Big(\sum_{i=1}^{b} \mathbf{X}_{elem} \Big) \Big], \tag{3.14}$$

$$\mathbf{L} = [T_1]^{-1} \sum_{j=1}^{b} \Big[[T_2]^{-1} r_{hinge} \bar{r} [T_3]^{-1} \Big(\sum_{i=1}^{b} \mathbf{X}_{elem} \Big) \Big] + (r_{hub} - r_{cg}) \bar{r} \mathbf{X}, \tag{3.15}$$

where $\mathbf{X}_{elem} = \mathbf{X}_{elem}^{aero} + \mathbf{X}_{elem}^{inert}$. See Appendix 3.2 about further details of these transformation matrices and the derivation of Eqs. (3.14) and (3.15). Based on those aerodynamic and inertial forces and moments, the control inputs vector, $\mathbf{u}$, and state vector, $\mathbf{x}$, are expressed in the state-space form,

$$\frac{d\mathbf{x}}{dt} = [A]\mathbf{x} + [B]\mathbf{u}, \tag{3.16}$$

where

$$\mathbf{x} = {}^t(u, v, w, p, q, r, \phi, \theta, \psi, \Omega), \tag{3.17}$$

or

$$\mathbf{x} = {}^t(u, v, w, p, q, r, \phi, \theta, \psi, \Omega, v_0, v_{1s}, v_{1c}), \tag{3.18}$$

wherein $\mathbf{u} =^{t} (\delta_r, \eta_s, \eta_c, \Omega_p)$ for gyroplanes[50]. Note that the model can be linearised either in the classical 7 DOF rigid-body form with Eq. (3.17) when the inflow dynamics are effectively treated quasi-statically, or linearised in 10 DOF form with Eq. (3.18) to encapsulate inflow dynamics. In either case, Eqs. (3.11), (3.12) and (3.13) form a closed loop together with the dynamic inflow model. (Recall Fig. 1-2.)

Equation (3.16) comprises nearly one hundred non-linear ordinary equations, though the exact number depends on several parameters including the number of blades. The set of simultaneous differential equations is to be numerically solved by the Runge-Kutta method in RASCAL. Further detail about the code can be found in Refs. (34) and (152). Stability and natural response characteristics of a state described by Eq. (3.16) can be studied by the eigenvalues of the state matrix, $[A]$. When the real part of an eigenvalue is positive, the state (mode) is unstable. Likewise, when negative, then stable. The imaginary part of an eigenvalue means the modal frequency.

3.4 Results from Numerical Simulation

The numerical simulation was computed to see how much the difference between V_{m+} and V_{m-} would influence the induced velocity and flight controls under different trim conditions. Used therein are two types of rotorcraft: Montgomerie, which is a two-seater medium gyroplane, and Westland Puma (see Fig. 3-1), which is a much heavier helicopter. Their brief specifications are shown in Table 3-1.

Fig. 3-1 [Montgomerie (left) and Westland Puma (right).][51]

[50] It is characteristic to the gyroplane that the propeller speed is in the control inputs vector.
[51] The left picture in Fig. 3-1 is reproduced from the webpage of Flight Dynamics Group at Glasgow University. The right picture is kindly provided by AgustaWestland, with copyright approved.

	Montgomerie	Puma
M (kg)	350	5810
I_{xx} (kgm^2)	73	9638
I_{yy} (kgm^2)	297	33240
I_{zz} (kgm^2)	224	25889
I_{xz} (kgm^2)	0	2226
b	2	4
R (m)	3.81	7.498
m (kg)	15	91

Table 3-1 [Specification of the Montgomerie and Puma.]

Since the rotor of a gyroplane is always in the windmill-brake state, simulations for the Montgomerie were done over a wide range of practical forward flight speeds and descent rates. On the other hand, the Puma was assumed to be descending with a fixed collective pitch, which is the most practical case where a helicopter rotor enters the windmill-brake state, because helicopter rotors usually enter the windmill-brake state only in emergency situations such as sudden power failure, where collective pitch should be minimized so as to keep the rotor speed as high as possible.

Figures 3-2 to 3-8 are related to the Montgomerie: Fig. 3-2 shows the resultant variation between the magnitude of dimensional mass-flow parameters of v_{m+} and v_{m-}; Fig. 3-3 to 3-8 show the influence of the difference in the mass-flow parameters in terms of forward flight speed and the descent rate against the inflow components, airframe attitudes and flight controls in trim, respectively.

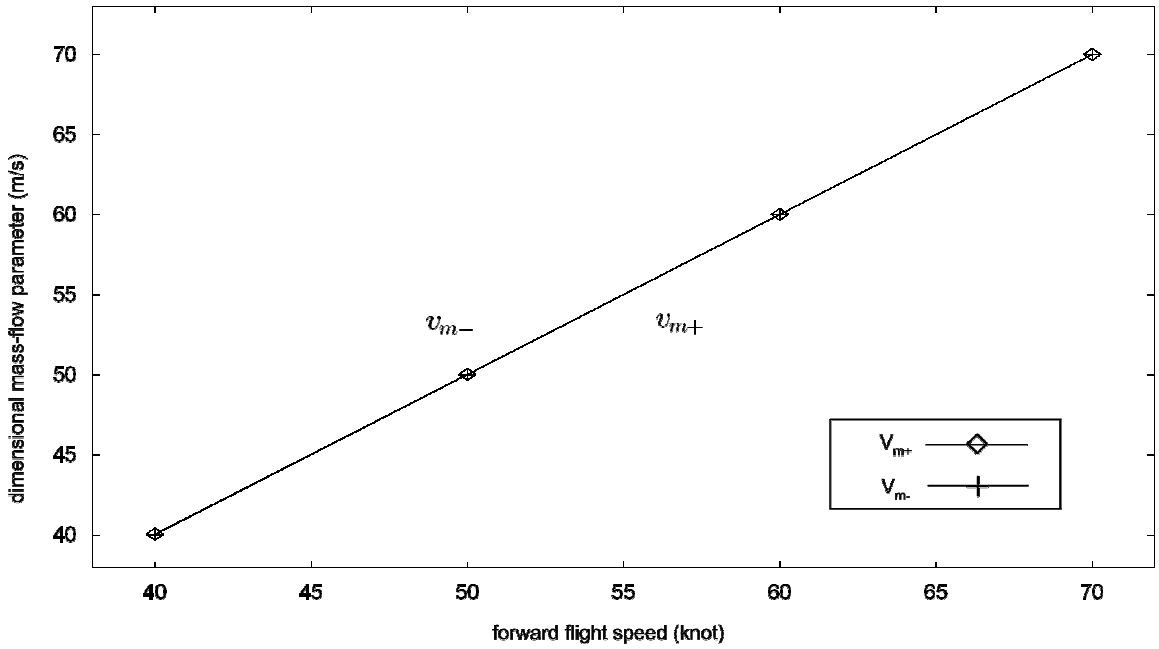

Fig. 3-2 [Comparison of forward flight speed and mass-flow parameters, Montgomerie.]

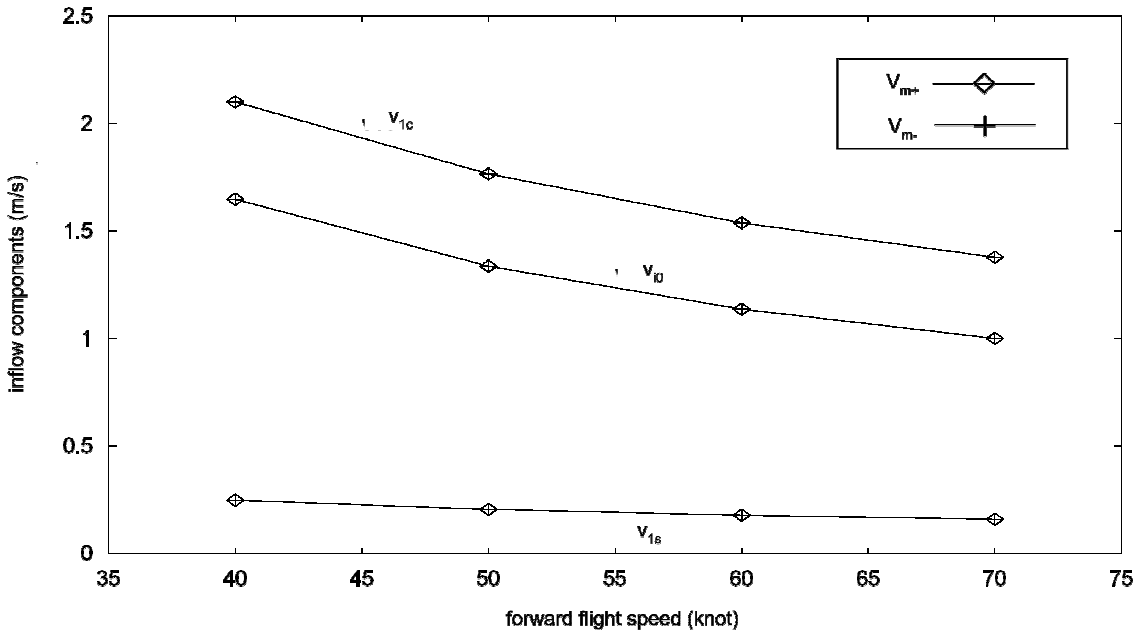

Fig. 3-3 [Comparison of forward speed and inflow components, Montgomerie.]

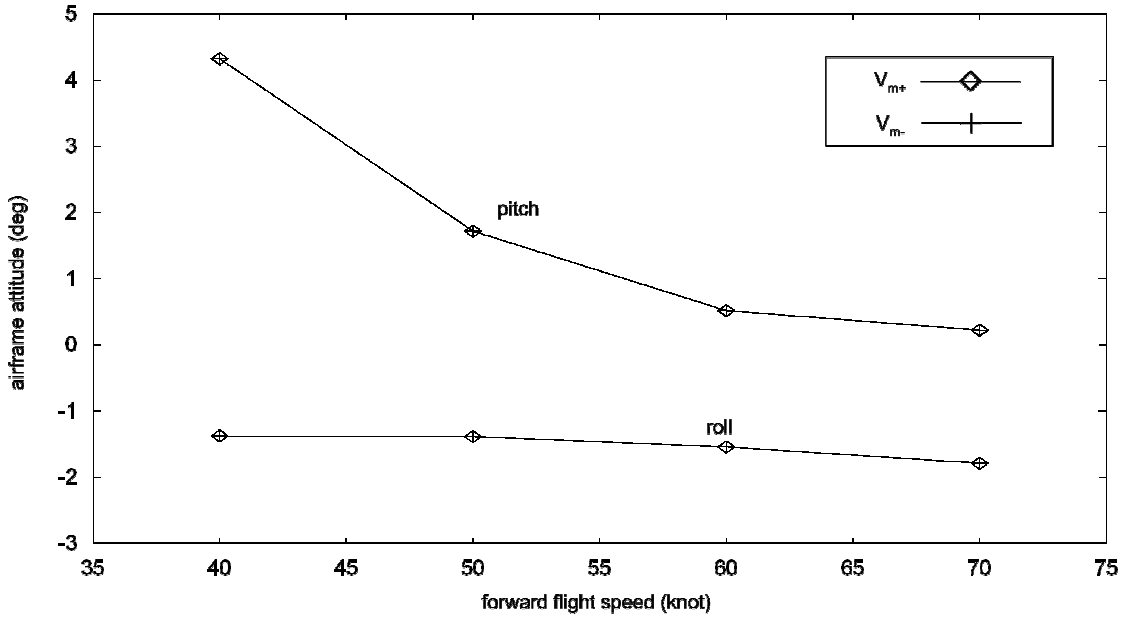

Fig. 3-4 [Comparison of forward speed and airframe attitude, Montgomerie.]

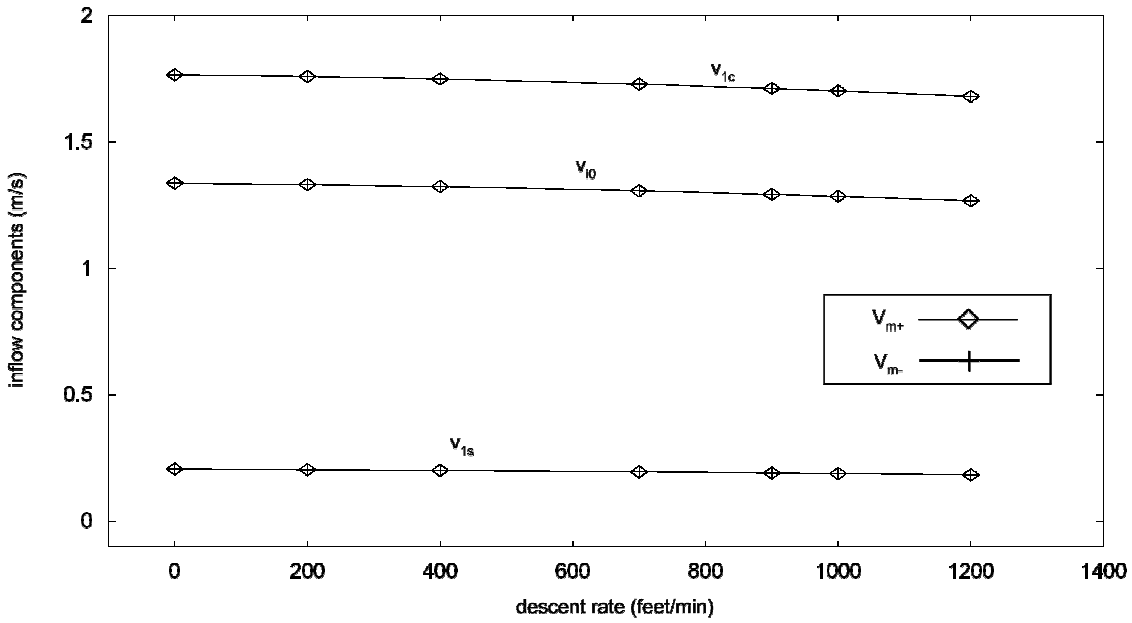

Fig. 3-5 [Comparison of descent rate and inflow components at 50 knots, Montgomerie.]

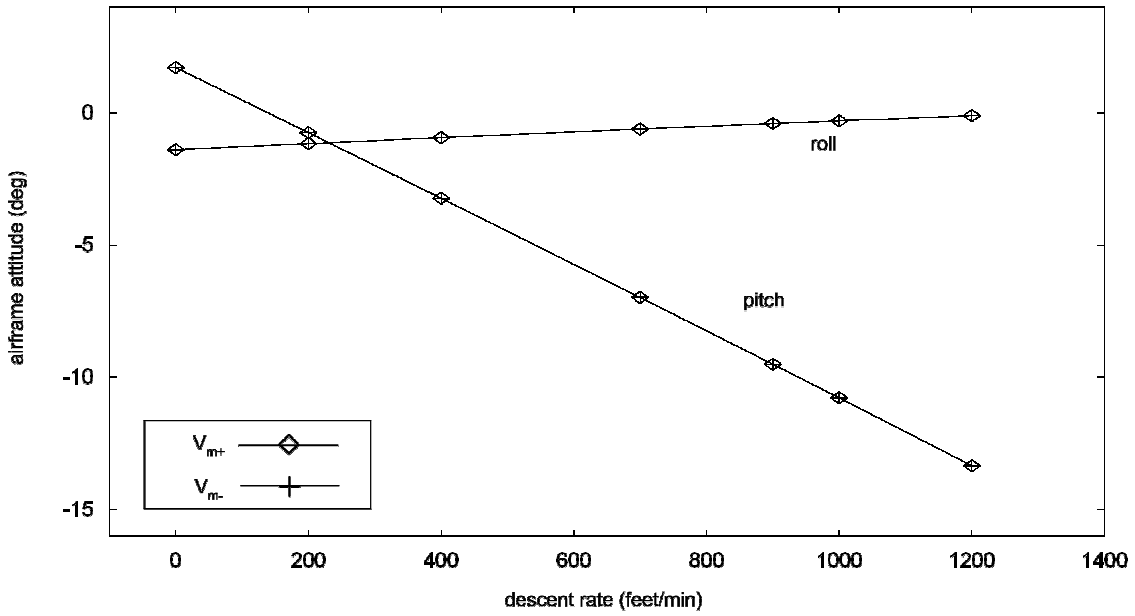

Fig. 3-6 [Comparison of descent rate and airframe attitude at 50 knots, Montgomerie.]

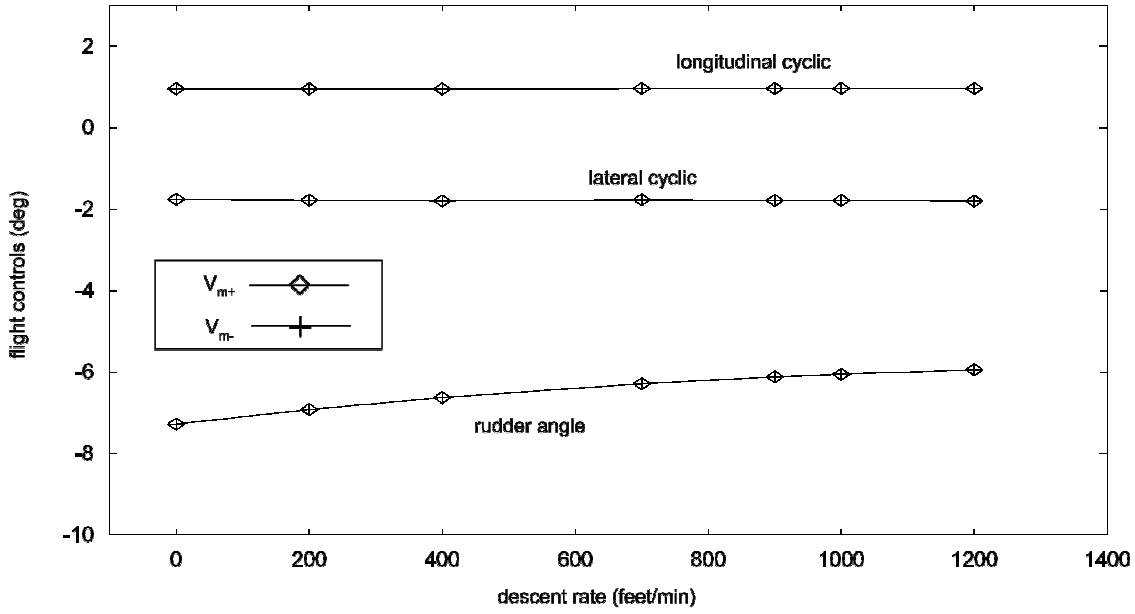

Fig. 3-7 [Comparison of descent angle and flight controls, Montgomerie.]

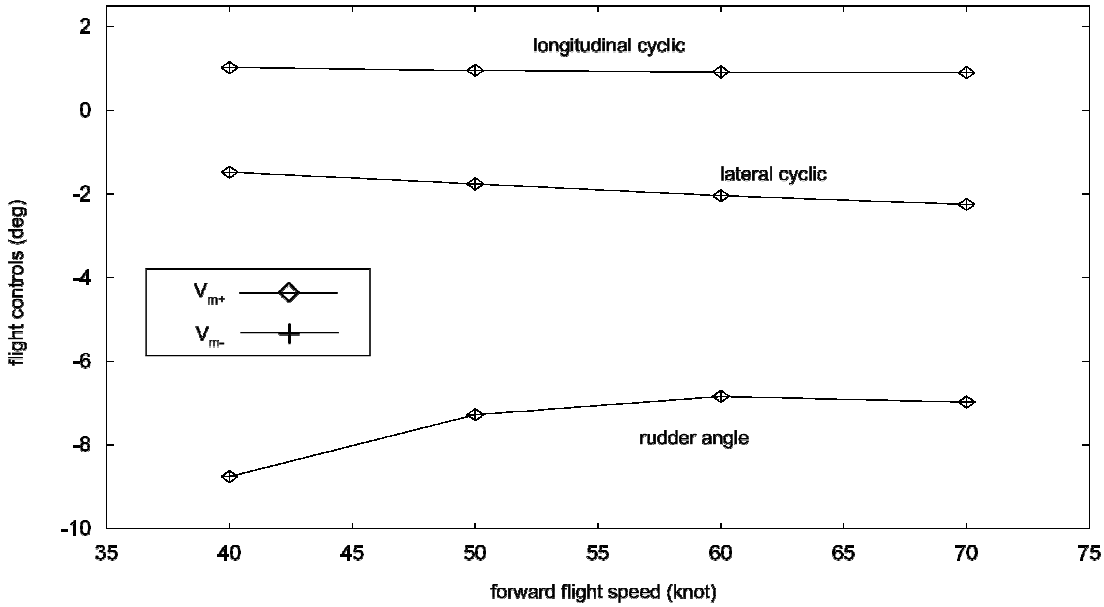

Fig. 3-8 [Comparison of forward flight speed and flight controls, Montgomerie.]

Figures 3-9 to 3-15 are related to the Puma. Figures 3-9 and 3-10 show the resultant variation between the magnitude of dimensional mass-flow parameters of v_{m+} and v_{m-} with respect to the forward flight speed and descent angle, respectively.

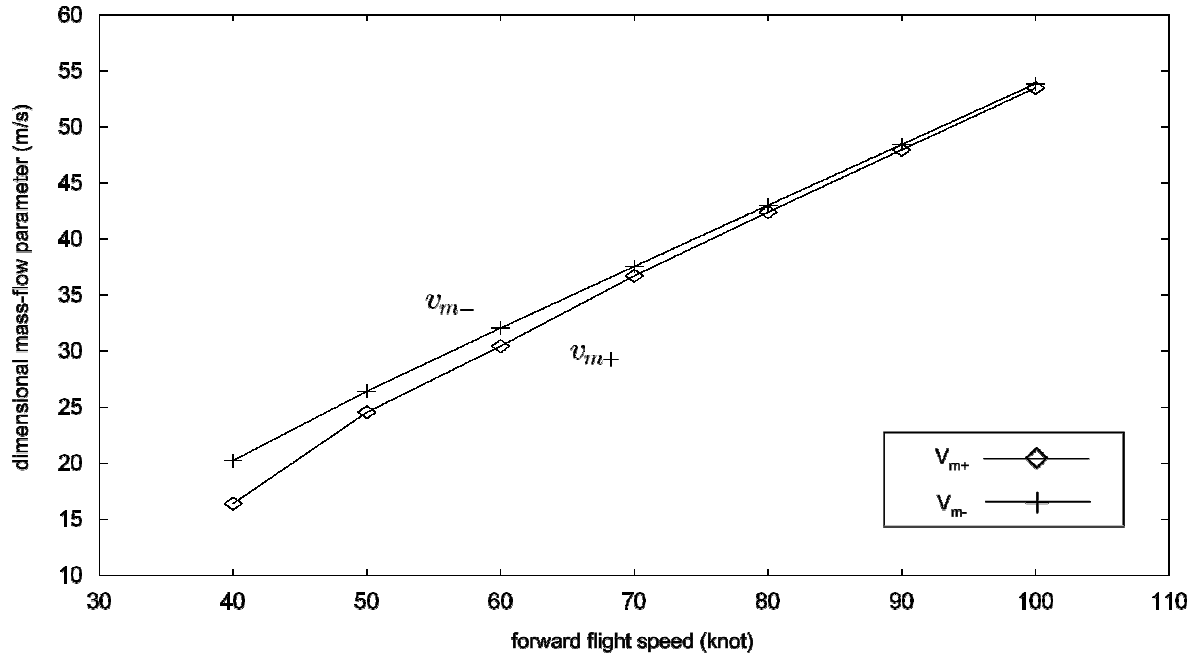

Fig. 3-9 [Comparison of forward flight speed and mass-flow parameters with collective pitch at $6.5°$, Puma in the windmill-brake state.]

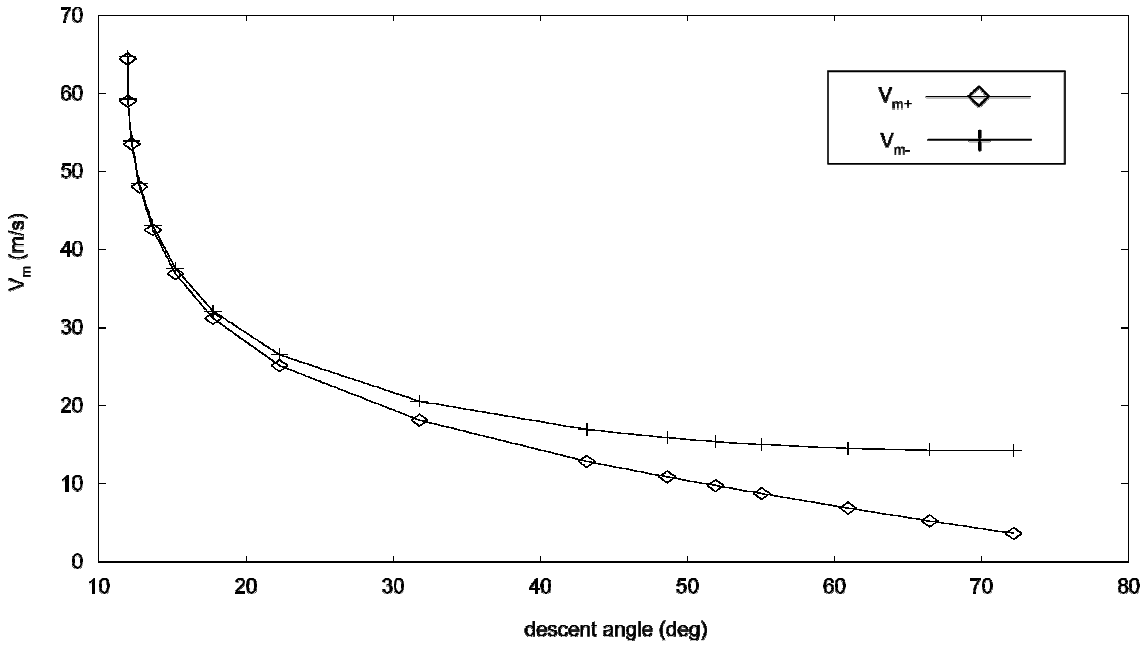

Fig. 3-10 [Comparison of inflow velocity for V_{m+} and V_{m-} with collective pitch at $6.5°$, Puma in the windmill-brake state.]

When comparing Eqs. (3.3) and (3.4), it can be predicted that when μ increases (i.e. high-speed flight or deep descent), the difference between V_{m+} and V_{m-} would be smaller, because μ becomes dominant in the numerators. This indicates that the difference between V_{m+} and V_{m-} should be larger in either low-speed flight or shallow descent. Indeed, Fig. 3-9 and 3-10 show this tendency. Through the comparison between the second terms in the numerators of Eqs. (3.4) and (3.5) (i.e. $\lambda(\lambda+\lambda_m)=(\lambda_f+\lambda_m)(\lambda_f+2\lambda_m)$ and $\lambda(\lambda-\lambda_m)=(\lambda_f+\lambda_m)\lambda_f$), it can be said that $V_{m+}<V_{m-}$ when in descent ($\lambda_f<0$) because $\lambda_f<\lambda_f+2\lambda_m$ and $\lambda_f+\lambda_m<0$. (Note that λ_m should always be positive by definition.) Both Fig. 3-9 and 3-10 are configured for full autorotation, and are indeed consistent with the observation above.

Figures 3-11 and 3-12 show the influence of forward flight speed with the fixed collective pitch at 6.5° upon the airframe attitude and the cyclic controls in trim conditions, respectively.

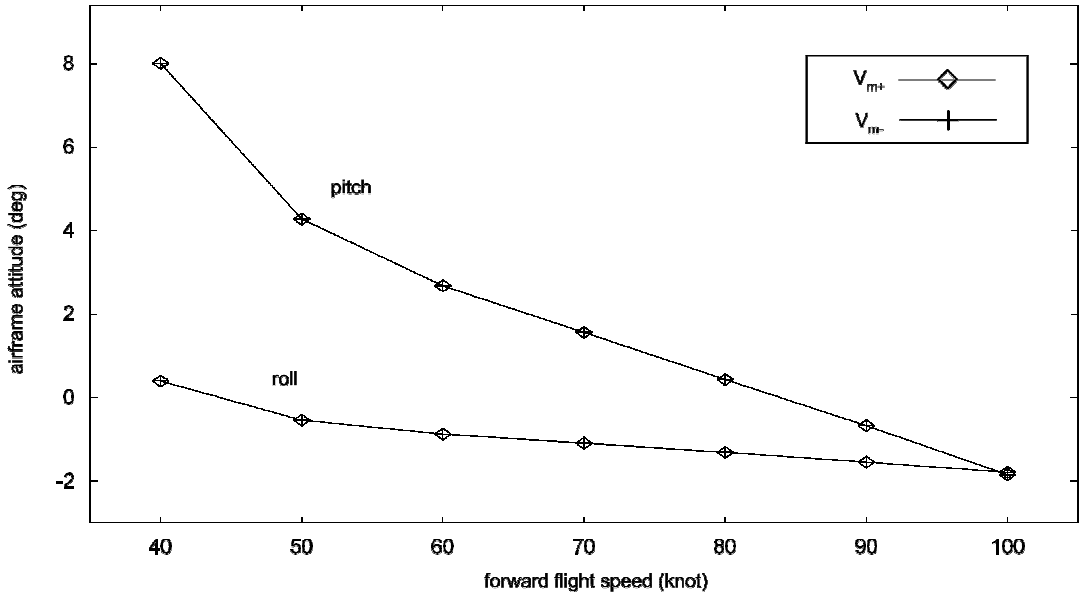

Fig. 3-11 [Comparison of descent rate and airframe attitude, Puma.]

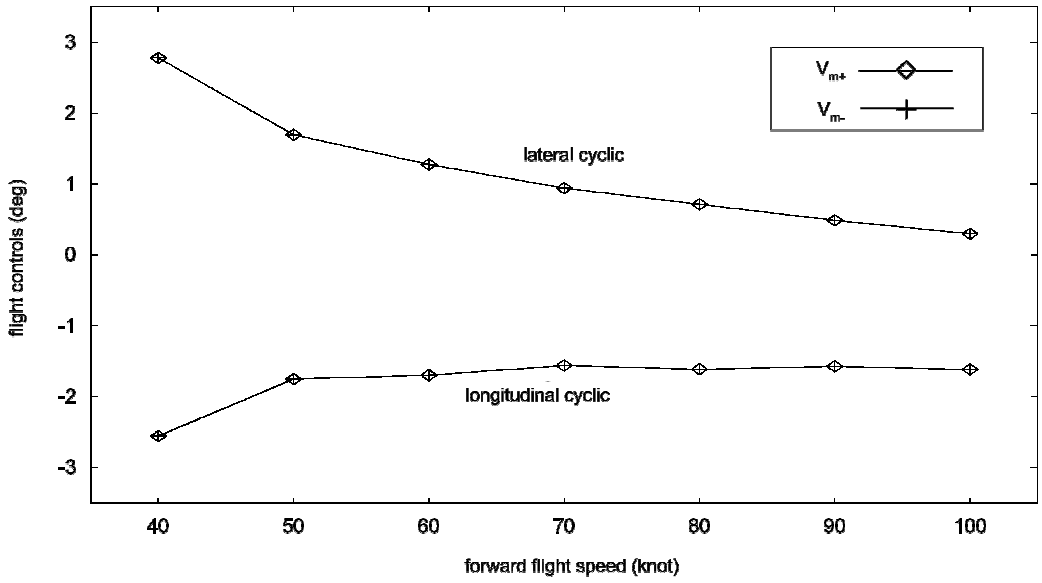

Fig. 3-12 [Comparison of Forward Flight Speed and Flight Controls, Puma.]

The stability analysis was also conducted configuring Puma helicopter alone, for which detailed configuration data exist[171]. It was trimmed in autorotative descents at the minimum collective pitch angle of 6.5 degree at the root.

Figure 3-13 shows the magnitude of the lateral inflow component, v_{1s}, calculated from Peters' original formulation (i.e., with V_{m+}) and the modified dynamic inflow model (i.e., with V_{m-}) with respect to the descent angle. Figure 3-14 shows the stability characteristics in the lateral inflow mode, and Fig. 3-15 shows the stability characteristics in the uniform/longitudinal mode. The resultant eigenvalues are shown in Tables 3.2 to 3.5 for both 7 DOF and 10 DOF simulations.

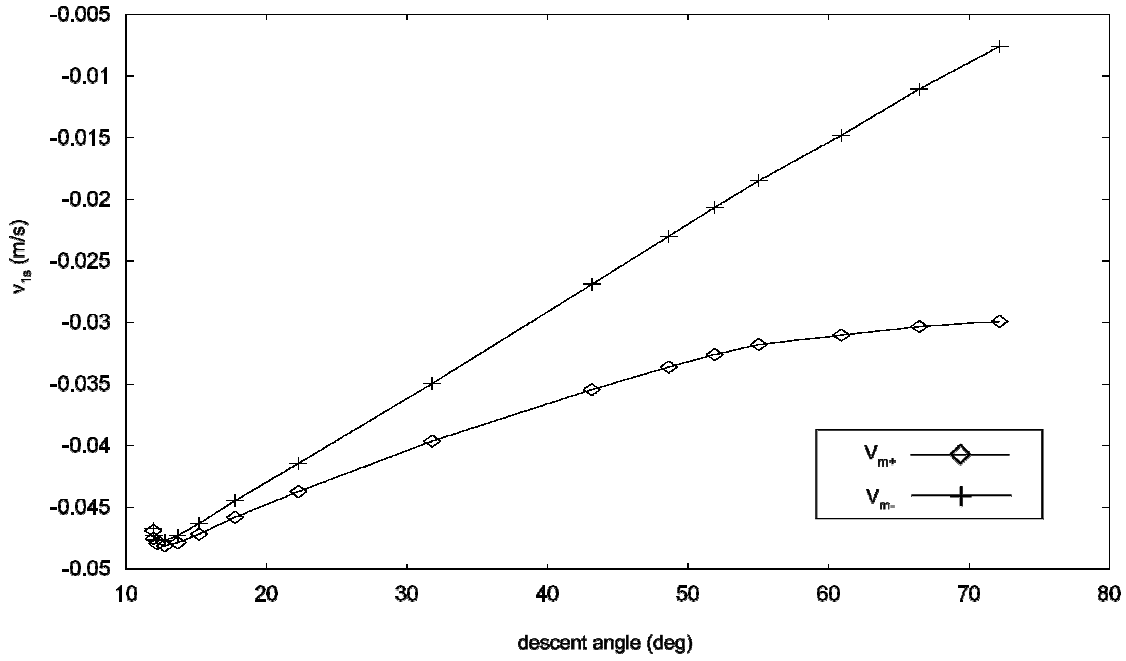

Fig. 3-13 [Comparison of lateral inflow component for V_{m+} and V_{m-}.]

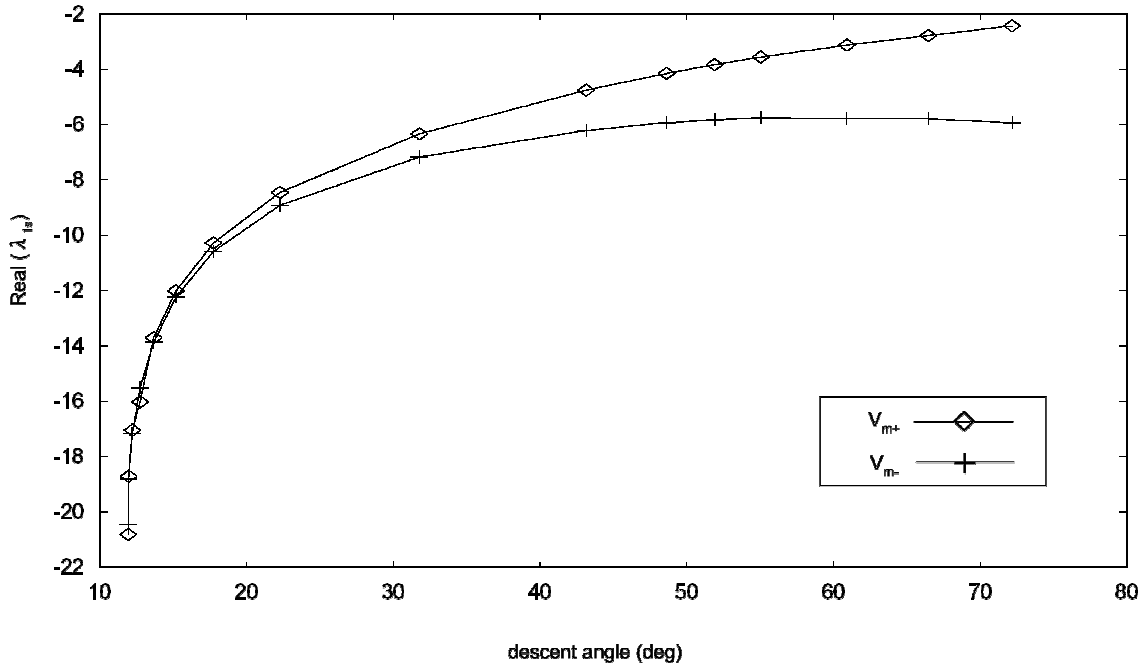

Fig. 3-14 [Lateral inflow mode; comparison for V_{m+} and V_{m-}.]

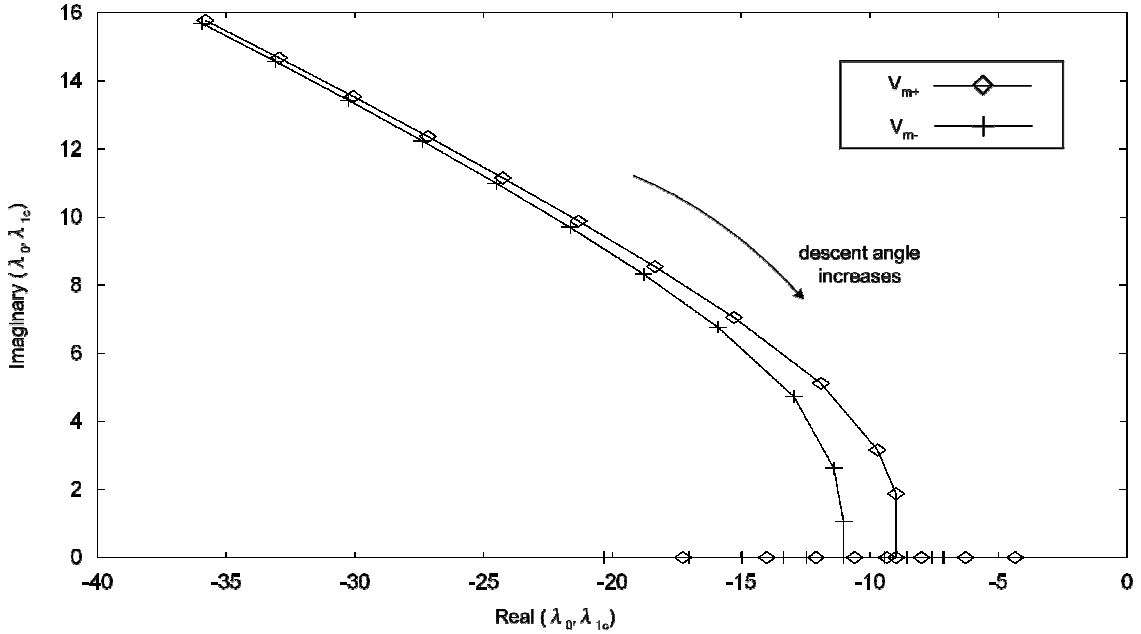

Fig. 3-15 [Coupled uniform/longitudinal inflow modes;
comparison for V_{m+} and V_{m-}.]

modes	7 DOF	10 DOF
lateral / directional	-1.7256±1.3189i	-1.9149±1.4127i
longitudinal	-0.5709±0.3350i	-0.7909±0.9535i
longitudinal	-0.2660±0.1519i	-0.5179±0.0434i
lateral	-0.4314	0.2128
lateral / longitudinal	-0.1818	-0.1179
longitudinal	0.8512	-0.7753
wake (uniform / longitudinal)	n/a	-17.2634
wake (lateral)	n/a	-2.4283
wake (uniform / longitudinal)	n/a	1.5525

*n.b. - Longitudinal modes include the rotor speed mode.

Table 3-2 [Linearised system eigenvalues - V_{m+};
35 KIAS, 3500 feet/min. $v_m = 3.6\ \mathrm{m/s}$.]

modes	7 DOF	10 DOF
lateral / directional	-1.6846±1.3975i	-1.5493±1.4667i
longitudinal	-0.6641±0.3103i	-0.6123±0.1654i
longitudinal	-0.2142±0.1743i	-0.2982±0.3543i
lateral	-0.4286	-0.2533
lateral / longitudinal	-0.1727	-0.1444
longitudinal	0.8726	0.8590
wake (uniform / longitudinal)	n/a	-20.3226
wake (lateral)	n/a	-7.1206
wake (uniform / longitudinal)	n/a	-5.9260

*n.b. - Longitudinal modes includes the rotor speed mode.

Table 3-3 [Linearised system eigenvalues - V_{m-};
35 KIAS, 3500 feet/min. $v_m = 14.3\ \mathrm{m/s}$.]

modes	7 DOF	10 DOF
lateral / directional	-0.9059±0.7283i	-0.8938±0.7401i
longitudinal	-0.2615±0.3352i	-0.2899±0.3151i
longitudinal / lateral	-1.5448	-1.4008
lateral	-1.6468	-1.6973
longitudinal	-0.1229	-0.1233
longitudinal	0.5407	0.5304
longitudinal	0.1797	0.1654
wake (uniform / longitudinal)	n/a	-11.9044±5.1166i
wake (uniform / lateral)	n/a	-6.3293

*n.b. - Longitudinal modes includes the rotor speed mode.

Table 3-4 [Linearised system eigenvalues - V_{m+};
40 KIAS, 2250 feet/min. $v_m = 18.2\ \mathrm{m/s}$.]

modes	7 DOF	10 DOF
lateral / longitudinal	-0.9064±0.7283i	-0.8958±0.7375i
longitudinal	-0.2623±0.3344i	-0.2915±0.3138i
longitudinal / lateral	-1.5955±0.0459i	-1.4185
lateral	n/a	-1.6765
longitudinal	-0.1229	-0.1233
longitudinal	0.5411	0.5308
longitudinal	0.1792	0.1644
wake (uniform / longitudinal)	n/a	-12.9543±4.7248i
wake (uniform / lateral)	n/a	-7.1681

*n.b. - Longitudinal modes includes the rotor speed mode.

Table 3-5 [Linearised system eigenvalues - V_{m-};
40 KIAS, 2250 feet/min. $v_m = 20.6\ \mathrm{m/s}$.]

3.5 Analysis of the Results Obtained

Firstly, results about Montgomerie are to be discussed. The two mass-flow parameters are hardly different in Fig. 3-2 (the difference numerically calculated is only about $0.05\ m/s$), and the influence of the difference upon flight controls, airframe attitudes and induced flow are also negligible. (In point of fact, the largest differences numerically obtained are not more than 1.0×10^{-5} % in the inflow components, and less than 2.5×10^{-4} deg. in the airframe attitude. These are not beyond the possible numerical errors in magnitude, and the differences are hardly visible in the diagrams.)

On the other hand, the difference in two mass-flow parameters is more obvious in the case of Puma, Fig. 3-9 and 3-10. It is likely that the weight of vehicle is reflected in the difference. However, the difference in two mass-flow parameters does not affect the flight controls, airframe attitudes or induced flow at all. (The differences numerically obtained are less than 2.3×10^{-2} % in the inflow components, and less than 8.3×10^{-4} deg. in the airframe attitude.) The cyclic controls do not show recognisable differences either.

The possible reason why the difference in the mass-flow parameters is negligible may be explained as follows; the uniform and longitudinal components of induced velocity in trim conditions are determined by the product of the gain matrix and the rotor load vector, where V_T is multiplied with the thrust and V_m is multiplied with the pitching moment. Since the thrust is two orders of magnitude greater than the aerodynamic pitching moment in trim condition, the difference in V_m hardly affects the uniform and longitudinal components of induced velocity. On the other hand, the lateral component of the induced flow is a function of the aerodynamic rolling moment alone, and hence is inversely proportional to the mass-flow parameter (indeed, Fig. 3-13 confirms the relative difference expected from inspection of Fig. 3-9), but the magnitude of v_{1s} is negligible in both cases due to the small aerodynamic rolling moment. As a result, control angles required to trim are therefore negligibly affected by the change in V_m proposed here, and, consequently, the airframe attitude and the induced velocity in trim conditions are hardly affected by V_m either.

On the other hand, the difference between V_{m+} and V_{m-} substantially affects the results from the stability analysis. Differences between the two mass-flow parameters become significant for descent angles steeper than about 30 deg. For the vehicle mass simulated (5810 kg), this equates to airspeeds less than 40 knots with corresponding to

rates of descent in excess of 2300 feet/min. The elements of the time constant matrix, $[L][M]$, associated with the longitudinal and lateral components of the dynamic inflow model are inversely proportional to V_m. The longitudinal and uniform components are coupled due to the off-diagonal terms and it might be thus expected that the dynamic inflow modes will all be characterised by differences between V_{m+} and V_{m-}. Figures 3-14 and 3-15 confirm that this is indeed the case. For the case of V_{m+}, the lateral mode decreases in magnitude with increasing descent angle, and the coupled longitudinal/uniform mode degenerates from an oscillatory character to a pair of aperiodic modes, one of which also migrates towards the right-hand (unstable) plane.

This is not the case for V_{m-}, where the corresponding behaviour is asymptotic to a stable value of large modulus, with increasing descent angle. Low modulus inflow modes will couple with the rigid-body dynamics, tending to invalidate the quasi-steady assumption underpinning the linearisation of the model. (See Table 3-2.) However, corresponding results for the V_{m-} case, where the inflow modes are of relatively large modulus, illustrate that the quasi-steady linearisation is a good approximation to the fully coupled case, Table 3-3.

3.6 Discussion

As is surveyed in Section 1.5, the study of rotorcraft flight mechanics in autorotation receives scant treatment in the literature after the advent of helicopters. It is certainly the case that those references such as Refs. (172) and (173) cover only elementary theory of autorotation and typically limited only to axial flight conditions. Also, most of the books available about gyroplanes such as Refs. (174) and (175) are just for amateur gyroplane pilots, and thus their contents are academically quite insufficient. Recently, Leishman did extend in the second edition of his textbook the treatment of flight in autorotation through considering gyroplane theory and application, and it is indeed the gyroplane problem that has served as the focus for studies in the application of dynamic inflow to autorotation[173]. However, the approach taken previously has been to accept the dynamic inflow theory, testing its applicability implicitly through validation (against flight test data) of the wider issues of vehicle trim, stability and control. The dynamic inflow model such as the Pitt and Peters model can be used also for rotors in the windmill-brake state without any change in the matrix elements.

For steady flight conditions, the only change required is in the mass-flow parameter

where V_{m-} should be used for rotors in the windmill-brake state instead of V_{m+}. The literature suggests that this should be the first time that the difference between V_{m+} and V_{m-} has been explicitly identified. The simple discussion in Section 3.1 may be essentially applicable to other variations of dynamic inflow model such as the Peters and He model and its updated variations[7,129].

The dynamic inflow modelling was revisited from the first principles in this Chapter, in an explicit attempt to assess its applicability for autorotation. This study has identified a modification to the mass-flow parameter. Note that the angle between the rotor disc and the free stream, α, and the wake skew angle, χ, should be defined differently, because of the geometric difference in the relation between the inflow and the rotor disc.

Numerical simulations of the Montgomerie and Puma confirm the analytical assessment that the change will have a negligible impact on the trim calculation, but can have a significant effect on the stability of inflow modes. This difference only becomes evident in steep descents with low forward speed, in an area of the flight envelope that is of little practical utility for the helicopter even in autorotation. The modified mass-flow parameter, V_{m-}, retains the inflow modes well-separated in modulus from the rigid-body modes, but this is not the case with V_{m+}, where body and inflow modes are coupled.

The gyroplane can of course conduct steep, power-off descents, and, moreover, the gyroplane rotor will tend to operate in an analogous state if flown in steady level flight at very low speed. However, simulation of a typical light gyroplane shows that the minimum level flight speed is too fast to cause significant differences in V_m. The change to V_m is thus not practically significant for gyroplane flights either.

Therefore, those works such as Refs. (9) and (10), in which the dynamic inflow model for the normal working state with V_{m+} was used, can still be considered practically quite reasonable in their results in spite of the theoretical incorrectness. Note that by looking at Eq. (2.128), it can be expected that the difference between V_{m+} and V_{m-} would be more strongly related with C_L and C_M than with C_T, and thus in those situations where C_L and C_M are much larger, the difference would be more evident. Such a manoeuvre is not very realistic with a helicopter descending in autorotation, but can be meaningful to take into account when estimating the overall performance of a

gyroplane.

Comparing Fig. 3-2 and Fig. 3-9, it can be said that the weight of the aircraft has the dominant influence in the magnitude of mass-flow parameter, and hence when designing jumbo-gyroplanes, whose conceptual designs are seriously under way by some companies[157], the difference in the mass-flow parameters may play a more crucial role.

3.7 Chapter Summary

The necessary modification to dynamic inflow modelling for autorotative rotors is proposed with regard to steady flight conditions. The definition of α and χ are also confirmed so as to be consistently applicable for rotors both in the normal working and windmill-brake states. Numerical simulations are conducted to examine the control inputs, airframe attitudes, induced flow and the stability in trim steady conditions. On the basis of findings and results above, the following general conclusive remarks are to be made:

1. It is theoretically confirmed that the apparent and gain matrices can hold the same elements in either the normal working or the windmill-brake states;
2. It is identified that the mass-flow parameter for the windmill-brake state should be dissimilar to that for the normal working state;
3. With regard to the definitions of χ, it was shown that Chen's definition[28] is not valid for autorotative rotors. Peters' definition, Eq. (3.2), is usable for rotors both in the normal working and windmill-brake states;
4. Numerical simulation indicates that the difference in the mass-flow parameter causes only negligible effects on the control inputs, airframe attitudes and the induced flow to trim a state;
5. Numerical simulation indicates that the difference in the mass-flow parameter affects the stability. Still, considerable differences only become apparent for steep descents with low forward speed;
6. The behaviour of the inflow modes are affected by the difference in the mass-flow parameter; without modification for autorotation, they will tend to slow and couple strongly with the rigid-body modes as the descent angle steepens. With the modification, the inflow modes become well-separated from the rigid-body modes;
7. Some inflow modes without modification for autorotation are found in the unstable

region. These modes become stable with modification to V_{m-}. The author suggests that stable modes should be more physically realistic than unstable modes of inflow, and therefore that V_{m-} should produce more meaningful inflow in autorotation.

8. Due to the limited area of the flight envelope of autorotating rotorcraft where the modification is practically required, those reference works such as Refs. (9), (10) and (151), (154) and (155), where unmodified dynamic inflow model is used for autorotative rotors, can be considered still reasonable about their results.

Chapter 4

Consideration of the Small Wake Skew Angle Assumption

4.1 Introduction

Peters and He derived their dynamic inflow model invariably based on the small wake skew angle assumption (Subsection 2.2.11), but proceeded to state that this model can be applied to a wide range of wake skew angles from 0° to 90°[37]. Since the model is extensively compared with experimental data and the correlation is found overall excellent[7], the practical validity of the model for a wide range of wake skew angles should be considered acceptable. Still, there is clearly a need to theoretically elucidate the validity of this approach in the model derivation.

In point of fact, the original authors have never discussed mathematically the validity of the assumption; indeed the small wake skew angle assumption appears only in the appendix of Ref. (7) (Appendix C, page 168)[52], and the pertinent part of the derivation is not mentioned in any other relevant published papers.

This author thus believes that the validity of the small wake skew angle assumption needs to be theoretically re-examined. Note that since the rotor is supposed to be working in the normal working state in the original works of Peters and He, the normal working state shall be used as the representative rotor state also in this Chapter. However, the general coverage of this Chapter shall not be limited to the normal working state alone.

4.2 New Gain Matrix Model

4.2.1 Derivation of a New No-Assumption Model

In an attempt to examine the small wake skew assumption, a new gain matrix is proposed without using the assumption. In this formulation, Eqs. (2.77.1) - (2.77.3) are used instead of Eq. (2.87).

Although all the derivation in Chapter 2 from Eq. (2.77) to (2.104) is applicable to

[52] In Ref. (7), the assumption is suddenly introduced with a phrase, “Now we will examine the integral behaviour for small wake skew angle χ for which we have...” However, it is not analytically explained in any other places why the resultant model can later be extended up to $\chi = \pi/2$.

Eqs. (2.77.1) - (2.77.3) except Eqs. (2.83.1) - (2.83.3), the Taylor series of the pressure potential, Eq. (2.84), should be modified as

$$\begin{aligned}\Phi_n^{mc(c)}(x,y,z) &= \Phi_n^{mc(c)}(x_0 - \tan\chi z, y_0, z) \\ &= \sum_{k=0}^{\infty} \frac{(-1)^k}{k!}\Big(z\tan\chi\Big)^k \frac{\partial^k \Phi_n^{mc(c)}}{\partial x^k}\bigg|_{x=x_0}. \end{aligned} \tag{4.1}$$

Note that although it may appear that Eqs. (2.77.1) - (2.77.3) would diverge to infinity at $\chi = \pi/2$, this case is already excluded when Eq. (2.69.1) is derived from Eq. (2.67.3)[53]. Equations (2.77.1) - (2.77.3) and (4.1) lead to the following final representations for the new gain matrix elements.

$$[\hat{L}_{jn}^{0m}]^c = \frac{1}{\cos\chi}(Y^m)[\Gamma_{jn}^{0m}], \tag{4.2}$$

$$[\hat{L}_{jn}^{rm}]^c = \frac{1}{\cos\chi}[Y^{|r-m|} + (-1)^{min(r,m)}Y^{|r+m|}][\Gamma_{jn}^{rm}], \tag{4.3}$$

$$[\hat{L}_{jn}^{rm}]^s = \frac{1}{\cos\chi}[Y^{|r-m|} - (-1)^{min(r,m)}Y^{|r+m|}][\Gamma_{jn}^{rm}], \tag{4.4}$$

where

$$Y = \frac{\tan\chi}{2}. \tag{4.5}$$

Note that when $\chi \ll 1$, Eqs. (4.2) - (4.5) reduce to Eqs. (2.99.1) - (2.99.3) and X, respectively. Therefore, it can be said that Eqs. (4.2) - (4.5) hierarchically imply Peters and He's gain matrix elements for axial flight.

Some examples of Eq. (4.2) - (4.5) are as follows.

$$\hat{L}_{11}^{00c} = \frac{3}{2\cos\chi}, \tag{4.6}$$

[53] Therefore, the extension of the Peters and He model up to edgewise flight is incompatible not only with the small wake skew angle assumption, but also with the derivation of Eq. (2.69.1). This indicates that the edgewise flight case should be discussed separately, if it is possible to deal with analytically. This is indeed the case, and perfectly edgewise flight shall be discussed later in this Chapter.

$$\hat{L}_{12}^{01c} = -\frac{\pi \tan\chi}{\sqrt{10}\cos\chi}, \tag{4.7}$$

$$\hat{L}_{21}^{10c} = \frac{\pi \tan\chi}{\sqrt{10}\cos\chi}, \tag{4.8}$$

$$\hat{L}_{22}^{11s} = \frac{5}{2}\left(1 + \frac{1}{4}\tan^2\chi\right), \tag{4.9}$$

$$\hat{L}_{22}^{11c} = \frac{5}{2}\left(1 - \frac{1}{4}\tan^2\chi\right). \tag{4.10}$$

Note also that when $\chi \ll 1$, Eqs. (4.6) - (4.10) reduce down to Eqs. (2.102.1) - (2.102.5).

4.2.2 The Modified Pitt and Peters Model

The difference of the gain matrices between the Pitt & Peters and Peters & He models are only in the coefficients and thus the trigonometric parts are the same[54]. Thus, it should be possible to propose a modified Pitt & Peters model as well by replacing the trigonometric parts in the original Pitt and Peters model with those appearing in Eq. (4.6) - (4.10). The specific form of the modified model will be as follows;

$$\begin{pmatrix} \frac{8}{3\pi} & 0 & 0 \\ 0 & -\frac{16}{45\pi} & 0 \\ 0 & 0 & -\frac{16}{45\pi} \end{pmatrix} \begin{pmatrix} \dot{\lambda}_0 \\ \dot{\lambda}_{1s} \\ \dot{\lambda}_{1c} \end{pmatrix} + \begin{pmatrix} \frac{1}{2\cos\chi} & 0 & \frac{15\pi}{64}\cdot\frac{\tan\chi}{\cos\chi} \\ 0 & -2\left(1+\frac{1}{4}\tan^2\chi\right) & 0 \\ \frac{15\pi}{64}\cdot\frac{\tan\chi}{\cos\chi} & 0 & -2\left(1-\frac{1}{4}\tan^2\chi\right) \end{pmatrix}^{-1} \frac{1}{V}\begin{pmatrix} \dot{\lambda}_0 \\ \dot{\lambda}_{1s} \\ \dot{\lambda}_{1c} \end{pmatrix} = \begin{pmatrix} C_T \\ C_L \\ C_M \end{pmatrix} \tag{4.11}$$

For $\chi = 0$ (hover), Eq. (4.11) is identical with the original Peters and He formulation. However, with progression into edgewise flight, the $(1,1)$ element in the gain matrix, $1/2\cos\chi$, tends to infinity. This means that the uniform induced velocity will increase with the wake skew angle, but this is counter to reality. Therefore, despite the derivation of this model should be mathematically more consistent, it can be predicted that this model would not provide realistic solutions when χ is fairly large.

In the next Subsection, numerical simulation of this model is provided.

[54] While the Peters and He model is given the general formulation for any combination of m, n, r and j, the Pitt and Peters model is provided only up to the five-state model. Therefore, strictly speaking, the simple replacement in Subsection 4.2.2 can de done only up to the five-state model.

4.2.3 Numerical Simulation

Numerical simulation is conducted by RASCAL in order to compare the Peters' original formulation and the new no-assumption model, using the Westland Puma as the reference vehicle. Since the Pitt and Peters model is used in the simulation code, the modified Pitt and Peters model is used in the simulation[55].

Figures 4-1 to 4-8 show comparisons between those two models about trim solutions between hover and 20 knots.

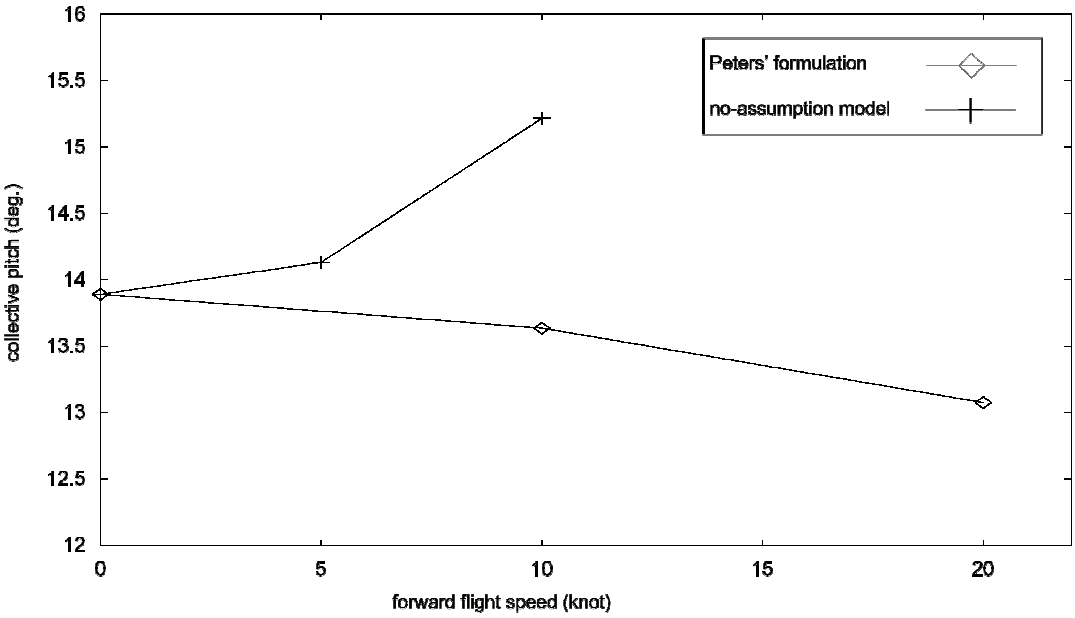

Fig. 4-1 [Comparison of collective pitches against forward flight speed.]

[55] It should be acknowledged that the coding of RASCAL was done by Dr. Stewart Houston at the University of Glasgow.

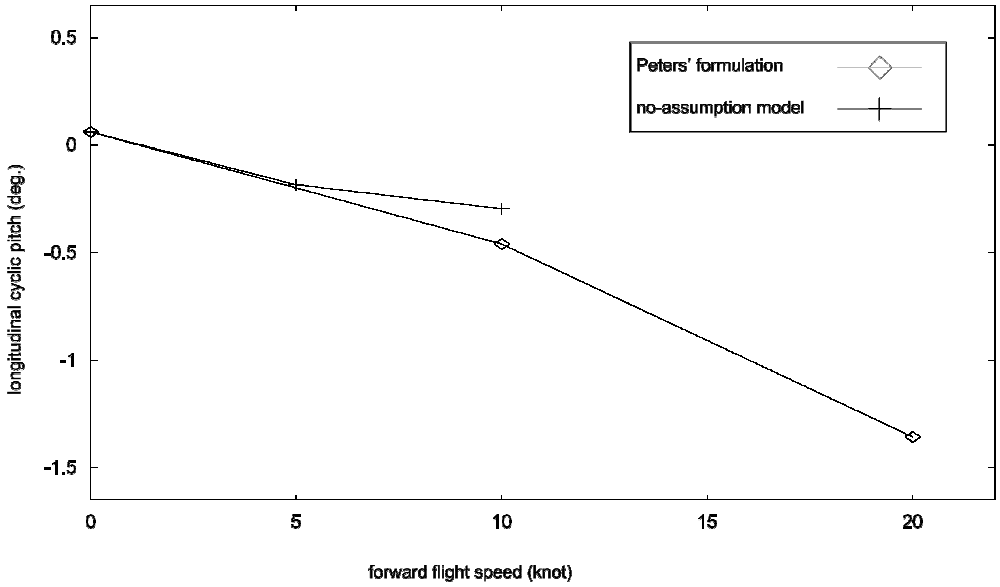

Fig. 4-2 [Comparison of longitudinal cyclic pitches against forward flight speed.]

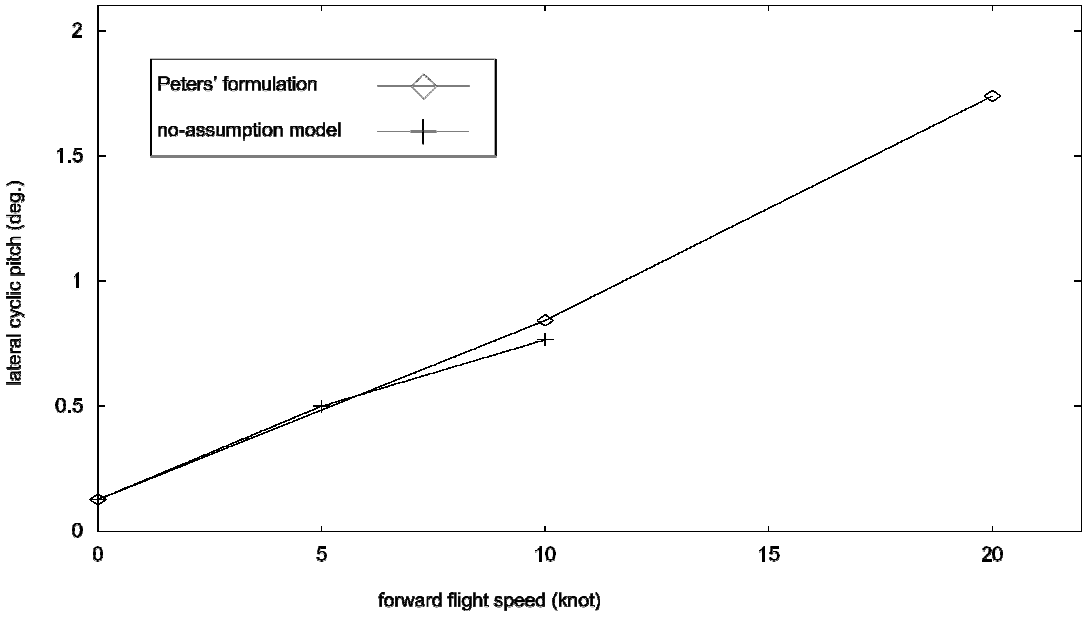

Fig. 4-3 [Comparison of lateral cyclic pitches against forward flight speed.]

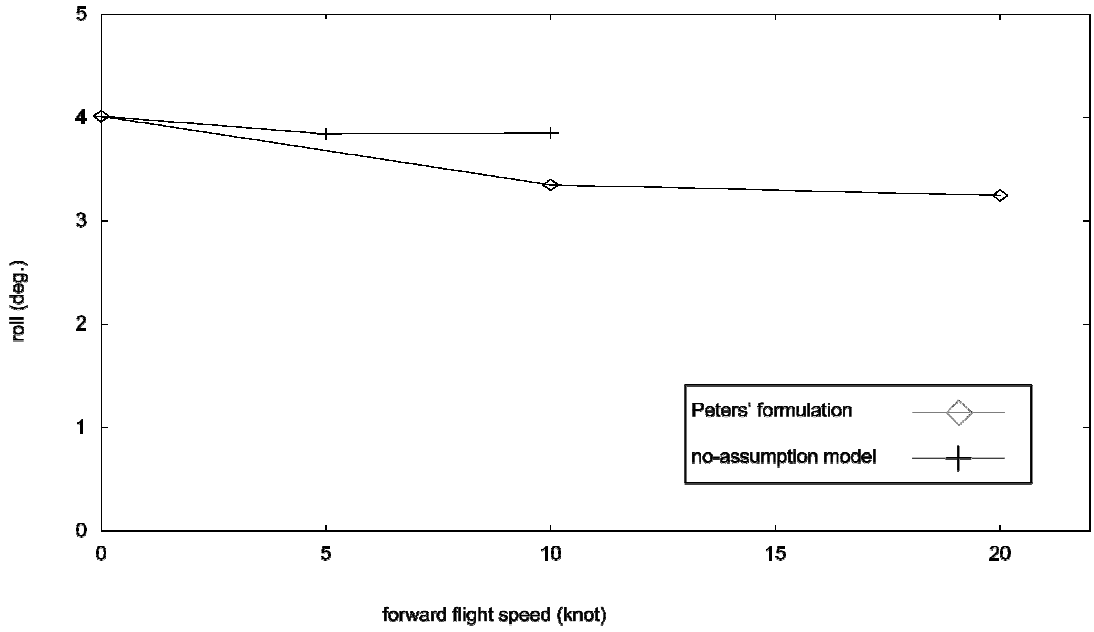

Fig. 4-4 [Comparison of roll attitudes against forward flight speed.]

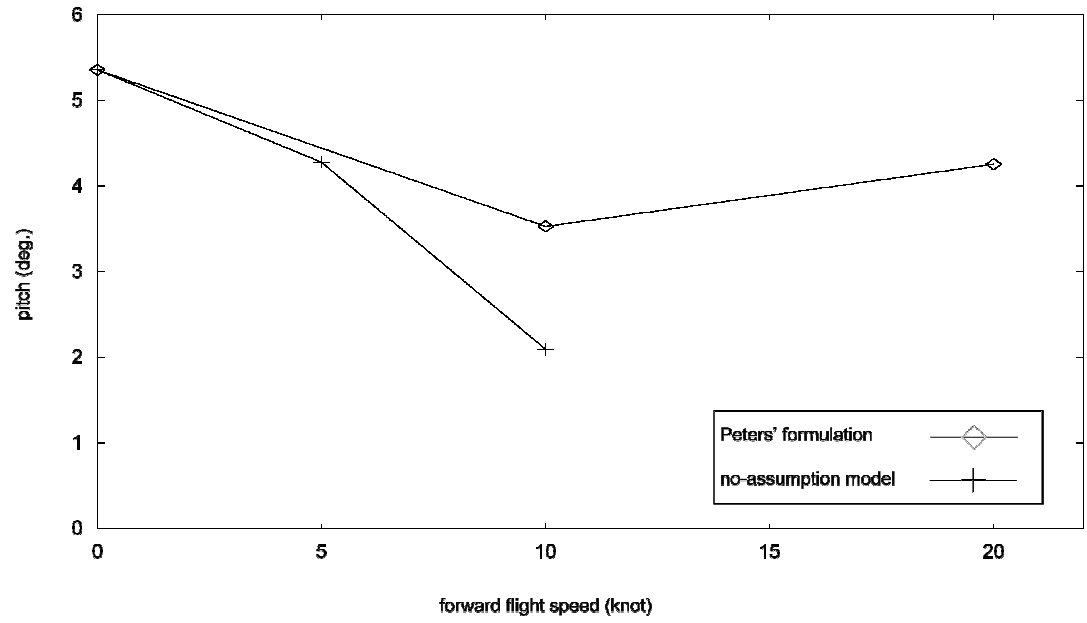

Fig. 4-5 [Comparison of pitch attitudes against forward flight speed.]

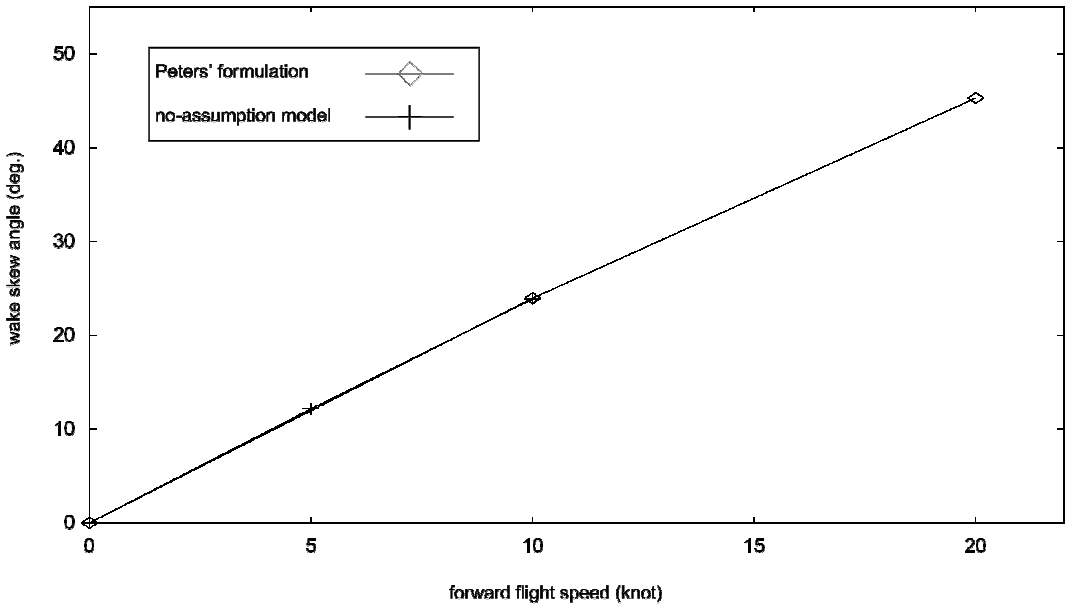

Fig. 4-6 [Comparison of wake skew angles against forward flight speed.]

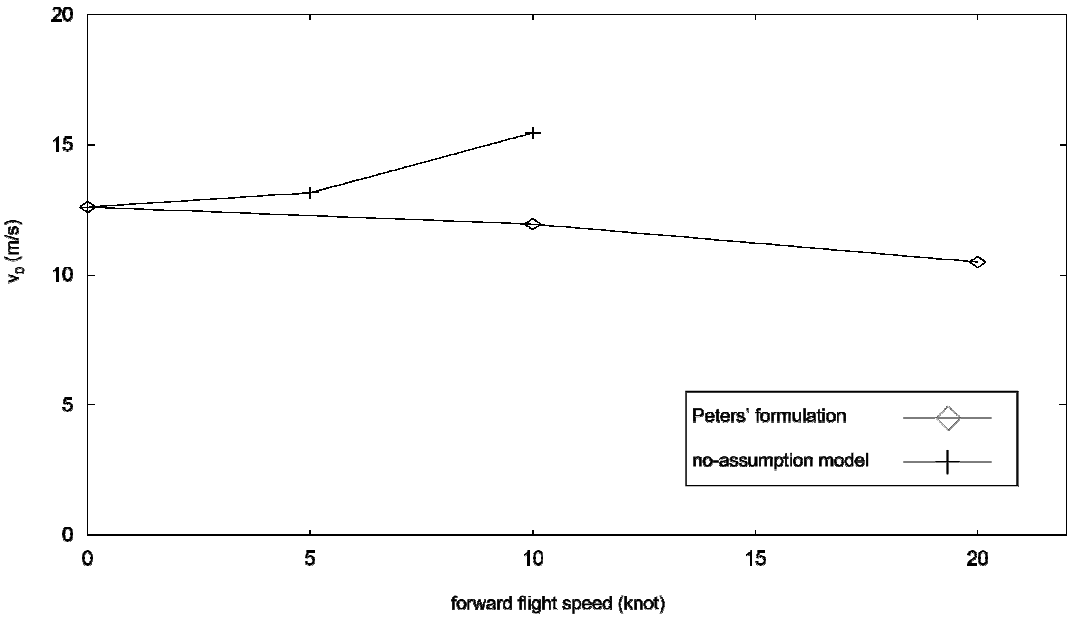

Fig. 4-7 [Comparison of uniform components of induced velocity against forward flight speed.]

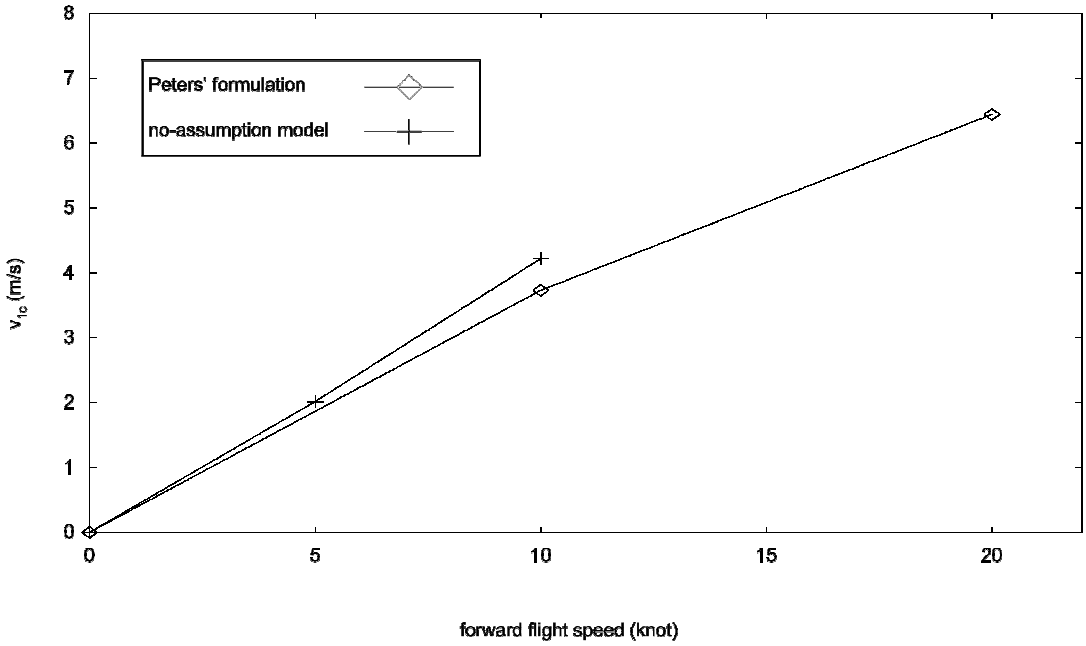

Fig. 4-8 [Comparison of the longitudinal components of induced velocity against forward flight speed.]

It can be observed that the new formulation fails to trim beyond about 10 knots[56] due to blade stall caused by excessive angle of attack following from the requirement for large collective pitch. These flight mechanics solutions suggest excessive drag due to a large angle of attack, which is caused by the pitch attitude rapidly decreasing with increasing airspeed. This is indeed the case, and the induced drag increases markedly with flight speed as the uniform component of induced velocity follows a trend opposite to Peters' formulation with the small wake skew angle assumption.

It can be said that this is physically counter-intuitive as well. In Eq. (4.11), the denominators tend to zero with the increasing wake skew angle (which increases with airspeed) as $\chi \to 90^\circ$ then $\cos\chi \to 0$. Solutions appear to be most sensitive to the leading term element in the gain matrix, which increases in magnitude with airspeed driving the uniform component of induced velocity to do likewise. Note that the time constant matrix, $[L][M]$, is also subject to the gain matrix elements, and thus the modes also take on a dissimilar form, Fig. 4-9.

[56] Generally speaking, small angle assumptions such as $\cos\theta \simeq 1$ and $\sin\theta \simeq \theta$ can be thought practically applicable for $|\theta| \leq 10^\circ$ or so. The forward flight speed of 10 knots corresponds more or less with a wake skew angle of 10°. Thus, it may be suggested that the unrealistic results beyond 10 knots or so should indicate that the model will be simply unrealistic without the small wake skew angle assumption.

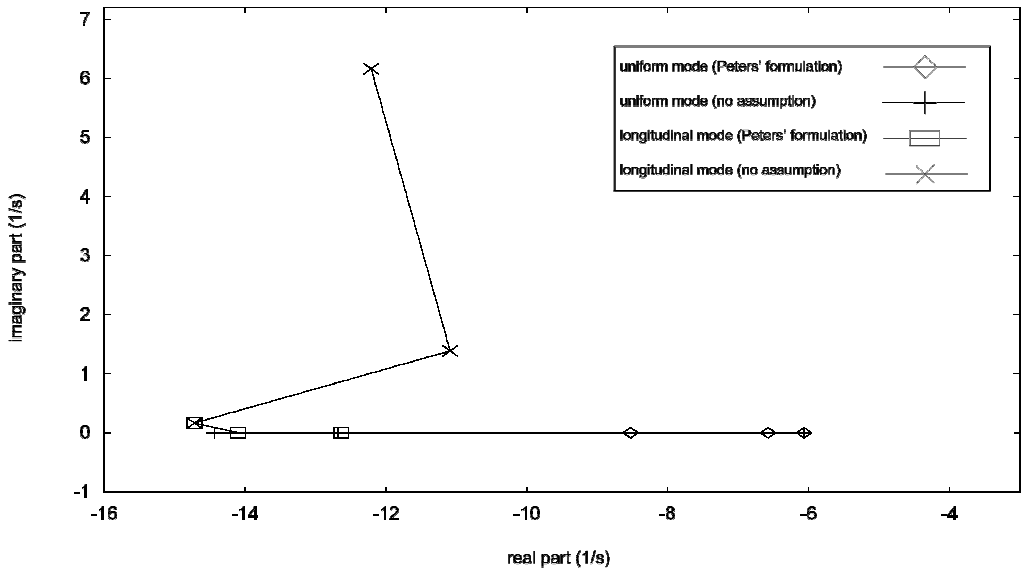

Fig. 4-9 [Comparison of modes.]

Regarding axial flight, it is confirmed that the modified Pitt and Peters model hierarchically complies with the original Pitt and Peters model both analytically and numerically. Hence those validation works for the Pitt and Peters model such as Refs. (62) and (102) can automatically verify the new model in axial flight cases, where the new model is reduced to their model.

However, when χ tends to $\pi/2$, the gain matrix elements in the new model tend to infinity unlike Pitt and Peters' formulation, and, indeed, the simulation results confirm and quantify the extent to which the new model provides unrealistic solutions when the forward flight speed increases; drag increases as the forward flight speed increases, and collective pitch and induced velocity need to be large too. (Recall that L_{11} is constant in the original Pitt and Peters model. The behaviour of the leading element in the gain matrix is the key to the divergence.)

It is argued that the validity of the small wake skew angle assumption is mathematically quite questionable, but the fact that the Peters and He model with the assumption practically works better indicates that the reason why their model works should be clarified on the theoretical ground.

4.3 Further Discussion

4.3.1 Deductive and Inductive Approaches

The simulation results indicate that the new formulation without the small wake skew assumption is unrepresentative despite the fact that the derivation must mathematically be more consistent than that of the Peters and He model. Considering the facts that the Peters and He model was numerically validated in Refs. (7), (92) and (112) showing excellent correlation with experimental data and also that its advanced models such as Refs. (131), (132) and (135) are widely used today, the practical validity of the Peters and He model can be considered to be fully validated in spite of the questionable assumption[57].

Questions naturally arising from this situation should include an argument *if it is possible to prove why the Peters and He model is practically valid in spite of the mathematically questionable application of the small wake skew angle assumption.* In order to respond to this question, the possibility to deductively present a proof shall be first discussed. (A deductive approach can generally provide a logically rigorous proof.)

Generally mathematically speaking, an approximated equation based on an assumption can approximate the original equation only when the underlying assumption is valid; hence when the assumption breaks down, the original and the approximated equations should formally be regarded as different equations. (For example, it is plainly evident that $\tan\chi$ and $2\tan(\chi/2)$ are different functions, though $\tan\chi$ can be well approximated by $2\tan(\chi/2)$ when χ is sufficiently small. They would behave quite differently when χ is fairly large.)

It can be thus believed that an attempt to apply the Peters and He model, which is derived on the small wake skew angle assumption, for larger angles, for which the assumption breaks down, is mathematically inappropriate or even meaningless in itself, regardless how the results are experimentally validated. Since the mathematical consistency in the derivation breaks down when the model is extended to larger wake skew angles, it is impossible to mathematically discuss the resultant model any further.

There seems to be no mathematically cogent reason available which makes it possible

[57] This author informally enquired after the mathematical validity of the assumption to Dr. ChengJian He by email, but his reply reads only that the model was numerically validated in correlation with experimental data. The present author believes that such a numerical validation is weak as a theoretical proof for the validity of the assumption, but any further replies were given. Thus, it still remains unclear how the original authors consider the validity of the assumption purely from the analytical point of view.

to extend the approximated equations up to those cases in which the approximations are not valid any longer. Therefore, it can be said that the inappropriateness of the application of the resultant model for larger wake skew angles is mathematically evident.

Another mathematically inconsistent point in the derivation is the way of applying the small wake skew angle assumption. If χ is really small, then Eqs. (2.67.1) and (2.67.3) could be further approximated as

$$\begin{aligned} x &= \xi \sin\chi + x_0, \\ &\simeq \xi\chi + x_0 \end{aligned} \tag{4.12}$$

$$\begin{aligned} z &= -\xi \cos\chi. \\ &\simeq -\xi \end{aligned} \tag{4.13}$$

Equations. (2.83.2) - (2.83.3) could also be further approximated as

$$\sin\chi \simeq \chi, \tag{4.14}$$

$$\tan\chi \simeq \chi. \tag{4.15}$$

The reasons why the small wake skew angle assumption is not applied before Eq. (2.85) in the derivation or why Eqs. (2.83.2) and (2.83.3) are not approximated down to χ are not explained in Ref. (7) at all. The way of applying the assumption in the original derivation is thus considered mathematically inconsistent.

Since logical debâcles with regard to the above-mentioned points are evident, the gap between the questionable derivation and the experimental validity of the resultant model cannot be filled by a deductive discussion within the present frame of the derivation.

This may indicate that the only possibility to deductively justify the assumption, if any, may lie in a fundamental extension of the model derivation by introducing new (more reasonable) assumptions, which shall be related to those physical phenomena that are hugely simplified or not considered at all in the original model, to construct consistent logics. Indeed, there are quite a few ignored or oversimplified physical phenomena in the original derivation. (For example, the cylindrical description of the wake tube itself is a crudest modelling of a wake tube and thus quite unrealistic.) When extending the original model derivation by taking new physical aspects into

consideration, there are generally two possible approaches; (i) building a completely new model from scratch with the aim to outperform the Peters and He model with a more mathematically consistent derivation, and (ii) modifying the present derivation of Peters and He model with the aim to have the same resultant model with a more mathematically consistent derivation.

With regard to the former approach, if the new model outperforms or works at least as well as the Peters and He model, then the paradox with the small wake skew angle assumption may be considered to be ascribed to the newly incorporated physical aspects. However, even if the new model performs well, the new model should also require experimental validation, and thus this cannot be a conclusive *mathematical proof* against the small wake skew angle assumption. (Recall that the Peters and He model is *already experimentally validated* implying that the small wake skew angle assumption is practically useful. As long as the extension of the present model should (even partly) rely on an experimental method, it is logically difficult to rigorously refute the small wake skew assumption thereby.) In addition, new assumptions related to the new physical aspects shall be new problems to experimentally validate because the effects of these physical phenomena are not easily evaluated theoretically. In any case, a new model should be considered as a different model from the Peters and He model and thus cannot be a theoretical counter-proof against the derivation of the Peters and He model. Also, building a completely new dynamic inflow model together with its validation should be beyond the scope of this thesis.

With regard to the latter approach, even though it were possible to ascribe the paradox with the small wake skew angle assumption to some new physical phenomena, since there should still be many simplifications and neglected physical phenomena in the original derivation, the selection of those physical phenomena which to newly introduce should inevitably be purposeful and intentional to some extent, as long as the derivation is aimed to result in the same representation as that of the Peters and He model. In order to theoretically verify the selection, it is required to exclude all the other possibilities which may be related to the wake skew angle; otherwise the selection can be considered as a purposefully far-fetched. However, this *probatio diabolica* is logically impossible to carry out.

Based on the discussion above, this author concludes that a deductive approach towards the paradox regarding the small wake skew angle assumption is impossible

even by extending the present frame of the derivation with new physical phenomena taken into consideration.

Those points discussed so far can be summarised as;

(E1) the small wake skew angle assumption is mathematically evidently questionable, regardless of the practical validity of the model. It cannot mathematically be acceptable and rather meaningless to apply a large χ to an equation which is derived on assumption that $\chi \ll 1$;

(E2) within the present frame of the derivation, there is no mathematically cogent reason available which verifies the application of those equations which are derived based on the small wake skew assumption even to those cases in which the assumption breaks down;

(E3) the way of applying the assumption in the derivation is not consistent (e.g. Eqs. (4.12) - (4.15));

(E4) the gap between the practical validity of the model and the mathematical inconsistency with the small wake skew angle assumption cannot theoretically be elucidated. The mathematical inconsistency is evident and thus the model's practical validity cannot be further theoretically discussed within the present frame of derivation;

(E5) even if it were possible to build a new model without the small wake skew angle assumption by newly incorporating some physical phenomena, the selection should inevitably be purposeful. Also, the validity of the selection needs to prove that all other possibilities are excluded, but this proof is logically impossible;

(E6) it is impossible to quantitatively evaluate complicated physical phenomena in a theoretical approach. In any case, the effect of new physical phenomena should be validated experimentally, thus this approach is weak as a theoretical counter-proof against the derivation of Peters and He model;

(E7) there is a theoretical possibility that a model without the small wake skew angle assumption can be built from scratch to outperform the Peters and He model. However, the validation of the new model should also be provided experimentally. This is weak as a mathematical counter-proof against the Peters and He model because the possible new model should be regarded as a different model from the original Peters and He model.

Although this author concludes that the application of the small wake skew angle assumption cannot theoretically validated by a deductive approach, it is possible to inductively discuss the small wake skew angle assumption approving as the starting point that the Peters and He model is practically valid. This approach cannot logically provide any rigorous proof, but can provide a reasonable explanation of the problem, and hence must be meaningful to make an insight into this issue deeper.

4.3.2 Characteristics of the Gain Matrix Elements of the Peters and He Model

The properties of the gain matrix elements of the Peters and He model should be now discussed. Figure 4-10 shows comparisons between the trigonometric parts contained in the gain matrix elements of the Peters and He model and their counterparts in the no-assumption model derived in Section 4.2.

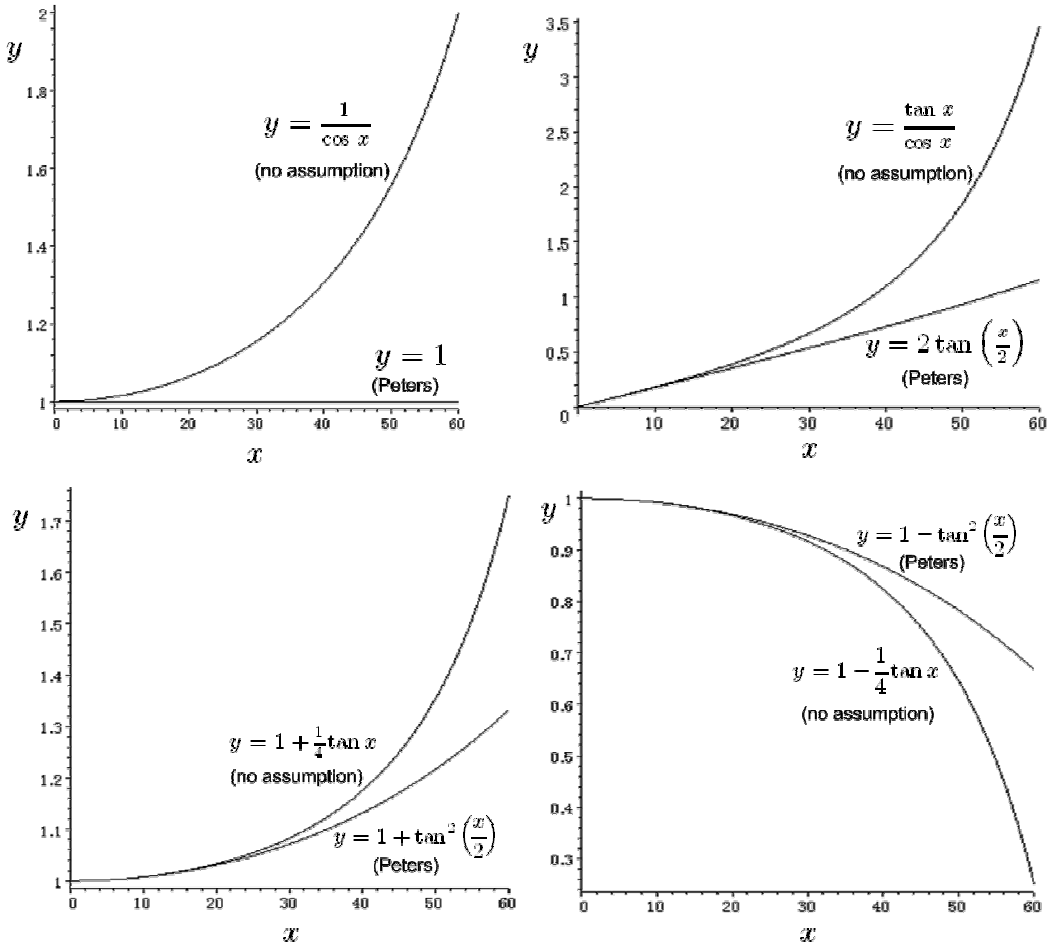

Fig. 4-10 [Comparisons of trigonometric parts in the gain matrices.]

It can be seen that the non-approximated equations are well approximated by the approximated functions up to around $10°$, then the non-approximated equations rapidly diverge to either $\pm\infty$ as $x \to 90°$, whereas the approximated equations remain finite. In fact, compared to the rapid divergence of the non-approximated equations, the behaviours of approximated equations at larger wake skew angles are considerably gentle (somewhat linear or parabolic), Fig. 4-11; they remain only within the range from 0 to 2 at $x = 90°$.

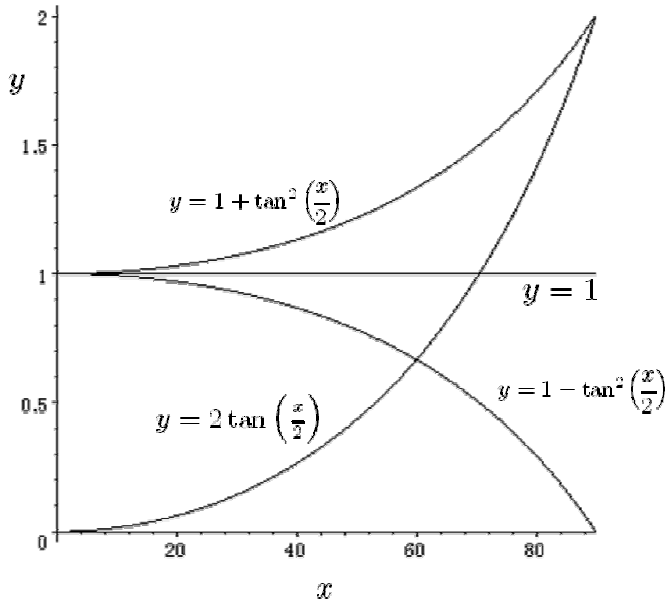

Fig. 4-11 [Trigonometric parts based on the small wake skew angle assumption.]

Recalling (E1) and (E2), this author believes that the only possibility to explain the small wake skew angle assumption is to assume;

(F1) the small wake skew angle assumption may be merely an expediency to derive Eqs. (2.83.2) and (2.83.3), which gently behave as χ increases, and hence have physically little to do with actual small wake skew angles;
(F2) Equations. (2.83.2) and (2.83.3) may approximate not only those cases in which the wake skew angle is small but also some cases in which the wake skew angle is pretty large.

Regarding (F1), it is quite possible to assume that the resultant forms of gain matrix elements of the Peters and He model are pre-aimed, because the trigonometric parts of the resultant gain matrix are identical with those of the Pitt and Peters model[(1)]. In fact,

this view explains the apparently inconsistent way of applying the small wake skew angle assumption, (E3), and also why the resultant model is later extended up to $\chi = 90°$.

Point (F2) above can be also considered as a reasonable inference when comparing with the Pitt and Peters model, because no assumption about the range of wake skew angles is underlying in the derivation of the Pitt and Peters model, that is to say, the same trigonometric functions as those of the Peters and He model can be therein derived without the small wake skew angle assumption. Interestingly, edgewise flight case, in which the gain matrix elements of no-assumption model in Subsection 4.2.2 diverge to infinity, is also analytically dealt with in the derivation of Pitt and Peters model to provide finite values to the gain matrix elements.

Now, in order to examine the conjectures of (F1) and (F2) above, the derivation of the Pitt and Peters model should be revisited in comparison with that of the Peters and He model with the foci on (i) how the trigonometric functions are therein derived without using the small wake skew angle assumption, and (ii) how the edgewise flight case is analytically dealt with in the derivation.

4.3.3 The Pitt and Peters Model and the Edgewise Flight Case

In the Pitt and Peters model, the gain matrix elements are determined based on Eq. (2.15),

$$w = \frac{1}{V}\int_{\infty}^{0} \frac{\partial \Phi}{\partial z} d\xi, \qquad (2.15)$$

in the same manner as in the Peters and He model. The pressure potential function is also represented by the associated Legendre functions of the first and second kinds, and the model derivation is not essentially different from that of the Peters and He model up to this point. However, Eq. (2.15) is treated in quite a different way in the derivation of Pitt and Peters model than that in the Peters and He model.

While the skewed cylindrical description of the wake tube is necessarily introduced in the Peters and He model to explicitly carry out the integral of Eq. (2.15) with the wake skew angle as a variable, the gain matrix elements of the Pitt and Peters model are determined in the following manner(1);

(i) analytically performing the integral of Eq. (2.15) for axial flight;
(ii) analytically performing the integral of Eq. (2.15) for edgewise flight;
(iii) *guessing* functions which can bridge the results from processes (i) and (ii);
(iv) numerically validating the resultant model.

In the process (iii) above, the suitable functions are chosen from Mangler's Fourier coefficients, Refs. (48) and (176)[58]. It is interesting that the edgewise flight case is analytically calculated in the derivation of the Pitt and Peters model, while the edgewise flight case is excluded in the derivation of the Peters and He model at this stage because otherwise the right-hand term of Eq. (2.69.1) tending to $0/0$ when $\chi \to 90^\circ$ is impossible to define.

Therefore, it should be worth trying to deal with the edgewise flight case for the Peters and He model in the same manner as in the derivation of the Pitt and Peters model. Note that since the wake skew angle is not explicitly used in the derivation of the Pitt and Peters model, no assumption is therein required about the wake skew angle. In perfectly edgewise flight, the ξ-axis coincides with the x-axis and is described in the ellipsoidal coordinate system as; (i) $\eta = 0, \quad -1 \le \nu \le 1$ on the rotor disc; and (ii) $\nu = 0, \quad 0 \le \eta \le \infty$ outside the rotor disc (see Fig. A2-1).

Following the same manner as in the Pitt and Peters model in Ref (1), the gain matrix elements of the Peters and He model for edgewise flight should be able to be represented as

$$\hat{L}_{jn}^{rmc} = \frac{1}{2\pi}\int_0^{2\pi}\int_0^1\int_{\sqrt{1-y_0^2}}^{\infty}\left[\frac{\partial}{\eta\partial\nu}\left(\bar{P}_n^m(\nu)\bar{Q}_n^m(i\eta)\cos(m\psi)\right)\right]_{\nu=0} dx\cdot\bar{P}_j^r(\nu_0)d\nu_0 d\psi$$
$$+\frac{1}{2\pi}\int_0^{2\pi}\int_0^1\int_{x_0}^{\sqrt{1-y_0^2}}\left[\frac{\partial}{\nu\partial\eta}\left(\bar{P}_n^m(\nu)\bar{Q}_n^m(i\eta)\cos(m\psi)\right)\right]_{\eta=0} dx\cdot\bar{P}_j^r(\nu_0)d\nu_0 d\psi . \tag{4.16}$$

[58] Mangler represented the induced velocity distribution in the form of the Fourier series, and $\tan\frac{\chi}{2} = \sqrt{\frac{1-\sin\alpha_e}{1+\sin\alpha_e}}$ appears as the coefficient for first harmonics, Ref. (48). However, Mangler put some assumptions including that the rotor is lightly loaded, that the distribution is symmetrical about the x-axis and so on, and hence the rotor described in Mangler's theory may be different from that for the Pitt and Peters model, in which those assumptions are not underlying. Considering the facts that the cosine components alone in the dynamic inflow model describe a symmetrical distribution about the x-axis and that the first harmonics describe only linear unevenness in the distribution, it may be reasonable to suppose that the coefficient for $\cos\psi$ can be $\tan(\chi/2)$. Still, the process for determining the gain matrix elements, process (iii) above, is not analytically clear at all.

See Fig. 4-12 about the integral domains.

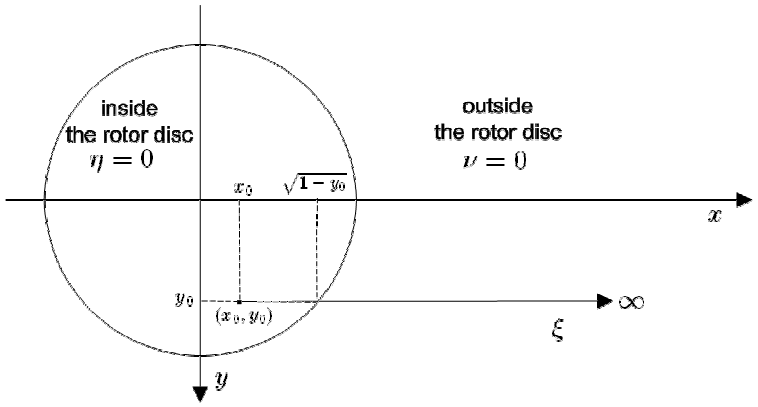

Fig. 4-12 [Integral Domains of the ξ-axis for the Edgewise Flight Case.]

Unlike the original derivation of the Peters and He model, the gain matrix elements for edgewise flight as represented above should be able to analytically be determined by the integral in Eq. (4.16), because there is no essential difference in the pressure potentials between the Pitt & Peters and Peters & He models except $\pm$ signs and coefficients related to normalisation.

In order to calculate the right-hand side of Eq. (4.16), the derivation of the Pitt and Peters model can be utilised. Reference (1) shows as an analytical result;

$$\lambda_0 = -\frac{1}{V}\int_{\infty}^{\sqrt{1-y_0^2}} \frac{1}{\eta}\cdot\frac{\partial\tilde{\Phi}}{\partial\nu}\Big|_{\nu=0,m=0,n=1} dx - \frac{1}{V}\int_{\sqrt{1-y_0^2}}^{x_0} \frac{1}{\nu}\cdot\frac{\partial\tilde{\Phi}}{\partial\eta}\Big|_{\eta=0,m=0,n=1} dx$$

$$= \frac{1}{2V}C_T + \frac{15\pi}{64V}C_M, \qquad (4.17)$$

where $\tilde{\Phi}$ is the pressure potential for the Pitt and Peters model defined as $\tilde{\Phi} = -\sum_{m,n=-,\ m\le n}^{\infty} P_n^m(\nu)Q_n^m(i\eta)\left[C_n^m\cos m\psi + D_n^m \sin m\psi\right]$.

Considering $\bar{P}_1^0(\nu)\bar{Q}_1^0(i\eta) = -\sqrt{3}\,P_1^0(\nu)Q_1^0(i\eta)$ and $\int_0^{2\pi}\int_0^1 \bar{P}_1^0(\nu_0)d\nu_0 d\psi = \sqrt{3}\,\pi$, it can be predicted from Eq. (4.17) that when $m=0,\ n=j=1$,

$$\hat{L}_{nj}^{0mc} = \frac{3}{2}. \qquad (4.18)$$

This result coincides with Eq. (2.102.1), which is derived on the small wake skew angle assumption. This coincidence is highly interesting when recalling the no-assumption model in Section 4.2, whose gain matrix elements diverge to infinity at $\chi = 90°$.

In the derivation of the Pitt and Peters model, other gain matrix elements such as L_{13}, L_{31} and L_{33} are also analytically obtained. (Note that it is stated in Ref. (1) that L_{22} is an exception, and only a numerical result of $L_{22} \simeq 2$ is therein shown.) Since there is no essential difference in the pressure potentials between the Pitt & Peters and Peters & He models except coefficients it can be considered that Eq. (4.16) is possible to analytically calculate also for other combinations of m, n, r and j for edgewise flight. The coincidence between Eqs. (4.18) and (2.102.1) should strengthen views (F1) and (F2) above that the small wake skew angle assumption has little to do with actual wake skew angles; the assumption rather seems to be playing a role in bridging axial and edgewise flights.

Since both Eq. (4.18) and the no-assumption model, in which $\bar{L}_{11}^{00c} \to \infty$ for edgewise flight, are analytically derived, there must be another analytical difference which made their results so different in their derivations. When comparing Eq. (4.16) and Eq. (2.65), it can be noticed that while Eq. (4.16) have two terms related to $\partial/\partial\nu$ and $\partial/\partial\eta$, respectively, Eq. (2.65) has only one term related to $\partial/\partial\eta$. At the stage when Eq. (2.65) is derived, the small wake skew angle assumption is not yet applied, and hence it can be believed that the difference is brought independently of the small wake skew angle assumption. Indeed, the $\partial/\partial\nu$ term is missed out from the derivation of the Peters and He model when Eq. (2.49) is simplified to Eq. (2.50)[59]. This simplification should be fully justified for the derivation of the apparent mass matrix elements because the derivation is based on Eq. (2.17) without any integrals. However, the simplification is maybe not appropriate for the derivation of the gain matrix elements because the integral path along the ξ-axis is not restricted only in the domain which is described as $\eta = 0$. Thus, even for obtaining the induced velocity distribution on the rotor disc, it is considered that $\eta = 0$ should be substituted only after the integral along the ξ-axis is

[59] The derivation of the no-assumption model in Section 4.2 is entirely based on that of the Peters and He model, except for the small wake skew angle assumption. The fact that the no-assumption model, which must mathematically be more consistent, breaks down for edgewise flight should indicate that the key to explain the difference between Eq. (4.18) and the divergence to infinity would lie in other part of the original derivation of the Peters and He model than the small wake skew angle assumption itself. This observation is consistent with the identification of the difference between Eqs. (4.19) and (2.65).

completed.

Based on this view, Eq. (2.65.1) can be extended by using Eq. (2.49) as

$$\hat{L}_{jn}^{rmc} = -\frac{1}{2\pi}\int_0^{2\pi}\int_0^1\int_0^\infty \left[\frac{\eta(1-\nu^2)}{\nu^2+\eta^2}\cdot\frac{\partial}{\partial\nu}\left(\bar{P}_n^m(\nu)\bar{Q}_n^m(i\eta)\cos(m\psi)\right) + \frac{\nu(1+\eta^2)}{\nu^2+\eta^2}\cdot\frac{\partial}{\partial\eta}\left(\bar{P}_n^m(\nu)\bar{Q}_n^m(i\eta)\cos(m\psi)\right)\right] d\xi\Big|_{\eta=0}\cdot\bar{P}_j^r(\nu_0)\cos(r\psi)d\nu d\psi. \tag{4.19}$$

Now, the possibility of further pressing on the integral of Eq. (4.19) analytically shall be examined. The ξ-axis is represented in the ellipsoidal coordinates as

$$\xi = -\sqrt{2-\nu_0^2-\nu^2+\eta^2-2y_0^2-2\sqrt{[(1+\eta^2)(1-\nu^2)-y_0^2](1-y_0^2-\nu_0^2)}}, \tag{4.20}$$

and thus

$$d\xi = \frac{\nu J-\nu(1+\eta^2)(1-y_0^2-\nu_0^2)}{J\sqrt{2-\nu^2+\eta^2-\nu_0^2-2y_0^2-2J}}d\nu - \frac{\eta J-\eta(1-\nu^2)(1-y_0^2-\nu_0^2)}{J\sqrt{2-\nu^2+\eta^2-\nu_0^2-2y_0^2-2J}}d\eta, \tag{4.21}$$

where $J=\sqrt{[(1+\eta^2)(1-\nu^2)-y_0^2](1-y_0^2-\nu_0^2)}$.

Also, along the ξ-axis, ν and η satisfy

$$\sqrt{1+\eta^2-\nu^2-\eta^2\nu^2-y_0^2}-\sqrt{1-y_0^2-\nu_0^2} = -t\nu\eta, \tag{4.22}$$

where

$$t \equiv \tan\chi = -\frac{\sqrt{(1+\eta^2)(1-\nu^2)-y_0^2}-\sqrt{1-y_0^2-\nu_0^2}}{\nu\eta}. \tag{4.23}$$

Therefore, along the ξ-axis,

$$d\nu = -\frac{\nu(1-\nu^2-y_0^2-\sqrt{(1-\nu^2+\eta^2-\eta^2\nu^2-y_0^2)(1-y_0^2-\nu_0^2)})}{\eta(1+\eta^2-y_0^2-\sqrt{(1-\nu^2+\eta^2-\eta^2\nu^2-y_0^2)(1-y_0^2-\nu_0^2)})}d\eta. \qquad (4.24)$$

Also, from Eq. (4.22), ν can be represented as a function of η along the ξ-axis,

$$\nu = \frac{\eta\sqrt{1-y_0^2-\nu_0^2}\sin\chi+\sqrt{K}}{\cos^2\chi+\eta^2}\cos\chi, \qquad (\text{for } \nu > 0) \qquad (4.25)$$

where

$$K = \eta^2(\eta^2+1)+\nu_0^2(\eta^2+1)\cos^2\chi-\eta^2y_0^2\sin^2\chi. \qquad (4.26)$$

Inserting Eqs. (4.21), (4.24), (4.25) and (4.26) into Eq. (4.19) gives an integral of η alone with the integral domain of η from 0 to ∞.

It can be easily confirmed that when $m = r = 0$, $n = j = 1$, $\nu_0 = 1$, $\chi = 0$, $y_0 = 0$,

$$\int_0^\infty \frac{\partial\Phi}{\partial z}d\xi = \int_\infty^0 \left(\sqrt{3}\tan^{-1}\left(\frac{1}{\eta}\right)-\frac{\sqrt{3}\,\eta}{1+\eta^2}\right)d\eta = \sqrt{3}. \qquad (4.27)$$

Thus, for this special case, Eq. (4.19) will be

$$\hat{L}_{11}^{00c} = \frac{3}{2\pi}\int_0^{2\pi}\int_0^1 d\nu_0 d\psi = \frac{3}{2}. \qquad (4.28)$$

The coincidence between Eqs. (4.28) and (2.102.1) indicates that Eq. (4.19) hierarchically covers the axial flight case of the Peters and He model. Also, it can be shown that Eq. (4.19) naturally accommodate Eq. (4.16), which is derived from Eq. (4.19) by assuming two extreme cases, $\nu = 0$ and $\eta = 0$, respectively. Therefore, it can be said that Eq. (4.19) should describe more general cases varying from axial to edgewise flights. Equation (4.19) can also naturally reduce down to Eq. (2.50) when $\eta = 0$ for the derivation of the apparent mass matrix.

It should be hoped that an analytical solution could be provided from Eq. (4.19) for an arbitrary combination of ν_0, y_0, m, n, r, j and χ. However, it is turned out to be

extremely difficult to analytically carry out the integrals appearing in Eq. (4.19) even for some simple cases such as $m = r = 1$ and $n = j = 2$. Since the primary aim of this Chapter is not providing a new model but clarifying the paradox with the small wake skew angle assumption, an attempt to analytically complete the integrals in Eq. (4.19) for a general case can be abandoned now. Instead, the two terms in the right-hand side of Eq. (4.19) shall be qualitatively discussed below.

When ν equals 1 (i.e. axial flight for a streamline running through the hub centre), $\eta(1-\nu^2)/(\nu^2+\eta^2)$ becomes zero and thus only the second term remains. As long as the wake skew angle is sufficiently small, ν is nearly zero over the most part of the streamline, and hence the contribution of the first term can still be considered small. On the other hand, $\nu(1+\eta^2)/(\nu^2+\eta^2)$ becomes nearly 1 when ν is close to 1. Also, $\eta \to \infty$ as $\xi \to \infty$, and thus $\nu(1+\eta^2)/(\nu^2+\eta^2) \to 1$ as $\xi \to \infty$ regardless of ν_0 or χ $(\neq \pi/2)$, thus the contribution of the second term cannot generally be ignored. This is indeed the case with the formulation of the Peters and He model, in which the first term is ignored but the wake skew angle is assumed to be small. Thus, the derivation of Peters and He model and the small wake skew angle assumption can be considered consistent in this case.

In perfectly edgewise flight (when exactly $\chi = \pi/2$), the ξ-axis coincides with the x-axis and ν becomes constantly zero outside the rotor disc, and thus the second term of Eq. (4.19) is scored out in the domain. In this case, it is believed that the first term is playing a crucial role. The huge difference between the no-assumption model, in which $\bar{L}_{11}^{00c} \to \infty$ as $\chi \to \pi/2$, and Eq. (4.28) is thus likely ascribed to the fact that the first term is ignored in the derivation of the Peters and He model.

It should be difficult to make a general comment for an arbitrary combination of m, n, r, j and χ, but based on the discussion above, what can be therefrom predicted include that (i) if the wake skew angle is sufficiently small, the contribution of the first term of Eq. (4.19) should be negligible regardless of ν_0, and (ii) if the wake skew angle is close to $\pi/2$, the first term of Eq. (4.19) may largely affect the results.

Point (i) above is consistent with the formulation of the Peters and He model including the small wake skew angle assumption, and point (ii) is underpinned when considering the difference between the edgewise cases between Eqs. (4.18) and the no-assumption model in Section 4.2, because edgewise flight and other flight scenarios

($0 < \chi < \pi/2$) must be continuously bridged from the physical point of view, and thus the gap should be explained by an analytical difference in the formulation, which must be the first term of Eq. (4.19).

Note also that in the formulation of Eq. (4.19) together with Eqs. (4.21), (4.24), (4.25) and (4.26), the wake skew angle appears only in Eqs. (4.25) and (4.26). Since Eq. (4.25) contains both $\cos\chi$ and $\sin\chi$ in its denominator, it will not diverge to infinity (or to zero either). This indicates that the general formulation based on Eq. (4.19) is free from diverging to infinity even at $\chi = \pi/2$. This is consistent with the qualitative discussion above and also with a continuous transition from axial to edgewise flights, which is intuitively required, too.

4.3.4 How the Small Wake Skew Angle Assumption Works

Recalling the difference between the derivations of the Pitt & Peters and Peters & He models, discussion in the previous Subsection indicates that introducing the small wake skew angle assumption works as if the first term of Eq. (4.19) were not ignored. In order to analytically examine this conjecture, a special case that $m = r = 0$, $n = j = 1$, $y_0 = 0$ and $\nu_0 = 1$ shall be checked. For this simplest case, the first and second terms in Eq. (4.19), which shall be designated as FT and ST hereinafter, can explicitly be expressed as

$$\begin{aligned} FT \equiv & \int_0^\infty \frac{\eta(1-\nu^2)}{\nu^2+\eta^2} \cdot \frac{\partial}{\partial \nu}\left(\bar{P}_1^0(\nu)\bar{Q}_1^0(i\eta) \right) d\xi \\ = & \sqrt{3}\int_0^\infty \left(\frac{\eta(\eta^3\cos^4\chi + \eta^3(\eta^2-1)\cos^2\chi - \eta^5)\arctan(1/\eta)}{\eta^6 + (2\eta^2+1)\cos^4\chi + \eta^2(3\eta^2+1)\cos^2\chi} \right. \\ & \left. + \frac{\eta^4 - \eta^2(\eta^2-1)\cos^2\chi - \eta^2\cos^4\chi}{\eta^6 + (2\eta^2+1)\cos^4\chi + \eta^2(3\eta^2+1)\cos^2\chi}\cos^2\chi \right) d\eta, \end{aligned} \tag{4.29}$$

$$\begin{aligned} ST \equiv & \int_0^\infty \frac{\nu(1+\eta^2)}{\nu^2+\eta^2} \cdot \frac{\partial}{\partial \eta}\left(\bar{P}_1^0(\nu)\bar{Q}_1^0(i\eta) \right) d\xi \\ = & -\sqrt{3}\int_0^\infty \left(\frac{(\eta^2+1)^2(\eta^2+\cos^2\chi)\cos^2\chi\arctan(1/\eta)}{\eta^6 + (2\eta^2+1)\cos^4\chi + \eta^2(3\eta^2+1)\cos^2\chi} \right. \\ & \left. + \frac{\eta^5 + \eta^3 + \eta(\eta^2+1)\cos^2\chi}{\eta^6 + (2\eta^2+1)\cos^4\chi + \eta^2(3\eta^2+1)\cos^2\chi}\cos^2\chi \right) d\eta. \end{aligned} \tag{4.30}$$

This author analytically calculated Eqs. (4.29) and (4.30) by using MAPLE, which is a mathematics software package for symbolic computation, for axial and edgewise

flights. For axial flight ($\chi = 0$),

$$\text{Eq. (4.29)} \Rightarrow 0, \tag{4.31}$$
$$\text{Eq. (4.30)} \Rightarrow \sqrt{3}. \tag{4.32}$$

For edgewise flight ($\chi = \pi/2$),

$$\text{Eq. (4.29)} \Rightarrow \sqrt{3} \tag{4.33}$$
$$\text{Eq. (4.30)} \Rightarrow 0. \tag{4.34}$$

Thus, the results of Eqs. (4.31) - (4.34) indicate that $FT + ST$ gives the same value both for axial and edgewise flights. These results are consistent with the conjecture in the previous Subsection, with the derivation of the Pitt and Peters model (in which the same values are analytically derived for both axial and edgewise flights), with the Peters and He model based on the small wake angle assumption (in which $\bar{L}_{11}^{00c}$ is assumed to be constant) and also with Eq. (2.130). However, for other flight scenarios between axial and edgewise flights ($0 < \chi < \pi/2$), it can be predicted that FT and ST would not that beautifully set off each other because of the differences noticed between Eqs. (4.29) and (4.30).

Since FT and ST behave in somewhat opposite ways as χ increases to balance each other to some extent, as discussed in the previous Subsection, it may be a good approximation to use only one of them with its behaviour moderated with regard to χ. It is hence understandable that the small wake skew angle assumption may approximate the model well not only for axial flight but also edgewise flight. Yet, any symmetry cannot be clearly recognised between Eqs. (4.29) and (4.30) with regard to χ, it is therefore indicated that FT and ST would not generally result in $\sqrt{3}$ when $0 < \chi < \pi/2$. (If Eqs. (4.29) and (4.30) had a symmetry with regard to χ, it would have been the case that FT and ST may have balanced each other resulting in a constant value for the $\bar{L}_{11}^{00c}$ for any χ; but this is highly likely not the case.)

This further indicates that although the result based on the small wake skew angle assumption (i.e. a constant value for $\bar{L}_{11}^{00c}$) is well consistent with the analytical results above and thus well bridge axial and edgewise flight cases, the assumption would likely not always coincide with analytical results when $0 < \chi < \pi/2$. With regard to the small wake skew angle assumption, naturally arising questions should include an argument

whether the assumption provides analytical solutions for some reason or it provides mere approximations. In point of fact, the sheer coincidence of the trigonometric functions in the gain matrix of the Peters and He model with those of the Pitt and Peters model would naturally make readers face a question if there is a hidden mathematical reason which allows the questionable application of the assumption to provide analytical solutions.

This author discussed only a special case of $\bar{L}_{11}^{00c}$, but believes that the discussion above should suffice as a counter-proof in response to the question above to show that the small wake skew angle assumption does not provide analytically rigorous results for all $\chi \in [0, \pi/2]$. Moreover, the present author adds following two reasons to conclude that the small wake skew angle assumption does not provide analytical solutions; (i) the way of applying the assumption in the original derivation is analytically not consistent, E(3), and; (ii) in the derivation of the Pitt and Peters model, it is stated that L_{22} for edgewise flight cannot analytically derived unlike other gain matrix elements, and it is only numerically shown that $L_{22} \simeq 2$. This indicates that $\bar{L}_{22}^{11s} = 2$ for $\chi = \pi/2$ in the Peters and He model is not consistent with its fully analytical result[60]. This conclusion should be consistent with points (E1), (E2) and (E3), and also with conjectures (F1) and (F2).

In any case, in order to more generally and rigorously discuss if ST together with the small wake skew angle assumption can well approximate those results which are derived from FT and ST for axial and edgewise flight cases, Eq. (4.19) ideally needs to be analytically calculated to a closed-form as a function of χ. However, it is turned out that it is extremely difficult to press on the integrals for more general cases. This potentially intensive calculation must be well beyond the scope of this thesis, and hence this author believes that this problem can be left as a good future problem.

It is believed that this problem needs to be concluded through more concrete proofs and discussion. Especially, it is necessary that the original authors would join the discussion to provide clear and coherent explanations about (i) the difference between the Pitt & Peters and Peters & He models in the treatments of the edgewise flight cases, and (ii) how the small wake skew angle assumption can be analytically validated. It is

[60] Indeed, there is a certain symmetry recognised between the two terms in Eq. (4.19) with regard to ν and η. For example, Eq. (4.19) approximately reduces to $(1/\nu)(\partial\Phi/\partial\eta)$ and $(1/\eta)(\partial\Phi/\partial\nu)$ for axial and edgewise flights, respectively. However, the present author was not able enough to draw a conclusion to the problem if there is any logical connection between this symmetry and the practical validity of the small wake skew angle assumption.

hoped that this thesis would provoke further discussion of this problem.

4.4 Chapter Summary

This is arguably the first study which identified the paradoxical aspects of the small wake skew angle assumption in the derivation of Peters and He model. A new model based on the derivation of Peters and He model was proposed without the assumption, but this model does not work well. This further led to the discussion why the Peters and He model practically works so well in spite of the questionable assumption. In so doing, the difference between the Pitt & Peters and Peters & He models in the treatments of the edgewise flight cases was identified and the paradox with the small wake skew angle was explained in relation to the difference.

Discussed points and results in this Chapter can be summarised as follows:

1. Regarding the small wake skew angle assumption used in the derivation of the Peters and He model, this author points out its mathematical inconsistency and inappropriateness. A new model is proposed without using the assumption, but the results suggested by the model are counter to reality;
2. This author discussed why the Peters and He model practically works well in spite of the questionable application of the small wake skew angle assumption in the derivation. In so doing, the possibility of deductively proving the validity of the assumption is ruled out, and thus only inductive discussions are made on the assumption that the Peters and He model is practically valid;
3. Due to the mathematical inconsistency that the resultant model is extended to large wake skew angles, this author conjectured that the small wake skew angle assumption has little to do with an actual wake skew angle, but may play a role in approximating the model for some specific flight cases including a flight case with a large wake skew angle such as edgewise flight;
4. Since the gain matrix elements in the Pitt and Peters model for edgewise flight are analytically determined, this author applied the same approach for the gain matrix elements of the Peters and He model without using the small wake skew angle assumption, and obtained the same result as those of the original model, which is derived based on the assumption;
5. By comparing the equation for edgewise flight in the derivation of Pitt and Peters model and the Peters and He model, this author points out that the base equation of the Peters and He model, Eq. (2.50), lacks one term related to $\partial/\partial\nu$. It is identified

that the pertinent term is left out when Eq. (2.49) is simplified to Eq. (2.50), but the simplification is maybe not appropriate for generally deriving the gain matrix elements;

6. The properties of two terms contained in Eq. (2.49) are qualitatively discussed. It is confirmed that the first term, which is left out at the simplification, may not hugely affect the result when the wake skew angle is nearly zero. Thus, the derivation of the Peters and He model, in which the first term is ignored but the wake skew angle is assumed to be small, is consistent in this point;
7. It is qualitatively discussed that the two terms contained in Eq. (2.49) behave somewhat in opposite ways as the wake skew angle increases. Thus, it can be considered reasonable to think that only the second term in Eq. (2.49) together with the small wake skew angle assumption may approximate the equation both for axial and edgewise flights to some extent;
8. Since it is turned out that analytically carrying out the integrals in Eq. (4.19) should be extremely difficult, only the simplest special case with $\bar{L}_{11}^{00c}$ is examined to test the prediction above. It is confirmed that the axial and edgewise flight cases result in the same value, as if the small wake skew angle assumption were therein assumed, due to the opposite tendencies that the two terms in Eq. (4.19) have. Still, the two terms do not have a perfect symmetry with regard to the wake skew angle. This likely indicate that they would not always balance out for $0 < \chi < \pi/2$;
9. It can be predicted that the small wake skew angle assumption may more generally approximate the axial and edgewise flight cases. However, in order to confirm this conjecture more rigorously, it is to be hoped in the future that the integrals in Eq. (4.19) will be fully analytically completed to a closed-form as a function of χ.

Chapter 5

Conclusions and Future Directions

5.1 Introductory Remarks - *Review of the Research Aim and Objectives*

The predefined aim of this research project is to theoretically build a dynamic inflow model that is suitable for autorotative rotors. The dynamic inflow model for the helicopter has been intensively developed by Peters and his co-workers over the last two decades, but little theoretical attention has hitherto been paid to the possible application of the model to the autorotative rotors, which include rotors of gyroplanes and autorotating helicopters.

The literature suggests that this should be the first time that the dynamic inflow model has been theoretically examined for autorotative rotors, and it is hoped that this thesis will offer a valuable contribution to control analyses of gyroplanes and helicopters in autorotation. Since this thesis sought to develop a new application of the dynamic inflow mode, the theory of the dynamic inflow model needed to be thoroughly re-examined in order to identify the necessary modification. Consequently, the research objectives were defined as the following three steps:

(i) to critically review the theoretical derivation of the contemporary dynamic inflow models in detail;
(ii) to examine whether these contemporary dynamic inflow models can also be applied to autorotative rotors;
(iii) to identify necessary modifications to the contemporary dynamic inflow model in order that this model can be applied to autorotative rotors.

Clearly a desired outcome of this investigation would have been the determination that existing dynamic inflow models can be applied to autorotative rotors without modification. In such a scenario step (iii) above would be unnecessary, while steps (i) and (ii) would still have been required establishing a theoretical verification of the modified model.

The next Section summarises these results.

5.2 Conclusions

The author first examined in detail the derivation of the Peters and He dynamic inflow model, which is originally designed for helicopters in the normal working state, and also considered whether it can be used also for gyroplanes. As a result, the following results and observations are obtained:

1. The Peters and He model can be used for autorotative rotors without any change in the matrix elements, but a modification is necessary in the mass-flow parameter.
2. Other dynamic inflow models such as the Pitt and Peters model also follow Conclusion 1 above, since the matrix elements can be determined regardless of the geometric difference, whereas the difference in the mass-flow parameter arises from the fundamental geometric difference between rotors in the normal working and windmill-brake states.
3. The modified mass-flow parameter for the windmill-brake state is proposed. In the course of the study of the mass-flow parameter, the difference between Chen's and Peters' definitions of the mass-flow parameter is clarified. It is confirmed that Chen's definition is not appropriate to be used for the wind-mill brake state.
4. It is confirmed from numerical simulations that the difference in results of the models using the modified and unmodified mass-flow parameters is generally negligible in controls and airframe attitudes during trim flights. The difference becomes more pronounced in the stability characteristics, but only in steep descents.
5. The difference between V_{m+} and V_{m-} significantly affects stability analysis. Some modes for steep descent in autorotaion obtained with V_{m+} are in the unstable region, but these modes become stable with V_{m-}. Stable modes can be considered physically more realistic than unstable modes.
6. It is confirmed that the difference in the modified and unmodified mass-flow parameters does not significantly alter the results of previous studies such as Refs. (151) - (155), where the unmodified mass-flow parameter was used for the windmill-brake state.
7. The unified form of V_{m+} and V_{m-} is proposed so as to be consistent with Peters' definition of $\tan\alpha$.

It is believed that the predefined aim and objectives of this research project are successfully accomplished by Conclusions 1 - 7. Especially, Conlusion 5 underpins the necessity of modifying the original mass-flow parameter in Peters' dynamic inflow

models, V_m, into V_{m-} for the windmill-brake state. This issue, however, needs further investigation, because no flight data for steep descent in autorotation is available to confirm the simulation results and observations above.

Furthermore, in the course of re-examining the dynamic inflow model in detail, the following critical views concerning the dynamic inflow model are expressed:

8. The view that the Pitt and Peters model may not be hierarchically included by the Peters and He model is expressed on theoretical grounds.
9. The theoretical unreasonableness of the application of the small wake skew angle assumption, which is an indispensable part of the derivation of Peters and He's dynamic inflow model, to a wide range of wake skew angle is pointed out.

From a purely practical point of view, this author does not disagree that the Peters and He model may approximately cover the Pitt and Peters model in most flight cases, as are reported in Refs. (7), (92) and (102). In point of fact, Conclusions 8 is not a conclusive counter-proof against those validation works. However, those references did not show any rigorous mathematical derivations, but only stated their conclusions supported by experimental or simulational results. Since both the Pitt & Peters and Peters & He models are arguably analytically derived by the same authors, the present author believes that this situation awaits theoretical works clarifying relations between existing dynamic inflow models. It is hoped that Conclusions 8 and 9 would provoke further theoretical discussions.

This author further discussed the small wake skew angle assumption in Chapter 4 in depth, and a new model was derived on trial following the derivation of Peters and He model but without the small wake skew angle assumption:

10. A new representation of the gain matrix is theoretically derived and proposed so that the small wake skew angle approximation is not required based on the derivation of Peters and He model, and that the Peters and He model is hierarchically therein contained as an approximation in the limit that the wake skew angle tends to zero. However, the simulation results indicate that the newly proposed model does not perform well.

Based on Conclusion 10 and the practical validity of the Peters and He model[7,92,

[102,107], this author discussed why the Peters and He model works so well in spite of the questionable assumption, and the following points are identified:

11. While the new no-assumption model above breaks down for edgewise flight, the edgewise flight case is also dealt with analytically in the derivation of the Pitt and Peters model, though their theoretical bases should not be markedly different from the Peters and He model. Comparing the Peters & He and Pitt & Peters models for edgewise flight, it is identified that the Pitt and Peters model has an extra term. The term is ignored in the derivation of Peters and He model before the small wake skew angle assumption is introduced in the model.
12. Considering the facts that the Pitt & Peters and Peters & He models have identical trigonometric functions for their gain matrices and that the derivation of Pitt and Peters model does not require any assumption about the wake skew angle, it can be assumed that equations based on the small wake skew angle assumption may describe not only those cases in which the wake skew angle is small, but also those cases in which the wake skew angle is pretty large.
13. It was qualitatively discussed that the two terms contained in Eq. (4.19) behave in somewhat opposite ways as the wake skew angle increases. This tendency is analytically confirmed for a special case that $m = r = 0$, $n = j = 1$, $y_0 = 0$ and $\nu_0 = 1$.
14. From Conclusions 11, 12 and 13, it can be predicted that introducing the small wake skew angle assumption may work as if both two terms of Eq. (4.19) were retained.
15. The asymmetry between Eqs. (4.29) and (4.30) with respect to χ indicates that $\bar{L}_{11}^{00c}$ is not always constant depending on χ. This observation is against the result based on the small wake skew angle assumption, in which $\bar{L}_{11}^{00c}$ is constant. This further indicates that the small wake skew angle assumption should not provide analytical results to the model but provide only approximations thereto.

The identification that the small wake skew angle assumption is inconsistent can be regarded as a significant result by itself, and it is believed that this is the first study to question the validity of its application on theoretical grounds. Conclusions 10 - 15 above were held in an inductive way on the assumption that the small wake skew angle assumption and the resultant model are practically acceptable. In order to theoretically confirm more rigorously Conclusions 14 and 15, it is ideally necessary that Eq. (4.19) should be calculated analytically to a close-form as a function of the wake skew angle. However, it was turned out that this calculation is extremely difficult. Conclusion 13 is

examined about only one special case, but this is considered to be enough as a counter-proof to show that the small wake skew angle assumption does not provide analytical results to the model but provide only approximations thereto.

In summary, it can be said that the predefined aim of this thesis to theoretically examine the availability of contemporary dynamic inflow models for autorotative rotors has been successfully accomplished. Also, a detailed discussion was held about the small wake skew angle assumption. It is expected that the results and observations presented in this dissertation will contribute to the relevant fields of study and lend a deeper and valuable insight into the dynamic inflow model theory.

5.3 Future Directions

The present author shall suggest some future research topics following the present research.

(i) Further Theoretical Sophistications of the Dynamic Inflow Model

With regard to possible further sophistications of the dynamic inflow model for autorotative rotors, modelling more detailed wake geometry should be worth considering, because the description of the wake tube as a skewed cylinder is the crudest approximation of reality. It must be next to impossible to analytically describe a realistic wake tube, which is highly turbulent (even though it were possible, the implementation of the wake geometry in the integral path of Eqs. (2.65) must be impossible), but even a slight improvement in the description should be important.

Conclusion 1 above is based on the present frame of the derivation of the Peters and He model, in which an autorotative rotor can be regarded the upside-down of a rotor in the normal working state, but the conclusion may change if differences in the wake geometry between normal working and wind-mill brake states such as wake contraction and expansion are taken into account in the derivation.

In addition to the static wake geometry, the dynamic behaviour of the wake tube should be important too. Dynamic effects caused by cyclic controls are discussed in Refs. (130) - (133). The dynamic response of the wake and induced flow to dynamically changing free stream may also be important in relation to autorotative rotors, because this situation may happen in an ever-increasing oscillation of poorly balanced autogyros,

which is often misconceivably called *PIO*, highly likely resulting in fatal accidents. Such dynamic problems should need a new modelling, in which those effects such as the momentum and inertia of wake tube, time-delay in the response of wake geometry and so on should be fully taken into consideration. The first thing which is worth trying for such an advanced dynamic model for gyroplanes may be to give some modifications to the gain matrix following Ref. (132).

(ii) More Consistent Model to Explain the Small Wake Skew Angle Assumption

Since Conclusions 12 and 14 are derived in an inductive approach, they cannot be logically rigorous proofs, although the prediction was confirmed about a special case. Thus, it is hoped that a new model would be build based on Eq. (4.19). It is extremely difficult (maybe impossible) to analytically complete the integrals in Eq. (4.19) to a closed-form as a function of the wake skew angle, but this is necessary to ultimately clear up the problem with the paradoxical small wake skew angle assumption.

The new model will likely be involved with extensive numerical calculations based on Eq. (4.19). The possibility of introducing new assumptions, which are more reasonable than the small wake skew angle assumption, to build a more comprehensive dynamic inflow model can also be pursued. Note that it may be not always the case that the new model could provide better results than those from the present Peters and He model from a practical point of view because of many other assumptions used in the derivation such as the cylindrical description of a wake tube. (Generally speaking, it is sometimes the case that sophisticating only one aspect of a model will result in a poorer model.) However, the paradox with the small wake skew angle assumption must be concluded as an analytical problem at this stage because the model derivation is asserted to be analytical. It is believed that a truly better analytical model cannot be built in the future without the understanding of this problem.

5.4 Conclusive Remarks

A variety of results have fruitfully been obtained from the present research not only for the autorotative rotors but also for the dynamic inflow model itself in general. All of those results are believed to be unique and significant. It is hoped that this thesis can form a valuable contribution across a wide range of relevant research fields.

Appendix 2.1 Linearisation of the Euler Equation

The motion of incompressible fluid is governed by the Navier-Stokes Equations.

$$\frac{\partial \mathbf{U}}{\partial \bar{t}} + (\mathbf{U} \cdot \nabla)\mathbf{U} = -\nabla\Phi + \nu\triangle\mathbf{U}. \qquad \text{(A2.1.1)}$$

When the viscosity can be ignored, Eq. (A2.1.1) reduced to the Euler Equations, in which $\triangle\mathbf{U} = 0$. Provided that $\mathbf{U} = \mathbf{V} + \mathbf{u}$ where $\mathbf{V}$ is the steady base flow and $\mathbf{u}$ is the perturbation, the convection term in Eq. (A2.1.1) is linearised as follows,

$$\begin{aligned}(\mathbf{U} \cdot \nabla)\mathbf{U} &= ((\mathbf{V} + \mathbf{u}) \cdot \nabla)(\mathbf{V} + \mathbf{u}) \\ &= \mathbf{V} \cdot \nabla\mathbf{V} + \mathbf{V} \cdot \nabla\mathbf{u} + \mathbf{u} \cdot \nabla\mathbf{V} + \mathbf{u} \cdot \nabla\mathbf{u} \\ &= \mathbf{V} \cdot \nabla\mathbf{u} + o(|\mathbf{u}|^2). \qquad \text{(A2.1.2)}\end{aligned}$$

Appendix 2.2 Transformation from Cartesian to Polar Coordinates on the Rotor

The azimuth in the cylindrical coordinates on the rotor is conventionally taken to the negative direction of the x-axis (see Fig. 2-1).

$$x = -\bar{r}\cos\psi, \qquad \text{(A2.2.1)}$$

$$y = \bar{r}\sin\psi. \qquad \text{(A.2.2.2)}$$

The metric factors between these two coordinate systems are defined as

$$h_1^2 = \left(\frac{\partial x}{\partial \bar{r}}\right)^2 + \left(\frac{\partial y}{\partial \bar{r}}\right)^2 = 1, \qquad \text{(A2.2.3)}$$

$$h_2^2 = \left(\frac{\partial x}{\partial \psi}\right)^2 + \left(\frac{\partial y}{\partial \psi}\right)^2 = \bar{r}^2. \qquad \text{(A2.2.4)}$$

Thus, the differential operators are transformed as follows,

$$\begin{aligned}\frac{\partial}{\partial x} &= \frac{1}{h_1^2} \cdot \frac{\partial x}{\partial \bar{r}} \cdot \frac{\partial}{\partial \bar{r}} + \frac{1}{h_2^2} \cdot \frac{\partial x}{\partial \psi} \cdot \frac{\partial}{\partial \psi} \\ &= -\cos\psi \frac{\partial}{\partial \bar{r}} + \frac{\sin\psi}{\bar{r}} \cdot \frac{\partial}{\partial \psi}\end{aligned}$$

$$= \frac{1}{2}\Big\{ e^{i\psi}\Big(-\frac{\partial}{\partial \bar{r}} + \frac{1}{i\bar{r}} \cdot \frac{\partial}{\partial \psi}\Big) - e^{-i\psi}\Big(\frac{\partial}{\partial \bar{r}} + \frac{1}{i\bar{r}} \cdot \frac{\partial}{\partial \psi}\Big)\Big\}, \tag{A2.2.5}$$

$$\frac{\partial}{\partial y} = \frac{1}{h_1^2} \cdot \frac{\partial y}{\partial \bar{r}} \cdot \frac{\partial}{\partial \bar{r}} + \frac{1}{h_2^2} \cdot \frac{\partial y}{\partial \psi} \cdot \frac{\partial}{\partial \psi}$$

$$= \sin\psi \frac{\partial}{\partial \bar{r}} + \frac{\cos\psi}{\bar{r}} \cdot \frac{\partial}{\partial \psi}$$

$$= \frac{1}{2}\Big\{ e^{i\psi}\Big(\frac{\partial}{i\partial \bar{r}} + \frac{\partial}{\bar{r}\partial \psi}\Big) - e^{-i\psi}\Big(\frac{\partial}{i\partial \bar{r}} - \frac{\partial}{\bar{r}\partial \psi}\Big)\Big\}. \tag{A2.2.6}$$

Note that

$$\frac{\partial}{\partial \bar{r}} = \frac{\partial x}{\partial \bar{r}} \cdot \frac{\partial}{\partial x} + \frac{\partial y}{\partial \bar{r}} \cdot \frac{\partial}{\partial y} = -\cos\psi \frac{\partial}{\partial x} + \sin\psi \frac{\partial}{\partial y}, \tag{A2.2.7}$$

$$\frac{\partial}{\partial \psi} = \frac{\partial x}{\partial \psi} \cdot \frac{\partial}{\partial x} + \frac{\partial y}{\partial \psi} \cdot \frac{\partial}{\partial y} = \bar{r}\sin\psi \frac{\partial}{\partial x} + \bar{r}\cos\psi \frac{\partial}{\partial y}. \tag{A2.2.8}$$

Appendix 2.3 The Ellipsoidal Coordinate System

Ellipsoidal coordinates, (ν, ψ, η), are defined by (x, y, z) as follows,

$$x = -\sqrt{1+\eta^2}\sqrt{1-\nu^2}\cos\psi, \tag{A2.3.1}$$

$$y = \sqrt{1+\eta^2}\sqrt{1-\nu^2}\sin\psi, \tag{A2.3.2}$$

$$z = -\eta\nu. \tag{A2.3.3}$$

The coordinate surfaces and their domains of definition are given as follows:

(i) ellipsoids : $\eta = const. \quad 0 \le \eta < \infty$; (A2.3.4)

(ii) hyperboloids : $\nu = const. \quad -1 \le \nu \le 1$; (A2.3.5)

(iii) half planes : $\psi = const. \quad 0 \le \psi < 2\pi$. (A2.3.6)

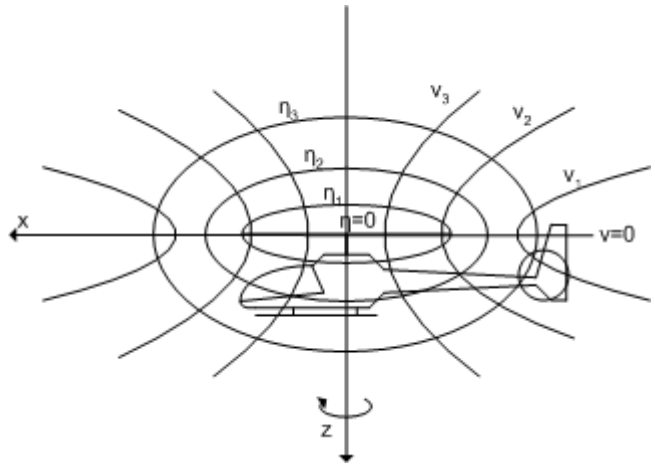

Fig. A2-1 [The ellipsoidal coordinate system.]

Examples of the representation in this coordinate system include

the hub centre	:	$\eta = 0,\ \ \nu = \pm 1,$	(A2.3.7)
the rotor surface	:	$\eta = 0,\ \ -1 \leq \nu \leq 1,$	(A2.3.8)
the edge of the rotor	:	$\eta = 0,\ \ \nu = 0.$	(A2.3.9)

Note that the upper and lower surfaces of the rotor are distinguished by the sign of ν.

$\nu < 0$	:	$z > 0,$	(the lower surface)	(A2.3.10)
$\nu > 0$	:	$z < 0.$	(the upper surface)	(A2.3.11)

The metric factors are given as follows. The subscripts of 1, 2 and 3 indicate (ν, ψ, η), respectively in this order.

$$h_1 = \sqrt{\frac{\nu^2 + \eta^2}{1 - \nu^2}}, \tag{A2.3.12}$$

$$h_2 = \sqrt{(1 + \eta^2)(1 - \nu^2)}, \tag{A2.3.13}$$

$$h_3 = \sqrt{\frac{\nu^2 + \eta^2}{1 + \eta^2}}. \tag{A2.3.14}$$

Vector differential operators (i.e. grad, div and $\triangle$) in ellipsoidal coordinates are expressed as

$$\mathrm{grad}\Phi = \mathbf{e}_\nu \sqrt{\frac{1-\nu^2}{\nu^2+\eta^2}}\frac{\partial \Phi}{\partial \nu} + \mathbf{e}_\psi \frac{1}{\sqrt{(1+\eta^2)(1-\nu^2)}}\frac{\partial \Phi}{\partial \psi} + \mathbf{e}_\eta \sqrt{\frac{1+\eta^2}{\nu^2+\eta^2}}\frac{\partial \Phi}{\partial \eta}, \tag{A2.3.15}$$

$$\mathrm{div}\mathbf{V} = \frac{1}{\nu^2+\eta^2}\Big[\frac{\partial}{\partial \nu}\Big(\sqrt{(1-\nu^2)(\nu^2+\eta^2)}\,V_1\Big) + \frac{\partial}{\partial \psi}\Big(\frac{\nu^2+\eta^2}{\sqrt{(1+\eta^2)(1-\nu^2)}}V_2\Big) + \frac{\partial}{\partial \eta}\Big(\sqrt{(\nu^2+\eta^2)(1+\eta^2)}\,V_3\Big)\Big], \tag{A2.3.16}$$

$$\triangle\Phi = \frac{1}{\nu^2+\eta^2}\Big[\frac{\partial}{\partial \nu}\Big((1-\nu^2)\frac{\partial \Phi}{\partial \nu}\Big) + \frac{\partial}{\partial \psi}\Big(\frac{(\nu^2+\eta^2)}{(1+\eta^2)(1-\nu^2)}\frac{\partial \Phi}{\partial \psi}\Big) + \frac{\partial}{\partial \eta}\Big((1+\eta^2)\frac{\partial \Phi}{\partial \eta}\Big)\Big], \tag{A2.3.17}$$

where Φ and $\mathbf{V} = (V_1, V_2, V_3)$ are arbitrary scalar and vector functions, respectively. The differential operators are formally transformed from Cartesian coordinates to ellipsoidal coordinates as follows,

$$\begin{aligned}\frac{\partial}{\partial z} &= \frac{1}{h_1^2}\cdot\frac{\partial z}{\partial \nu}\cdot\frac{\partial}{\partial \nu} + \frac{1}{h_2^2}\cdot\frac{\partial z}{\partial \psi}\cdot\frac{\partial}{\partial \psi} + \frac{1}{h_3^2}\cdot\frac{\partial z}{\partial \eta}\cdot\frac{\partial}{\partial \eta} \\ &= -\frac{\eta(1-\nu^2)}{\nu^2+\eta^2}\cdot\frac{\partial}{\partial \nu} - \frac{\nu(1+\eta^2)}{\nu^2+\eta^2}\cdot\frac{\partial}{\partial \eta},\end{aligned} \tag{A2.3.18}$$

$$\begin{aligned}\frac{\partial}{\partial x} &= \frac{1}{h_1^2}\cdot\frac{\partial x}{\partial \nu}\cdot\frac{\partial}{\partial \nu} + \frac{1}{h_2^2}\cdot\frac{\partial x}{\partial \psi}\cdot\frac{\partial}{\partial \psi} + \frac{1}{h_3^2}\cdot\frac{\partial x}{\partial \eta}\cdot\frac{\partial}{\partial \eta} \\ &= \frac{\nu(1-\nu^2)}{\nu^2+\eta^2}\sqrt{\frac{1+\eta^2}{1-\nu^2}}\cos\psi\frac{\partial}{\partial \nu} + \frac{\sin\psi}{\sqrt{(1-\nu^2)(1+\eta^2)}}\frac{\partial}{\partial \psi} - \frac{\eta(1+\eta^2)}{\nu^2+\eta^2}\sqrt{\frac{1-\nu^2}{1+\eta^2}}\cos\psi\frac{\partial}{\partial \eta},\end{aligned} \tag{A2.3.19}$$

$$\begin{aligned}\frac{\partial}{\partial y} &= \frac{1}{h_1^2}\cdot\frac{\partial y}{\partial \nu}\cdot\frac{\partial}{\partial \nu} + \frac{1}{h_2^2}\cdot\frac{\partial y}{\partial \psi}\cdot\frac{\partial}{\partial \psi} + \frac{1}{h_3^2}\cdot\frac{\partial y}{\partial \eta}\cdot\frac{\partial}{\partial \eta} \\ &= -\frac{\nu(1-\nu^2)}{\nu^2+\eta^2}\sqrt{\frac{1+\eta^2}{1-\nu^2}}\sin\psi\frac{\partial}{\partial \nu} + \frac{\cos\psi}{\sqrt{(1-\nu^2)(1+\eta^2)}}\frac{\partial}{\partial \psi} + \frac{(1+\eta^2)}{\nu^2+\eta^2}\sqrt{\frac{1-\nu^2}{1+\eta^2}}\sin\psi\frac{\partial}{\partial \eta}.\end{aligned} \tag{A2.3.20}$$

Appendix 2.4 Prandtl's Potential Function

From Eq. (A2.3.17), Laplace's Equation is expressed in the ellipsoidal coordinate system as follows,

$$\triangle\Phi = \frac{1}{\nu^2+\eta^2}\left[\frac{\partial}{\partial\nu}\left((1-\nu^2)\frac{\partial\Phi}{\partial\nu}\right) + \frac{\partial}{\partial\psi}\left(\frac{(\nu^2+\eta^2)}{(1+\eta^2)(1-\nu^2)}\cdot\frac{\partial\Phi}{\partial\psi}\right) + \frac{\partial}{\partial\eta}\left((1+\eta^2)\frac{\partial\Phi}{\partial\eta}\right)\right] = 0. \tag{A2.4.1}$$

Given that $\Phi(\nu,\psi,\eta) = \Phi_\nu(\nu)\Phi_\psi(\psi)\Phi_\eta(\eta)$, Laplace's Equation is separated into the following three differential equations corresponding to each variable.

$$\frac{d}{d\nu}\left[(1-\nu^2)\frac{d\Phi_\nu}{d\nu}\right] + \left[-\frac{m^2}{1-\nu^2} + n(n+1)\right]\Phi_\nu = 0, \tag{A2.4.2}$$

$$\frac{d}{d\eta}\left[(1+\eta^2)\frac{d\Phi_\eta}{d\eta}\right] + \left[\frac{m^2}{1+\eta^2} - n(n+1)\right]\Phi_\eta = 0, \tag{A2.4.3}$$

$$\frac{d^2\Phi_\psi}{d\psi^2} + m^2\Phi_\psi = 0. \tag{A2.4.4}$$

Equation (A2.4.2) is *the associated Legendre equation*, and its solutions are given in the form of the associated Legendre function of the first and second kinds, i.e. $P_n^m(\nu)$ and $Q_n^m(\nu)$. Equation (A2.4.3) will also result in the associated Legendre equation by replacing η with $i\eta$. Thus, the solutions are obtained as $P_n^m(i\eta)$ and $Q_n^m(i\eta)$. The solutions to Eq. (A2.4.4) are given by sine and cosine.

$$\Phi_\psi = A\cos m\psi + B\sin m\psi, \tag{A2.4.5}$$

where A and B are arbitrary constants. Among these solutions to Eqs. (2.4.2) - (2.4.4), $P_n^m(i\eta)$ and $Q_n^m(\nu)$ tend to infinity at the rotor edge ($\eta = 0,\ \nu = 0$), and thus they must be abandoned in order to satisfy the boundary condition of (B2). Therefore,

$$\Phi(\nu,\eta,\psi) = \sum_m^\infty\sum_n^\infty P_n^m(\nu)Q_n^m(i\eta)\left[C_n^m\cos(m\psi) + D_n^m\sin(m\psi)\right], \tag{A2.4.6}$$

where C_n^m and D_n^m are arbitrary constants. In addition, only those combinations in which $n = m+1, m+3, m+5, \ldots$ satisfy the boundary condition (B2). Hence,

$$\Phi(\nu,\eta,\psi)=\sum_{m}^{\infty}\sum_{m+1,m+3,\ldots}^{\infty}P_n^m(\nu)Q_n^m(i\eta)\Big[C_n^m\cos(m\psi)+D_n^m\sin(m\psi)\Big]. \tag{A2.4.7}$$

This is called *Prandtl's Potential Function* after the German physicist, Ludwig Prandtl (1875-1953), who was a great pioneer of aerodynamics.

Appendix 2.5 The Associated Legendre Functions

The associated Legendre function of the first kind is defined as a solution to the associated Legendre equation, which is described in the form of Eq. (A2.4.2). It can also be defined as polynomials,

$$P_n^m(x)=(1-x^2)^{\frac{m}{2}}\frac{d^m}{dx^m}P_n(x),\quad (-n\le m\le n) \tag{A2.5.1}$$

where $P_n(x)$ is the Legendre function of the first kind, which will be introduced later in Appendix 2.6[61]. Important relations derived from Eq. (A2.5.1) include

$$P_n^{-m}(x)=(-1)^m\frac{(n-m)!}{(n+m)!}P_n^m(x), \tag{A2.5.2}$$

$$P_n^0(x)=P_n(x). \tag{A2.5.3}$$

Note that the variable of x in this Appendix is no more than a general variable, and thus should not be interpreted as x in rotor Cartesian coordinates. In a context of rotorcraft problems, x in this Appendix is usually interpreted as $\bar{r}$. Some specific examples of the associated Legendre function of the first kind include

$$P_n^0(x)=P_n(x)=\sum_{k=0}^{[\frac{n}{2}]}(-1)^k\frac{(2n-2k)!}{2^n k!(n-k)!(n-2k)!}x^{n-2k}, \tag{A2.5.4}$$

$$P_1^1(x)=\sqrt{1-x^2}=\sin\theta, \tag{A2.5.5}$$

[61] The associated Legendre functions are occasionally defined with an additional factor of $(-1)^m$ depending on textbooks, especially in those books concerning quantum mechanics. This factor is related to the spherical harmonics, and is not necessary in a context of rotorcraft problems. The reader should pay attention to the variation in the definition when consulting references.

$$P_2^1(x) = 3x\sqrt{1-x^2} = 3\cos\theta\sin\theta, \tag{A2.5.6}$$

$$P_2^2(x) = 3(1-x^2) = 3\sin^2\theta, \tag{A2.5.7}$$

$$P_3^1(x) = \tfrac{3}{2}(5x^2-1)\sqrt{1-x^2} = \tfrac{3}{2}(5\cos^2\theta - 1)\sin\theta, \tag{A2.5.8}$$

$$P_3^2(x) = 15x(1-x^2) = 15\cos\theta\sin^2\theta, \tag{A2.5.9}$$

$$P_3^3(x) = 15(1-x^2)^{\frac{3}{2}} = 15\sin^3\theta, \tag{A2.5.10}$$

$$P_4^1(x) = \tfrac{5}{2}(7x^3-3x)\sqrt{1-x^2} = \tfrac{5}{2}(7\cos^3\theta - 3\cos\theta)\sin\theta, \tag{A2.5.11}$$

$$P_4^2(x) = \tfrac{15}{2}(7x^2-1)(1-x^2) = \tfrac{15}{2}(7\cos^2\theta - 1)\sin^2\theta, \tag{A2.5.12}$$

$$P_4^3(x) = 105x(1-x^2)^{\frac{3}{2}} = 105\cos\theta\sin^3\theta, \tag{A2.5.13}$$

$$P_4^4(x) = 105(1-x^2)^2 = 105\sin^4\theta. \tag{A2.5.14}$$

Note that some of the examples above have the substitution of $x = \cos\theta$, and this is utterly reasonable because it is proven that the set of associated Legendre functions can be a perfect set which can form a functional space spanned only by cosines[(163)]. Figure A2-2 shows some of the examples above.

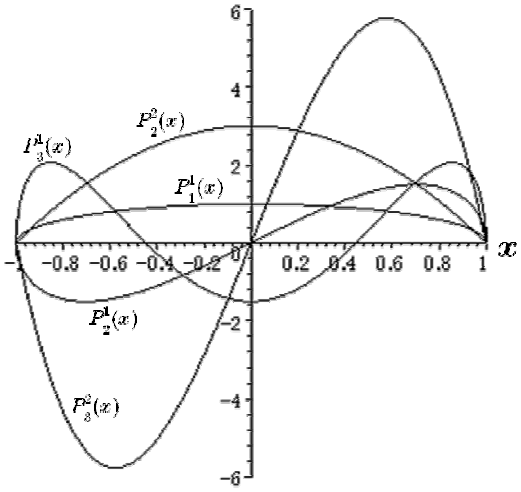

Fig. A2-2 [The associated Legendre functions of the first kind.]

It can be seen from the diagram that only those associated Legendre functions in which $m+n \equiv 1 \mod 2$ is satisfied become zero at $x=0$. Thus, only those combinations of m and n which satisfy $m+n \equiv 1 \mod 2$ are to be used in rotor problems. This property can be more rigorously proven by the following recurrence formula,

$$(2n+1)xP_n^m = (n+m)P_{n-1}^m + (n-m+1)P_{n+1}^m. \tag{A2.5.15}$$

Equation (A2.5.15) is straightforwardly given by mathematical induction from Eqs. (A2.5.4) - (A2.5.6). The orthogonality of the associated Legendre function of the first kind is represented as

$$\int_{-1}^{1} P_n^m(x)P_l^m(x)dx = \frac{2}{2n+1}\cdot\frac{(n+m)!}{(n-m)!}\delta_{nl}. \tag{A2.5.16}$$

Thus, the associated Legendre function of the first kind can be normalised as

$$\bar{P}_n^m(\nu) = (-1)^m\left(\frac{P_n^m(\nu)}{\rho_n^m}\right), \tag{A2.5.17}$$

where

$$\rho_n^m = \sqrt{\frac{2}{2n+1}\cdot\frac{(n+m)!}{(n-m)!}}. \tag{A2.5.18}$$

Note that since the radial position on the rotor disc is usually normalised by the rotor radius, the integral interval used in the rotor analysis is $[0,1]$, and hence the following equations can be useful alternatives to Eqs. (A2.5.16) and (A2.5.18) to define the orthogonality.

$$\int_{0}^{1} P_n^m(x)P_n^m(x)dx = \frac{1}{2}\int_{-1}^{1} P_n^m(x)P_n^m(x)dx = \frac{2}{2n+1}\cdot\frac{(n+m)!}{(n-m)!}\delta_{nl}. \tag{A2.5.19}$$

$$\rho_n^m = \sqrt{\frac{1}{2n+1}\cdot\frac{(n+m)!}{(n-m)!}}. \tag{A2.5.20}$$

The associated Legendre function of the second kind is the conjugate function of the associated Legendre function of the first kind defined as the conjugate solution of the associated Legendre function of the first kind to Eq. (A2.4.2). Still, the associated Legendre function of the second kind alone can be defined as

$$Q_n^m(x) = (-1)^m(1-x^2)^{\frac{m}{2}}\frac{d^m}{dx^m}Q_n(x). \quad (-n \le m \le n) \tag{A2.5.21}$$

It is known that the differentiation of the associated Legendre function of the second kind can be represented as a simple recurrence relation,

$$\frac{\partial Q_n^m(x)}{\partial x} = \frac{1}{x^2-1}\Big[nxQ_n^m(x) - (m+n)Q_{n-1}^m(x)\Big]. \tag{A2.5.22}$$

When $x = 0$,

$$Q_n^m(0) = -\frac{2^{m-1}\pi^{\frac{3}{2}}}{\Gamma\left(\frac{1-m-n}{2}\right)\Gamma\left(\frac{n-m}{2}+1\right)}\tan\left[\frac{\pi(m+n)}{2}\right], \tag{A2.5.23}$$

where Γ is the gamma function defined as

$$\Gamma(s) = \int_0^\infty x^{s-1}e^{-x}dx \quad (s>0). \tag{A2.5.24}$$

Some specific examples of the associated Legendre function of the second kind include

$$Q_0^0(x) = \frac{1}{2}\ln\frac{1+x}{1-x}, \tag{A2.5.25}$$

$$Q_1^0(x) = \frac{x}{2}\ln\frac{1+x}{1-x} - 1, \tag{A2.5.26}$$

$$Q_3^0(x) = \frac{x(5x^2-3)}{4}\ln\frac{1+x}{1-x} + \frac{2}{3} - \frac{5}{2}x^2, \tag{A2.5.27}$$

$$Q_1^1(x) = \frac{(x^2-1)\ln\frac{1+x}{1-x} - 2x}{2\sqrt{1-x^2}}, \tag{A2.5.28}$$

$$Q_2^1(x) = \frac{4-6x^2+3x(x^2-1)\ln\frac{1+x}{1-x}}{2\sqrt{1-x^2}}, \tag{A2.5.29}$$

$$Q_2^2(x) = \frac{2x(3x^2-5) - 3(x^2-1)^2\ln\frac{1+x}{1-x}}{2(x^2-1)}, \tag{A2.5.30}$$

$$Q_3^3(x) = \frac{30x^5 - 80x^3 + 66x + 15(1-x^2)^3\ln\frac{1+x}{1-x}}{2(1-x^2)^{\frac{3}{2}}}. \tag{A2.5.31}$$

Since the associated Legendre function of the second kind in Prandtl's potential function, Eq. (A2.4.7), has an imaginary variable, the definition should be extended to a complex function. The extension itself can be simply done by regarding x in equations above as a complex variable. Figure A2-3 shows the real part of some examples of the above.

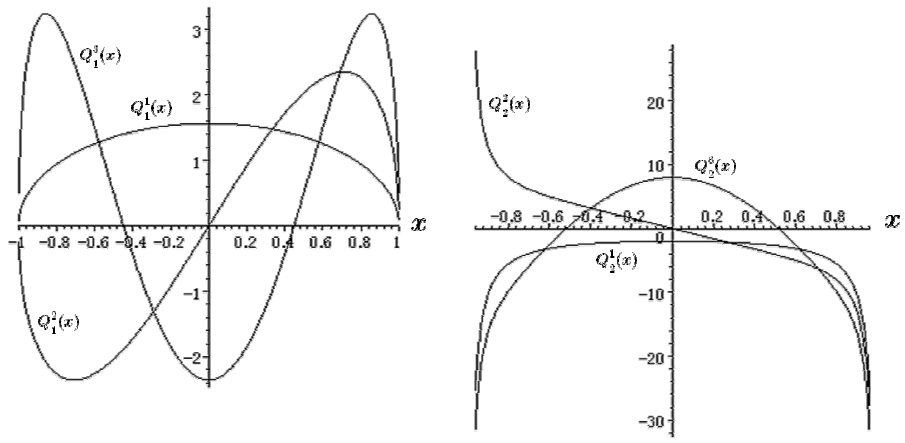

Fig. A2-3 [Real parts of the associated Legendre functions of the second kind.]

Note that at $|x| = 1$, those functions in the left diagram become zero and the others in the right diagram diverge to infinity, depending on the combination of m and n. The imaginary parts of the same functions are shown in Fig. A2-4.

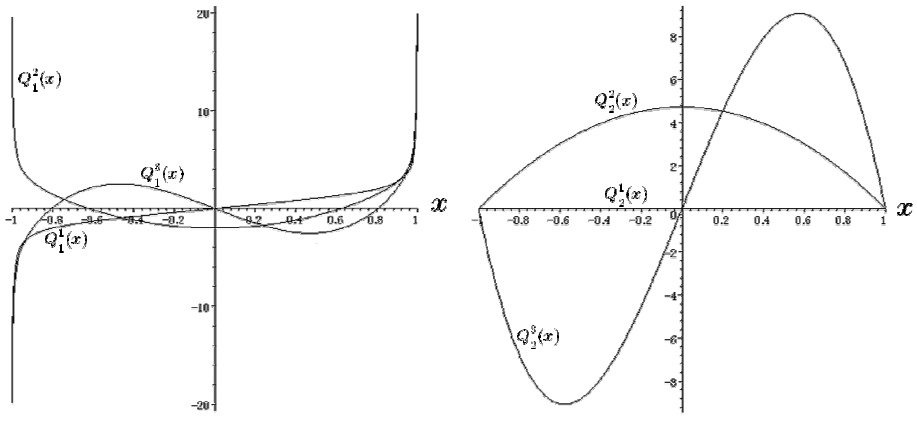

Fig. A2-4 [Imaginary parts of the associated Legendre functions of the second kind.]

Appendix 2.6 The Legendre Functions

The Legendre functions of the first and second kinds are conjugate solutions to each other to *Legendre's equation*,

$$(1-x^2)\frac{d^2y}{dx^2}-2x\frac{dy}{dx}+n(n+1)y=0. \tag{A2.6.1}$$

The Legendre function of the first kind can be regarded as a special case of the associated Legendre function, $P_n^m(x)$, when $m=0$, yet the Legendre function of the first kind alone can independently be defined as

$$P_n(x)=\sum_{k=0}^{\left[\frac{n}{2}\right]}(-1)^k\frac{(2n-2k)!}{2^n k!(n-k)!(n-2k)!}x^{n-2k}. \tag{A2.6.2}$$

The following recurrence relation is useful.

$$(2n+1)xP_n(x)=(n+1)P_{n+1}(x)+nP_{n-1}(x),\quad (n=1,2,3...) \tag{A2.6.3}$$

where $P_0(x)=1$ and $P_1(x)=x$. Some specific examples of the Legendre functions of the first kind include

$$P_0(x)=1, \tag{A2.6.4}$$

$$P_1(x)=x, \tag{A2.6.5}$$

$$P_2(x)=\frac{3}{2}x^2-\frac{1}{2}, \tag{A2.6.6}$$

$$P_3(x)=\frac{5}{2}x^3-\frac{3}{2}x, \tag{A2.6.7}$$

$$P_4(x)=\frac{35}{8}x^4-\frac{15}{4}x^2+\frac{3}{8}, \tag{A2.6.8}$$

$$P_5(x)=\frac{63}{8}x^5-\frac{35}{4}x^3+\frac{15}{8}x, \tag{A2.6.9}$$

$$P_6(x)=\frac{231}{16}x^6-\frac{315}{16}x^4+\frac{105}{16}x^2-\frac{5}{16}, \tag{A2.6.10}$$

$$P_7(x)=\frac{429}{16}x^7-\frac{693}{16}x^5+\frac{315}{16}x^3-\frac{35}{16}x. \tag{A2.6.11}$$

On the other hand, the Legendre function of the second kind is defined as

$$Q_n(x) = (-1)^{\frac{n}{2}} \frac{\left[\left(\frac{n}{2}\right)!\right]^2 2^n}{n!} q_n(x) = (-1)^s \frac{(2s)!!}{(2s-1)!!} q_{2s}(x) \qquad for\ \ n = 2s, \tag{A2.6.12}$$

$$Q_n(x) = (-1)^{\frac{n+1}{2}} \frac{\left[\left(\frac{n-1}{2}\right)!\right]^2 2^{n-1}}{n!} p_n(x) = (-1)^{s+1} \frac{(2s)!!}{(2s+1)!!} p_{2s+1}(x) \qquad for\ \ n = 2s+1, \tag{A2.6.13}$$

where

$$p_n(x) = 1 - \frac{n(n+1)}{2!}x^2 + \frac{(n-2)n(n+1)(n+3)}{4!}x^4 - \cdots, \tag{A2.6.14}$$

$$q_n(x) = x - \frac{(n-1)(n+2)}{3!}x^3 + \frac{(n-3)(n-1)(n+2)(n+4)}{5!}x^5 - \cdots, \tag{A2.6.15}$$

Some specific examples of the Legendre functions of the second kind include

$$Q_0(x) = \frac{1}{2}\ln\left(\frac{1+x}{1-x}\right), \tag{A2.6.16}$$

$$Q_1(x) = \frac{x}{2}\ln\left(\frac{1+x}{1-x}\right) - 1, \tag{A2.6.17}$$

$$Q_2(x) = \frac{3x^2-1}{4}\ln\left(\frac{1+x}{1-x}\right) - \frac{3x}{2}, \tag{A2.6.18}$$

$$Q_3(x) = \frac{5x^2-3x}{4}\ln\left(\frac{1+x}{1-x}\right) - \frac{5x^2}{2} + \frac{2}{3}. \tag{A2.6.19}$$

The Legendre functions of the second kind diverge to infinity at $x = \pm 1$. This property corresponds to the fact that the Legendre functions of the first kind have singular points at $x = \pm 1$. Some examples of the Legendre functions of the first and second kinds are shown in Fig. A2-5.

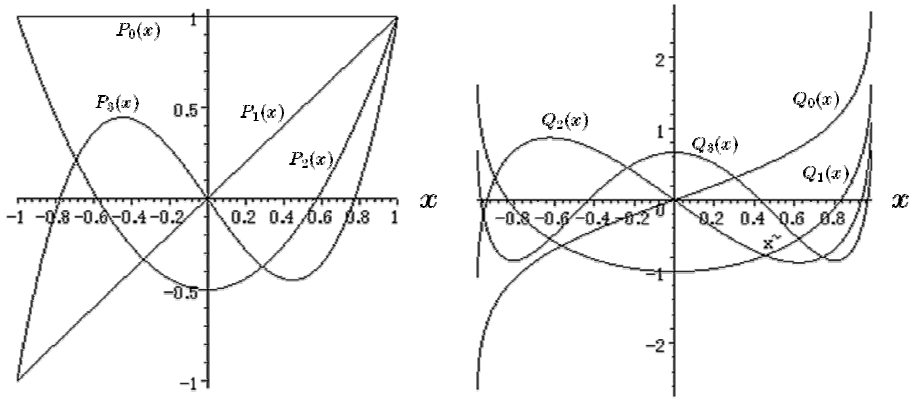

Fig. A2-5 [The Legendre functions of the first and second kinds.]

Appendix 2.7 A Complement to Eq. (2.38)

From (A2.5.1),

$$\frac{1}{\nu}\bar{P}_n^m(\nu) = \frac{1}{\rho_n^m}(1-\nu^2)^{\frac{m}{2}}\frac{d^m}{d\nu^m}P_n(\nu). \qquad \text{(A2.7.1)}$$

On the other hand, there is a formula called *Rodrigue's formula* to represent the Legendre function of the first kind as follows,

$$P_n(\nu) = \frac{1}{2^n n!}\left(\frac{d}{d\nu}\right)^n (\nu^2-1)^n. \qquad \text{(A2.7.2)}$$

The derivation of Rodrigue's formula is provided in Ref. (163). Substituting Eq. (A2.7.2) into Eq. (A2.7.1) and using $\bar{r}^2 = 1-\nu^2$ yields Eq. (2.38).

Appendix 2.8 Comments on the Coefficients of $\hat{L}_{jn}^{rmc}$ and $\hat{L}_{jn}^{rms}$

$\hat{L}_{jn}^{0mc}$ has the coefficient of $1/4$ while $\hat{L}_{jn}^{rmc}$ and $\hat{L}_{jn}^{rms}$ have $1/2$, following the definition of Peters, Eq. (2.65.1) - (2.65.3). This implies that $\hat{L}_{jn}^{rmc}$ and $\hat{L}_{jn}^{rms}$ are Fourier coefficients of a Fourier series which is defined as

$$f(x) \sim \sum_{n=1}^{\infty}(a_n \cos nx + b_n \sin nx), \tag{A2.11.1}$$

$$\begin{cases} a_0 = \dfrac{1}{2\pi}\displaystyle\int_{-\pi}^{\pi} f(x)dx, & \text{(A2.11.2)} \\ a_n = \dfrac{1}{\pi}\displaystyle\int_{-\pi}^{\pi} f(x)\cos nx dx, & \text{(A2.11.3)} \\ b_n = \dfrac{1}{\pi}\displaystyle\int_{-\pi}^{\pi} f(x)\sin nx dx. & \text{(A2.11.4)} \end{cases}$$

where $f(x)$ is an arbitrary periodical functions defined in $[-\pi, \pi]$.

In the representations above, while Eq. (A2.11.1) has a pleasing symmetry between a_n and b_n, the symmetry breaks in Eqs. (A.2.11.2) - (A2.11.4) between a_0 and the others.

There is another definition of Fourier expansion, in which Fourier coefficients are consistently and symmetrically defined for all n, but the general representation of the expanded function needs to contain the case selection between $n = 0$ and $n \neq 0$.

$$f(x) \sim \frac{a_0}{2} + \sum_{n=1}^{\infty}(a_n \cos nx + b_n \sin nx), \tag{A2.11.5}$$

$$\begin{cases} a_n = \dfrac{1}{2\pi}\displaystyle\int_{-\pi}^{\pi} f(x)\cos nx dx, & \text{(A2.11.6)} \\ b_n = \dfrac{1}{2\pi}\displaystyle\int_{-\pi}^{\pi} f(x)\sin nx dx. & \text{(A2.11.7)} \end{cases}$$

If the dynamic inflow model were developed based on Eqs. (A2.11.5) - (A2.11.7), then Eqs. (2.66.1) and (2.66.3) could have been defined in a unified form, but representations of the pressure potential and induced flow such as Eq. (2.25) must have had an extra term, for example $\zeta_n^0/2$ for Eq. (2.25), in the same form as Eq. (2.11.5).

Many of textbooks including Ref. (163) have Eqs. (A2.11.5) - (A2.11.7) for the definition of a Fourier series, but Peters used Eqs. (A2.11.1) - (A2.11.4) for his studies. The variations in the definition should be paid special attention when consulting the literature.

Appendix 2.9 Variation in the Representation of the Pressure Potential

With regard to the gain matrix elements, in some references such as Ref. (37), Γ_{jn}^{rm} for $r+m \equiv 0 \mod 2$ is given as follows,

$$\Gamma_{jn}^{rm} = \frac{(-1)^{\frac{n+j-2r}{2}}}{\sqrt{H_n^m H_j^r}} \cdot \frac{4\sqrt{(2n+1)(2j+1)}}{(n+j)(n+j+2)[(n-j)^2-1]}. \tag{A2.12.1}$$

Allow Eq. (2.101.1) to be re-carried here again for the comparison,

$$\Gamma_{jn}^{rm} = \frac{(-1)^{\frac{n+j-2r}{2}}}{\sqrt{H_n^m H_j^r}} \cdot \frac{2\sqrt{(2n+1)(2j+1)}}{(n+j)(n+j+2)[(n-j)^2-1]}. \tag{2.101.1}$$

Reference (92) contains Eq. (2.101.1). Equations (2.101.2) and (2.101.3) are also doubled in Ref. (37). There is also a variation in the representation of the dynamic inflow model. In Ref. (92), the dynamic inflow model for the cosine part is supposed to have the form of

$$[M](\dot{a}_j^r) + 2V[L^c]^{-1}(a_j^r) = (\tau_{mc}^n), \tag{A2.12.2}$$

while in Ref. (37) it is formulated as

$$[M](\dot{a}_j^r) + V[L^c]^{-1}(a_j^r) = (\tau_{mc}^n). \tag{A2.12.3}$$

The reader may notice that the second term in Eq. (A2.12.2) has an extra coefficient of 2 compared to Eq. (A2.12.3). This variation is due to the variation in the representation of pressure potential. In Ref. (92), the Fourier coefficients, τ_n^{mc}, are associated with the Lift, Eq. (2.13), while in Ref. (37), the Fourier coefficients, τ_n^{mc}, are associated with Eq. (2.12). In either way, the induced flow can be associated with the pressure potential, but depending on how to define the pressure potential and the dynamic inflow model (i.e. the combination of whether Eqs. (2.12) or (2.13) and whether Eqs. (A2.12.2) or (A2.12.3)). This thesis is based on the definitions in Ref. (7). Readers have to avoid the possible confusion when reading a plural of relevant literature.

Appendix 3.1 Further Discussion about the Mass-flow Parameter

In addition to high-speed flight cases discussed in Subsection 3.2.4, the axial flight case shall be examined in this Appendix in order to underpin the validity of the definition of $V_{m\pm}$. In axial flight ($\mu = 0$),

$$V_T = \sqrt{\lambda^2} = |\lambda| \tag{A3.1.1}$$

in order to maintain $C_T > 0$. Also,

$$V_{m\pm} = \frac{\lambda^2 + \lambda_m|\lambda|}{|\lambda|} = \lambda_m + |\lambda_f + \lambda_m|. \tag{A3.1.2}$$

Especially when the vehicle is climbing, as $\lambda_f > 0$,

$$V_{m\pm} = 2\lambda_m + \lambda_f. \qquad \text{(climbing)} \tag{A3.1.3}$$

Likewise, when in descent, as $\lambda_f < 0$,

$$V_{m\pm} = -\lambda_f. \qquad \text{(descent)} \tag{A3.1.4}$$

Note that $\lambda_m > 0$ in both cases by definition. On the other hand, Peter's definition of mass-flow parameter, V_{m+}, yields the following values in axial flight,

$$V_{m+} = 2\lambda_m + \lambda_f, \qquad \text{(climbing)} \tag{A3.1.5}$$

$$V_{m+} = -2\lambda_m - \lambda_f. \qquad \text{(descent)} \tag{A3.1.6}$$

Since $V_{m\pm}$ and V_{m+} provide the same value with the climbing case, and the sign change found between Eqs. (A3.1.5) and (A3.1.6) is reflection of the modulus sign implemented in the definition of $V_{m\pm}$, and this is consistent with the observation about high-speed fligh in Subsection 3.2.4.

Appendix 3.2 Forces and Moments on a Blade Element

The derivation of Eqs. (3.17) and (3.18) are enunciated in this Chapter. References (5) and (152) should be referred about further details.

The hub velocity vector in aircraft axes, $\mathbf{u}_{\mathbf{hub(vehicle)}}$, can be expressed as

$$\mathbf{u}_{\mathbf{hub(vehicle)}} = \mathbf{u}_{vehicle(vehicle)} + \mathbf{w} \times (\mathbf{r}_{c.g.} - \mathbf{r}_{hub}), \tag{A3.2.1}$$

where $\mathbf{u}_{vehicle(vehicle)}$ is the vehicle velocity in aircraft axes, $\mathbf{w}$ is the vehicle angular velocity, $\mathbf{r}_{c.g.}$ is the centre of mass position vector with respect to the airframe reference and $\mathbf{r}_{hub}$ is the position of the rotor hub with respect to the airframe reference.

Then, $\mathbf{u}_{\mathbf{hub(vehicle)}}$ can be transformed to the shaft-oriented axes, in which the z-axis lies along the rotor shaft, as

$$\mathbf{u}_{hub(shaft)} = [T_1]\mathbf{u}_{hub(vehicle)}, \tag{A3.2.2}$$

where $[T_1]$ is the matrix that transforms a vector from airframe to shaft axes defined as

$$[T_1] = \begin{bmatrix} \cos\theta_s & 0 & -\sin\theta_s \\ \sin\theta_s \sin\phi_s & \cos\phi_s & \sin\phi_s \\ \sin\theta_s \cos\phi_s & -\sin\phi_s & \cos\theta_s \cos\phi_s \end{bmatrix}, \tag{A3.2.3}$$

where θ_s and ϕ_s are longitudinal and lateral tilt of the rotor shaft with respect to the airframe, respectively. Next, $\mathbf{u}_{hub(shaft)}$ is transformed to a rotating frame of reference about the shaft,

$$\mathbf{u}_{hub(hub)} = [T_2]\mathbf{u}_{hub(shaft)}, \tag{A3.2.4}$$

where $\mathbf{u}_{hub(hub)}$ is the hub velocity in the rotating frame of reference and $[T_2]$ is defined as

$$[T_2] = \begin{bmatrix} \sin\psi & -\cos\psi & 0 \\ \cos\psi & \sin\psi & 0 \\ 0 & 0 & 1 \end{bmatrix}, \tag{A3.2.5}$$

where ψ is the azimuthal position of the reference blade. When the rotor has a hinge-offset, the hinge velocity, $\mathbf{u}_{hinge}$, is obtained as

$$\mathbf{u}_{hinge} = \mathbf{u}_{hub(hub)} + \mathbf{w}_{hinge} \times \mathbf{r}_{hinge} + \begin{pmatrix} 0 \\ 0 \\ -v_i \end{pmatrix}, \tag{A3.2.6}$$

where $\mathbf{w}_{hinge}$ is the hinge angular velocity, $\mathbf{r}_{hinge}$ is the hinge position with respect to the shaft-based rotating frame of reference and v_i is the induced velocity. Note that v_i is a function of radial and azimuthal positions. The hinge angular velocity can be given as follows;

$$\mathbf{w}_{hinge} = [T_2][T_1]\mathbf{w} + \begin{pmatrix} 0 \\ 0 \\ \Omega \end{pmatrix}, \tag{A3.2.7}$$

where Ω is the rotor speed. By using a transformation matrix, $[T_3]$, that transforms a vector from hinge to blade axes, we have

$$\mathbf{w}_{blade} = [T_3]\mathbf{w}_{hinge} + \begin{pmatrix} \dot{\beta} \\ \dot{\theta} \\ \dot{\zeta} \end{pmatrix}, \tag{A3.2.8}$$

where β, θ and ζ are flap, pitch and lag angles, respectively, and

$$[T_3] = \begin{bmatrix} \cos\zeta & \sin\zeta & 0 \\ -\cos\beta\sin\zeta & \cos\beta\cos\zeta & \sin\beta \\ \sin\beta\sin\zeta & -\cos\zeta\sin\beta & \cos\beta \end{bmatrix}. \tag{A3.2.9}$$

The absolute velocity of the blade element in the blade axes, $\mathbf{u}_{blade}$, is thus defined as

$$\mathbf{u}_{blade} = \mathbf{u}_{hinge} + \mathbf{w}_{blade} \times \mathbf{r}_{bladeelem.}, \tag{A3.2.10}$$

where $\mathbf{r}_{bladeelem}$ is the radial position of the blade element with respect to the hinge in the blade axes. Then, the local angle of attack and the local absolute velocity at the blade element are calculated as

$$\alpha_{elem} = \theta_{elem} + \tan^{-1}\left(\frac{u_{blade} \cdot {}^t(0,0,1)}{u_{blade} \cdot {}^t(0,0,1)}\right), \tag{A3.2.11}$$

$$V_{elem} = \sqrt{(u_{blade} \cdot {}^t(0,0,1))^2 + (u_{blade} \cdot {}^t(1,0,0))^2}. \tag{A3.2.12}$$

The local lift and drag are defined as

$$L_{elem} = \frac{1}{2}\rho c_{elem} V_{elem}^2 r_{elem} a \alpha_{elem}, \tag{A3.2.13}$$

$$D_{elem} = \frac{1}{2}\rho c_{elem} V_{elem}^2 r_{elem} \delta, \tag{A3.2.14}$$

where c_{elem} is the chord of the blade element, r_{elem} is the radial length of the blade element, a is the lift curve slope and δ is the drag coefficient. Note that c_{elem} is generally a function of the radial position, and a and δ are generally functions of the local angle of attack and the local Mach number.

The local lift and drag are defined along the direction of V_{elem}. In the blade element frame of reference, they are expressed as

$$X_{elem}^{aero} = L_{elem} \sin\alpha_{elem} - D_{elem} \cos\alpha_{elem}, \tag{A3.2.15}$$

$$Y_{elem}^{aero} = 0, \tag{A3.2.16}$$

$$Z_{elem}^{aero} = -L_{elem} \cos\alpha_{elem} - D_{elem} \sin\alpha_{elem}. \tag{A3.2.17}$$

These are aeronautical loads working on a blade element. On the other hand, the inertial loads on the blade elements can be given as

$$\mathbf{X}_{elem}^{inertial} = -m_{elem} \mathbf{a}_{elem}^{elem}, \tag{A3.2.18}$$

where m_{elem} is the mass of the blade element and $\mathbf{a}_{elem}^{elem}$ is the absolute acceleration of the blade element defined as

$$\mathbf{a}_{elem}^{elem} = [T_3]\Big\{[T_2][T_1]\Big[\dot{\mathbf{u}} + w \times \mathbf{u} + \mathbf{w} \times (\mathbf{w} \times \mathbf{r}_{hub})\Big] + \mathbf{w}_{hinge} \times \mathbf{r}_{hinge} + \mathbf{w}_{blade} \times [T_3](\mathbf{w}_{hinge} \times \mathbf{r}_{hinge})\Big\}. \tag{A3.2.19}$$

Equations (3.17) and (3.18) can be obtained from equations above by defining that $\mathbf{X}_{elem} = \mathbf{X}_{elem}^{aero} + \mathbf{X}_{elem}^{inertial}$.

References

N.b.) Although highly convenient, the Internet is not as reliable a source of information as reviewed papers. Still, it is difficult to completely ignore electric on-line references available nowadays. The present author dares to include in the reference list a limited number of websites, which the author judges are relatively sustainable and reliable, for only supplementary information. It must be herein emphasised that this thesis essentially relied only on reviewed published papers.

1. Pitt, D.M. and Peters, D.A., "Theoretical Prediction of Dynamic-Inflow Derivatives," *Vertica*, Vol.5, No.1, Jan. 1981, pp.21-34
2. De La Cierva, J., "The Development of the Autogyro," *Journal of Royal Aeronautical Society*, 1926, Vol.30, No.181, pp.8-29
3. De La Cierva, J., "The Autogiro," *Journal of the Royal Aeronautical Society*, Vol.34, No.239, 1930, pp.902-921
4. De La Cierva, J., "New Development of the Autogiro," *Journal of the Royal Aeronautical Society*, Vol.39, Dec. 1935, pp.1125-1143
5. Bramwell, A.R.S., *Helicopter Dynamics*, Arnold, London, 1976
6. Peters, D.A. and Chen, S.Y., "Momentum Theory, Dynamic Inflow and the Vortex-Ring State," *Journal of the American Helicopter Society*, Jul. 1982, pp.18-24
7. He, C.-J., "Development and Application of a Generalized Dynamic Wake Theory for Lifting Rotors," Ph.D. dissertation, Georgia Inst. of Tech, 1989
8. Coton, F.N., Smrcek, L. and Pátek, Z., „Aerodynamic Characteristics of a Gyroplane Configuration," *Journal of Aircraft*, Vol.35, No.2, Mar.-Apr. 1998
9. Houston, S.S., "Modelling and Analysis of Helicopter Flight Mechanics in Autorotation," *Journal of Aircraft*, Vol.40, No.4, Jul.-Aug. 2003
10. Houston, S.S., "Analysis of Rotorcraft Flight Dynamics in Autorotation," *Journal of Guidance, Control and Dynamics*, Vol.25, No.1, Jan.-Feb. 2002, pp.33-39
11. The United Kingdom Air Accident Investigation Branch.
    Webpage: http://www.aaib.dft.gov.uk/home/index.cfm
12. Secretariat of the Aircraft and Railway Accident Investigation Commission of Japan, Printed reports available from: Ministry of Land, Infrastructure and Transport, 2-1-2, kasumigaseki, Chiyoda-ku, Tokyo, 100-8919, Japan.
    Electric forms available from: http://araic.assistmicro.co.jp/araic/aircraft/
13. Focke, E.H.H., "German Thinking on Rotor Wing Development," *Journal of Aeronautical Society*, Vol.69, No.653, 1965, pp.293-305

14. Focke, E.H.H., "The Focke Helicopter," *Journal of Aeronautical Society*, Vol.42, May. 1938, pp.577-590
15. Prouty, R.W., *Helicopter Aerodynamics*, PJS Publications Inc., 2003
16. Wheatley, J.B., "An Aerodynamic Analysis of the Autogiro Rotor with a Comparison Between Calculated and Experimental Results," NACA Report No.487, 1937
17. Wheatly, J.B., "Wing Pressure Distribution and Rotor-Blade Motion of an Autogiro as Determined in Flight," NACA Report No.475, 1933
18. Wheatly, J.B., "The Aerodynamic Analysis of the Gyroplane, Rotating-Wing System," NACA Report No.492, 1934
19. Wheatly, J.B., "Lift and Drag Characteristics and Gliding Performance of an Autogiro as Determined in Flight," NACA Report No.434, 1932
20. Lock, C.N.H. and Townend, H.C.H., "Wind Tunnel Experiments on a Model Autogyro at Small Angles of Incidence," Aeronautical Research Committee, R&M 1154, Mar. 1927
21. Lock, C.N.H., "Further Development of Autogyro Theory Parts I & II," Aeronautical Research Committee, R&M 1127, Mar. 1927
22. Lock, C.N.H, Bateman, H. and Townend, H.C.H., "An Extension of the Vortex Theory of Airscrews with Applications to Airscrews of Small Pitch, Including Experimental Results," R&M. No.1014, British A.R.C., 1926
23. Schad, J.L., "Small Autogyro Performance," *Journal of the American Helicopter Society*, Vol.10, 1965
24. McKillip, R.M. and Chih, M.H., "Instrumented Blade Experiments using a Light Autogyro," Proceedings of the 16th European Rotorcraft Forum, Vol.2, The Royal Aeronautical Society, Glasgow, 1990, pp. 8.4.1-8.4.8
25. Miln-Thomson, L.M., *Theoretical Hydrodynamics*, Dover Publication Inc.
26. Landau, L.D., *Fluid Mechanics*, Butterworth-Heinemann, 1987
27. Ormiston, R.A., "An Actuator Disc Theory for Rotor Wake Induced Velocities," AGARD Conference Proceedings, AGARD CP. cp.111, 1972
28. Chen, R.T., "A Survey of Nonuniform Inflow Models for Rotorcraft Flight Dynamics and Control Applications," *Vertica*, Vol.14, No.2, 1990, pp.147-184
29. Gaonkar, G.H. and Peters, D.A., "Review of Dynamic Inflow Modeling for Rotorcraft Flight Dynamics," *Vertica*, Vo.12, No.3, 1988, pp.213-242
30. Su, A. and Peters D.A., "The Effect of Hidden Dynamic States on Floquet Eigenvalues," *Journal of the American Helicopter Society*, TN, Vol.35, No.4, Oct. 1990
31. Lowis, O.J., "The Stability of Rotor Blade Flapping Motion at High Tip Speed

Ratios," Reports and Memoranda No.3544, Jan. 1963

32. Peters, D.A. and Hohenemser, K.H., "Application of the Floquet Transition Matrix to Problems of Lifting Rotor Stability," *Journal of the American Helicopter Society*, Vol. 16, No.2, Apr. 1971
33. Gaonkar, G.H. and Peters, D.A., "Review of Floquet Theory in Stability and Response Analyses of Dynamic Systems with Periodic Coefficients," Bisplinghoff Honorary Symposium, Boca Raton, Florida, Feb. 1986
34. Houston, S.S. and Tarttelin, P.C., "Validation of Mathematical Simulations of Helicopter Vertical Response Characteristics in Hover," *Journal of the American Helicopter Society*, Vol.36, No.1, 1991, pp.45-57
35. Ellenrieder, T.J., "Investigation of the Dynamic Wake of a Model Rotor," Ph.D. dissertation, University of Bristol, Oct. 1995
36. Chen, R. T. N. and Hindson, W. S., "Influence of Dynamic Inflow Derivatives," *Vertica*, Vol.5, 1987, pp.21-34
37. Peters, D.A. and He, C.-J., "Finite State Induced Flow Models Part II: Three-Dimensional Rotor Disk," *Journal of Aircraft*, Vol.32, No.2, Mar.-Apr., 1995
38. Turnour, S.R. and Celi, R., "Modelling of Flexible Rotor Blades for Helicopter Flight Dynamics Applications," *Journal of American Helicopter Society*, Vol.41, No.1, 1996, pp.52-61
39. Peters, D.A. and He, C.-J., "A Closed-Form Unsteady Aerodynamic Theory for Lifting Rotors in Hover and Forward Flight," the 43rd Annual National Forum of the American Helicopter Society, Missouri, May. 1987
40. Gaonkar, G.H., et al, "The Use of Actuator-Disc Dynamic Inflow for Helicopter Flap-Lag Stability," *Journal of the American Helicopter Society*, Vol.28, No.3, Jul. 1983
41. Glauert, H., "A General Theory of the Autogyro," Reports and Memoranda No.1111, Aeronaut Res. Council, 1926
42. Brotherhood, P., "An Investigation in Flight of Induced Velocity distribution Under a Helicopter Rotor When Hovering," Br. ARCRAE Report No.Aero.2211, Jun. 1947
43. Coleman, R.P., Feingold, A.M, and Stempin, C.W., "Evaluation of the Induced Velocity Field of an Idealized Helicopter Rotor," NACA ARR L5E10, 1945
44. Stepniewski, W.Z. and Keys, C.N., *Rotary-Wing Aerodynamics*, Dover Publication Inc., 1984
45. Harris, F.D. and McVeigh, M.A., "Uniform Downwash with Rotors Having a Finite Number of Blades," *Journal of the American Helicopter Society*, Vol.21, No.1, Jan. 1976

46. Harris, F.D., “Articulated Rotor Blade Flapping Motion at Low Advance Ratio,” *Journal of the American Helicopter Society*, Vol.17, No.1, Jan. 1972
47. Kinner, W., “Die Kreisfirmige Tragflasche auf Potentialtheorischer Grundlage,” Ingenier Archive VIII Band, 1937, pp.47-80
48. Mangler, K.W. and Squire, B., “Calculation of the Induced Velocity Field of a Rotor,” Royal Aircraft Establishment, Rept. Aero 2247, Sep. 1948
49. Joglekar, M. and Loewy, R., “An Actuator Disc Analysis of Helicopter Wake Geometry and the Corresponding Blade Response,” USAAU-LBS, Tech. Report, 1970
50. Carpenter, P.J. and Friedvich, “Effect of a Rapid Blade-Pitch Increase on the Thrust and Induced-Velocity Response of a Full-Scale Helicopter Rotor,” NACA TN 3044, 1953
51. Munk, M.M., “Some Tables of the Factors of Apparent Mass,” National Advisory Committee for Aeronautics, Technical Note NO.197, 1924
52. Castles, W. Jr. and De Leeuw, J.H., “The Normal Component of the Induced Velocity in the Vicinity of a Lifting Rotor and Some Examples of Its Application,” NACA Rept. 1184, 1954
53. Heyson, H.H. and Katzoff, S., “Induced Velocities Near a Lifting Rotor with Nonuniform Disk Loading,” NACA Rept. 1319, 1957
54. Jewel, I.W. and Heyson, H.H., “Charts of the Induced Velocities Near a Lifting Rotor,” NASA MEMO 4-15-59L, May. 1959
55. Sissingh, G.J., “The Effect of Induced Velocity Variation on Helicopter Rotor Damping in Pitch or Roll,” TN No.Aero 2132, Nov. 1951
56. Amer, K.B., “Theory of Helicopter Damping in Pitch and Roll and a Comparison with Flight Measurements,” NACA T.N. 2136, Oct. 1950
57. Brotherhood, P. and Steward, W., “An Experimental Investigation of the Flow Through a Helicopter Rotor in Forward Flight,” Aeronautical Research Council, Report and Memoranda No.2734, Sep. 1949
58. Curtiss, H.C. Jr., and Schupe, N.K., “Stability and Control Theory for Hingeless Rotors,” Ann. Forum AHS, May. 1971
59. Banerjee, D., Crews, S.T., Hohenemser K. and Yin, S., “Identification of State Variables and Dynamic Inflow from Rotor Model Dynamic Tests,” *Journal of the American Helicopter Society*, Vo.22, 1977
60. Kuczynski, W.A. and Sissingh, G.J., “Characteristics of Hingeless Rotors with Hub Moment Feedback Controls including Experimental Rotor Frequency Response,” NASA CR 114427 (Vol.1) and CR 114428 (Vol.II), 25048, Jan. 1972

61. Bousman, W.G., “An Experimental Investigation of the Effects of Aeroelastic Coupling on Aeromechanical Stability of a Hingeless Rotor Helicopter,” *Journal of the American Helicopter Society*, Vol.26, No.1, Jan. 1981, pp.46-54
62. Gaonkar, G.H. and Peters, D.A., “A Review of Dynamic Inflow and Its Effect on Experimental Correlations,” Second Decennial Specialists’ Meeting on Rotorcraft Dynamics, AHS-NASA, Ames, Moffet Field, California, Nov. 7-9, 1984
63. Wood, E.R. and Hermes, M.E., “Rotor Induced Velocities in Forward Flight by Momentum Theory,” AIAA Paper No.69-224, 1969
64. Azuma, A. and Kawachi, K., “Local Momentum Theory and Its Application to the Rotor Wing,” *Journal of Aircraft*, Vol.16, No.1, 1979, pp.6-14
65. Ormiston R.A. and Peters, D.A., “Hingeless Helicopter Rotor Response with Nonuniform Inflow and Elastic Blade Bending,” *Journal of Aircraft*, Vol.9, No.10, Oct. 1972
66. Peters, D.A., “Hingeless Rotor Frequency Response with Unsteady Inflow,” NASA SP-352 Rotorcraft Dynamics, 1974
67. Ormiston, R.A., “Application of Simplified Inflow Model to Rotorcraft Dynamic Analysis,” *Journal of American Helicopter Society*, Vol.21, No.3, Jul. 1976
68. Crews, S.T., Hohenemser, K.H. and Ormiston, R.A., “An Unsteady Wake Model for a Hingeless Rotor,” *Journal of Aircraft*, Vol.10, No.12, Dec. 1973
69. White, F. and Blade, B.B., “Improved Method of Predicting Helicopter Control Response and Gust Sensitivity,” Ann. Forum AHS, May. 1979
70. Johnson, W., “Influence of Unsteady Aerodynamics on Hingeless Rotor Ground Resonance,” *Journal of Aircraft*, Vol.29, No.9, Aug. 1982
71. Johnson, W., *Helicopter Theory*, Princeton Univ. Press, 1994
72. Peters, D.A. and Gaonkar, G.H., “Theoretical Flap-Lag Damping with Various Dynamic Inflow Models,” *Journal of the American Helicopter Society*, Vol.25, No.3, Jul. 1980, pp.29-36
73. Banerjee, D., Crews, S.T., Hohenemser K. and Yin, S., “Parameter Identification Applied to Analytic Hingeless Rotor Modeling,” *Journal of the American Helicopter Society*, Vo.24, No.1, Jan. 1979, pp.26-32
74. Gaonkar, G.H., Mitra, A.K. and Peters, D.A., “Feasibility of a Rotor Flight-Dynamics Model with First Order Cyclic Inflow and Multiblade Modes,” AIAA Dynamics Specialists’ Conference, Atlanta, Ga., Apr. 1981, AIAA Paper No. 81-0611-CP.
75. Van Holten, Th., “The computation of aerodynamic loads on helicopter blades in forward flight, using the method of the acceleration potential,” Rep. VTH-189,

Technische Hogeschool Delft, Netherlands, Mar. 1975

76. Pierce, G.A. and Vaidynathan, A.R., "Helicopter Rotor Loads Using a Matched Asymptotic Expansion technique," NASA CR-165742, May. 1981
77. Meijer Drees, J. and Hendal, W.P., "Airflow Patterns in the Neighbourhood of Helicopter Rotors," Aircraft Engineering, Vol.23, No.266, Apr. 1951
78. Pitt, D.M., "Rotor Dynamic Inflow Derivatives and Time Constants from Various Inflow Models," Ph.D. dissertation, Washington University, Dec. 1989
79. Glauert, H.M.A., "The Force and Moment of an Oscillating Aerofoil," R.&M. No.1292 ('Ae. 397), 1929
80. Theodorsen T., "General Theory of Aerodynamic Instability and the Mechanism of Flutter," NACA TR No.496, 1935
81. Isaacs, R., "Airfoil Theory for Rotory Wing Aircraft," *Journal of Aeronautical Sciences*, Vol.13, No.4, Apr. 1945, pp.218
82. Greenberg, J.M., "Airfoil in Sinusoidal Motion in Pulsating Stream," NACA TN No.1326, 1947
83. Willmer, M.A.P., "The Loading of Helicopter Blades in Forward Flight," RAE Report Naval 20N276935 No. 8, Apr. 1959
84. Brown, R.E. and Houston, S.S., "Comparison of Induced Velocity Models for Helicopter Flight Mechanics," *AIAA Journal*, Vol.37, No.4, 2000, pp.623-629
85. Miller, R.H., "Rotor Blade Harmonic Air Loading," *AIAA Journal*, Vol.2, No.7, 1964, pp.1254-1269
86. Loewy, R.G., "A Two-Dimensional Approximation to the Unsteady Aerodynamics of Rotary Wings," *Journal of the Aeronautical Sciences*, Vol.24, 1957
87. Jones, W.P. and Rao, B.M., "Compressibility Effects on Oscillating Rotor Blades in Hovering Flight," AIAA Journal, Vol.8, No.2, 1970, pp.321-329
88. Hammond, C.E. and Pierce, G.A., "A Compressible Unsteady Aerodynamic Theory for Helicopter Rotors," AGARD Specialists' Meeting on the Aerodynamics of Rotary Wings, Marseille, France, Sep. 13-15, 1972
89. Friedmann, P.P. and Venkatesan, C., "Influence of Various Unsteady Aerodynamic Models of the Aeromechanical Stability of a Helicopter in Ground Resonance," NASA CP-2400, 1985
90. Friedmann, P.P. and Venkatesan, C., "Finite State Modelling of Unsteady Aerodynamics and Its Application to a Rotor Dynamic Problem," 11th European Rotorcraft Forum, Paper No.72, London, Sep. 10-13, 1985
91. Venkatesan, C. and Friedmann, P.P., "New Approach to Finite-State Modelling of Unsteady Aerodynamics," *AIAA Journal*, Vol.24, No.12, 1986 pp.1889-1897

92. Peters, D.A. and He, C.-J., "Correlation of Measured Induced Velocities with a Finite-State Wake Model," *Journal of the American Helicopter Society*, Vol.36, No.3, 1991, pp.59-70
93. Heyson, H.H., "A Brief Survey of Rotary Wing Induced Velocity Theory," NASA TM78741, Jun. 1978
94. Landgrebe, A.J., "An Analytical Method for Predicting Rotor Wake Geometry," *Journal of the American Helicopter Society*, Vol.14, No.4, Oct. 1969
95. Sadler, S.G., "Development and Application of a Method for Predicting Free Wake Positions and Resulting Rotor Blade Air Loads," Vol.1 Model and Results, NASA CR-1011, 1971
96. Padfield, G.D., "Theoretical Modelling for Helicopter Flight Dynamics: Development and Validation," International Council for the Aeronautical Sciences, ICAS-88-6.1.3, Jerusalem, Israel, 1988, pp.165-177
97. Drazin, P.G., *Nonlinear System*, Cambridge Univ. Press, 1992
98. Basset, P.M., "Study of the Vortex Ring State Using Bifurcation Theory, " American helicopter Society 58th Annual Forum, Montreal, Canada, 2002
99. Houston, S.S. and Brown, R.E., "Rotor-Wake Modelling for Simulation of Helicopter Flight Mechanics in Autorotation," *Journal of Aircraft*, Vol.40, No.5, Sep. 2003
100. Faulkner, A.J. and Buchner, F., "Flight Investigations of a Helicopter low airspeed estimation system based on measurement of control parameters," 6th European Rotorcraft Forum, 1980
101. Nagabhushanam, J. and Gaonkar, G.H., "Rotorcraft Air Resonance in Forward Flight with Various Dynamic Inflow Models and Aeroelastic Couplings," *Vertica*, Vol.8, No.4, 1984, pp.373-394
102. Gaonkar G.H. and Peters, D.A., "Effectiveness of Current Dynamic Inflow Models in Hover and Forward Flight," *Journal of American Helicopter Society*, Vol.31, No.2, Apr. 1986
103. Siblski, K., "Non-Linear Flight Mechanics of a Helicopter Analysis by Application of a Continuation Methods," 20th European Rotorcraft Forum, Rome, Italy, 1999
104. Chen, R. and Hindson, W.S., "Influence of Dynamic Inflow on the Helicopter Vertical Response," NASA TM-88327, No. 87-24482, Jun. 1986
105. Pitt D.M. and Peters D.A., "Rotor Dynamic Inflow Derivatives and Time Constants from Various Inflow Models," 9th European Rotorcraft Forum, No.55, 1983
106. Pitt, D.M., "Rotor Dynamic Inflow Derivatives and Time Constants from Various Inflow Models," USATSARCOM-TR81-2, Dec. 1980

107. Peters, D.A. and HaQuang, N., "Dynamic Inflow for Practical Applications," *Journal of the American Helicopter Society*, TN, vol.33, No.4, Oct. 1988, pp.64-68
108. Schrage, D.P., Peters D.A. and Prasad, V.R., "Helicopter Stability and Control Modeling Improvements and Verification," 14th European Rotorcraft Forum, Part I, No.77, Milan, 1988
109. Su, A., Yoo, K.M. and Peters, D.A., "Extension and Validation of an Unsteady Wake Model for Rotors," *Journal of Aircraft*, Vol.29, No.3, 1992, pp.374-383
110. Su, A., "Application of a State-Space Wake Model to Elastic Blade Flapping in Hover," Ph.D. dissertation, Georgia Inst. of Technology, Atlanta, GA, Dec. 1989
111. De Andrade, D. and Peters, D.A., "Correlation of Experimental Flap-Lag Torsion Damping - A Case Study," Proceedings of the 49th Annual National Forum of the American Helicopter Society, St. Louis, 1993, pp.1011-1028
112. Peters, D.A., Boyd, D.D. and He, C.-J., "Finite-State Induced-Flow Model for Rotors in Hover and Forward Flight," *Journal of the American Helicopter Society*, Vol. 34, No.4, 1989, pp.5-17
113. Nibbelink, B.D. and Peters, D.A., "Flutter Calculations for Fixed and Rotating Wing with State-Space Inflow Dynamics," Proceedings of AIAA/AHS/ASME Structural Dynamics and Materials Conference, La Jolla, Apr. 1993
114. Elliot, J.W., Althoff S.L. and Sailey, R.H., "Inflow Measurements Made with a Laser Velocimeter in Forward Flight, Volume 3, Rectangular Planform Blades at an Advance Ratio of 0.15," NASA TM 100541, AVSCOM TM 88-B-004, Apr. 1984
115. Elliot, J.W., Althoff S.L. and Sailey, R.H., "Inflow Measurements Made with a Laser Velocimeter in Forward Flight, Volume 3, Rectangular Planform Blades at an Advance Ratio of 0.23," NASA TM 100542, AVSCOM TM 88-B-005, Apr. 1984
116. Elliot, J.W., Althoff S.L. and Sailey, R.H., "Inflow Measurements Made with a Laser Velocimeter in Forward Flight, Volume 3, Rectangular Planform Blades at an Advance Ratio of 0.30," NASA TM 100543, AVSCOM TM 88-B-006, Apr. 1984
117. Xin, H., Prasad, J.V.R. and Peters, D.A., "Dynamic Inflow Modelling for Simulation of a Helicopter Operating in Ground Effect," AIAA Modeling and Simulation Technologies Conference and Exhibit, Portland, OR, Collection of Technical Papers, Aug. 9-11, 1999, pp.182-192
118. Xin, H., Prasad, J.V.R. and Peters, D.A., "Ground Effect Aerodynamics of Lifting Rotors Hovering above Inclined Ground Plane," the AIAA 17th Applied Aerodynamics Conference, Norfolk, VA, Jun. 1999
119. Takahashi, M.D., "A Flight Dynamic Helicopter Mathematical Model with a Single Flap-Lag-Torsion Main Rotor," NASA TM 102267, USAAVSCOM TM 90A004,

Feb. 1990

120. Chaimovitch, M., Rosen, A., Mansur, M.H. and Tschler, M.B., "Investigation of the Flight Mechanics Simulation of a Hovering Helicopter," the 48th Annual Forum of the American Helicopter Society, Washington D.C., Jun. 1999, pp.1237-1256
121. He, C.-J. and Lewis, W.D., "A Parametric Study of Real-Time Mathematical Modeling Incorporating Dynamic Wake and Elastic Blades," the 48th Annual Forum of the American Helicopter Society, Washington D.C., Jun. 1999, pp.1181-1196
122. Harding, J.W. and Bass, S.M., "Validation of a Flight Simulation Model of the AH-64 Apache Attack Helicopter against Flight Test Data," the 46th Annual Forum of the American Helicopter Society, Washington D.C., May. 1990
123. Prouty, R.W., "The Case of the Cross-Coupling Mystery," *Rotor and Wing*, Vol.28, No.6, 1994, pp.48-49
124. Von Grünhagen, W., "Dynamic Inflow Modelling for Helicopter Rotors and Its Influence on the Prediction of Cross-Couplings," Proceedings of the AHS Aeromechanics Specialists Conference, Bridgeport, CT, Oct. 1995
125. Ballin, M.G. and Dalang-Secretan, M.A., "Validation of the Dynamic Response of a Blade-Element UH-60 Simulation Model in Hovering Flight," Proceedings of the American Helicopter Society 46th Annual Forum, Washington D.C., May. 1990
126. Simons, I.A. and Modha, A.N., "Gyroscopic Feathering Moments and the Bell Stabilizer Bar on Helicopter Rotors," the 2002 European Rotorcraft Forum, Bristol, England, Sep. 17-20, 2002, pp.90.1-90.8
127. Rosen, A. and Isser, A., "A New Model of Rotor Dynamics During Pitch and Roll of a Hovering Helicopter," *Journal of the American Helicopter Society*, Vol.40, No.3, Jul.1995, pp.17-28
128. Rosen, A. and Isser, A., "A Model of the Unsteady Aerodynamics of a Hovering Helicopter Rotor that Includes Variations of the Wake Geometry," *Journal of the American Helicopter Society*, Vol.40, No.3, Jul.1995, pp.6-16
129. Krothapalli, K.R., Prasa, J.V. and Peters, D.A., "Helicopter Rotor Dynamic Inflow Modeling for Maneuvering Flight," *Journal of the American Helicopter Society*, 2001, Apr. pp129-139
130. Barocela, E.B., Peters, D.A., Krothapalli, K.R. and Prasad, J.V.R., "The Effect of Wake Distortion on Rotor Inflow Gradients and Off-Axis Coupling," Proceedings of the Atmospheric Flight Mechanics Conference of the American Institute of Aeronautics and Astronautics, New Orleans, Louisiana, Aug. 1997
131. Krothapalli, K.R., Prasa, J.V. and Peters, D.A., "Improved Wake Geometry Model for a Maneuvering Rotor," Proceedings of the American Helicopter Society

Technical Specialists' Meeting for Rotorcraft acoustics and Aerodynamics, Williamsburg, Virginia, Oct. 1997

132. Krothapalli, K.R., Prasa, J.V. and Peters, D.A., "Development of a Comprehensive Wake Theory for Lifting Rotors," Proceedings of the Atmospheric Flight Mechanics Conference of the American Institute of Aeronautics and Astronautics, San Diego, California, Jul. 1996
133. He, C.-J., Lee, C.-S. and Chen, W., "Rotorcraft Simulation Model Enhancement to Support Design, Testing and Operational Analysis," the American helicopter Society 55th Annual Forum, Montreal, Canada, May 25-27, 1996
134. Zhao, J.-G., Prasad, J. and Peters, D.A., "Simplified Dynamic Wake Distortion Model for Helicopter Transitional Flight," AIAA Atmospheric Flight Mechanics Conference and Exhibit, Monterey, California, Aug. 5-8, 2002
135. Zhao, J.-G., "Dynamic Wake Distortion Model for Helicopter Maneuvering Flight," Ph.D. dissertation, Georgia Inst. of Technology, Atlanta, GA, Mar. 2005
136. Peters, D.A. and Morillo, J.A., "Towards a Complete Dynamic Wake Model in Axial Flow," Proceedings of the American Helicopter Society Aeromechanics Specialists' Meeting, Atlanta, Georgia, Nov. 13-14, 2000
137. Morillo, J. and Peters, D.A., "Extension of Dynamic Inflow Models to Include Mass Injection and Off-disk Flow," AIAA Aerospace Sciences Meeting and Exhibit, 40th, Reno, Jan. 14-17, 2002
138. De La Cierva, J., "A Letter to RAeS with Comments on the Paper Presented by H. Glauert on 20 January 1927," *Journal of the Royal Aeronautical Society*, Vol.31, No.198, 1927, pp.5060-506
139. Beavan, J.A. and Lock, C.N.H., "The Effect of Blade Twist on the Characteristics of the C-30 Autogyro," Aeronautical Research Council, ARC R&M 1727, London, 1939
140. Glauert, H., "Lift and Torque of an Autogyro on the Ground," Aeronautical Research Committee, R&M 1131, Jul. 1927
141. Glauert H. and Lock, C.N.H., "A Summary of the Experimental and Theoretical Investigations of the Characteristics of an Autogyro," Aeronautical research Committee R&M 1162, Apr. 1928
142. Glauert, H., "The Analysis of Experimental Results in the Windmill Brake and Vortex Ring States of an Airscrew," R&M. No.1026, British A.R.C., 1926
143. Glauert, H., "The Theory of the Autogiro," *Journal of the Royal Aeronautical Society*, Vol.31, No.198, 1927, pp.483-505
144. Moreno-Caracciolo, M, "The Autogiro," Technical Memorandum No.216, 1923

145.Leishman, J.G., “Development of the Autogiro: A Technical Perspective,” *AIAA Journal*, 0021-8669 Vol.41, No.4, 2004

146.Popular Rotorcraft Association. Webpage: http://www.pra.org

147.Ken Wallis’ personal webpage: http://www.kenwallisautogyro.com

148.Anon, “British Civil Airworthiness Requirements Section T: Light Gyroplane design Requirements,” U.K. Civil Aviation Authority, Paper T860, Jul. 1993

149.Houston S.S., “Identification of Gyroplane Lateral/Directional Stability and Control Characteristics from Flight Test,” Proceedings of the Institute of Mechanical Engineers, Pt. G, Vol.212, No. G4, 1998, pp.1-15

150.Houston, S.S., “Longitudinal Stability of Gyroplanes,” *The Aeronautical Journal of the Royal Aeronautical Society*, Jan. 1996

151.Houston, S.S. and Brown, R.E., “Rotor-Wake Modelling for Simulation of Helicopter Flight Mechanics in Autorotation,” *Journal of Aircraft*, Vol.40, No.5, Sep. 2003, pp.938-945

152.Houston, S.S., “Validation of a Non-linear Individual Blade Rotorcraft Flight Dynamics Model Using a Perturbation Method,” *Aeronautical Journal*, Aug.-Sep. 1994, pp.260-266

153.Houston, S.S. and Tarttelin, P.C., “Validation of Mathematical Simulations of Helicopter Vertical Response Characteristics in Hover,” *Journal of the American Helicopter Society*, Vol.36, No.1, 1991, pp.45-57

154.Spathopoulos, V.M., “The Assessment of a Rotorcraft Simulation Model in Autorotation by Means of Flight Testing a Light Gyroplanes,” Ph.D. dissertation. Dept. of Aerospace Engineering, Univ. of Glasgow, Scotland U.K., Aug. 2001

155.Bagiev, M., “Gyroplane handling Qualities Assessment Using Flight Testing and Simulation Technique,” Ph.D. dissertation. Dept. of Aerospace Engineering, Univ. of Glasgow, Scotland U.K., Aug. 2005

156.Carter Jr. J., “The Carter Heliplane Transport Slowed/Compound Aircraft: Candidate for the Air-Maneuver Transport(AMT),” *Carter Aviation Technologie.*
Webpage: http://www.cartercopters.com/

157.Groen Brothers Aviation Incorporated. Company.
Webpage: http://www.groenbros.com

158.PAL-V Europe BV. Webpage: http://www.pal-v.com/

159.Lopez, C.A. and Wells, V.L., “Dynamic and Stability of an Autorotating Rotor/Wing Unmanned Aircraft,” *Journal of Guidance, Control, and Dynamics*, Vol.27, No.2, Mar.-Apr. 2004, pp.258-270

160.Skews, B.W., “Autorotation of Rectangular Plates,” *J. Fluid Mech*. Vol. 217, 1990,

pp.33-40

161. Lugt, H.J., “Autorotation,” Ann. Rev. *Fluid Mech*. 1983, 15:123-47

162. Hislop, G.S., “The Fairy Rotordyne,” Meetings of the Helicopter Association of Great Britain &The Royal Aeronautical Society, London, Nov. 1958

163. Arfken, G.. and Weber, H., *Mathematical Methods for Physicists*, 3rd ed. Academic Press, 1995

164. Mathworld Website: http://mathworld.wolfram.com/

165. Abramovich, M. and Stegun, I., *Handbook of Mathematical Functions*, Dover Publications, Inc., 1972

166. Peters, D.A. and Cao, W.M., “Finite State Induced Flow Models Part I: Two-Dimensional Thin Airfoil,” *Journal of Aircraft*, Vol.32, No.2, Mar.-Apr. 1995

167. The Wolfram Functions Site. Webpage: http://functions.wolfram.com/

168. Murakami, Y. and Houston, S., “Dynamic inflow modelling for autorotating rotors” *Aeronautical Jouranal*, Vol.112, No.1127, Jan. 2008, pp 47-53

169. Peters, D.A. and He, C.-J., “Modification of Mass-Flow Parameter to Allow Smooth Transition Between Helicopter and Windmill States,” *Journal of the American Helicopter Society*, TN, 51, No 3, Jul. 2006, pp.275-278

170. He, C.-J., Lee, C.-S. and Chen, W., “Finite State Induced Flow Model in Vortex Ring State,” *Journal of the American Helicopter Society*, TN, 45, No 4, Oct. 2000, pp.318-320

171. Padfield, G.D., *Helicopter Flight Dynamics*, Blackwell Science, Oxford, 1996

172. Done, G. and Balmford, D., *Bramwell's Helicopter Dynamics*, 2nd ed. Butterworth Heinemann, 2001

173. Leishman, J.D., *Principles of Helicopter Aerodynamics*, 2nd ed. Cambridge University Press, 2006

174. Abbott, P.B., *The Gyroplane Flight Manual*, Abbott Co., 1996

175. Abbott, P.B., *Understanding the Gyroplane*, Abbott Co., 1994

176. Mangler, K.W., “Fourier Coefficients for Downwash at a Helicopter Rotor,” R.A.E. Technical Note No. Aero. 1958, May, 1948